AD NUMBER

AD489451

NEW LIMITATION CHANGE

TO

Approved for public release, distribution unlimited

FROM

Distribution authorized to U.S. Gov't. agencies and their contractors; Administrative/Operational Use; JUN 1966. Other requests shall be referred to Air Force Aero Propulsion Lab., Wright-Patterson AFB, OH 45433.

AUTHORITY

AFAPL ltr, 12 Apr 1972

AD 484457

UTILIZATION OF ELASTIC RECOVERY MATERIALS FOR THE DEVELOPMENT OF CREW TRANSFER TUNNELS, AIRLOCKS, AND SPACE MAINTENANCE HANGARS

Part II. Expandable Modular Crew Transfer Tunnel Design, Fabrication, and Testing

T. L. Hoffman

FOREWORD

This report was prepared by Goodyear Aerospace Corporation (GAC), Akron, Ohio under USAF Contract AF33(615)-2114. The contractor's number for this report is GER-12335. The effort was initiated under Project No. 8170, "Aerospace Site Support Techniques." In particular it was a development effort in compliance with Task No. 817004 "Expandable and Modular Structures for Aerospace." The work was administered under the direction of the Aero Propulsion Laboratory, Research and Technology Division (RTD). Mr. F.W. Forbes and Lt. A.J. Zappanti of this laboratory (APFT) were project engineers for the Air Force.

The program began in November 1964 and was concluded in January 1966. The program was directed by the Space Systems and Analytics Division, managed by Mr. S.J. Pipitone of GAC.

This program was a group effort headed by Mr. L. Jurick, project manager of the Astronautics Programs Department, assisted by T. L. Hoffman, project engineer; K. L. Cordier, materials; B.H. Burzlaff, environmental effects; R. L. Ginter, thermodynamics; J.D. Marketos, structural analysis; D.S. Kimes, fabrication; R.D. Lilley, test operations; and L. L. Swinehart, administration and planning.

This report was submitted by the author March 1966.

This technical report has been reviewed and is approved.

James A. McMillan, Major, USAF
Chief, Space Technology Branch
Support Technology Division

ABSTRACT

This report summarizes the design, analysis, fabrication, and testing performed by GAC on the expandable Gemini to Manned Space Station (MSS) modular crew transfer tunnel under USAF Contract AF33(615)-2114 for the Air Force Aero Propulsion Laboratory. The program established the design of a 3.5-foot diameter modular tunnel to be used as a pressurized meteoroid protective enclosure for astronauts transferring from the Gemini capsule to the MSS. The transfer tunnel, which has an expanded length of 12 feet, attaches to the elliptical Gemini hatch at one end and to the circular MSS hatch at the other end.

A prototype expandable crew transfer tunnel was fabricated, and preliminary qualification testing was conducted to establish the feasibility of the design. The expandable tunnel construction is a composite wall consisting of an inner triple-barrier pressure bladder for gas retention, a four-ply Dacron cloth structural layer, a 2-inch thick polyether foam meteoroid barrier, and a film-cloth laminate outer cover with a thermal coating. The expandable composite wall is structurally bonded to a rigid aluminum honeycomb sandwich floor to which the packaging canister is attached when the tunnel is folded to constitute a modular unit.

Pressure proof testing for 7 days at 10 psi and cyclic pressure testing from vacuum to the nominal operating pressure of 7.5 psi for 60 cycles established the structural integrity. Pressure leak testing under ambient conditions for 7 days at 7.5 psi established the gas tightness of the structure with a leak rate of 0.50 lb/day of inflation gas under orbital conditions. Pressure leak testing in a vacuum chamber at an average vacuum of 4×10^{-5} mm Hg for one day established a leak rate of 0.40 lb/day of inflation gas under orbital conditions. Tunnel deployment testing in a vacuum chamber confirmed the operational aspects of the design.

Fabrication of an operational expandable crew transfer tunnel, which is estimated to weigh 375 pounds including the packaging canister, is entirely feasible and within the present state of the art.

TABLE OF CONTENTS

LIST OF ILLUSTRATIONS

LIST OF TABLES

LIST OF SYMBOLS

THERMAL ANALYSIS (SECTION V, SUBSECTION B)

A	Surface area (ft^2)
C	Specific heat (Btu/lb-^oF)
$\bar{C}$	Solar constant (Btu/hr-ft^2)
C'	Solar flux on surface (Btu/hr-ft^2)
E	Earth reradiation flux (Btu/hr-ft^2)
F	Radiation view factor
K	Thermal conductivity (Btu-in./hr-ft^2-^oF)
Q	Albedo flux (Btu/hr-ft^2)
T	Temperature (^oR)
U	Thermal conductance (Btu/hr-^oF)
U'	Thermal conductance from interior to external surface of tunnel (Btu/hr-ft^2-^oF)
W	Mass (lb)
WC	Thermal mass (Btu/^oF)
WC/A	Thermal mass per unit area (Btu/ft^2-^oF)
α	Solar absorptance
β	Oribital angle measured from high noon position (degrees)
δ	Angle around tunnel (degrees)
ϵ	Emittance
θ	Time (hr)
σ	Stefan-Boltzmann constant (Btu/hr-ft^2-$^oR^4$)

Subscripts:

C-E	From cylinder to earth
i	Of or on indicated node
i-E	From indicated node to earth
i-j	Between indicated nodes
S-E	From sphere to earth

LIST OF SYMBOLS (Continued)

STRUCTURAL ANALYSIS (SECTION V, SUBSECTION C)

A	Location point
A'	Cross section area (in^2.)
a	Designated dimension (in.)
B	Location point
b	Designated dimension (in.)
C	Location point
C'	Deflection coefficient
c	Designated dimension (in.)
$\bar{c}$	Distance from neutral axis to outermost bending fiber (in.)
D	Location point
D'	Flexural rigidity (in.-lb)
d	Designated dimension (in.)
d( )	Differential indicator
E	Modulus of elasticity (psi)
e	Designated dimension (in.)
F	Load (lb/in.)
f	Stress (psi)
f'	Stress (lb/in.)
G	Acceleration of gravity (ft/sec^2)
H	Reaction (lb/in.)
h	Flange thickness (in.)
I	Cross section moment of inertia ($in.^4/in.$)
I'	Cross section moment of inertia ($in.^4$)
L	Length (in.)
M	Moment (in.-lb/in.)
M'	Moment (in.-lb)
MS	Margin of safety

LIST OF SYMBOLS (Continued)

P	Load (lb)
p	Pressure (psi)
R	Radius of sphere, Gemini end (in.)
R'	Radius of sphere and cylinder, MOL end (in.)
R''	Radius of transition torus (in.)
r	Cross section radius (in.)
S	Membrane stress (psi)
S'	Bending stress (psi)
s	Arc length (in.)
t	Thickness (in.)
U	Strain energy (in.-lb/in.)
V	Shear; reaction (lb/in.)
W	Load (lb)
w	Distributed load on cylinder (lb/in.)
w'	Distributed load on bolt circle (lb/in.)
w''	Distributed load on flange (lb/in.)
x	Reference axis
$\bar{x}$	Neutral axis
y	Distance from reference axis to item centroid (in.)
$\bar{y}$	Distance from reference axis to neutral axis (in.)
β	Designated angle (degrees)
δ	Linear deflection (in.)
θ	Angular deflection (radians)
λ	Coefficient for radius-thickness relationship ($in.^{-1}$)
μ	Poisson's ratio
ϕ	Designated angle (degrees)
∂ ( )	Partial differential indicator

Subscripts:

A	Location A
B	Location B
b	Bond
br	Bearing
C	Location C; cylinder
c	Compression
D	Location D
F	Flange
M	Moment
max	Maximum
o	Item neutral axis
P	Pressure
s	Shear
T	Twisting
t	Tension
u	Ultimate
V	Shear
w	Distributed load
x	Reference axis
$\bar{x}$	Neutral axis
θ	Angular location
0	Redundant
1	Meridional, axial
2	Hoop
3, 4, 5, 6	Coefficient identification

LIST OF SYMBOLS (Continued)

ENVIRONMENTAL HAZARDS (SECTION V, SUBSECTION D)

A	Area (ft^2)
c	Velocity of light (cm/sec)
d( )	Differential indicator
E	Kinetic energy (mev)
$\bar{E}$	Average incident energy (mev)
E'	Average energy with which particles leave after penetration (mev)
F	Ratio of shower meteoroids to sporadic meteoroids
K	Short-term mission factor
m	Mass (g)
N	Designated flux (particles/ft^2-day or particles/cm^2)
$\bar{N}$	Designated flux (particles/cm^2)
N'	Total number of impacts
n	Nano (prefix)
P	Designated probability (day^{-1} or $mission^{-1}$)
p	Particle momentum (mev-sec cm)
R	Rigidity (million volts)
r	Average range of particles (g cm^2)
S	Shielding factor
T	Sum of kinetic energy and rest energy (mev)
t	Thickness (in.)
t'	Material thickness (areal density) (g cm^2)
U'	Total number of meteoroid impacts ($mission^{-1}$)
Ze	Nuclear charge of the particle (electron charges)
ΔD	Energy absorbed per unit mass (rads)
ΔE	Incremental energy (mev)
ΔN	Flux with incidental energy in a designated energy range (particles cm^2)
N[>E]	Flux as a function of energy (particles cm^2)

LIST OF SYMBOLS (Continued)

$N[>R]$	Flux as a function of rigidity (particles/cm^2)
$N[E + \Delta E]$	Flux as a function of a designated energy range (particles/cm^2)
$N[E - \Delta E]$	Flux as a function of a designated energy range (particles/cm^2)
$P[N]$	Probability as a function of flux (day^{-1} or mission^{-1})
μ	Micro (prefix)
τ	Time (days)

Subscripts:

al	Aluminum
E	Earth shielding
$\bar{E}$	Designated energy
E'	Designated energy
e	Electrons
F	Total shielding
foam	Polyether flexible foam
I	Interference
M	Particular mission duration
o	Rest
p	Projected
s	Exposed surface
SH	Shower meteoroids
SP	Sporadic meteoroids
$x = 0$	Of no impacts; of zero penetrations
τ	Time in days
300_{nmi}	For a 300-nautical mile orbit

PRELIMINARY QUALIFICATION TESTING (SECTION VI)

C	Proportionality constant (lb/Mach No.)
G	Acceleration of gravity (ft/sec^2)

LIST OF SYMBOLS (Continued)

M	Molecular weight (lb/mole)
p	Pressure
'	Pressure for Mach number determination (psia)
R	Specific gas constant (ft-lb/lb-^{o}R)
R'	Universal gas constant (ft-lb/mole-^{o}K)
T	Temperature (^{o}F)
$\overline{T}$	Temperature (^{o}K)
T'	Temperature (^{o}R)
V	Volume (ft^3)
v	Velocity
w	Weight (lb)
$\Delta p'$	Pressure differential for Mach number determination (psia)
ρ	Density (pcf)
τ	Time (days)

Subscripts:

A	Absolute pressure
$\overline{A}$	Average absolute pressure
B	Barometric pressure
C	Corrected to reference temperature of 75^{o}F
c	Due to cylinder weight decrease
D	Daily
F	Final value
G	Gage pressure
H	In. Hg
I	Initial value
L	Loss
M	MM of Hg or torr
m	Due to molecular weight difference

LIST OF SYMBOLS (Continued)

N	Gas mixture, 50 percent nitrogen and 50 percent oxygen
O	Orbital conditions
P	Psi
p	Due to pressure difference
T	Leak test
V	Vacuum chamber
v	Due to velocity difference
1	Designated condition
2	Designated condition

SECTION I

INTRODUCTION

A. GENERAL

This final report presents the results of GAC's program effort conducted under USAF Contract AF33(615)-2114 for the Aero Propulsion Laboratory. The contract effort was fundamentally directed toward demonstrating the technical feasibility of utilizing an expandable crew transfer tunnel for manned space stations utilizing current re-entry modules such as the Gemini capsule, hereinafter called the Gemini-Manned Space Station (MSS) system. The program effort was performed in three successive phases.

B. PHASE I - CONCEPT DEFINITION

The objective of the Phase I effort was to define a modular expandable crew transfer tunnel in conceptual form. This was established within certain constraints stipulated by Air Force in-house Development relative to the mission objective with regard to general operational, human factors, and packaging requirements; and attachment, environmental, structural, and materials requirements. Design studies were conducted, and a specific concept was established. This concept is shown in Figure 1.

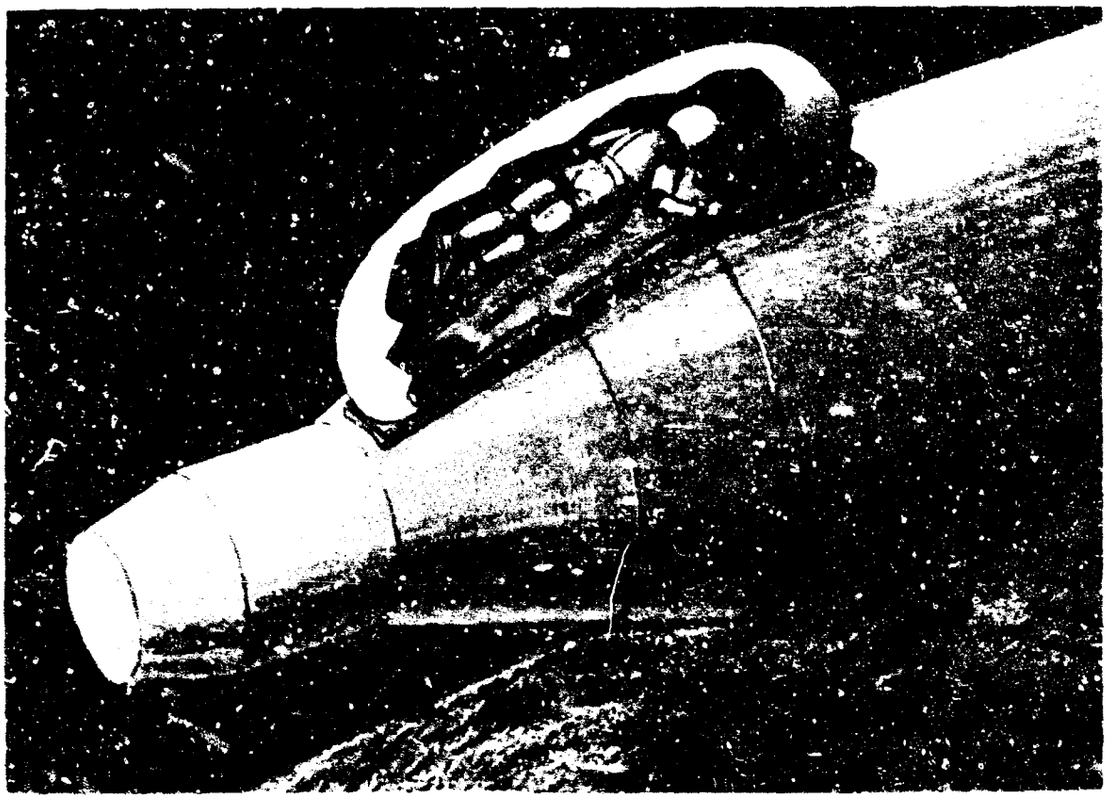

Figure 1. Expandable Crew Transfer Tunnel

C. PHASE II - DETAILED DESIGN, ANALYSIS, AND TEST

The Phase II effort was initiated to translate the concept into a detailed preliminary design. The following supporting analyses were conducted to substantiate the preliminary design:

(1) Evaluation of the passive thermal control system.

(2) Determination of structural integrity of the tunnel.

(3) Analysis of environmental hazards including micrometeoroids and radiation.

(4) Substantiation of proposed materials for the tunnel construction.

The general arrangement of the detailed design is shown in Figure 2.

D. PHASE III - PROTOTYPE FABRICATION AND PRELIMINARY QUALIFICATION

In Phase III, a full-scale prototype tunnel was fabricated and subjected to preliminary qualification testing. To perform the testing, a test carrier mock-up simulating the Gemini and MSS hatches and a packaging canister were fabricated. Packaging, pressure proof, pressure leak, and vacuum chamber deployment tests were conducted. The prototype tunnel design is shown in Figure 3.

Zero-G flight tests of the tunnel will be performed when the government-furnished zero-G aircraft at Wright-Patterson AFB is available. The results of these tests will be reported in Part III of this report.

Figure 4 shows the fully expanded prototype tunnel, which has successfully passed the acceptance pressure proof test at 10 psi and the pressure leak test at 7.5 psi. Figure 5 shows the same structure folded prior to installation of the packaging canister.

E. CONTINUED DEVELOPMENT

In view of the successful preliminary qualification tests on the prototype tunnel, it is recommended that the program be continued with the development and flight testing of a modular design expandable tunnel for man-rated orbital flight operation. In line with this recommendation, a program development plan has been prepared and is submitted in this report.

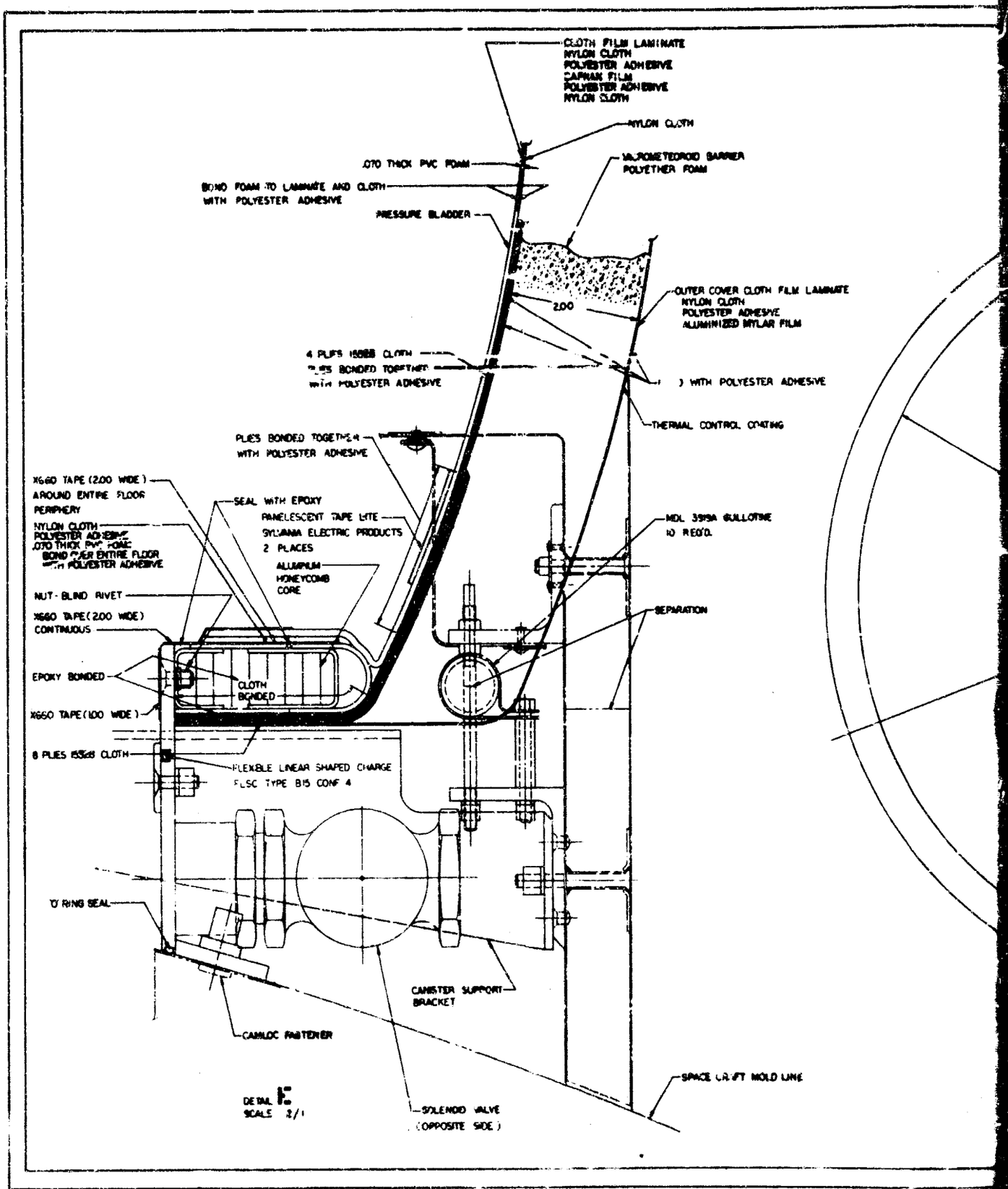
CLOTH FILM LAMINATE
NYLON CLOTH
POLYESTER ADHESIVE
CAPRAN FILM
POLYESTER ADHESIVE
NYLON CLOTH
NYLON CLOTH
.070 THICK PVC FOAM
VALROMETEDROID BARRIER
POLYETHER FOAM
BOND FOAM TO LAMINATE AND CLOTH
WITH POLYESTER ADHESIVE
PRESSURE BLADDER
2.00
OUTER COVER CLOTH FILM LAMINATE
NYLON CLOTH
POLYESTER ADHESIVE
ALUMINIZED MYLAR FILM
4 PLIES 181SS CLOTH
) WITH POLYESTER ADHESIVE
THERMAL CONTROL COATING
PLIES BONDED TOGETHER
WITH POLYESTER ADHESIVE
X660 TAPE (2.00 WIDE)
AROUND ENTIRE FLOOR
PERIPHERY
SEAL WITH EPOXY
PANELESCENT TAPE LITE
SYLVANIA ELECTRIC PRODUCTS
2 PLACES
NYLON CLOTH
POLYESTER ADHESIVE
.070 THICK PVC FOAM
BOND OVER ENTIRE FLOOR
WITH POLYESTER ADHESIVE
ALUMINUM
HONEYCOMB
CORE
MDL 3919A GUILLOTINE
TO REQ'D.
NUT - BLIND RIVET
X660 TAPE (2.00 WIDE)
CONTINUOUS
SEPARATION
EPOXY BONDED
CLOTH
BONDED
X660 TAPE (1.00 WIDE)
8 PLIES 181SS CLOTH
FLEXIBLE LINEAR SHAPED CHARGE
FLSC TYPE B15 CONF 4
O RING SEAL
CANISTER SUPPORT
BRACKET
CAMLOC FASTENER
SPACE CRAFT MOLD LINE
SOLENOID VALVE
(OPPOSITE SIDE)
DETAIL E
SCALE 2/1

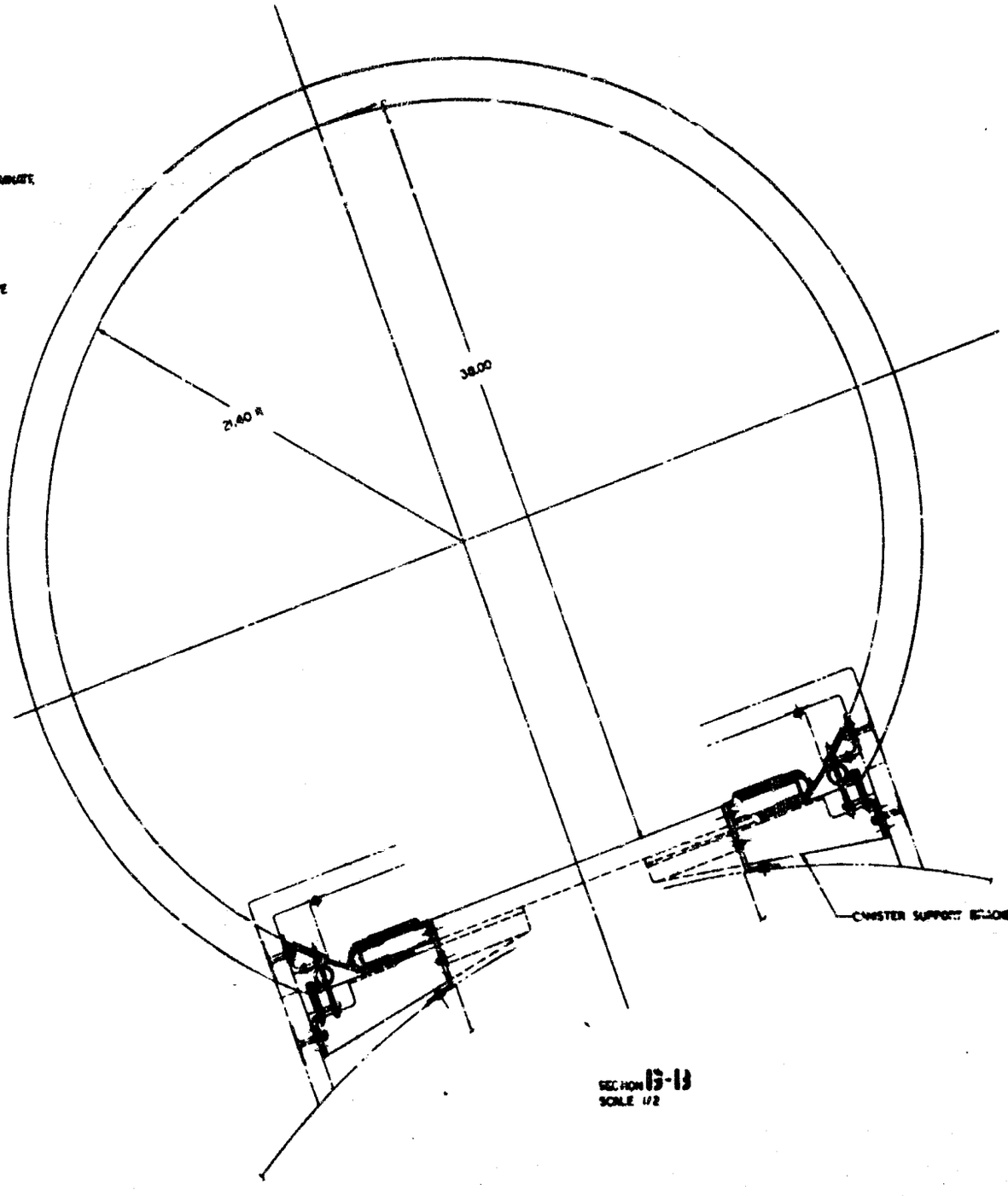

SECTION B-B
SCALE 1/2

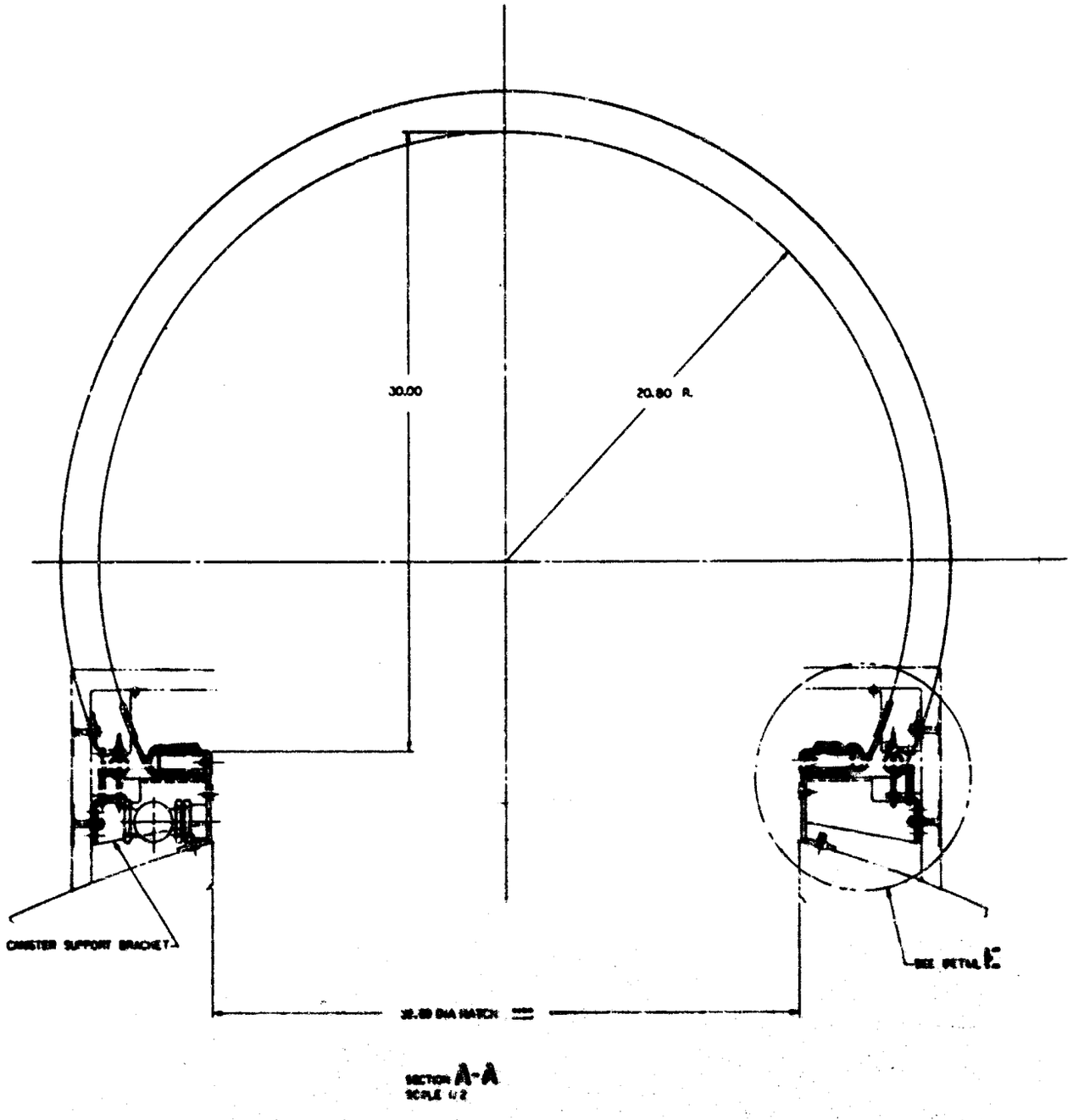

Figure 2. General Arrangement Drawing of Expandable Crew Transfer Tunnel (Sheet 1 of 3)

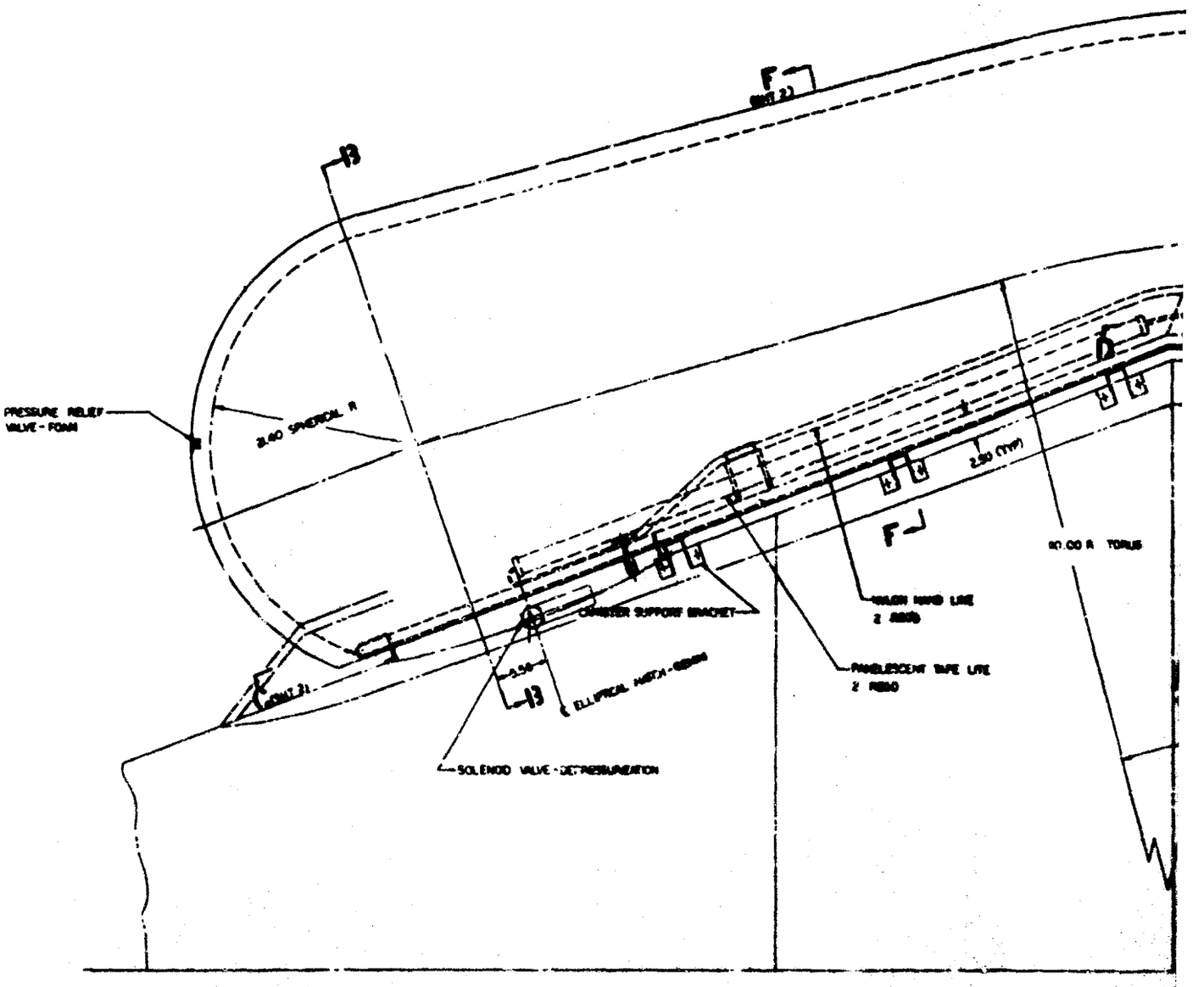

DETAIL E

Sheet (Sheet 1 of 2)

3

4

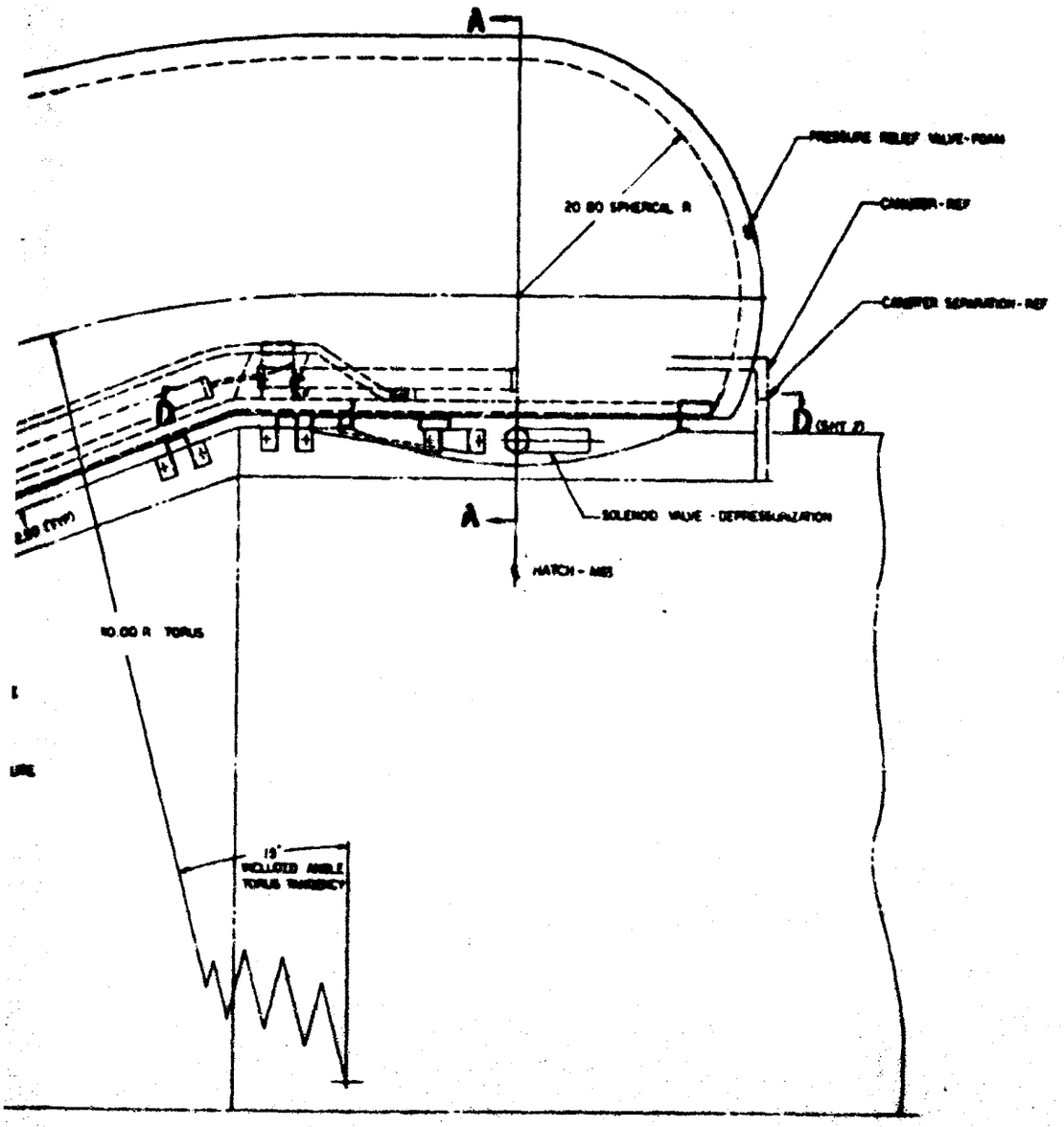
A
PRESSURE RELIEF VALVE - FOAM
20.80 SPHERICAL R
CANISTER - REF
CANISTER SEPARATION - REF
D (SHT 2)
SOLENOID VALVE - DEPRESSURIZATION
A
HATCH - MB
10.00 R TORUS
15°
WELDED ANGLE
TORUS TANGENCY

4

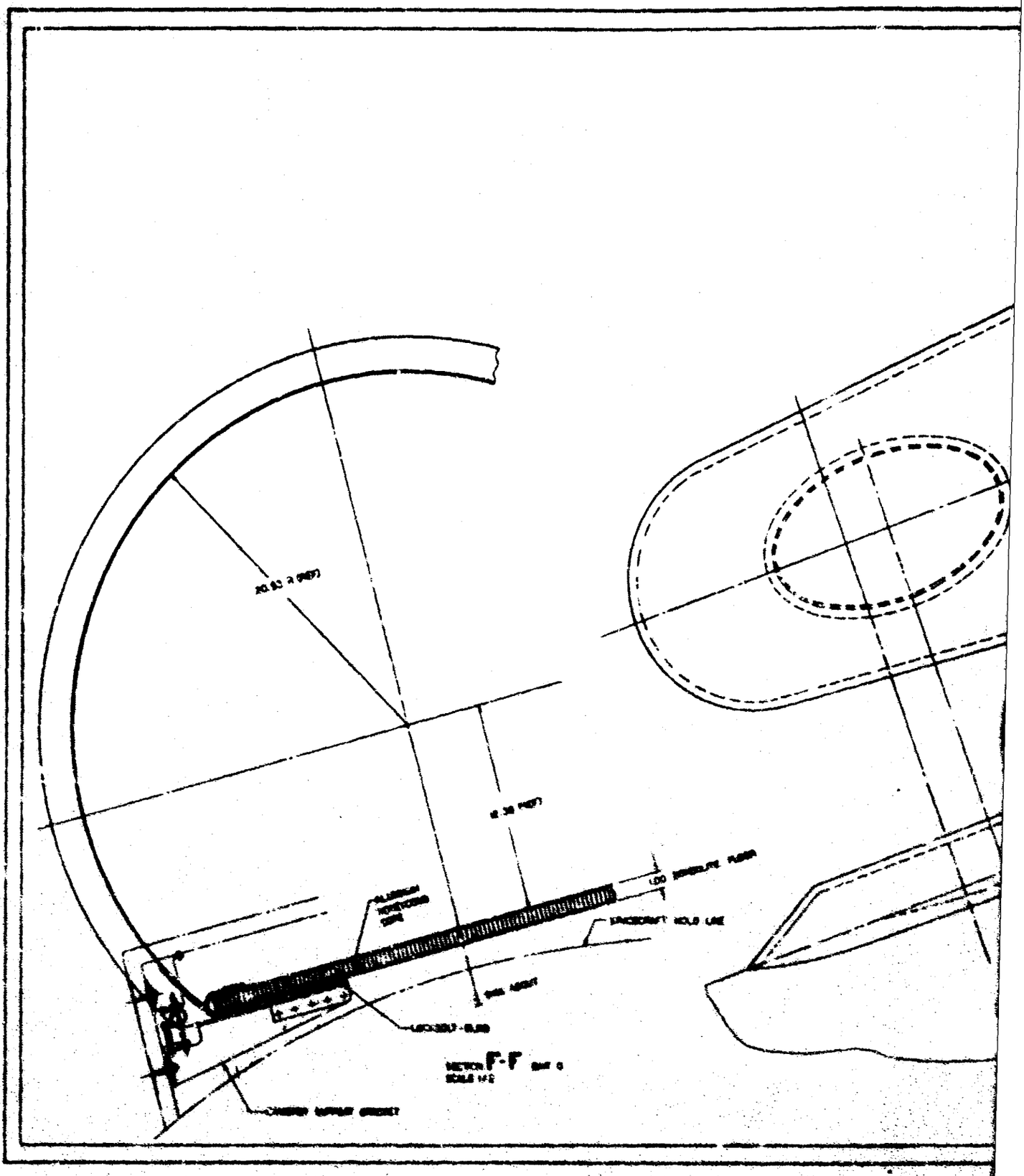
SECTION F-F

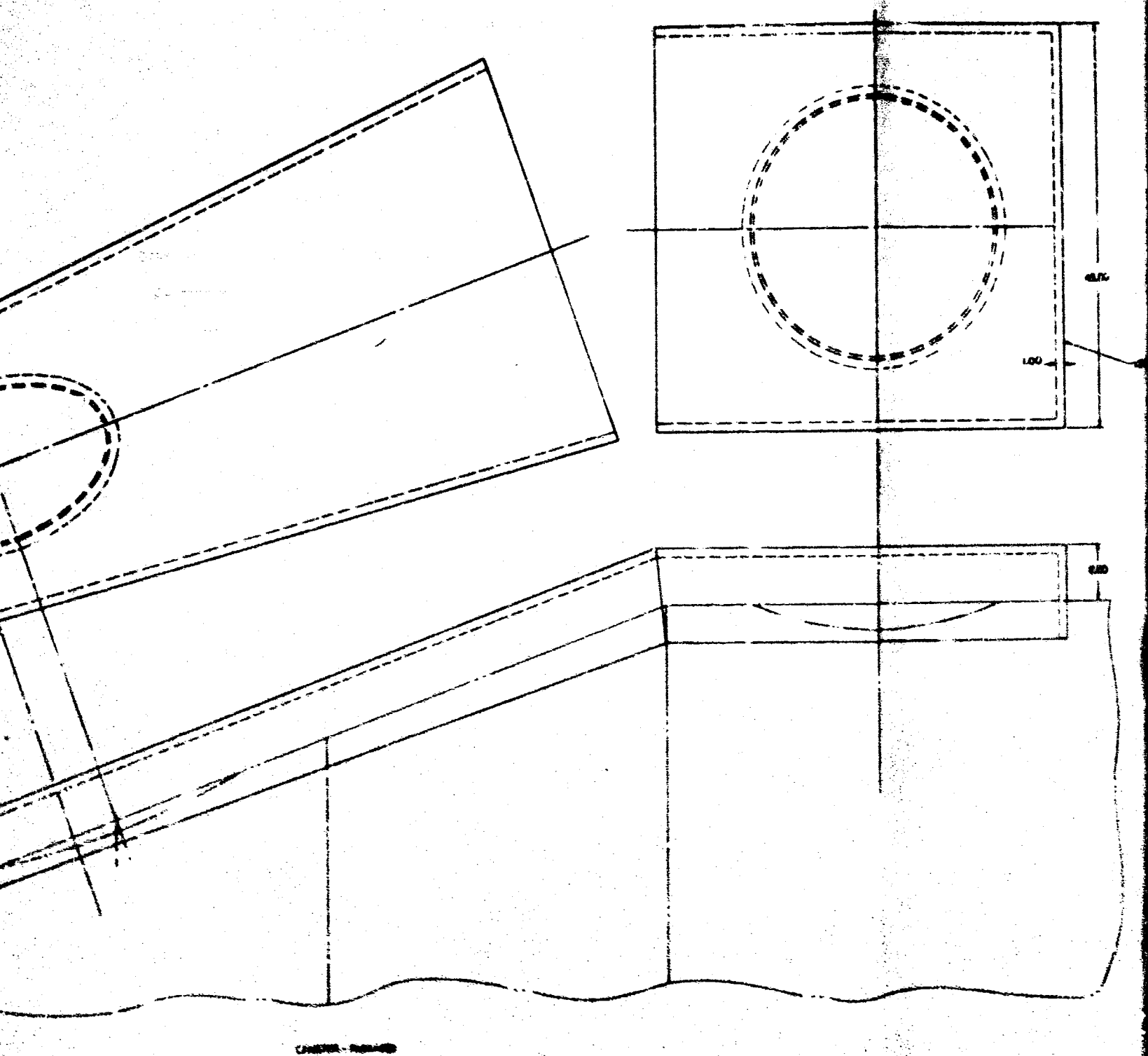

Figure 2. General Arrangement Drawing of [illegible]

2

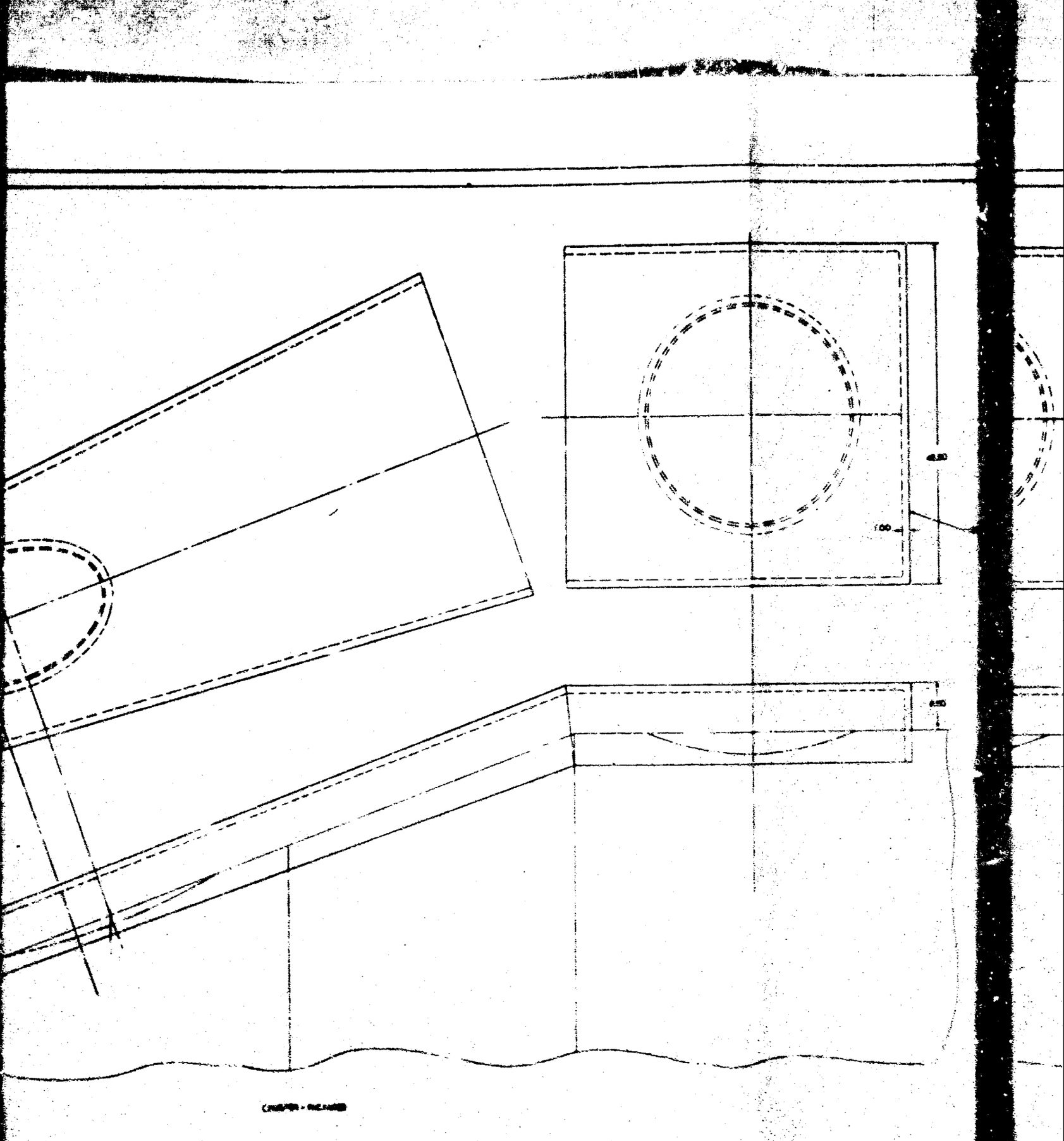

Figure 1. General Arrangement Drawing of

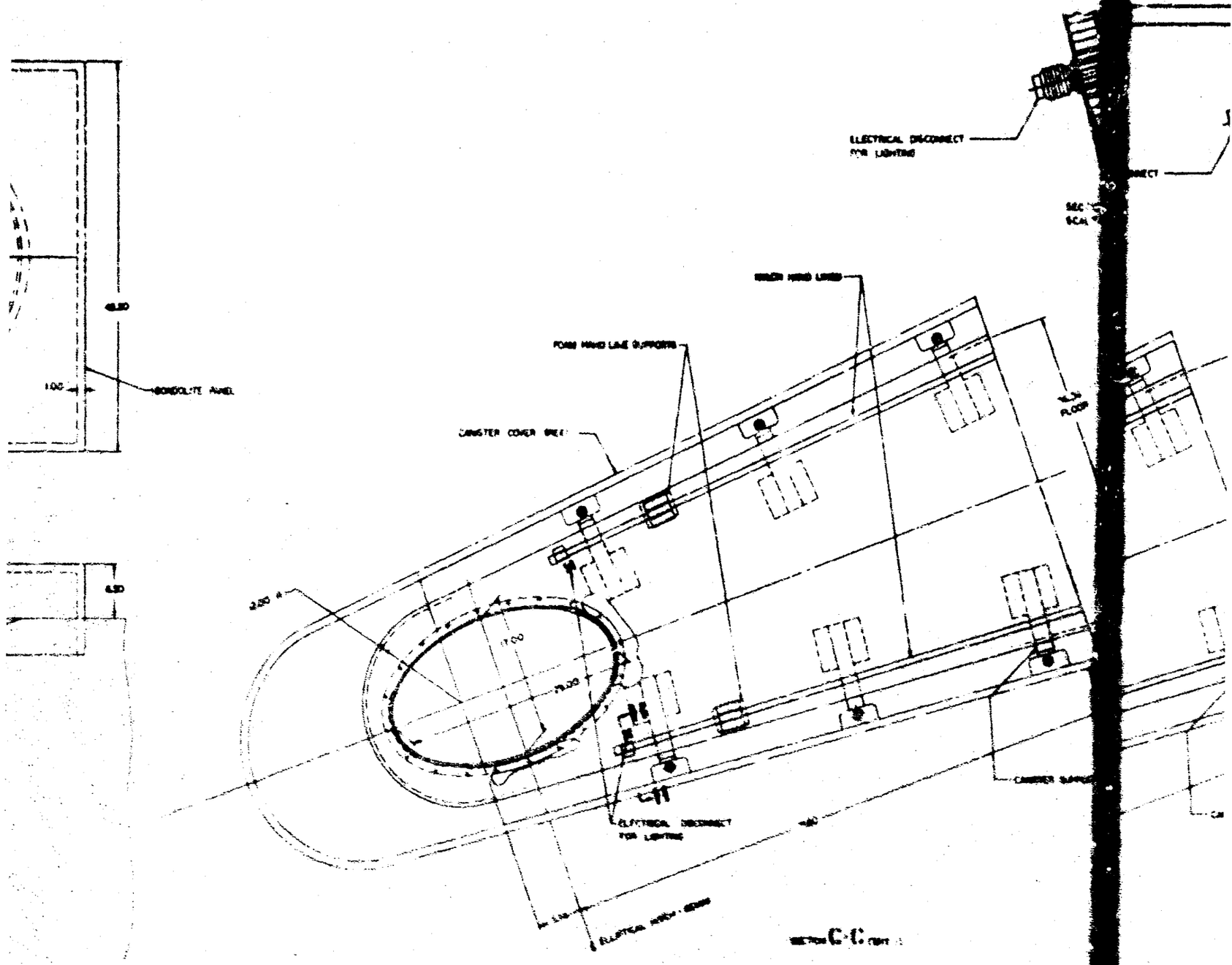

ring of Expandable Crew Transfer Tunnel (Sheet 2 of 2)

2

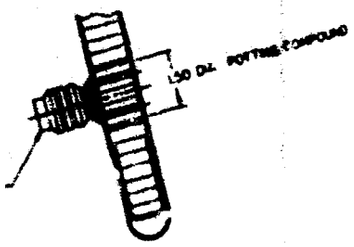

SECTION H-H
SCALE 1/1

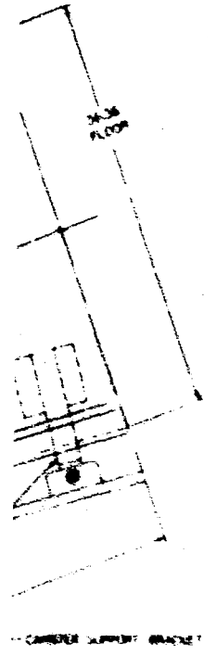

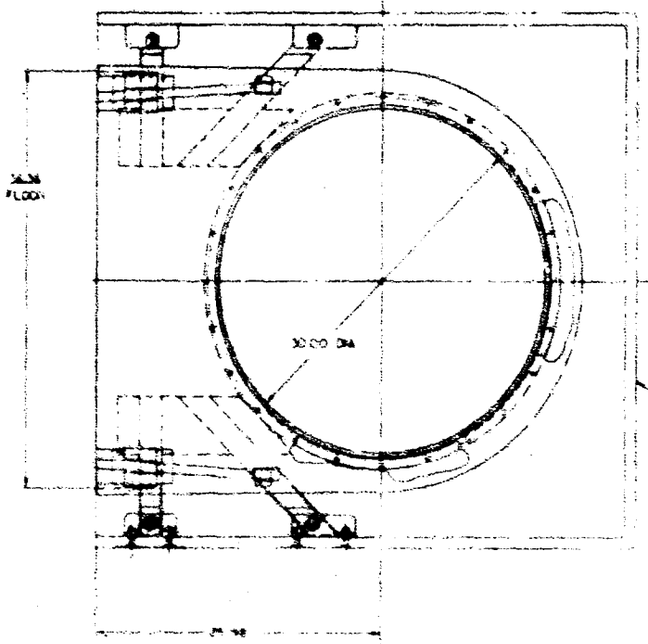

SECTION D-D

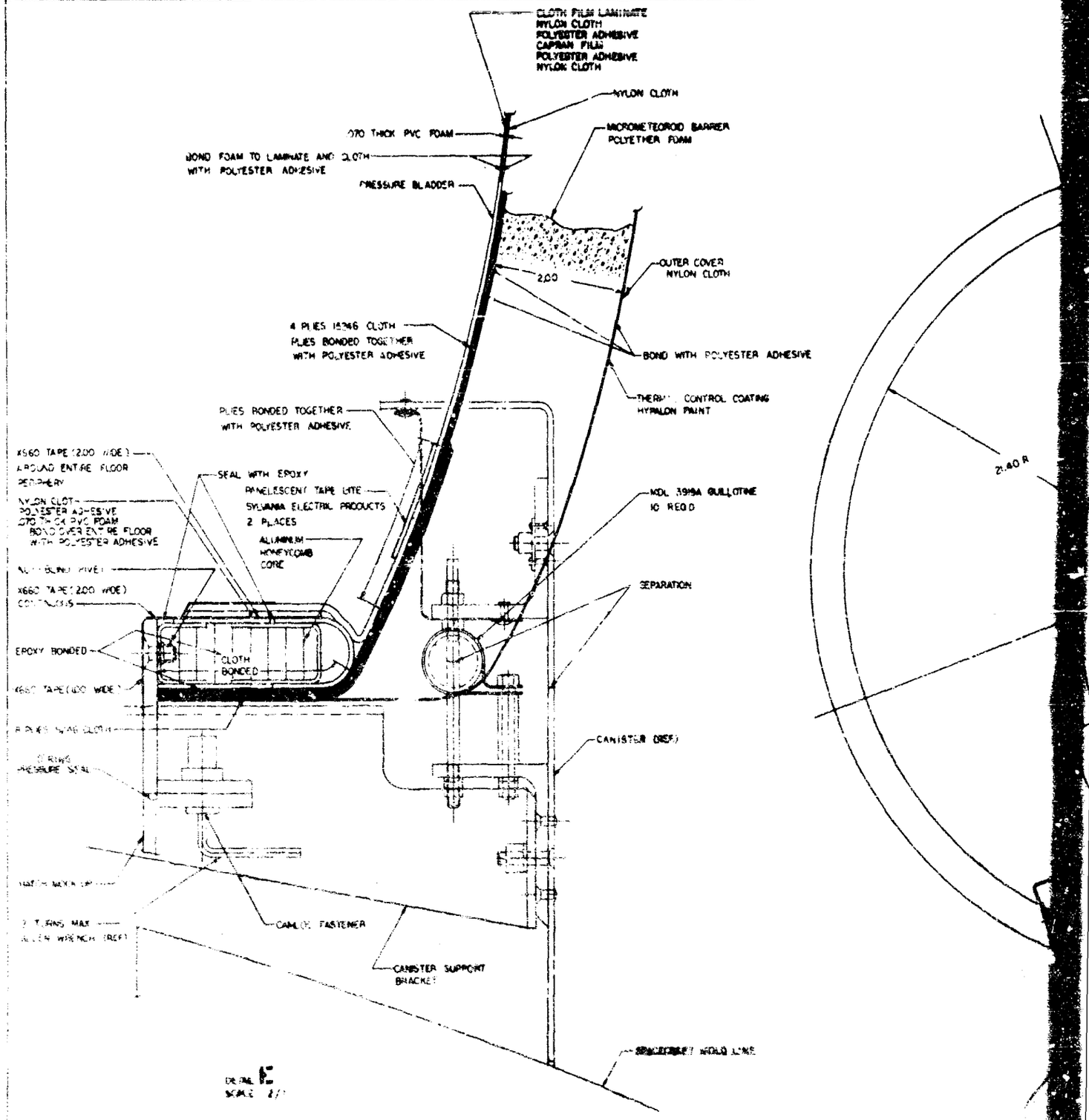
CLOTH FILM LAMINATE
NYLON CLOTH
POLYESTER ADHESIVE
CAPRAN FILM
POLYESTER ADHESIVE
NYLON CLOTH
NYLON CLOTH
.070 THICK PVC FOAM
MICROMETEOROID BARRIER
POLYETHER FOAM
BOND FOAM TO LAMINATE AND CLOTH
WITH POLYESTER ADHESIVE
PRESSURE BLADDER
OUTER COVER
NYLON CLOTH
2.00
4 PLIES 181/66 CLOTH
PLIES BONDED TOGETHER
WITH POLYESTER ADHESIVE
BOND WITH POLYESTER ADHESIVE
THERMAL CONTROL COATING
HYPALON PAINT
PLIES BONDED TOGETHER
WITH POLYESTER ADHESIVE
X560 TAPE (2.00 WIDE)
AROUND ENTIRE FLOOR
PERIPHERY
SEAL WITH EPOXY
PANELESCENT TAPE LITE
SYLVANIA ELECTRIC PRODUCTS
2 PLACES
NYLON CLOTH
POLYESTER ADHESIVE
.070 THICK PVC FOAM
BOND OVER ENTIRE FLOOR
WITH POLYESTER ADHESIVE
ALUMINUM
HONEYCOMB
CORE
MDL 3919A GUILLOTINE
10 REQ'D
SEPARATION
X660 TAPE (2.00 WIDE)
EPOXY BONDED
CLOTH
BONDED
CANISTER (REF.)
CANISTER FASTENER
CANISTER SUPPORT
BRACKET
21.80 R

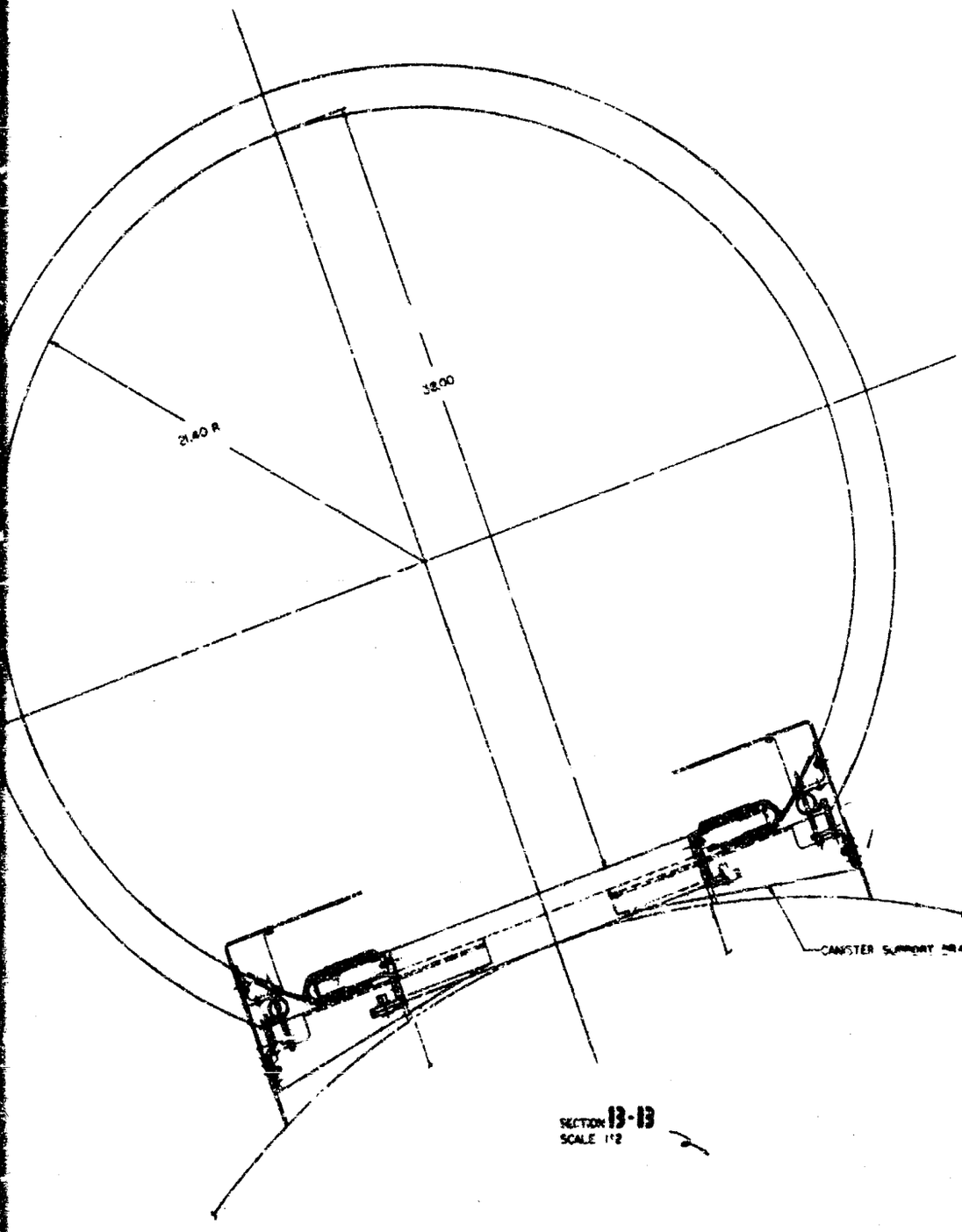

SECTION B-B
SCALE 1"2

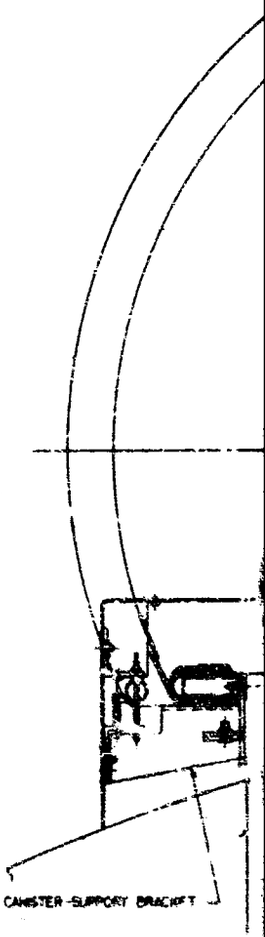

Figu

2

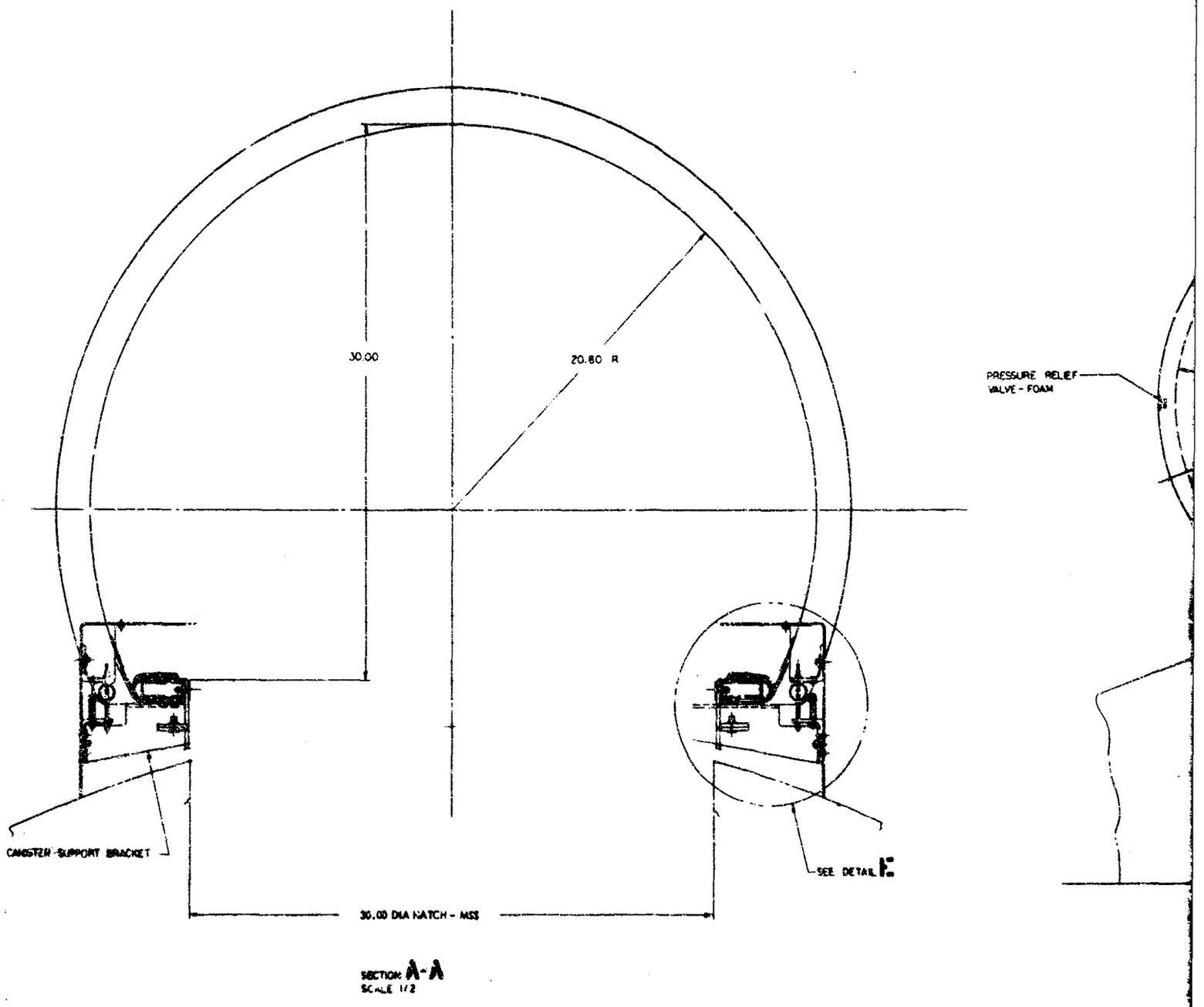

Figure 3. General Arrangement Drawing of Prototype Crew Transfer Tunnel (Sheet 1 of 2)

2

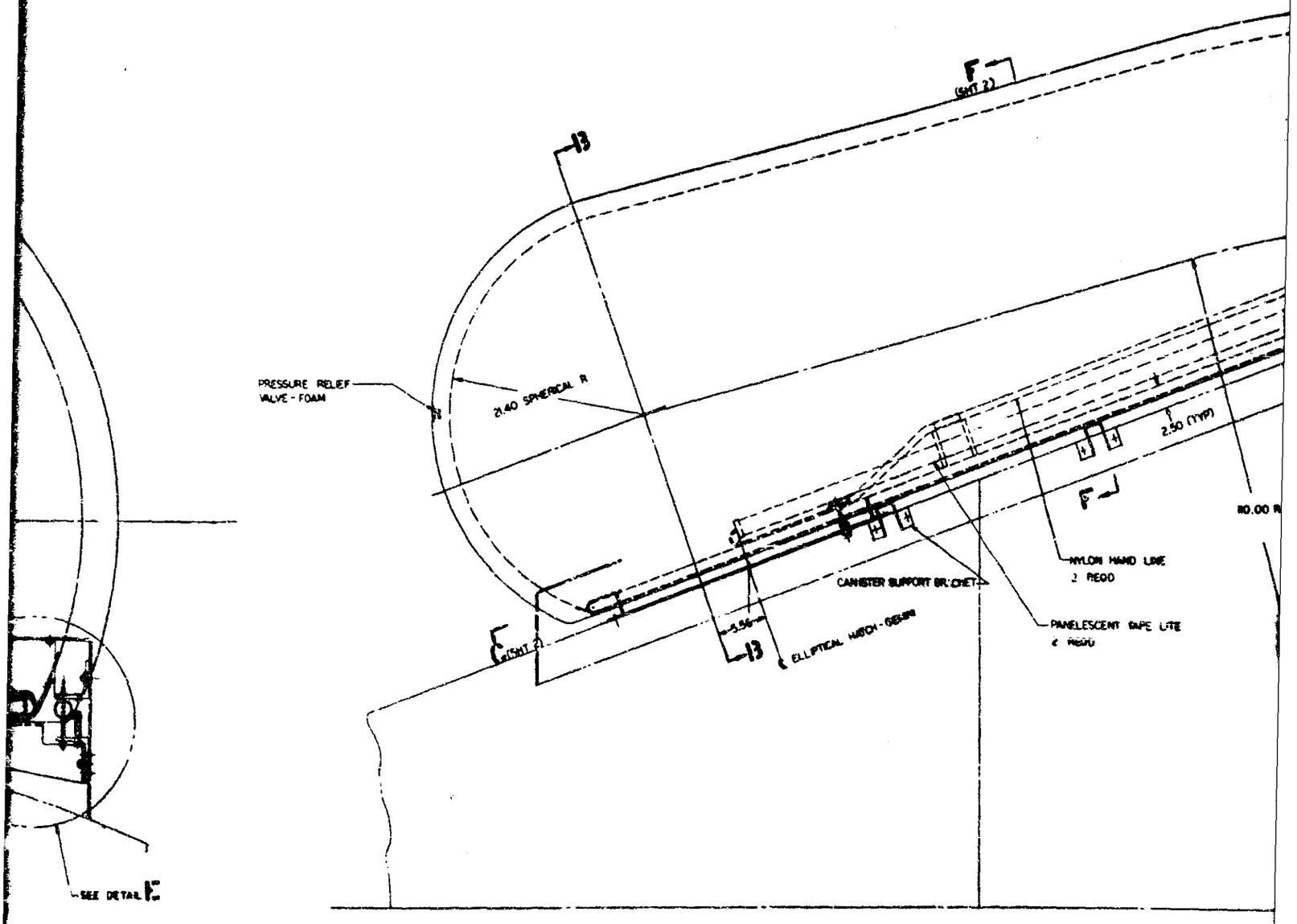

nafer Tunnel (Sheet 1 of 2)

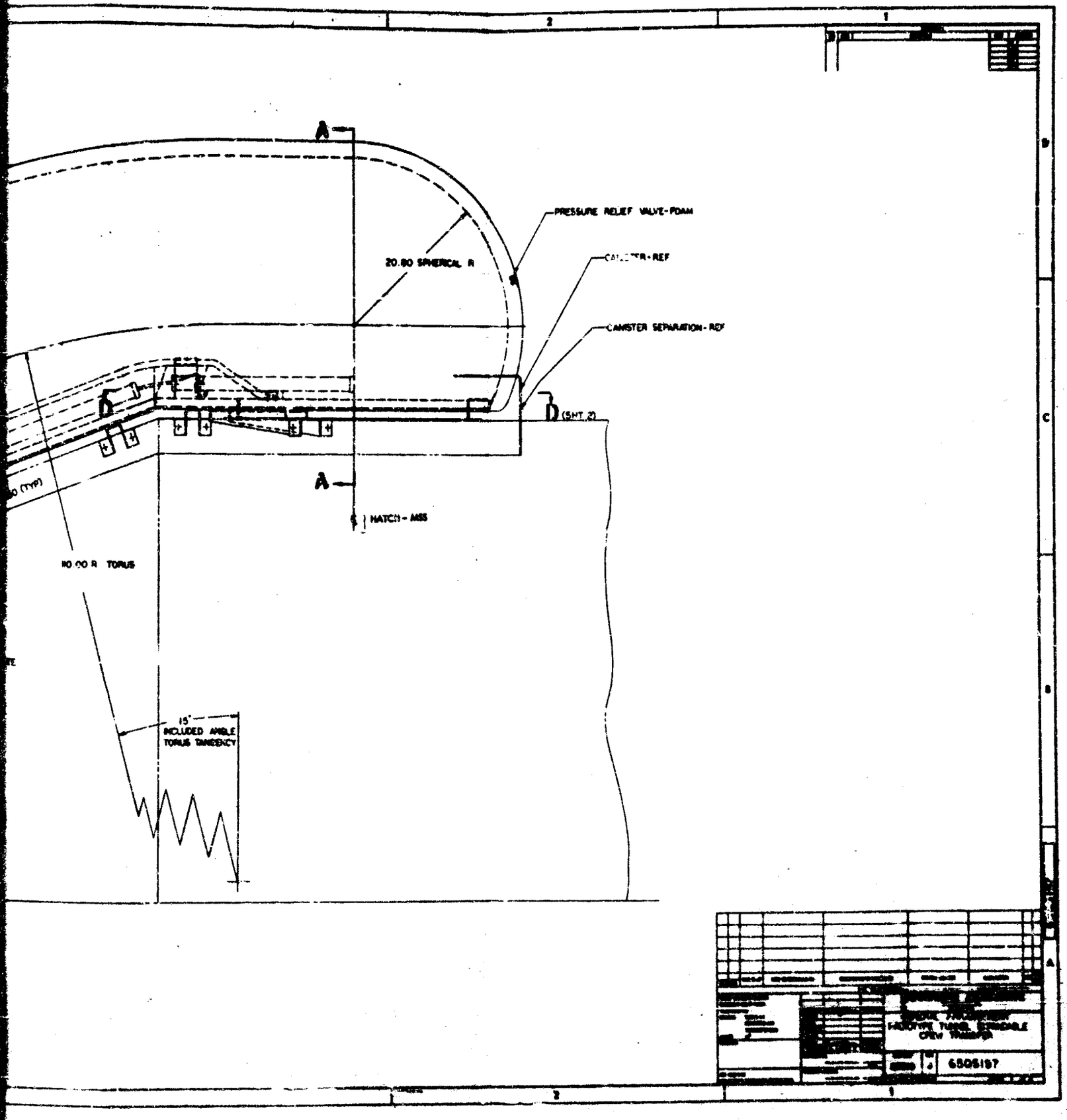
A
PRESSURE RELIEF VALVE-FOAM
20.80 SPHERICAL R
CANISTER-REF
CANISTER SEPARATION-REF
D (SHT 2)
A
HATCH-MBS
10.00 R TORUS
15°
INCLUDED ANGLE
TORUS TANGENCY
6505157

3

4

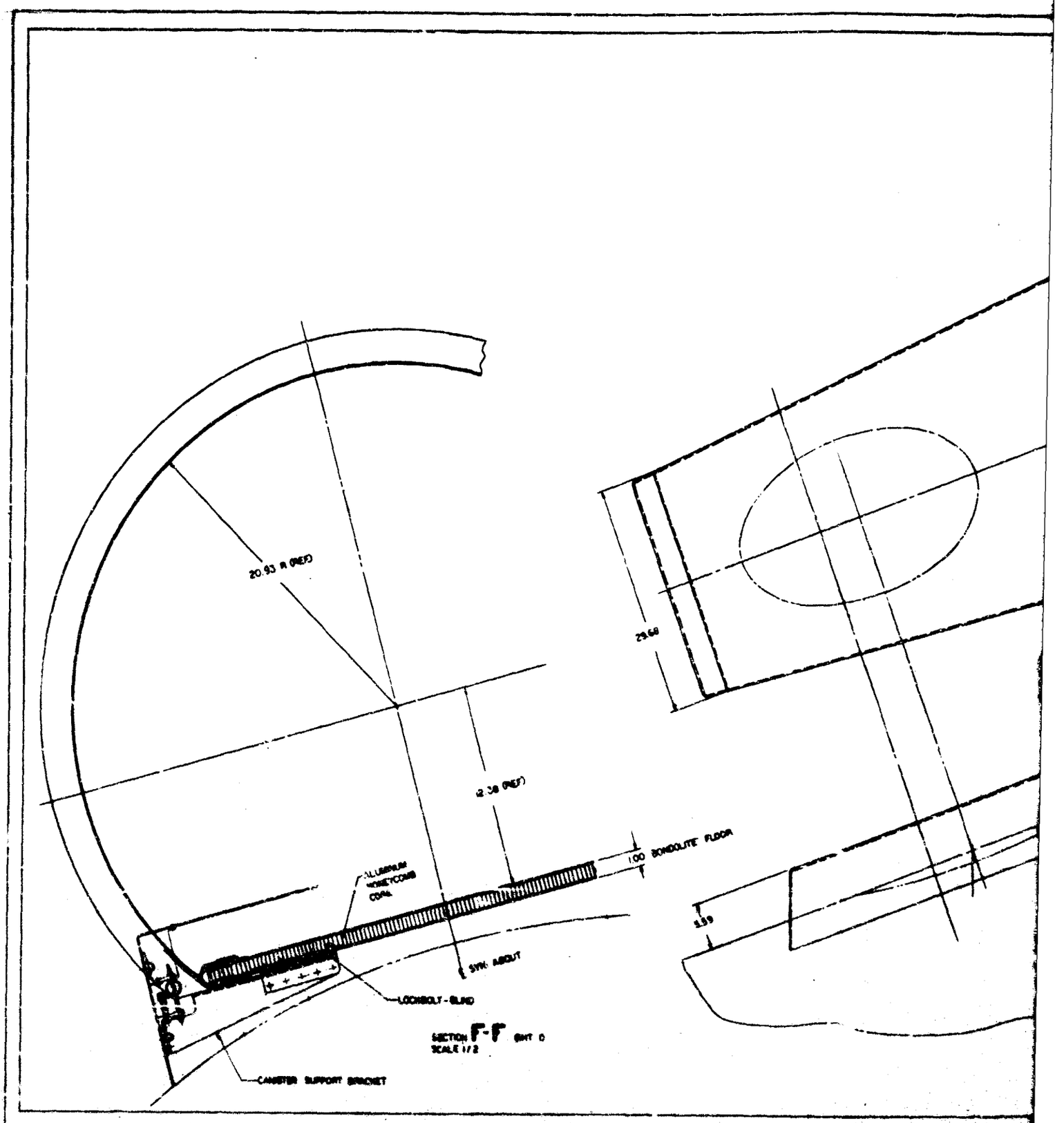
20.93 R (REF)
23.68
12.38 (REF)
1.00 BONDOLITE FLOOR
ALUMINUM HONEYCOMB CORE
5.59
SYM. ABOUT
LOCKBOLT - SEE
CANISTER SUPPORT BRACKET
SECTION F-F SHT 0
SCALE 1/2

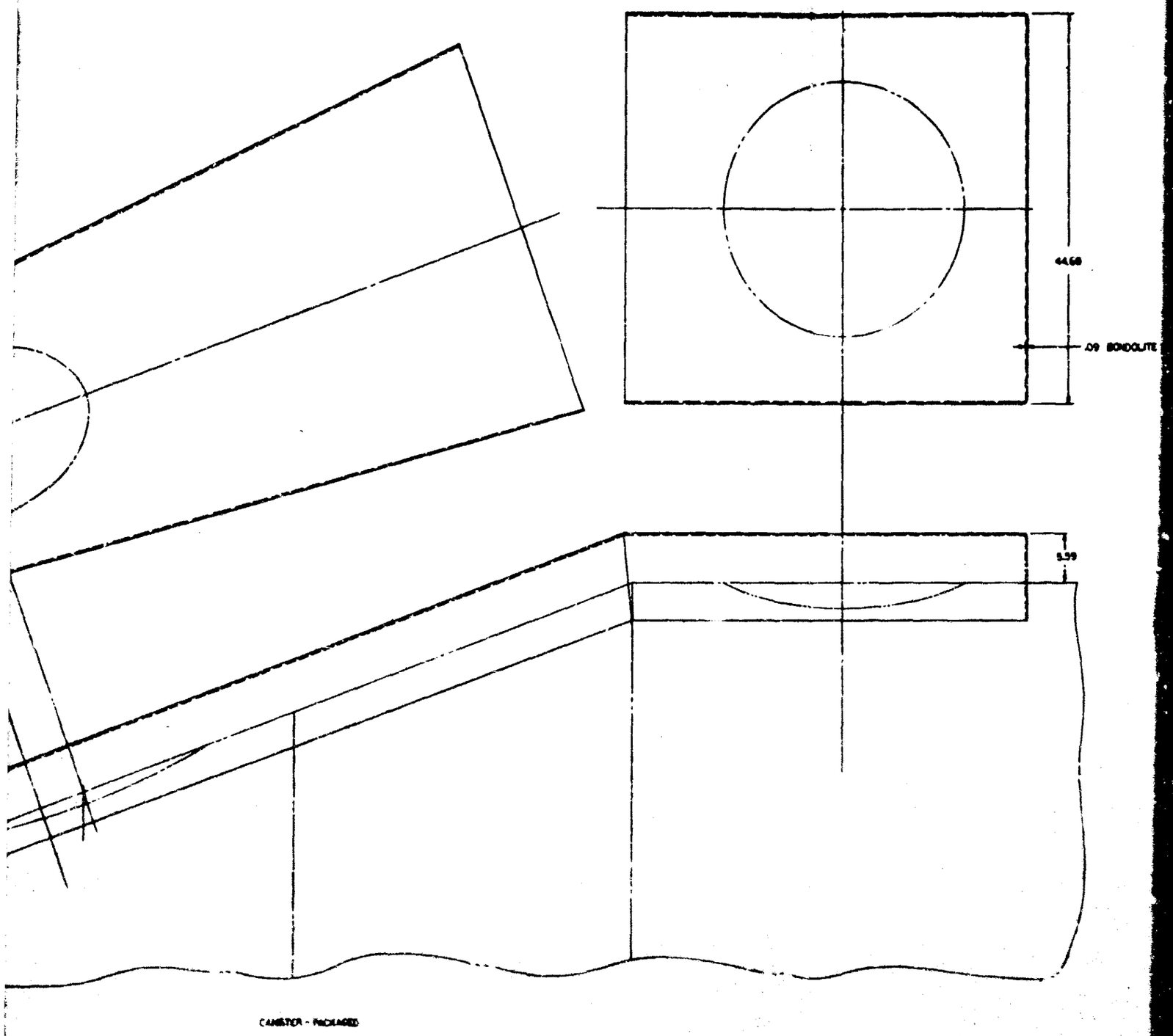

Figure 3. General Arrangement Drawing of Prototype Cr

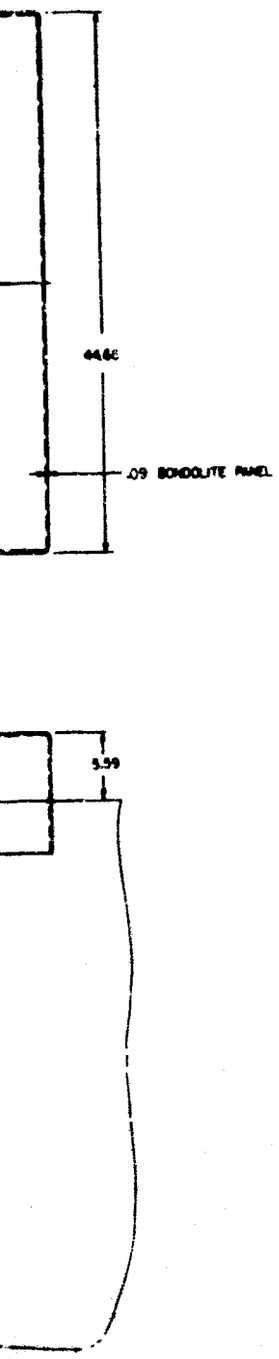

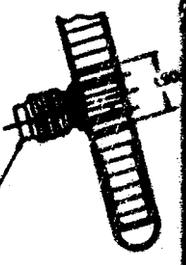

SECTION H-H
SCALE 1/1

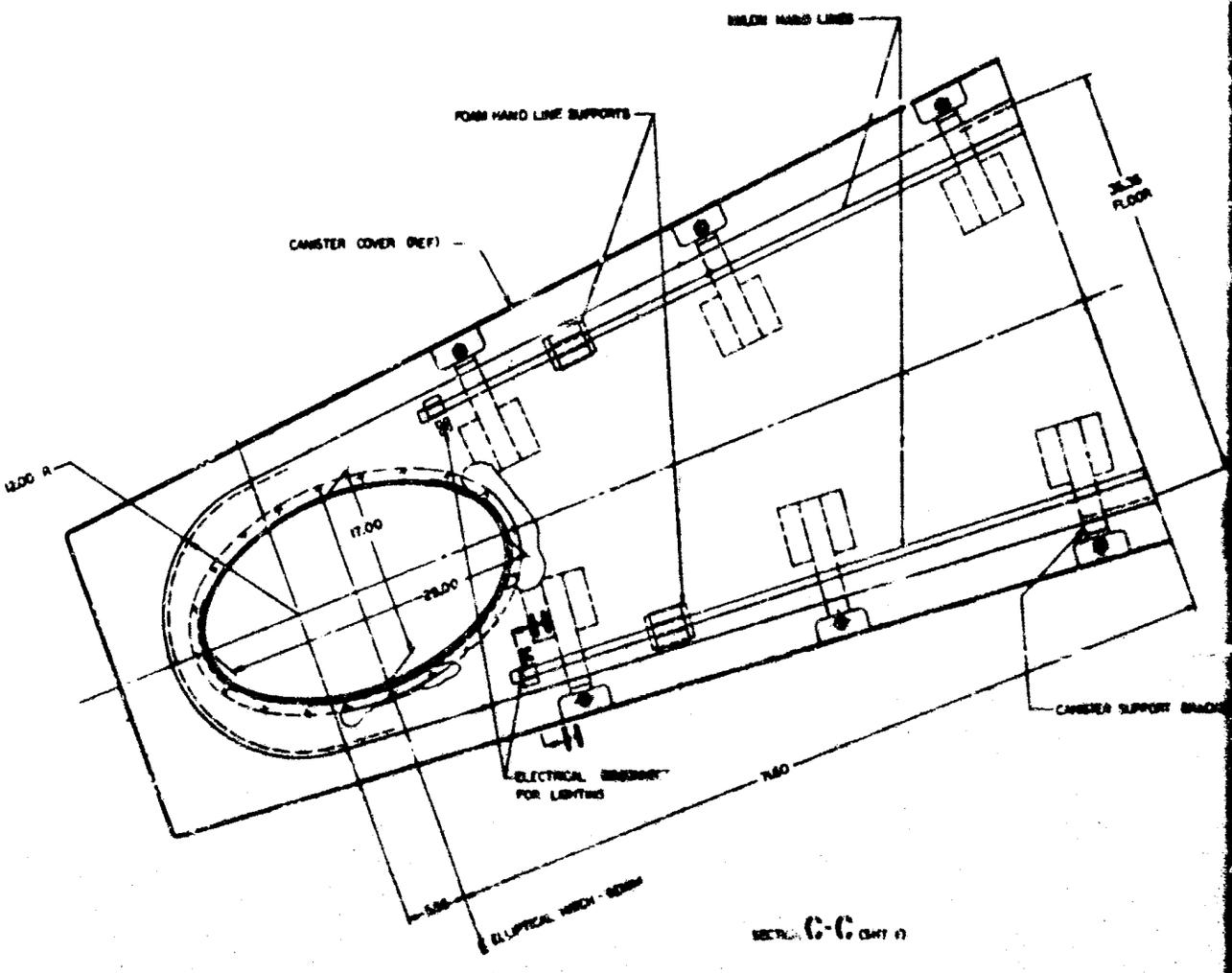

SECTION C-C (SHT 1)

g of Prototype Crew Transfer Tunnel (Sheet 2 of 2)

9

3

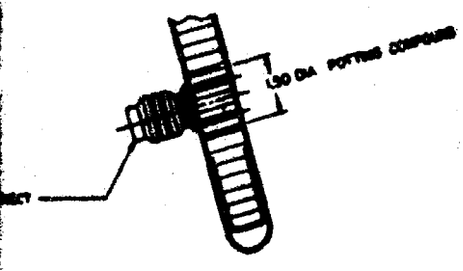

SECTION H-H
SCALE 1/1

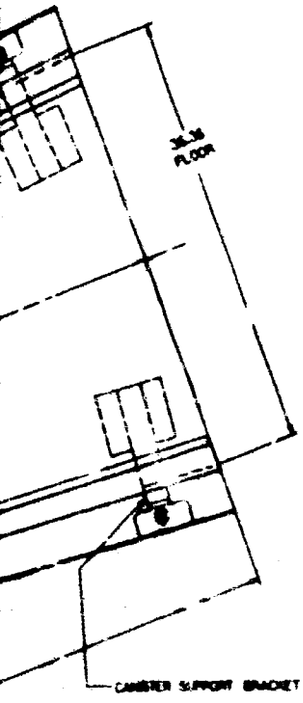

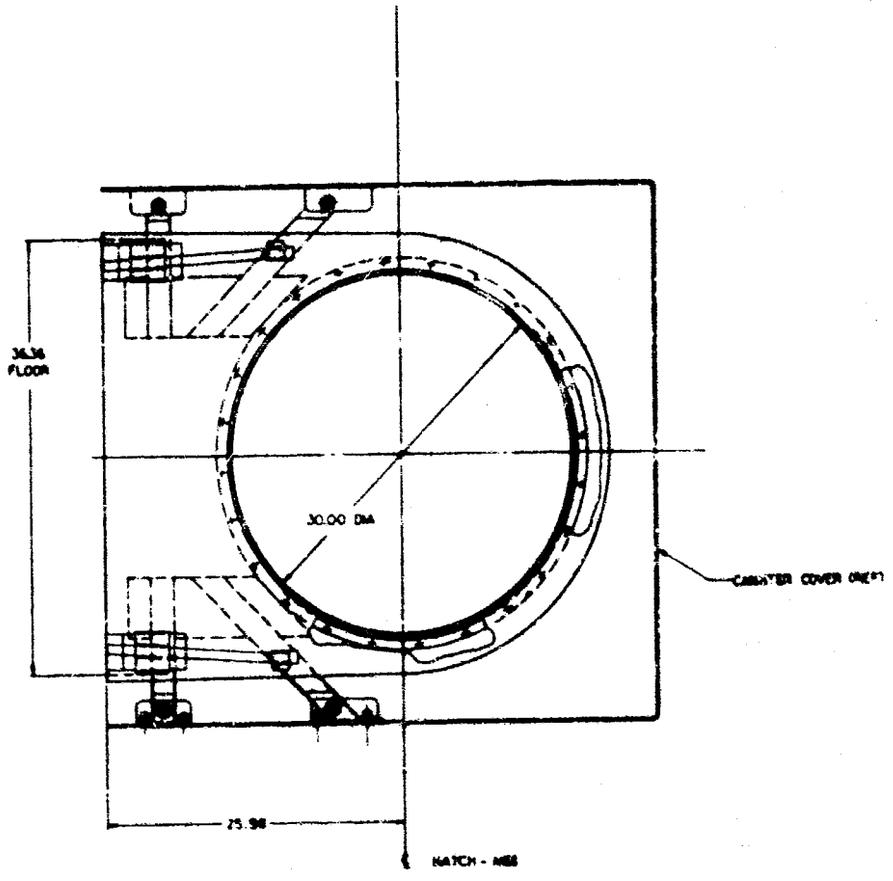

SECTION D-D (SH) 1

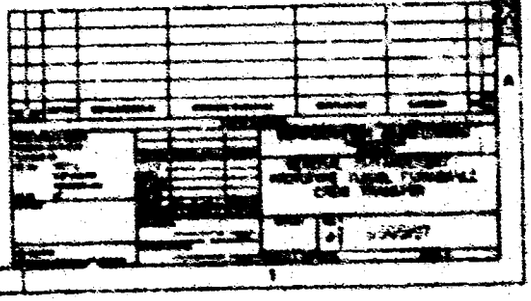

3

4

Figure 4. Fully Expanded Prototype Tunnel

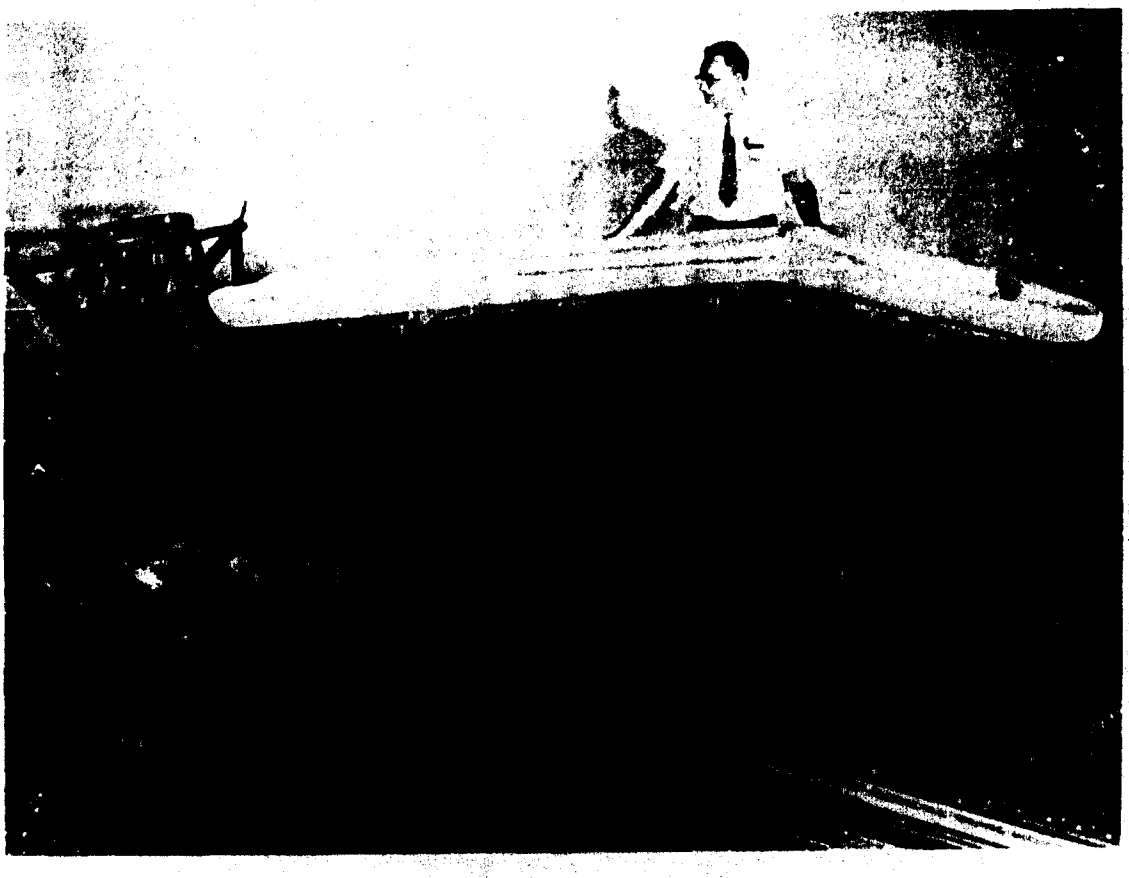

Figure 5. Folded Prototype Tunnel

SECTION II

SUMMARY

A. GENERAL

A modular expandable crew transfer tunnel conceptual design was defined to satisfy the mission objective within the constraints regarding human factors considerations and operational and environmental requirements established by Air Force in-house development by the AF Aero Propulsion Laboratory, the AF Aero Medical Laboratory, and the AF Experimental Fabrication Division. A detailed design of this concept, substantiated by supporting analysis and specimen testing, was completed, and a prototype tunnel was fabricated. The prototype tunnel was then subjected to preliminary qualification tests that proved that the concept is completely satisfactory and entirely feasible. The tunnel design is shown in Figure 2, and the prototype design is shown in Figure 3.

B. SYSTEM REQUIREMENTS

1. General

The Gemini-MSS crew transfer system has four phases of operation for which general operational requirements were established.

2. Launch Pad Requirements

A modular tunnel design is required which will permit prepackaging of the expandable tunnel prior to mounting on the Gemini-MSS system. The packaging canister is required to provide protection from the terrestrial environment encountered on the launch pad.

3. Boost Phase Requirements

In addition to having a minimal effect on the aerodynamics of the total system and protecting the packaged tunnel from the damaging effects of aerodynamic heating, the modular design is required to have the capability of being instantly jettisoned from the Gemini-MSS system in case of mission abort.

4. Orbital Flight Phase Requirements

The crew transfer tunnel is required to resist the total space environment to be encountered in orbits ranging from 100 to 300 nautical miles for a 45-day mission. The tunnel may or may not be pressurized 100 percent of the mission, and the inflation pressure may be as high as 7.5 psia.

5. Re-Entry Phase Requirements

The modular tunnel is required to be jettisoned away from the Gemini-MSS system prior to separation of Gemini from MSS for the re-entry sequence.

C. SYSTEM DESCRIPTION

1. General

The modular crew transfer tunnel consists of an expandable tunnel with a composite wall structure attached to a rigid sandwich structure floor that spans the distance between the Gemini and MSS hatches. The floor is attached to the Gemini-MSS vehicle at the hatch locations by metal ring structures bolted to both the floor and the vehicle. Pyrotechnic devices

are incorporated in the ring design for separation of the tunnel from the Gemini-MSS vehicle for mission termination or for mission abort during the launch phase. The packaged tunnel is protected during the launch pad and boost phases by a packaging canister that is attached to the floor structure only and rests against the Gemini-MSS vehicle without being attached directly to it. Pyrotechnic devices are incorporated in the canister design for jettisoning the canister from the floor structure in orbit to allow the expandable portion of the modular tunnel to deploy. Flexible strip lighting is provided along each side of the tunnel for interior lighting, and hand ropes are provided on each side of the tunnel above the floor as locomotion aids for the astronauts.

The operational advantages of the modular design are numerous. With the canister attached only to the rigid floor structure, the folded expandable tunnel and the canister can be prepackaged as a unit before delivery to the launch pad, thereby reducing the required mounting time and eliminating the packaging operations from the pad mounting routine. In case of mission abort, the entire unit can be jettisoned from the Gemini-MSS system by the same ejection system designed at the Gemini and MSS hatches for jettisoning the tunnel at mission termination. The design eliminates the necessity of jettisoning the canister as a separate unit before jettisoning the tunnel assembly in case of mission abort.

2. Composite Wall Structure

The composite wall structure consists of a triple-seal inner gas pressure bladder, a multi-ply Dacron cloth structural layer, a flexible-foam meteoroid barrier, an outer cover, and a thermal coating on the exterior surface. The unit weight is 0.690 psf.

The nonstructural triple-seal pressure bladder utilized in this design comprises an inner sealant of nylon cloth and Capran film laminate, an intermediate sealant of 0.070-inch thick closed-cell polyvinyl chloride (PVC) foam with a density of 10 pcf, and an outer sealant of nylon cloth coated with polyester resin. The multiple plies of the pressure bladder are bonded together with polyester adhesive. The unit weight is 0.126 psf.

The structural layer is four-ply Dacron cloth laminated with polyester adhesive and attached to the sandwich floor structure with a rigid epoxy bond. The seams in each ply of the structural layer are staggered so that no two plies have coincidental seams and so that there are three uninterrupted plies over the seam in the fourth ply. The material then acts as an essentially seamless structure. The unit weight is 0.210 psf.

The meteoroid barrier is 2-inch thick flexible polyether foam with a density of 1.2 pcf. The unit weight is 0.200 psf.

The outer cover is a nonstructural film-cloth laminate. The thermal coating on the outer cover consists of vapor-deposited aluminum on the film covered in part by aluminum powder in silicone paint or by silicon monoxide, depending upon the particular orbit and orientation involved. The outer cover unit weight is 0.015 psf, and the thermal coating is estimated to weigh 0.026 psf.

3. Sandwich Structure Floor

The sandwich structure floor consists of two flat metal honeycomb bonded sandwich panels that are mechanically joined to form a 160-degree included angle between the panels, paralleling the longitudinal contour of the Gemini-MSS vehicle. There is a circular hole in the panel over the MSS hatch and an elliptical hole in the panel over the Gemini hatch to allow ingress and egress of the astronauts.

4. Attachment and Separation Systems

The tunnel is attached to the launch vehicle at the hatch areas with aluminum rings containing provisions for pyrotechnic separation devices. The rings are attached to the floor

structure with bolts and Rivnuts, and attached to the launch vehicle with Camloc quick-disconnect fasteners. The rings contain machined notch areas around their circumferences to receive the DuPont flexible linear shaped charge (FLSC) pyrotechnic separation devices. The FLSC achieves separation by burning through the ring metal in the notched area and supplying pressure to force the separated portions apart.

5. Packaging Canister

During the launch phase, the packaging canister is subjected to dynamic pressure loads and aerodynamic heating. Lack of a specific launch trajectory precludes the detailed design of the canister. The weight summary given in Table I assumes the use of titanium sandwich construction with interior insulation to control the temperature of the packaged tunnel during the launch phase. The packaging canister design shown in Figure 2 provides a packaging volume of about 20.8 cubic feet while presenting a drag area of about 2.6 square feet. The prototype canister is aluminum.

The canister is constructed in two parts. The lower part, which rests against the launch vehicle, is bolted to canister support brackets attached to the tunnel floor structure. The upper part of the canister, which contains the packaged tunnel, is attached to the lower part with separation screws that pass through the openings in pyrotechnic guillotines. This design allows the upper part of the canister to be jettisoned for deploying the tunnel by detonating the guillotines. Detonation of the guillotines cuts the separation screws and supplies a separating force between the upper and lower canister parts. This design also allows the canister to be jettisoned with the tunnel as a unit in case of mission abort.

6. Fabrication Technique

The fabrication tool for the transfer tunnel involves the use of a rigid polyurethane foam mandrel machined to the interior contour of the tunnel and mounted on a movable fixture. The prototype mandrel and fixture are shown in Figure 6. The sandwich floor panels are fabricated as subassemblies by proven bonding procedures meeting military specifications. After the two floor panels are mechanically joined to form a complete tunnel floor structure, the floor structure becomes part of the fabrication tool. The completed prototype tunnel floor is shown in Figure 7.

The mandrel is sprayed with a separating material to prevent adhesion of the pressure bladder to the mandrel, and the pieces of the pressure bladder that are cut to size from patterns are placed on the mandrel and spliced together. The film-cloth laminate ply of the prototype pressure bladder is shown in Figure 8. The floor is coated with adhesive and placed in position against the foam mandrel so that the pressure bladder becomes attached to the floor as required. The tool is then complete and is ready to receive the remaining layers of the composite wall. The completed prototype pressure bladder with the floor attached is shown in Figure 9.

The cloth patterns for the structural cloth wall are then placed on the mandrel with each ply of cloth coated with adhesive for interply adhesion and with the seams in each ply staggered so that no seams are coincidental, and the cloth layer is attached to form the wall-floor joint. The completed prototype tunnel 4-ply Dacron cloth structural layer with the completed wall-floor epoxy joint is shown in Figure 10. The entire assembly is then vacuum bagged and oven cured to provide the pressure and heat required to allow the adhesives to reach full strength. The 2-inch polyether foam and the outer cover are fabricated in a similar manner. The prototype foam barrier is shown in Figure 11.

When the composite wall lay-up is complete, the rigid foam mandrel is removed by chipping it out in chunks through the hatch-matching holes in the tunnel floor. The prototype tunnel, complete except for the thermal coating, with the rigid foam mandrel removed is shown in Figure 12.

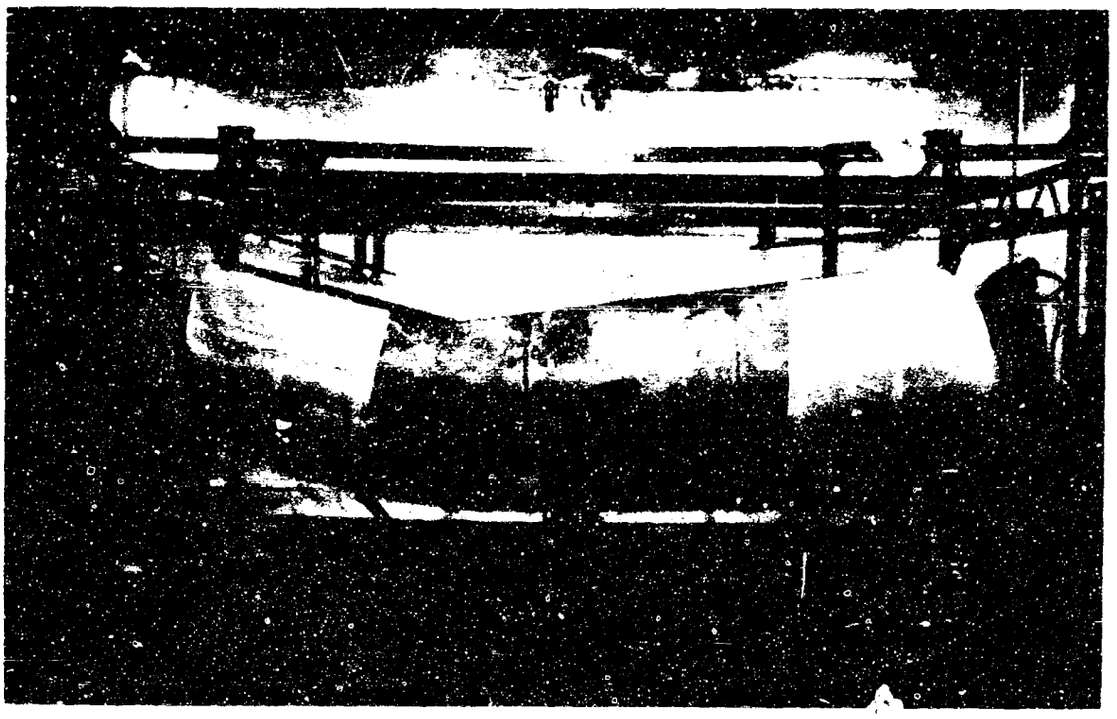

Figure 6. Prototype Tunnel Rigid Foam Mandrel and Fixture

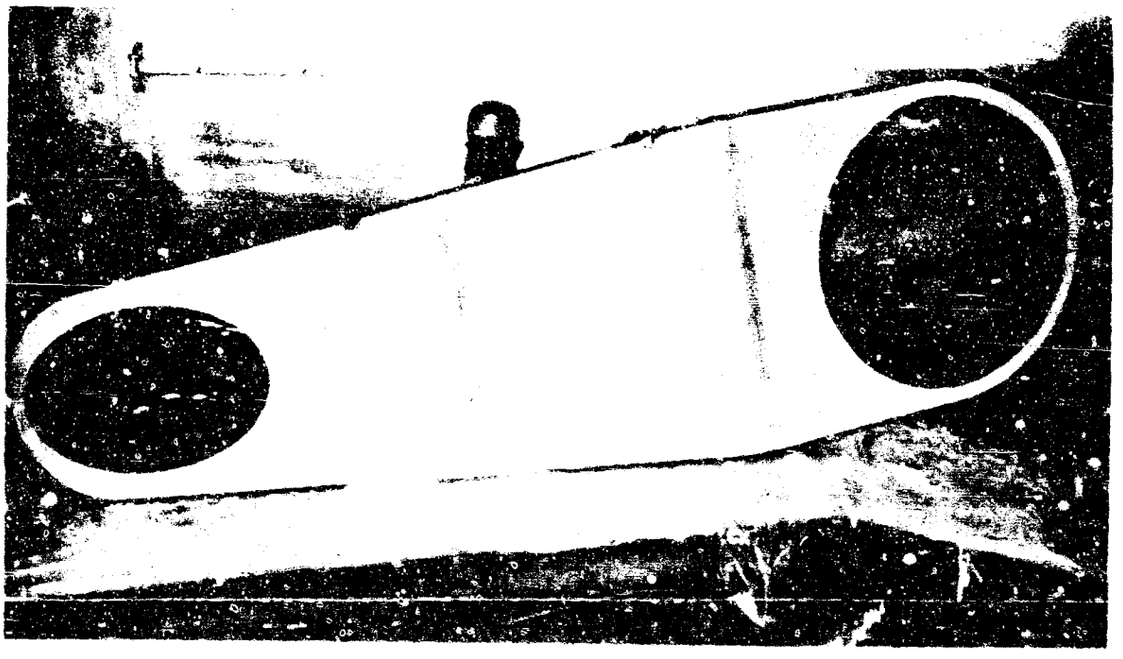

Figure 7. Prototype Tunnel Rigid Structure Floor

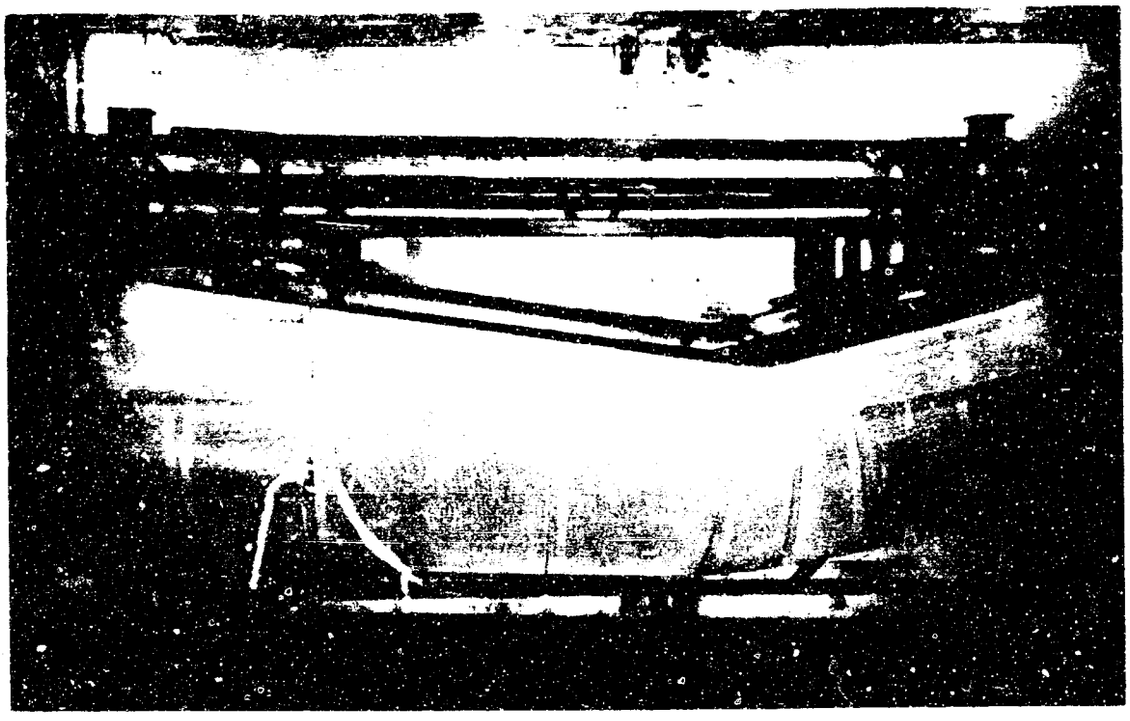

Figure 8. Film-Cloth Laminate Ply of the Prototype Tunnel Pressure Bladder

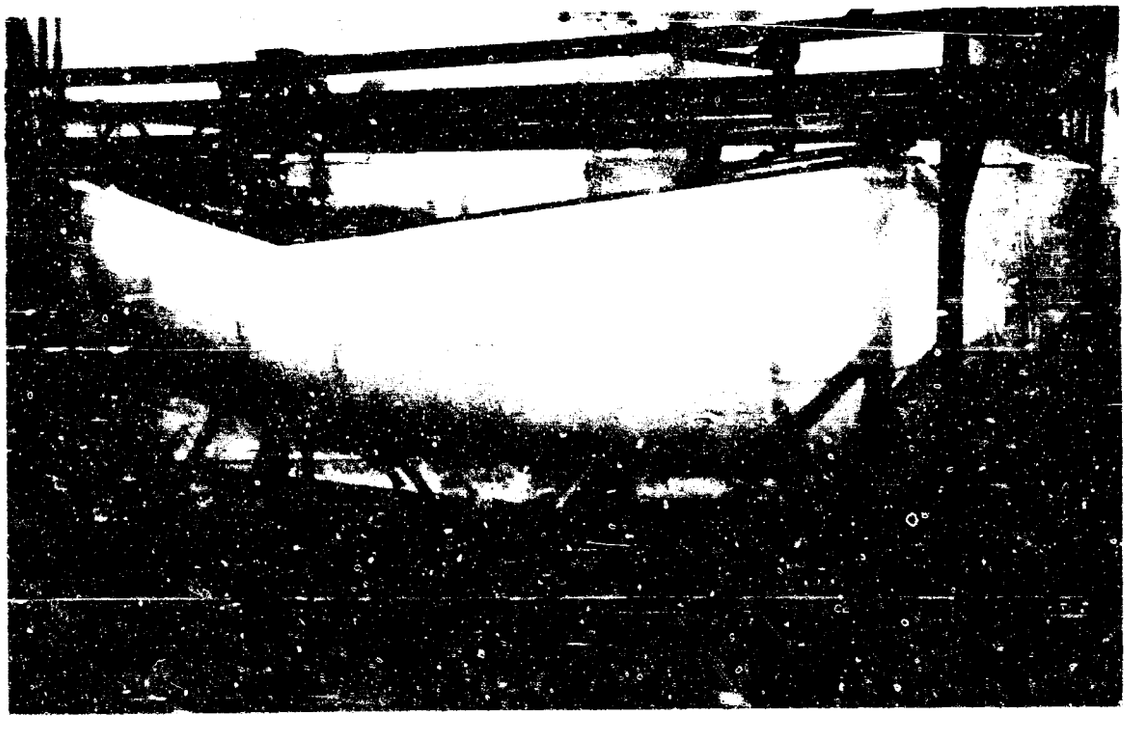

Figure 9. Completed Prototype Pressure Bladder with Floor Attached

Figure 10. Dacron Cloth Structural Layer with Epoxy Wall-Floor Joint

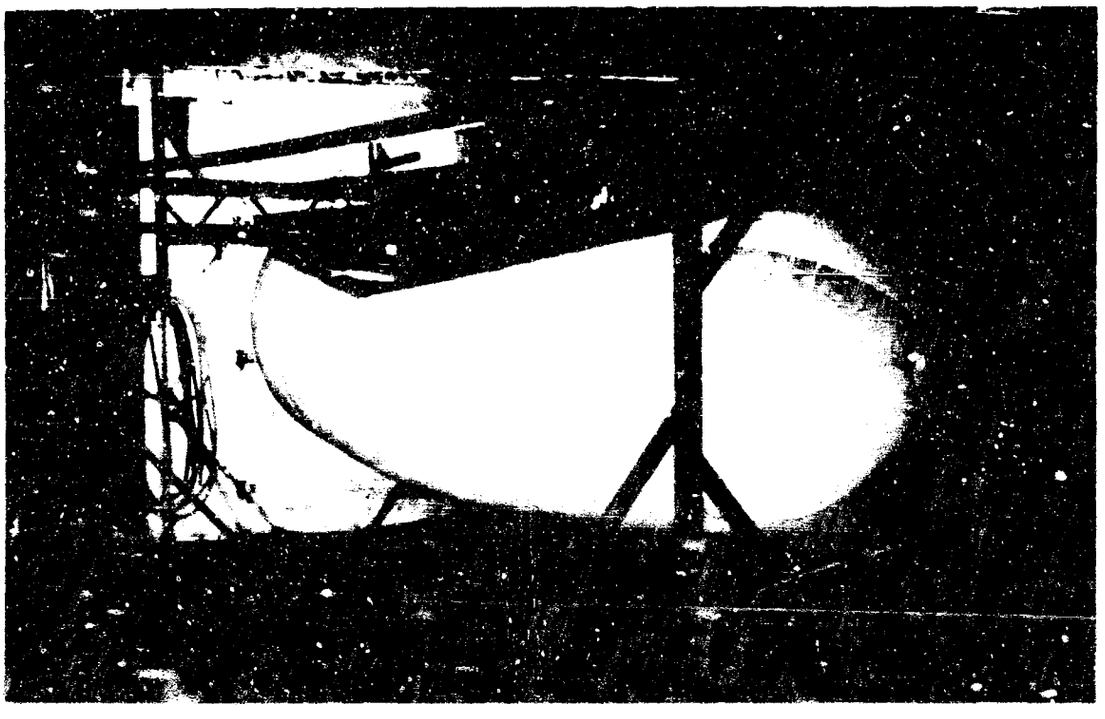

Figure 11. Prototype Tunnel Foam Meteroid Barrier

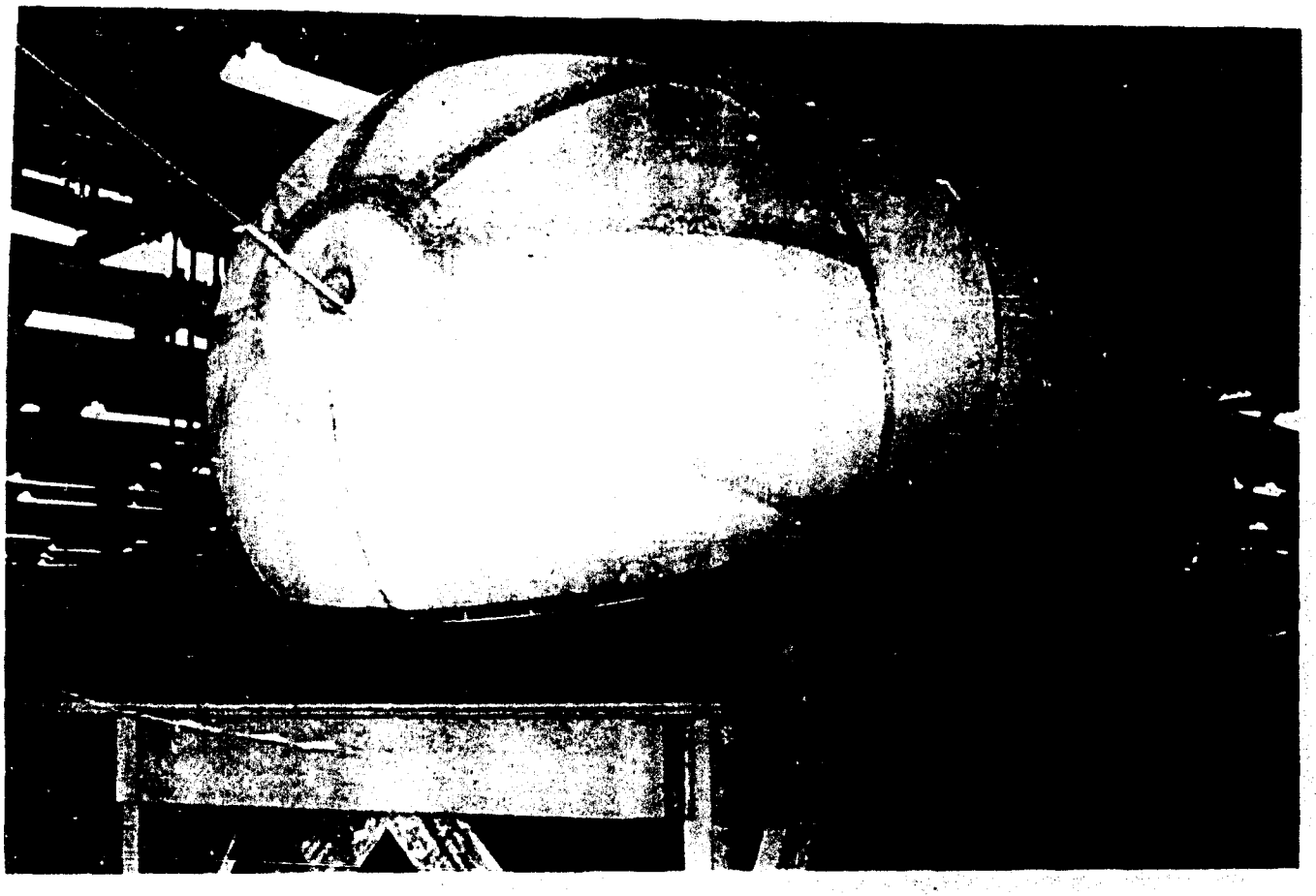

Figure 12. Prototype Tunnel with Mandrel Removed

7. Human Factors Considerations

The crew transfer tunnel interior dimensions of 28 inches clear height at the MSS end and 38 inches clear height at the Gemini end were established by RTD as a result of zero-G transfers through a mock-up tunnel. Types and locations of crew locomotion aids and tunnel interior lighting were studied by the human factors engineers in the Life Sciences Research Department of GAC. The results of these studies are incorporated in the tunnel design and are included in the fabrication of the prototype tunnel.

Locomotion aids consist of 0.75-inch diameter nylon cords extending along each side of the floor from the Gemini hatch opening to the MSS hatch opening. The ends of the hand cords are attached to the floor with clamps. The cords are held 4 inches above the floor by intermittently placed flexible foam cubes.

For tunnel interior lighting, two strips of Sylvania flexible strip lighting are cemented along each side of the tunnel wall about 1.5 inches above the floor. A 6-foot strip extends from the angular contour change in the tunnel floor to the Gemini hatch opening, and a 2-foot strip extends from the contour change to the MSS hatch opening. Evaluation of the lighting in the prototype tunnel indicates that the design is quite adequate for tunnel interior illumination.

D. SYSTEM SUPPORTING ANALYSES

1. General

The supporting analyses performed to substantiate the tunnel design are discussed in the following paragraphs.

2. Thermal Analysis

The primary objective of the thermal design is to maintain the tunnel interior at comfortable temperatures for astronaut transfer while limiting the exterior surface hot and cold spot temperatures to values within the material capabilities. Thermal design optimization would depend upon Gemini-MSS system parameters that are undefined, and optimization is therefore considered beyond the scope of this study.

The only major difficulty involved in the thermal design is passively maintaining the required internal temperature of 75 (± 25)^{o}F. Three possible thermal design systems are presented which would satisfy this requirement reasonably well for most orbits and orientations provided that the orbit and orientation were specified before the thermal coatings are selected. There are some orbits and orientations, however, where the interior cannot be passively maintained at comfortable temperatures, and either a specific orientation or the addition of heat to the tunnel would be required.

The three possible thermal designs have the common features of the addition of thermal insulation to the floor, the application of a low solar absorptance to emittance ratio (α/ϵ) white paint to the tunnel interior, and the covering of the entire expandable wall with an aluminized film substrate. The three thermal design coating systems are as follows:

(1) The tunnel would be uniformly covered with stripes of aluminized silicone white paint for an average α/ϵ ratio of approximately 2.

(2) The thermal coating of (1) would be used with the quantity of painted stripes varied locally to alleviate hot spots.

(3) The tunnel would be covered with thin layers of silicon monoxide applied in some locations and stripes of aluminized silicone white paint applied unevenly over the entire surface.

From a thermal viewpoint, the expandable crew transfer tunnel is definitely feasible and within the state of the art.

3. Structural Analysis

The structural analysis was performed to demonstrate the structural integrity of the tunnel. The structural cloth layer of the composite wall has a factor of safety of 5 for an inflation pressure of 7.5 psi after consideration of plying and seaming efficiencies and creep-rupture effects due to long periods of time under load. The metal floor structure, the attachments, and the separation rings are designed to have safety factors of 2 on yield strength and 3 on ultimate strength. The analysis shows that all parts have a positive margin of safety when compared to these criteria.

4. Meteoroid Hazard Analysis

The composite wall puncture hazard due to micrometeoroids is assessed in terms of a probability of zero penetrations of 0.995 for a 60-day mission. The analysis shows that the critical mass is 8.12×10^{-4} g, which is the largest projectile the foam barrier material must be capable of stopping to ensure a 0.995 probability of zero penetrations. This critical mass would require a barrier of single sheet aluminum with a thickness of 0.2034 inch. Hypervelocity

particle impact tests have shown the foam barrier material to be 16 times as effective as single sheet aluminum on a weight per unit area basis. Thus, 2-inch thick polyether foam with a density of 1.2 pcf is quite adequate for the crew transfer tunnel application to ensure a probability of zero penetrations of at least 0.995.

5. Radiation Analysis

The radiation analysis was performed to ascertain the materials and biological implications of proton, alpha particle, and electron radiation in space. The tunnel will be subjected to electron radiation in any near-earth orbit, and to high energy proton and alpha particle radiation for approximately half the time in a polar orbit. Since it is felt that astronaut transfer could take place during periods of no radiation during a polar orbit, no consideration is given to the proton and alpha particle radiation dosage that an astronaut inside the tunnel might receive.

The maximum high energy proton and alpha particle radiation dose received by any part of the tunnel wall is 2×10^5 rads, most of which is absorbed by the outer cover, and the radiation dose received by the foam barrier and structural layer is less than 2×10^4 rads. A very conservative value for the electron radiation dose received by any part of the tunnel wall is less than 2×10^6 rads, most of which is absorbed by the outer cover. The remainder is mostly absorbed by the inner layers of the tunnel wall, and virtually no electron radiation will penetrate to the tunnel interior.

Since test data indicates that the tunnel wall material can withstand radiation dosages of 10^8 rads with virtually no damage, the radiation dose expected for the crew transfer tunnel presents no problem with regard to material damage.

6. Weight Summary

In conjunction with the design shown in Figure 2, a summary of the weight analysis for the expandable Gemini to MSS crew transfer tunnel is given in Table I.

E. MATERIALS EVALUATION AND TESTS

1. General

The materials approach of utilizing the composite material construction developed on previous in-house company-funded programs was selected as being the best suited to satisfy the requirements of the tunnel design. Although the materials selection required no further development effort, sufficient material qualification testing was conducted to ensure that the materials met the structural and environmental requirements.

2. Structural Aspects

The selection of four plies of Dacron cloth for the structural layer of the composite wall was based on the material's high strength to weight ratio, relatively low elongation, good creep-rupture resistance, and on the use of multiple plies to achieve the essentially seamless construction desired. Tests conducted on the four-ply material show that a factor of safety of 5 based on the stresses produced by an inflation pressure of 7.5 psi is attained after strength degradation due to multi-ply lamination and creep rupture effects.

Initial tests of the bonded wall to floor joint indicated a 50 percent load capability compared to the parent structural cloth strength. Consequently, the design evolved to the eight-ply splice bonded to the floor with rigid epoxy and bonded to the four-ply structural layer with flexible polyester adhesive. Subsequent testing substantiated the joint design as being fully capable of carrying the required loads.

Table I. Weight Estimate

Transfer Tunnel		227 lb
Expandable Composite Wall	81.3 lb	
Thermal Control Coating	2.7 lb	
Outer Cover Laminate	5.3	
Polyether Foam	23.3	
Dacron Structural Layer	30.5	
Pressure Bladder	16.3	
Inner Coating	3.2	
Sandwich Floor Structure	89.2 lb	
Sandwich Panels	69.7 lb	
Joints and Hardware	2.3	
Insulation	2.0	
Canister Support Brackets	15.2	
Wall-Floor Attachment	15.4 lb	
Hatch Attachment-Separation System	22.2 lb	
Circular Separation Ring	9.1 lb	
Elliptical Separation Ring	6.3	
FLSC and Backup Structure	2.4	
Hardware	4.4	
Lighting and Locomotion Aids	8.8 lb	
Inflation System	10.1 lb	
Packaging Canister		148 lb
Sandwich Cover	110.0 lb	
Lower Panels	24.0 lb	
Upper Panels	73.5	
Hardware	12.5	
Insulation	17.6 lb	
Pyrotechnic Separation System	20.4 lb	
Guillotines	4.6 lb	
Brackets	11.6	
Hardware	4.2	
Total Weight		375 lb

3. Permeability

To substantiate the gas pressure tightness of the pressure bladder, permeability tests were conducted on pressure bladder samples with an atmosphere of 100 percent oxygen and a 5-psia pressure differential. The maximum test permeability rate was 1×10^{-4} psf per day, or a gas loss for the tunnel of less than 0.02 pound per day.

4. Environmental Hazards Resistance

Environmental effects on the materials require the consideration of vacuum, thermal extremes, ultraviolet and high energy radiation, and micrometeoroids. Tests of the composite

materials under vacuum conditions indicated an initial off-gassing that subsequently leveled off with negligible weight losses. Structural integrity and foam elastic recovery were investigated after exposure to the expected temperature extremes. Although structural integrity was not adversely affected, the tests indicated that the packaged foam must be insulated against extreme cold if full recovery is to be achieved. The structural integrity is not affected by exposure to 10^6 rads of gamma radiation, and the tolerance of the other composite layers to high energy radiation is higher than the anticipated dose. The resistance to punctures from micrometeoroids, discussed earlier in this section, indicates that the probability of zero penetrations for the barrier material of polyether foam exceeds 0.995 for a 60-day mission.

F. PRELIMINARY QUALIFICATION TESTING

1. General

The prototype expandable crew transfer tunnel was subjected to preliminary qualification testing to substantiate the design. This program included a packaging test, pressure proof test, pressure leak test, cyclic pressure test, and vacuum chamber deployment test. Zero-G flight tests are to be conducted on the KC-135 zero-G aircraft at Wright-Patterson AFB, and these test results will be reported in Part III of this report.

A steel test carrier with mock-ups simulating the Gemini and MSS access hatches was fabricated to support the prototype tunnel during the preliminary qualification testing. Each access hatch is fitted with a hatch cover utilizing an O-ring seal for pressure tightness. The completed prototype tunnel mounted on the test carrier is shown in Figure 13.

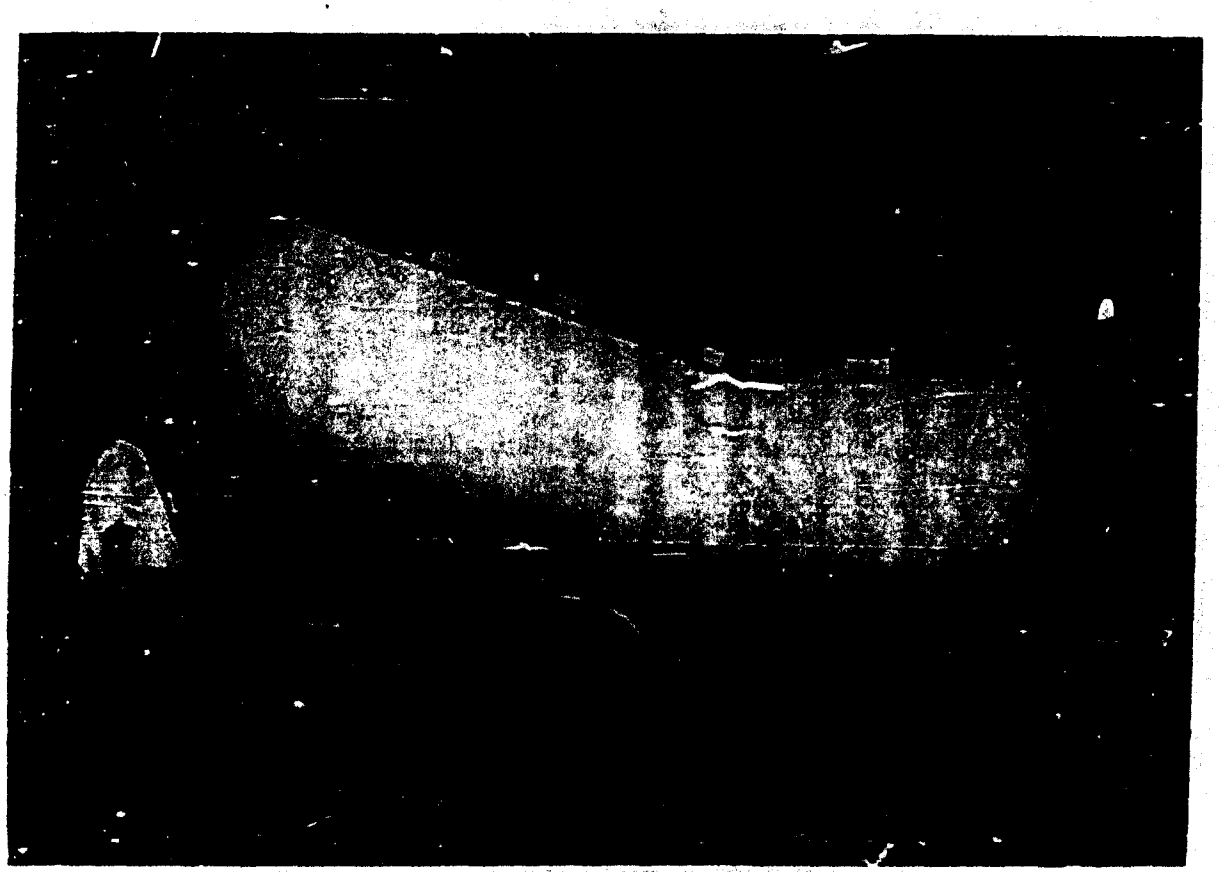

Figure 13. Prototype Tunnel Mounted on Test Carrier

2. Packaging Test

The packaging test was conducted to establish the minimum attainable packaging height. Both the tunnel interior and the meteoroid barrier foam were evacuated with vacuum lines so that the expandable wall material could be compressed as much as possible. The most efficient folding procedure utilized a vertical accordion fold with the creases running lengthwise along the tunnel and the hemispherical ends folded back across the lengthwise folds. When the minimum packaging height was established, the canister was match-drilled with the canister support brackets attached to the tunnel floor. The minimum packaging height was established as 5-3/8 inches from the top of the floor to the inside surface of the canister. The initial vacuum line evacuation is shown in Figure 14, and the packaged tunnel is shown in Figure 15. The folded tunnel with the canister removed is shown in Figure 5.

After the completion of the packaging test, the prototype tunnel mounted on the test carrier bed was placed in the GAC pressure test room for pressure proof and leak tests.

3. Pressure Proof Test

The purpose of the proof test was to establish the structural integrity of the tunnel by maintaining an inflation pressure of 10 psi, 1.33 times the design inflation pressure of 7.5 psi, for a period of seven days. The pressure was maintained during the test by regulators capable of maintaining pressure within ±0.2 inch of mercury, or ±0.1 psi. Pressure and temperature were recorded periodically during the seven-day period. The pressurized tunnel in the pressure test room at the end of the seven-day period is shown in Figure 16. The test instrumentation is shown outside the test room in Figure 17.

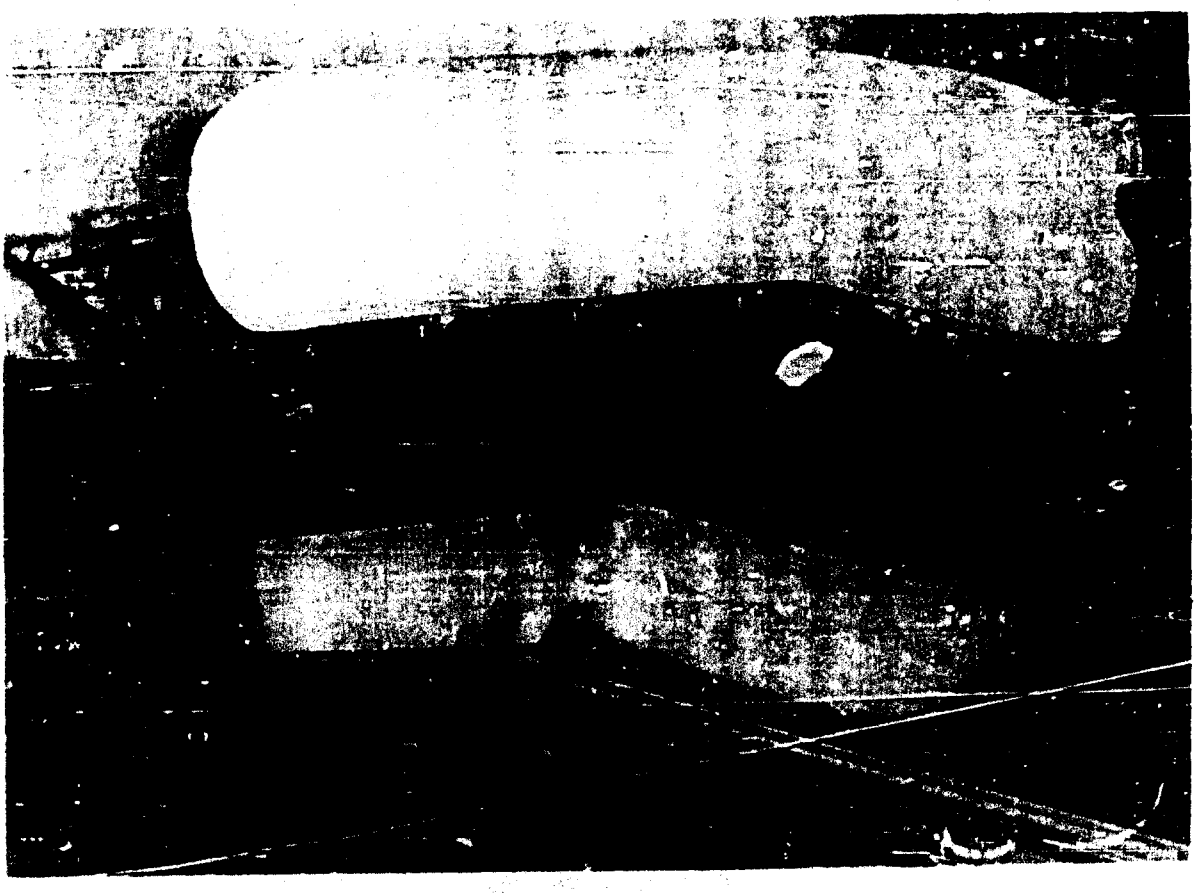

Figure 14. Vacuum Evacuation for Packaging Test

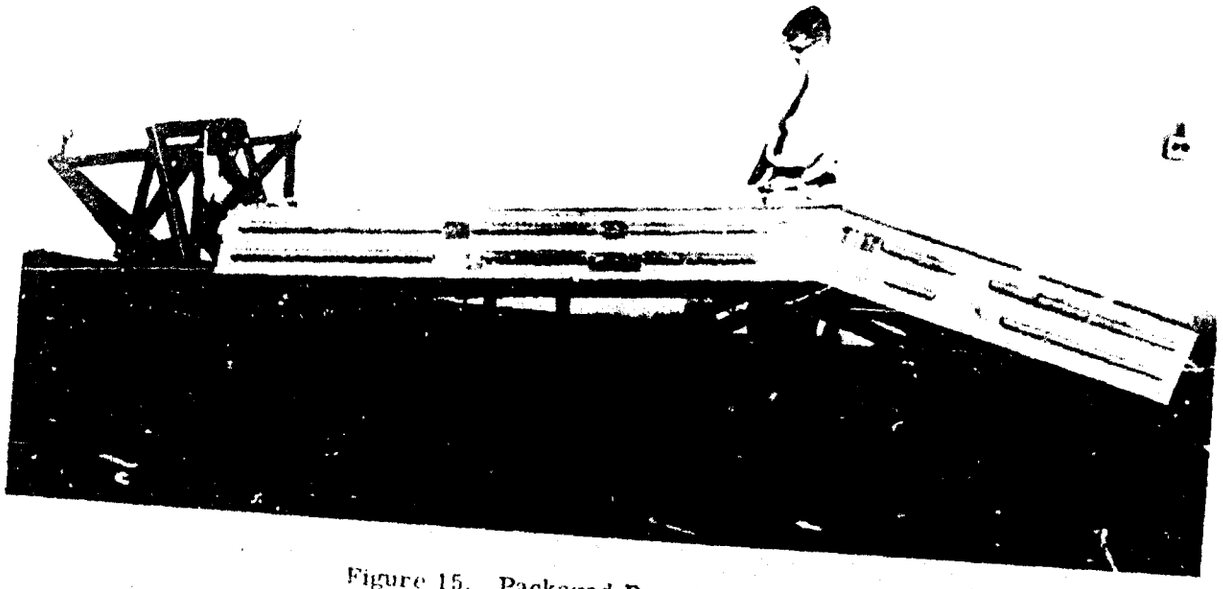

Figure 15. Packaged Prototype Tunnel

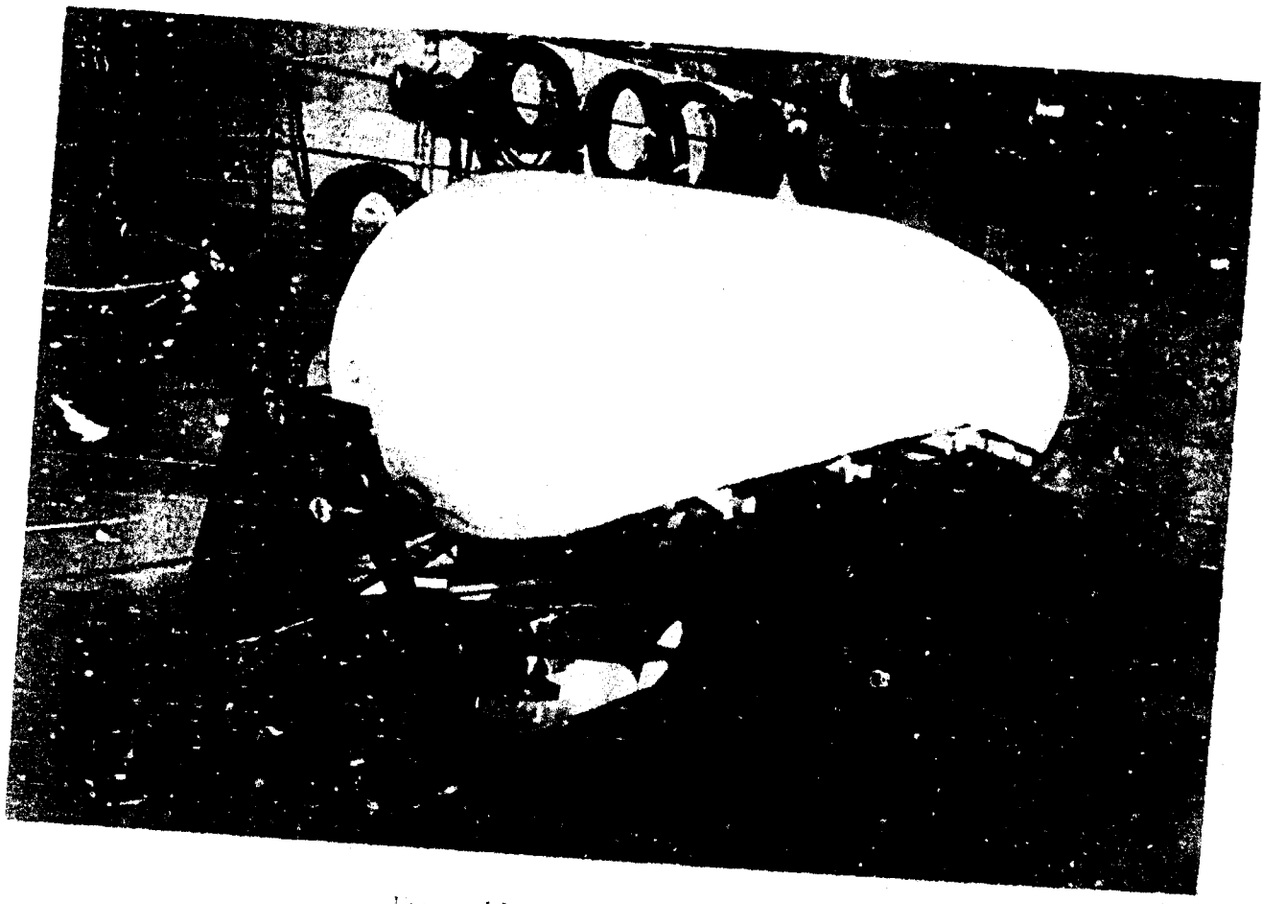

Figure 16. Pressure Proof Test

4. Pressure Leak Test

The pressure leak test was conducted to establish the tunnel leak rate for a period of seven days while being pressurized to the design pressure of 7.5 psi. The test arrangement was the same as for the proof test except that a bottle of compressed air placed on a calibrated platform scale was used as the pressurization air supply instead of shop air lines and the inflation pressure was reduced to 7.5 psi. Barometer readings, compressed air bottle weight, tunnel interior temperature, and inflation pressure were recorded at the beginning and the end of the seven-day period and were monitored periodically during the test. The leak rate was determined by calculating the initial weight of air contained in the tunnel, adding the weight loss of the compressed air bottle, subtracting the calculated final weight of air contained in the tunnel, and dividing the total weight change by the time involved. The total air weight loss was 7.70 pounds for the seven-day period. Converting this loss to a weight loss of a mixture of 50 percent nitrogen and 50 percent oxygen under orbital conditions established the leak rate to be 0.50 pounds of gas per day for an inflation pressure of 7.5 psia with the tunnel exterior in a vacuum.

5. Cyclic Pressure Test

The purpose of the cyclic pressure test was to establish the durability of the tunnel with respect to cyclic loading. The test arrangement was similar to the pressure proof test (inflation air supplied by shop air lines) except that a vacuum line was also attached to the test carrier hatch cover. The tunnel was pressurized to 7.5 psi in approximately 20 seconds. The

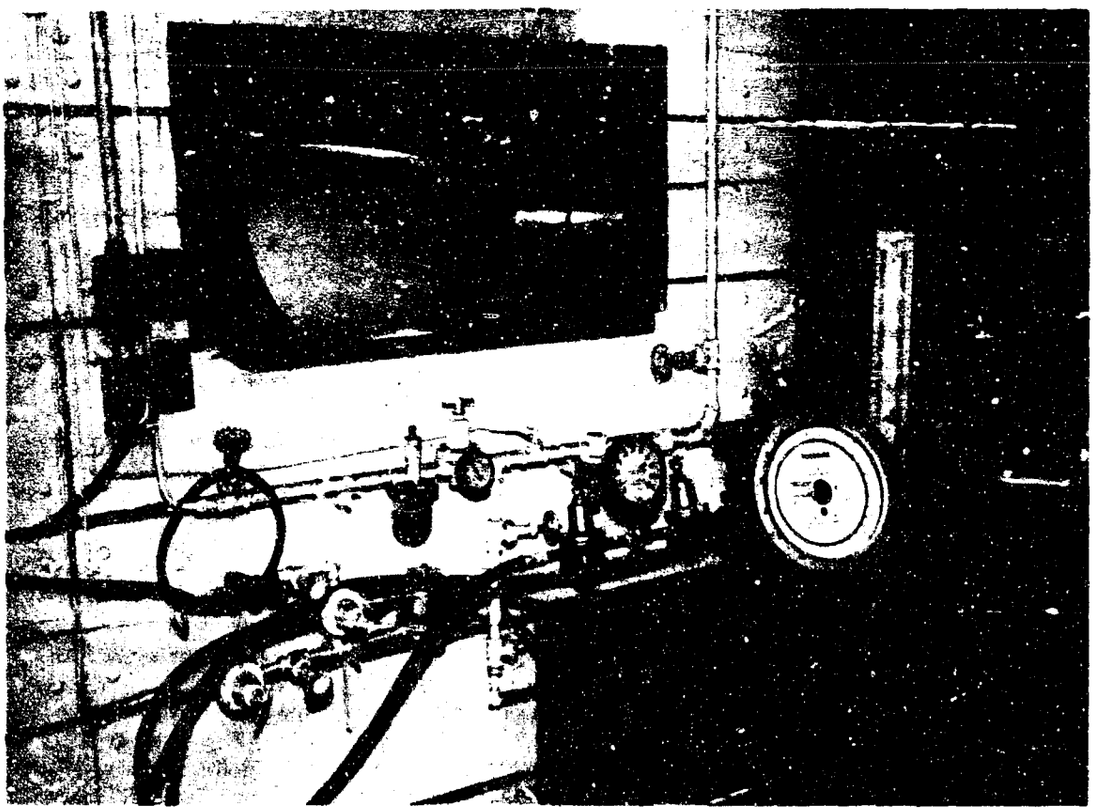

Figure 17. Pressure Proof Test Instrumentation

vacuum pump line was then opened, and the tunnel was evacuated until it started to collapse. It was then pressurized again to 7.5 psi. This procedure was repeated until the tunnel had been pressurized 60 times. There were no visible signs of rigid structure deformation during the test, and no visual signs of any damage were observed at the completion of the test.

6. Vacuum Chamber Deployment Test

The purpose of this test was to demonstrate the deployment of the expandable tunnel under vacuum conditions of 10^{-4} mm Hg, and to establish the leak rate for 24 hours under the same conditions. The test was conducted in the Aerospace Environmental Facility (AEF) new Mark I vacuum chamber, which is 40 feet in diameter and 80 feet high, at Arnold Engineering Development Center (AEDC), Tennessee.

The test carrier with the packaged tunnel attached was lowered into the chamber through the 22-foot diameter access port. This operation is shown in Figure 18. The test carrier bed was rotated so that the packaged tunnel was in an inverted position, and all instrumentation and controls were connected and checked. The chamber was sealed and pumped down to a vacuum of 3×10^{-5} mm Hg. During the pump-down, the solenoid valves mounted on the test carrier access hatch covers were opened to allow the packaged tunnel internal pressure to decrease with the chamber pressure. This was done in order to evaluate the elastic recovery action of the meteoroid barrier foam as a deployment device in expanding the packaged tunnel to the desired shape instead of expanding due to the pressure of the entrapped gas. When the chamber pressure was stabilized at 3×10^{-5} mm Hg, the solenoid valves were closed with a tunnel internal pressure of 4 mm Hg. The packaged tunnel in the vacuum chamber prior to deployment is shown in Figure 19.

The pyrotechnic guillotines were then fired to cut the 12 canister separation screws and eject the canister cover, allowing the folded tunnel to deploy. Canister separation and ejection occurred as planned. The guillotines supplied sufficient separating force to hurl the canister cover away. However, the elastic recovery energy of the foam was not sufficient to shape the tunnel, and it was necessary to pressurize the tunnel to approximately 0.25 psia to overcome the stiffness of the packaging folds and completely shape the tunnel. The deployed unpressurized tunnel is shown in Figure 20, and the almost completely shaped tunnel at 0.15 psia is shown in Figure 21. The completely shaped tunnel at 0.25 psia is shown in Figure 22.

The tunnel was then further pressurized to 7.5 psia with CO_2, and the pressure, growth, and temperature were allowed to stabilize for 2 hours before the 24-hour leak check was started. The actual stabilized pressure was 7.7 psia at the beginning of the 24-hour period. At the end of the 24-hour period the pressure was 7.0 psia. During the test period the chamber pressure decreased from 5.5×10^{-5} mm Hg to 2.4×10^{-5} mm Hg with a nearly linear decline. Converting the leakage to a weight loss of a mixture of 50 percent nitrogen and 50 percent oxygen established the leak rate to be 0.40 pound of gas per day under orbital conditions. This leak rate compares favorably with the rate of 0.50 pound of gas per day for the ambient atmosphere pressure leak test, indicating that the permeability is not unfavorably affected by the vacuum environment. The deployed tunnel after pressurization in the vacuum is shown in Figure 23. The tunnel pressurized to 2 psig after the chamber return to ambient pressure is shown in Figure 24.

7. Zero-G Flight Test

Zero-G flight tests are to be conducted on the KC-135 zero-G aircraft at Wright-Patterson AFB. The purpose of the tests is to ascertain man's ability to transfer through the tunnel in zero G. Also to be evaluated is man's ability to utilize the GAC repair kit in zero-G to repair simulated damage to the tunnel. The test results will be reported in Part III of this report. Since the tunnel expanded geometry was prescribed by the simulated tunnel mock-up previously used successfully to demonstrate zero-G transfers, no major problems are anticipated in this area.

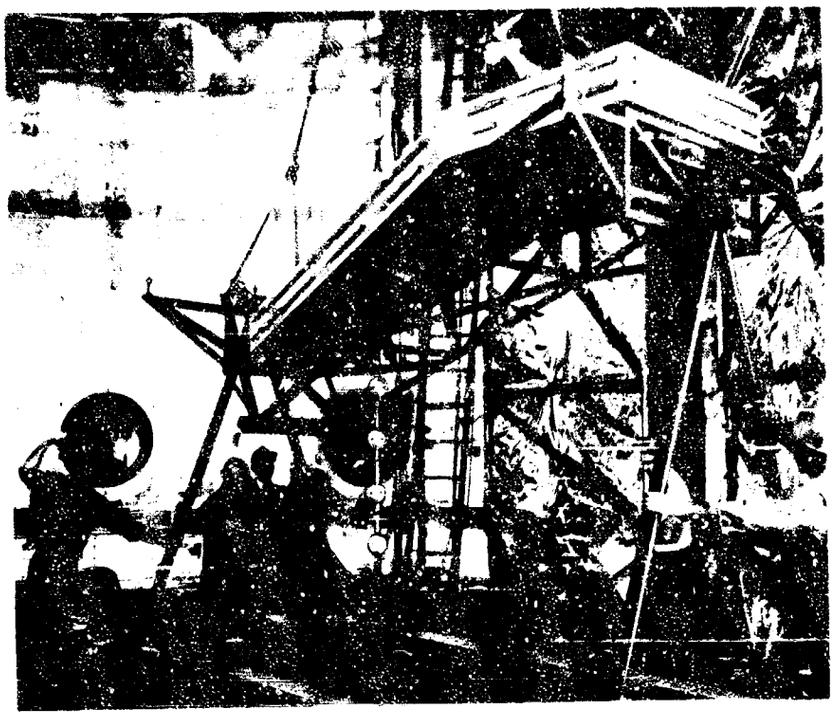

Figure 18. Packaged Tunnel Being Lowered into Vacuum Chamber

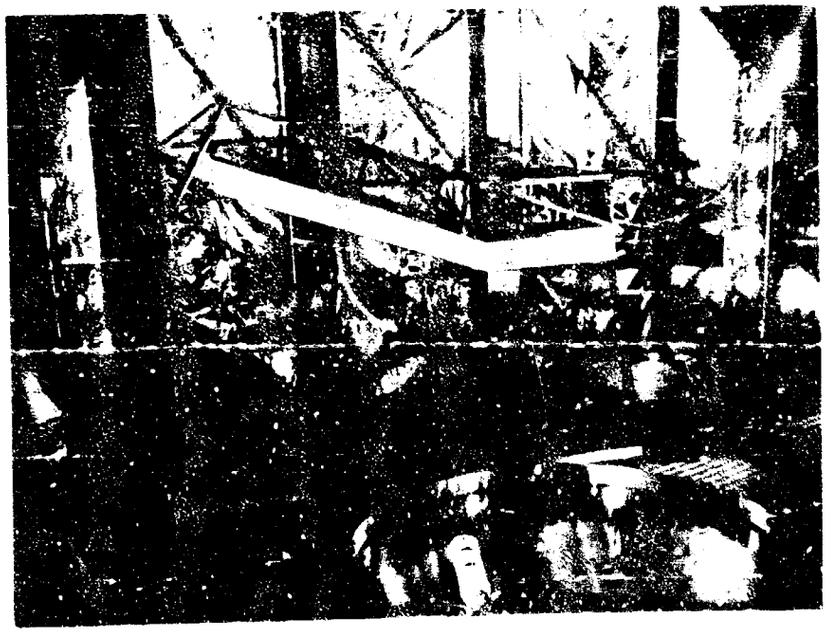

Figure 19. Packaged Tunnel in Vacuum Chamber prior to Deployment

Figure 20. Deployed Tunnel Unpressurized in a Vacuum

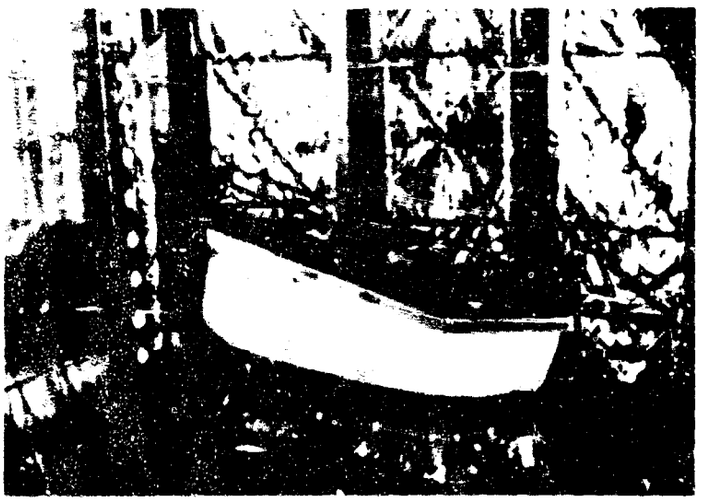

Figure 21. Deployed Tunnel at 0.15 PSIA in a Vacuum

Figure 22. Deployed Tunnel at 0.25 PSIA in a Vacuum

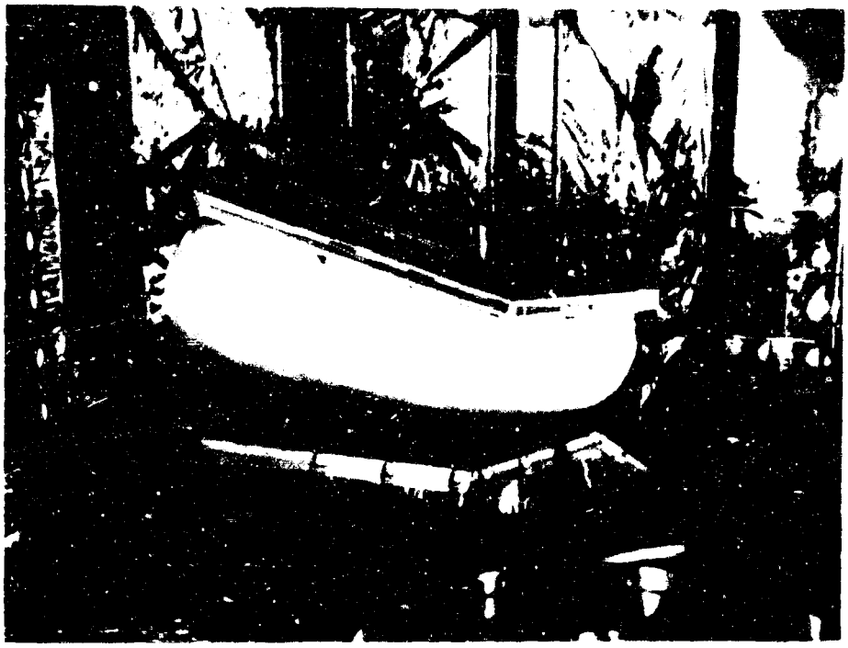

Figure 23. Deployed Tunnel at 7.5 PSIA in a Vacuum

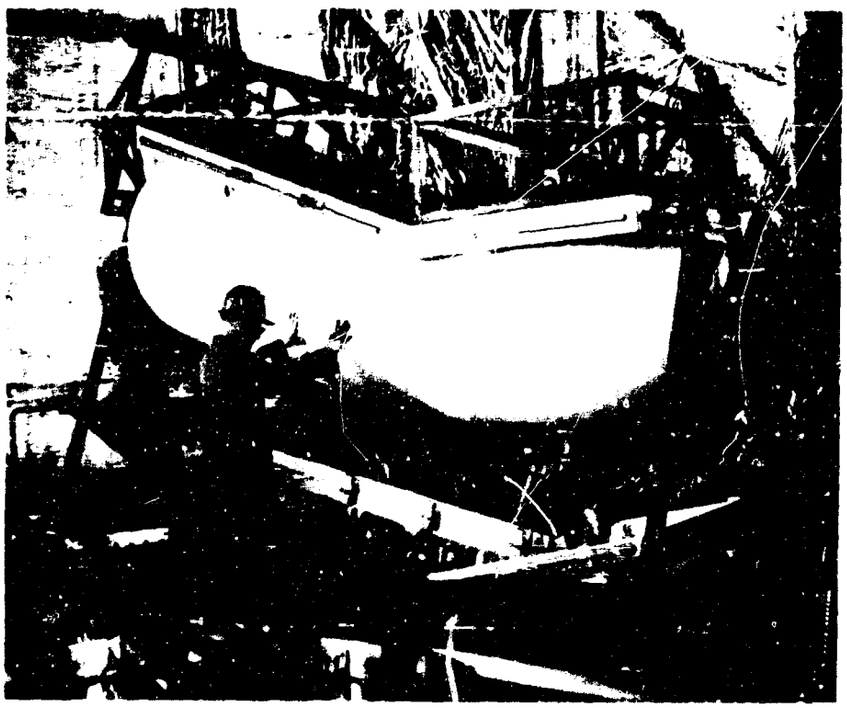

Figure 24. Deployed Tunnel at 2 PSIG in Ambient Conditions

SECTION III

CONCEPT CONSTRAINTS

A. MISSION OBJECTIVE

The crew transfer tunnel was designed to provide a safe method of transferring the crew from the Gemini capsule to the crew station in orbit. The major constraints imposed on the tunnel design by operational, human factors, structural and materials, attachment, environmental, and packaging requirements are discussed in this section.

B. GENERAL OPERATIONAL REQUIREMENTS

1. General

This Gemini-MSS system has four phases of operation (pad, boost, orbit, and re-entry) for which general operational requirements were established.

2. Launch Pad Requirements

A modular tunnel design is required that will permit prepackaging of the expandable tunnel prior to mounting on the Gemini-MSS system. The astronauts should have quick ingress and egress capability to and from the Gemini capsule with the modular tunnel attached. The packaging canister is required to provide protection from the terrestrial environment encountered on the launch pad at either the Pacific Missile Range or the Atlantic Missile Range.

3. Boost Phase Requirements

The packaged tunnel and canister are required to have a minimum effect on the aerodynamics of the total launch system. The canister design is required to provide sufficient insulation to prevent the encountered aerodynamic heating from thermally damaging the tunnel. The modular design is also required to have the capability of being instantly jettisoned away from the Gemini-MSS system in case of mission abort.

4. Orbital Flight Phase Requirements

Once the Gemini-MSS system is in orbit, the expandable crew transfer tunnel packaging canister is required to be jettisoned away. The expandable tunnel should then tend to deploy to about 90 percent of its fully expanded configuration without any internal pressurization. The deployed tunnel is required to be pressurized with an internal pressure as low as 3.5 psia or as high as 7.5 psia. The tunnel may or may not be pressurized 100 percent of the mission duration of 45 days, but is required to resist the total space environment to be encountered in orbits ranging from 100 to 300 nautical miles in either case.

5. Re-entry Phase Requirements

The modular tunnel is required to be jettisoned away from the Gemini-MSS system prior to separation of Gemini from MSS for the re-entry sequence.

C. HUMAN FACTORS REQUIREMENTS

1. General

The expanded tunnel configuration is required to provide space for the efficient transfer

of astronauts or disabled astronauts from Gemini to MSS and vice versa. Interior tunnel lighting is required, and locomotion aids are required for the crew.

2. Interior Size and Geometry

The tunnel interior size and geometry should provide space for an astronaut carrying limited size packages (1 cubic foot) or an astronaut transferring an injured astronaut to move freely and transfer efficiently. Astronauts will be dressed in space suits and will be wearing a chest- or back-mounted environmental life support system. In the event of tunnel pressurization failure, the astronaut is required to transfer in a pressurized space suit.

3. Locomotion Aids

Built-in locomotion aids that will not damage the astronaut's space suit or jeopardize the tunnel's structural integrity are required to facilitate the transfer of an astronaut or the transfer of an unconscious astronaut by another astronaut when the tunnel is either fully pressurized or non-pressurized.

4. Interior Lighting

The tunnel is required to have interior built-in lighting to provide sufficient light to permit crew transfer or small equipment transfer.

D. STRUCTURAL AND MATERIALS REQUIREMENTS

1. General

The tunnel expandable wall structure is required to be a minimum weight multilaminate composite consisting of a nonabrasive tunnel liner, pressure bladder, fiber load-carrying structure, flexible foam meteoroid barrier, and passive thermal control coating. There should be no delamination as a result of folding, packaging, residual air entrapment, or release of volatiles, which may be encountered during prelaunch, launch, and space environmental conditions. The tunnel is required to remain sufficiently rigid to allow astronauts to effect a crew transfer when the tunnel is not pressurized where, although in a zero-G environment, there would be dynamic loading resulting from the astronaut's motions. The tunnel load-carrying structure is required to resist 7.5-psia internal pressure, which is the principal load on the tunnel. A material system is also required that could be utilized to repair tears or particle penetrations in the tunnel.

2. Interior Nonabrasive Liner

A nonabrasive interior tunnel liner is required to minimize abrasion between the tunnel and an astronaut's space suit.

3. Airtight Pressure Bladder

The pressure bladder is required to be constructed of materials that will not give off toxic by-products in orbit regardless of whether the tunnel is pressurized or nonpressurized. The pressure bladder is required to maintain the total leak rate of the tunnel to no greater than 0.5 and 1 pound per day at internal pressures of 3.5 psia and 7.5 psia respectively.

4. Load-Carrying Structure

The modular tunnel load-carrying structure is required to resist an internal pressure of 7.5 psia. The fiber portion of the multilayer composite wall is required to resist the internal pressure with a safety factor of 5. The metal structure associated with the modular design is required to resist the internal pressure with a safety factor of 2 on yield strength and a safety factor of 3 on ultimate strength. These factors of safety are to be maintained after degradation

of the physical and mechanical properties of the materials due to temperature, load duration, vacuum, ultraviolet radiation, and electron radiation has been considered. Structural splices and joints are required to develop 100 percent of the required load-carrying capacity of the normal tunnel material.

5. Meteoroid Barrier

A 1 to 2 pcf density flexible foam meteoroid barrier 1 to 2 inches thick is required on the exterior of the fiber load-carrying structure to provide a probability of resisting puncture of 0.995 for a 60-day mission at an orbit of 100 to 300 nautical miles.

6. Passive Thermal Control Coating

A passive thermal control coating is required for the exterior surface of the tunnel. The coating must maintain an interior surface temperature of 75 (±25)°F while maintaining exterior surface temperatures within the capabilities range of the materials.

7. Repair Materials

A nontoxic material system is required that could be used on the inside of the tunnel in a vacuum, pure oxygen atmosphere, or a normal atmosphere to repair tears or particle penetrations in the tunnel. The materials should be able to activate nearly instantaneously and should be capable of being utilized in zero-G. Self-sealing systems are not applicable for this effort because of their high weight per unit area.

E. ATTACHMENT REQUIREMENTS

The attachments that secure the modular crew transfer tunnel to the Gemini-MSS system are required to minimize leakage, provide quick access to Gemini or MSS on the launch pad, and provide quick release in the event of abort.

F. ENVIRONMENTAL REQUIREMENTS

1. General

The environments to which the transfer tunnel will be exposed are internal pressurization and external space.

2. Internal Pressurization

The tunnel is required to be designed for an internal pressure of 7.5 psia for 45 days, although the tunnel will probably be pressurized and depressurized several times during the mission. For this reason the tunnel is required to withstand 60 repeated pressurization and depressurization cycles. The tunnel materials are required to be compatible with a pure oxygen atmosphere or a mixture of oxygen and nitrogen with a pressure range of 3.5 psia to 7.5 psia and a relative humidity range of 0 to 50 percent.

3. External Space Environment

The external space environment that the tunnel is required to resist is a vacuum of at least 1×10^{-7} mm Hg with solar ultraviolet radiation, high energy proton and alpha particle radiation, and low energy electron radiation, and the best available meteoroid environment.

G. PACKAGING REQUIREMENTS

The expandable crew transfer tunnel is required to be packaged in a modular design canister against the side of the Gemini-MSS vehicle in a minimum package volume that would have a minimum effect on the aerodynamics of the total launch system. The modular tunnel and packaging canister design is required to provide quick and easy ingress and egress from the Gemini capsule on the launch pad while also having the capability of being instantly jettisoned away from the Gemini-MSS system in case of mission abort.

SECTION IV

MODULAR CREW TRANSFER TUNNEL

A. GENERAL

The expandable Gemini to MSS modular crew transfer tunnel was specifically designed to satisfy the mission objective of providing a safe method of transferring the crew from the Gemini capsule to the crew station in orbit. The tunnel was designed under the major constraints imposed by human factors considerations and by general operational and environmental requirements. A prototype tunnel was fabricated and subjected to preliminary qualification testing to substantiate the design and verify the feasibility of the modular tunnel concept.

B. DESIGN OBJECTIVES

1. General

Human factors considerations controlled the general configuration of the tunnel, the design of the locomotion aids, and the tunnel interior lighting. The nontoxic requirement of tunnel construction materials is also a human factors consideration. The final design of the tunnel was then controlled by mission considerations including launch pad and boost requirements, orbital operations, and mission termination.

2. Human Factors

The human factors design requirements were established by Air Force in-house programs. By a cooperative effort between the Aero Propulsion Laboratory, the Aero Medical Laboratory, and the Materials Laboratory, a wood mock-up of the tunnel geometry was fabricated. This mock-up was flown in the KC-135 zero-G aircraft and thoroughly evaluated relative to human factors requirements in zero-G transfer.

The tunnel mock-up was attached to a mock-up of the left half of a two-man spacecraft with entry from the tunnel into the spacecraft through a 17 by 30 inch elliptical hatch in the main entry hatch of the spacecraft. Entry from the other end of the tunnel into a simulated orbital laboratory was through a 22-inch diameter circular hatch. Two ropes placed 21 inches apart served as handrails from the elliptical hatch to the circular hatch.

Human factors flight evaluation by a subject wearing a full pressure suit consisted of the following:

(1) Three unpressurized suit transfers from the spacecraft to the laboratory.

(2) Two unpressurized suit transfers from the laboratory to the spacecraft, one of which included a turnaround at the laboratory.

(3) Six pressurized suit transfers from the laboratory to the spacecraft, one of which included a turnaround at the laboratory. Another included the carrying of a specimen case, and the last included the transfer of a "completely disabled" shirt-sleeved subject.

(4) Four pressurized suit transfers from the spacecraft to the laboratory, one of which included a turnaround at the laboratory, and another included a turnaround at the spacecraft. The last included the carrying of a specimen case.

transfers in an unpressurized suit [illegible] suit required more time and were more [illegible] Figure 25 shows the typical mode of transfer in a pressurized suit. The results of these transfers can be summarized as follows:

(1) No problems were encountered in passing through the elliptical hatch.

(2) A specific technique must be worked out for transferring packages and equipment through the hatches.

(3) The two handrails were effective locomotion aids to crew transfer and should be incorporated in the tunnel design.

(4) The tunnel geometry, represented by the mock-up, was entirely compatible with effective crew transfer. There should be 28 inches clear height over the circular hatch and 38 inches clear height over the elliptical hatch. The final tunnel design should have no sharp protuberances that might snag the umbilicals or the space suit, and it should have a nonabrasive liner to avoid space suit damage.

Other human factors requirements that should be included in the tunnel design include the use of nontoxic materials in the tunnel construction and incorporation of interior tunnel lighting. Low-intensity lighting would appear to be adequate but should be evaluated in actual transfer experiments.

3. [illegible]tion Considerations

The general operational and environmental considerations that controlled the design were those necessary to satisfy the requirements discussed in Section III. A modular tunnel design approach should be followed that would permit prepackaging of the tunnel and on-the-ground check-out and repair prior to mounting on the launch vehicle. The packaged tunnel would be relatively easy to install on or remove from the launch vehicle, and should a mission abort be necessary, would allow the packaged tunnel and canister to be jettisoned away from the launch vehicle as a unit. In addition to protecting the packaged tunnel from the elements during hold or countdown on the launch pad, the flight canister should incorporate sufficient insulation to protect the packaged tunnel from damage due to aerodynamic heating during the boost phase. The packaging volume should be minimized so that the packaged tunnel and canister would impose a minimum effect on the aerodynamics of the launch vehicle.

For structural integrity, the expandable tunnel should be designed to withstand its design pressure of 7.5 psia for a mission duration of 45 days at orbital altitudes ranging from 100 to 300 nautical miles with a safety factor of 3. To withstand conditions encountered in the orbital environment, the tunnel materials must meet the following requirements:

(1) Provide a 0.995 probability of zero meteoroid penetrations.

(2) Maintain interior surface temperatures between 50 and 100°F.

(3) Be suitable for operations in hard vacuum of 10^{-7} torr.

(4) Absorb 10^6 rads of space radiation without serious degradation.

The design must incorporate provisions to jettison the transfer tunnel from the Gemini-MSS vehicle after the final transfer from the MSS to the Gemini capsule prior to reentry, preferably by utilizing the same system provided for ejecting the packaged modules in the event of mission abort.

EXITING FROM SPACE CRAFT HATCH

COMPLETELY WITHIN TUNNEL

TAUT ROPE USED AS LOCOMOTION AID

ENTERING LABORATORY HATCH

Figure 25. Crew Transfer Experiment under Zero G

C. DESIGN DESCRIPTION

1. General

Basically, the design incorporates an expandable tunnel configuration simulating the geometry used on the mock-up for human factors evaluation. The expandable structure has a rigid floor, which in turn is integrated with the packaging canister. In essence, the tunnel floor forms the lower half of the packaging canister and is connected to the upper half of the canister by separation screws that are cut by pyrotechnic guillotines for canister ejection. The advantages of this design are as follows:

(1) The tunnel can be prepacked prior to mounting on the launch vehicle.

(2) No attachments are required between the packaging canister and the launch vehicle.

(3) Mounting attachment points are required only at the hatch connections, simplifying installation and removal.

(4) The ejection systems are simplified. Requirements for launch abort and mission termination are combined into a single system.

Figures 26 through 30 show the operational sequence from prelaunch to mission termination. Figure 26 shows the prepackaged tunnel module attached to the Gemini capsule and MSS hatches. Figure 27 shows design provisions to meet abort requirements at launch. The hatch attachment rings incorporate a DuPont flexible linear shaped charge (FLSC) to burn through the rings for separation. In the event of abort, the canister and the packaged tunnel will be jettisoned as a single unit.

Deployment of the packaged tunnel in orbit is shown in Figure 28. The guillotines will be activated to cut the separation screws used to attach the canister cover to the tunnel floor, ejecting the canister cover and initiating tunnel deployment. The elastic recovery characteristics of the tunnel should then deploy the structure to its expanded volume. Figure 29 shows the geometry of the fully expanded tunnel. At mission termination, the expanded tunnel will be ejected, permitting separation of the Gemini capsule from the MSS. The jettisoning system shown in Figure 30 will be the same as that used for launch abort. The tunnel design is shown in Figure 2.

2. Composite Wall Structure

a. General. The materials approach selected to best meet the overall requirements of the tunnel design is a material composite that comprises four distinct layers bonded together into a homogeneous structure and painted on both inner and outer surfaces. The inner layer is an unstressed pressure bladder whose only function is to maintain pressure tightness and to transmit pressure loads to an adjacent structural layer. The structural layer carries structural loads resulting from internal pressure. Bonded to the structural layer is a flexible foam layer that performs a dual function. It acts first as a micrometeoroid barrier protecting the pressure bladder from penetration. Its secondary function is deployment and shaping of the structure through the use of stored energy inherent in the foam when compressed for packaging. The outer cover that is bonded to the foam barrier also serves a dual purpose. It is used as a smooth base for the application of a thermal coating and also encapsulates the total composite for evacuation and compression prior to packaging the tunnel in the canister. Two plastic pressure relief valves are incorporated in the composite wall design so that they penetrate the encapsulating outer cover and are embedded in the flexible foam layer. These valves also serve a dual purpose in providing a passageway for gas from the foam barrier through the outer cover, which is constructed from sealant material. One purpose is to provide a means of evacuating the air from the flexible foam for packaging. The other purpose is to provide an escape route for gas in the foam layer to prevent a pressure buildup within the outer cover due to environmental pressure reduction during launch and due to gas permeating the pressure bladder during the orbital mission.

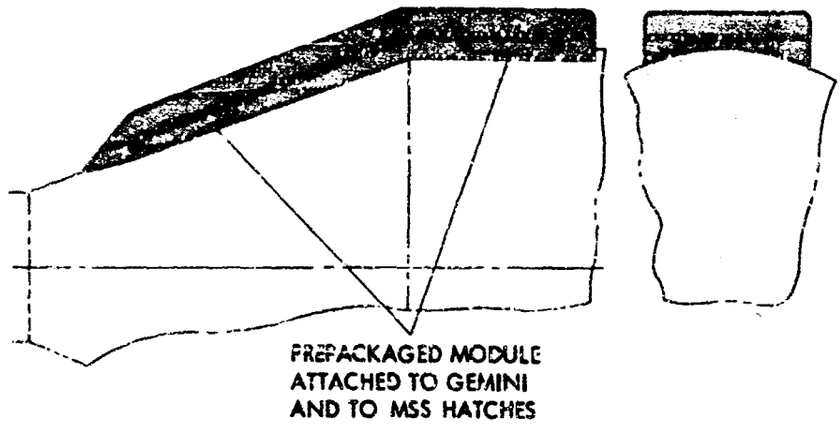

Figure 26. Launch Configuration of Prepackaged Tunnel

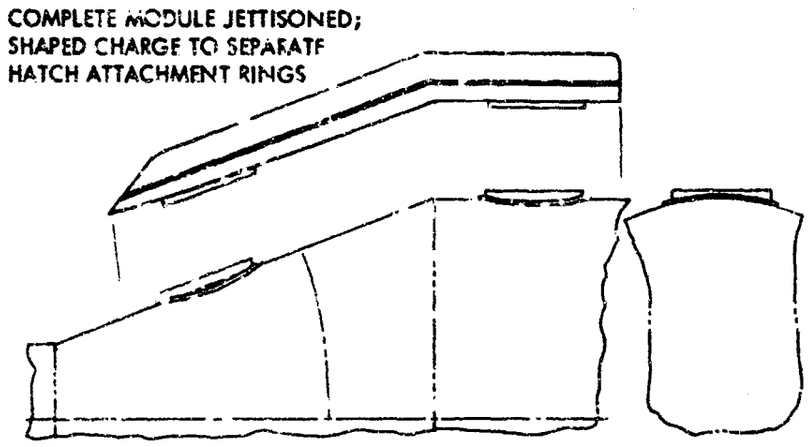

Figure 27. Tunnel Ejection at Launch Abort

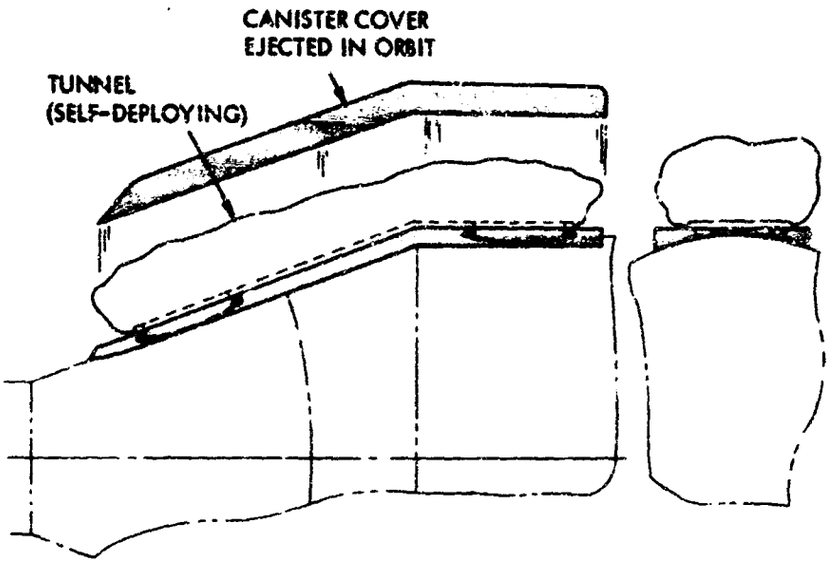

Figure 28. Canister Ejection and Tunnel Deployment

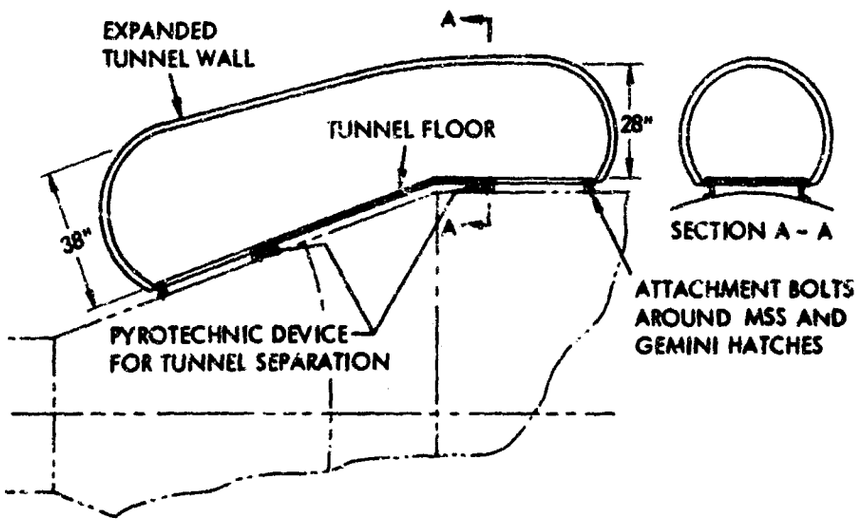

Figure 29. Deployed Tunnel

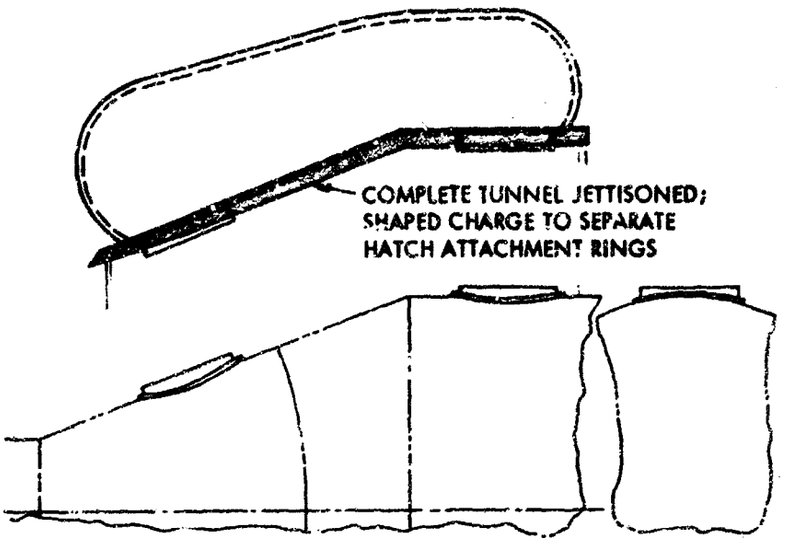

Figure 30. Tunnel Jettisoned at Mission Termination

The composite wall is discussed more thoroughly in Section V. The wall cross section is shown in Figure 82. The total weight of the composite wall is 0.890 psf.

b. Pressure Bladder. The pressure bladder is a laminate of three individual sealant layers. The inner layer is a laminate of Capran film sandwiched between two layers of lightweight nylon cloth. This layer is bonded with polyester adhesive to a second layer of closed-cell vinyl foam 1/16-inch thick. The outer sealant is a close-weave nylon cloth coated with a polyester resin. The total weight of the bladder composite is 0.126 psf and is independent of design pressure.

Tests were conducted on the pressure bladder to determine permeability rate, possible toxicity, and environmental effects due principally to vacuum. Permeability was determined with oxygen as a test gas at 5 psia, using a Dow cell. The measured rate was 10^{-4} psf per day. Relating this rate to the tunnel design, the anticipated gas loss is approximately 0.02 pound per day, substantially less than the maximum allowable of 1 pound per day. A survey of toxic materials known to be used in the construction of the pressure bladder indicated the possible presence of toluene, xylene, methyl ethyl ketone, methylene chloride solvents, and toluene diisocyanate. Although carbon monoxide was not known to be contained, tests for it were also included. The bladder material was exposed to 5 psia of oxygen for 24 hours prior to a chemical analysis and check for toxic gases. Test results indicated that all the above contaminants were below the threshold limits established by the National Bureau of Standards for occupational exposure.

The principal environmental effect for which the bladder was checked was a hard vacuum. This check was made first to ensure that delamination of the composite bladder would not occur and secondly to determine the degree of off-gassing to be expected. The bladder construction technique proved successful both in preventing delamination and in minimizing off-gassing. Off-gassing stabilized in about 96 hours with a 3.3 percent weight loss.

The pressure bladder is discussed more thoroughly in Section V. The laminate is shown in Figure 83.

c. Structural Layer. The structural layer is a four-ply laminate of Dacron cloth bonded together with polyester resin, then cured under heat and pressure. The design pressure of 7.5 psia, which along with a safety factor of five and allowance for creep rupture, requires an original load capability of 1300 pounds per inch. This load must be carried entirely by the

structural layer. The basic structural concept of the multi-ply technique is that joints in the individual plies are staggered in such a way as to offer an essentially seamless construction. Cylinder burst tests of this technique indicate an 81 percent load capability, as compared to that of the parent structural cloth. The degradation in strength is attributed to the "locked-in" crimp of the bonded polyester joint. A similar degradation also is incurred in elastomer-coated fabrics and is attributed to the same effect. Even in a mechanically sewn joint, seam efficiencies beyond 85 percent are unlikely. It thus appears that a 100 percent structural efficiency for a fabric structure is not attainable. However, because the structural weight of 0.210 psf is only 30 percent of the total composite weight, the weight penalty incurred by an 81 percent structural efficiency is not significant.

Particular emphasis was placed on the design and development of a structural joint between the rigid floor of the tunnel and the structural layer. The technique that evolved from this investigation uses an epoxy resin rigid bond. The locked-in crimp effect was again found in this joint design, resulting in an efficiency of 50 percent. Attempts to improve joint efficiency by using a more elastic epoxy bond were not successful and only resulted in shear failure of the joint. A polyester resin bond similar to that used in the multi-ply wall was also tested, but was wholly inadequate for the required bond. Consequently, the rigid epoxy bond technique was adopted as the required design technique and resulted in an eight-ply bond to the structural floor joined to the four-ply structural layer with a polyester resin bond. Strip tensile tests of this overall joint design indicated that the full load capability could be carried by both the joints and the basic four-ply structural layer.

Structural tests have been conducted to investigate environmental effects due to vacuum and high energy radiation. Strip tensile tests on Dacron have indicated negligible effects of hard vacuum on the structural characteristics. Similar tests on fabrics irradiated with 10^6 rads of 1.3-mev gamma radiation have also indicated negligible degradation. Accordingly, there is no reason why synthetic fiber structures should not be used in structural space applications, if their physical characteristics are known and related to the operational environment.

The structural layer and the structural joint between the structural layer and the rigid floor of the tunnel are discussed more thoroughly in Section V. The construction is shown in Figure 85.

d. Flexible Foam Layer. The tunnel will be protected from micrometeoroid penetration by a 2-inch layer of flexible polyether foam. Flexible foam of 1.2-pcf density has been selected as a suitable barrier material, based on hypervelocity particle impact tests conducted by GAC and on tests conducted at the micrometeorite testing facility at Wright-Patterson AFB. Both series of tests (the latter conducted at 27,000 fps with an average particle mass of 5 milligrams) indicate that a 2-inch foam barrier of 1.0-pcf density is equivalent in barrier effectiveness to single-sheet aluminum 3/16-inch thick (2.7 psf). Figure 60 shows the Air Force near-earth micrometeoroid environment spectrum in terms of particle mass and accumulative particle flux. When the previously mentioned test results are correlated with single-sheet aluminum penetration theory, the critical penetrating flux level is about 5.23×10^{-7} particles/ft^2-day. Relating the critical flux with the exposed surface area of the deployed tunnel (130 square feet) and the mission time (60 days), the probability of zero penetration is at least 0.995.

While the primary function of the foam will be as a micrometeoroid barrier, it can serve also as a tunnel deployment aid. During packaging, the foam layer will be compressed to about 10 percent of its original thickness and will be restrained by the packaging canister. Upon deployment in orbit, the canister will be jettisoned, and the elastic recovery characteristics of the foam will shape the tunnel to its fully expanded volume. Figure 90 shows the recovery characteristics of the foam under vacuum conditions and for varying temperatures. From Figure 90 it can be seen that the packaged structure must be insulated against extreme cold if full recovery is to be achieved.

Environmental effects should be evaluated to establish compatibility with the environment.

Of principal concern are the effects of vacuum, temperature, and high energy radiation. The effect of foam recovery in a vacuum has already been discussed. Off-gassing induced by vacuum was negligible; it amounted to a 0.5 percent weight loss and stablized in 1.5 hours. Expected temperature extremes should cause no problem. High energy radiation is not expected to present any problem, because the foam tolerance is about an order of magnitude higher than the anticipated dose of 10^6 rads.

The flexible foam micrometeoroid barrier is discussed more thoroughly in Section V. The weight of 2-inch thick foam of 1.2-pcf density is 0.200 psf.

e. Outer Cover. The outermost layer of the composite wall structure encapsulates the wall and provides a smooth base for the application of a thermal coating. The construction of this layer is shown in Figure 84. It is a film-cloth laminate weighing 0.015 psf. With an estimated thermal coating weight of 0.026 psf, the total combined layer weight is 0.041 psf.

Inasmuch as the outer cover encapsulates the composite wall, it serves as an aid in packaging the tunnel prior to launch. By a vacuum technique, the wall thickness can be compressed from the fully expanded 2 inches to about 3/8 inch, suitable for folding and subsequent packaging in the canister. Also, a certain amount of air will still be trapped in the composite wall, even after evacuation. This air can be used as a thickness recovery aid, augmenting the elastic recovery characteristics of the compressed foam. Thus, full recovery of the wall thickness, even under adverse temperatures, will be ensured.

The film side of the outer cover laminate will be coated with vacuum-deposited aluminum, which is part of the thermal control coating. Depending upon the Gemini-MSS system orbit and the tunnel orientation relative to the sun and the earth, the aluminized film will be partially covered by stripes of aluminized silicone white paint and possibly by thin layers of silicon monoxide in some locations to maintain comfortable internal tunnel temperatures and to maintain material temperatures within acceptable limits during full solar flux. The thermal control system is discussed more thoroughly in Section V.

Environmental effects compatibility requires the consideration of combined vacuum and ultraviolet radiation, the thermal environment, and high energy radiation from Van Allen electrons. The portion of the outer cover most sensitive to the orbital environment will be the thermal coating. The combined effect of vacuum and ultraviolet radiation will cause some degradation of the coating. The solar absorptance/emittance (α/ϵ) ratio is expected to increase by not more than 10 percent for a 60-day mission, resulting in a slight increase in materials temperature. Off-gassing due to vacuum is a minute effect, causing less than 0.5 percent weight loss, and stabilizes in 1.5 hours. Thermal effects relative to extremes in temperature are expected to produce no problems. Finally the thermal coating is expected to absorb 10^6 rads of electron radiation. However, the tolerance of the coating to high energy radiation is on the order of 10^7 to 10^8 rads.

3. Sandwich Structure Floor

The sandwich structure floor consists of two flat metal honeycomb bonded sandwich panels that are mechanically joined to form a 160-degree included angle between the panels, paralleling the longitudinal contour of the Gemini-MSS vehicle. There is a circular hole in the panel over the MSS hatch and an elliptical hole in the panel over the Gemini hatch to allow ingress and egress of the astronauts. The circular hole is 30 inches in diameter, and the elliptical hole has major and minor axes of 29 and 17 inches respectively.

The Bondolite[1] sandwich panel construction consists of 7.9-pcf density aluminum honeycomb core with 1/4-inch cells having 0.004-inch walls of 3003 aluminum bonded to 0.063-inch thick 7076-T6 aluminum faces with Epon 934 epoxy adhesive. The panels are edged around both the periphery and the hatch-access cutouts with shaped aluminum sections to provide a

[1]TM, Goodyear Aerospace Corporation, Akron, Ohio

structural surface for installation of the hatch attachment rings and to provide a smooth contour for bonding the structural layer of the composite wall to the floor. Doublers are installed inside the lower faces of the panels to provide reinforcement in the areas where the channel section canister support brackets are attached. The floor panels are fabricated as complete subassemblies by curing the adhesive under heat and pressure in an autoclave.

After the panels are attached together with aluminum plates on both the upper and lower surfaces, the interior tunnel surface and the edges are sealed with a film-cloth laminate tape bonded over the cracks and a foam-cloth laminate bonded over the entire interior surface. The tape is made from the same film-cloth laminate as the inner ply of the pressure bladder. The foam-cloth laminate "rug" is constructed from the closed-cell vinyl foam and nylon cloth used in the remainder of the pressure bladder construction.

4. Attachment and Separation Systems

The tunnel is attached to the launch vehicle at the hatch areas with 6061-T6 aluminum rings containing provisions for pyrotechnic separation systems. The rings, elliptical at the Gemini hatch and circular at the MSS hatch, are attached to the floor structure with countersunk bolts and Rivnuts, with the floor-ring joint sealed by the application of epoxy resin covered by a film-cloth laminate sealant tape. The separation rings have flanges shaped to fit the contours of the Gemini capsule and the laboratory. Each flange contains a machined groove for installation of an O-ring seal. The rings are attached to the launch vehicle with rows of Camloc quick-disconnect fasteners through the flanges.

Each ring contains machined circumferential grooves around its entire periphery in the wall area between the flange and the floor attachments for installation of the FLSC pyrotechnic separation devices. The FLSC is packed into the machined notches with epoxy adhesive and protected by backup plates of aluminum bolted to the separation rings. The FLSC achieves separation when detonated by burning through the ring metal in the notched thickness area and supplying pressure to force the separated portions apart. GAC has been quite successful in the utilization of the FLSC separation and jettison technique.

With the packaging canister attached to the floor structure with screws through the 10 canister support brackets on the floor, and not to the launch vehicle directly, the tunnel may be separated and jettisoned in the event of mission abort or for mission termination by the same FLSC separation system incorporated in the ring designs.

5. Packaging Canister

The packaging canister is designed to retain the folded tunnel in the packaged configuration and to protect the tunnel from the environmental elements on the launch pad and during the launch phase. Titanium sandwich construction is used for the canister design.

The canister is constructed in two parts. The lower part, an open frame approximately 12 feet long, has a width of about 4 feet at the MSS end tapered to a width of about 2-1/2 feet at the Gemini end. The depth along the long edges is about 5-1/2 inches, and the ends are shaped to fit the contours of the Gemini-MSS vehicle. The frame is constructed by mechanically joining the titanium sandwich panels at the edges. The interior surface of the frame is lined with sheet insulation. The lower part of the canister, which rests against the launch vehicle, is bolted to the canister support brackets attached to the tunnel floor.

The upper part of the canister is a long, narrow, open box-like structure that is constructed by joining titanium sandwich panels in the same manner used for the lower part. The interior surface is also lined with sheet insulation. The upper part of the canister, which contains the packaged tunnel, rests against the lower part and is attached to it with long separation screws that are attached to angular brackets mounted on the interior surfaces of both canister parts at 12 locations. Each of the separation screws passes through the access opening of a pyrotechnic guillotine bolt cutter mounted on the angular bracket of the lower part of the canister. This design allows the upper part of the canister to be separated from the lower part for

tunnel deployment by detonating the guillotines which cut the separation screws and supply a separating force for jettisoning the upper part of the canister.

The packaging canister design provides a packaging volume of about 20.8 cubic feet while presenting an aerodynamic drag area of about 2.6 square feet. The canister weight given in Table I is based on estimated titanium sandwich weight and estimated insulation weight. The sandwich material required for structural integrity depends upon the aerodynamic loads during launch. The insulation required to protect the packaged tunnel from thermal damage during launch depends upon the aerodynamic heating involved. A launch profile, which was not available, is required for analyses involving these parameters. Lack of these values does not detract from the feasibility of the preliminary design.

6. Interior Lighting and Locomotion Aids

Types and design locations of tunnel interior lighting and crew locomotion aids were studied by the human factors engineers in the Life Sciences Research Department of GAC. The results of these studies in conjunction with the recommendations of the Air Force as a result of the tunnel mock-up zero-G flight tests are incorporated in the tunnel design.

Locomotion aids consist of 0.75-inch diameter nylon cords extending along each side of the floor from the Gemini hatch opening to the MSS hatch opening. The ends of the hand ropes are attached to the rigid floor structure with clamps. The cords are held 4 inches above the floor by flexible foam cubes placed intermittently along the rope length. Flexible foam is used for the hand rope supports so that they may be easily compressed during the tunnel packaging operation.

Sylvania flexible strip lighting was selected for the tunnel interior lighting. Two strips of lighting are cemented along each side of the tunnel wall about 1.5 inches above the floor in the best position to illuminate the hand ropes. A 6-foot strip extends from the angular contour change in the tunnel floor to the Gemini hatch opening, and a 2-foot strip extends from the contour change to the MSS hatch opening. In addition to the strip lighting installation, the tunnel design includes an interior coating of a reflective white paint to assist in illuminating the tunnel interior.

7. Weight Estimate

The weight estimate given in Table I is based on the tunnel design shown in Figure 2. As shown in Table I, the total weight of the transfer tunnel (227 pounds) and the packaging canister (148 pounds) is 375 pounds. This weight is based on a design pressure of 7.5 psia. For a design pressure of 3.5 psia, the weight reduction would be small, since so many of the items included in the design are not controlled by the inflation pressure. The estimated weight reduction is 23.5 pounds. The contributing items are the structural layer of the expandable wall, the wall-floor joint, and the inflation system. It is possible that the sandwich floor might offer some weight reduction, depending on the canister aerodynamic loads. Based on inflation pressure loads alone, the floor weight reduction is about 21.5 pounds. This is a total weight reduction of 45 pounds, which would reduce the total weight to 330 pounds.

D. PROTOTYPE TUNNEL

1. General

The expandable Gemini to MSS modular crew transfer tunnel design was translated into a detail prototype tunnel design that could be fabricated and subjected to preliminary qualification tests in order to substantiate the design. The prototype tunnel design is shown in Figure 3. There are four areas in the design of the prototype tunnel in which the actual tunnel design is not faithfully reproduced. These changes were made in the interests of simplification and time savings, and [illegible]ay affect the feasibility of the design or the results of the prototype tunnel tests.

First, the design of the hatch attachment separation rings was simplified by omitting the machined notches for the FLSC separation system and by making the flanges in a flat plane rather than shaped to follow the contours of the launch vehicle. Since the utilization of the FLSC pyrotechnic system is a well proven separation technique and since demonstration of tunnel separation for mission termination or abort was not a preliminary test requirement, the elimination of this system from the prototype design is well justified. By making the separation ring flanges flat rather than contoured, considerable tooling and prototype fabrication time could be saved. In addition, the design and fabrication of the steel test carrier mock-up hatches that support the prototype tunnel were greatly simplified by the use of flat separation ring flanges. This change has no effect on the feasibility of the tunnel design or on the test results.

Secondly, a substitute Dacron cloth was used for the four-ply structural layer of the prototype tunnel. This substitution was necessary because the required cloth was unavailable at the time it was required for this program. Although the substitute cloth is slightly heavier and thicker than the required cloth, it has a lower breaking strength. Since the structural layer of the tunnel wall was designed to have a factor of safety of 5 with degradation due to creep rupture effects for 60 days under the load considered, the use of a substitute cloth with a factor of safety of 4 under [illegible] conditions is considered satisfactory for the prototype tunnel.

The third area of difference between the tunnel design and the prototype tunnel involves the packaging canister. To simplify fabrication of the prototype packaging canister, the decision was made to use lightweight aluminum sandwich panels rather than titanium panels of a greater thickness. Since no thermal testing was required, the insulation was not included in the prototype canister design.

The last area of the prototype tunnel deviation from faithful reproduction is the use of a substitute outer cover and thermal coating on the composite wall of the prototype tunnel. Since no thermal testing was required on the prototype tunnel and since the required materials could not be obtained for use on the prototype tunnel, the decision was made to use materials that would satisfy the nonthermal requirement of the outer cover. The nonthermal requirement is to provide a gas-tight barrier for encapsulating the flexible foam. In order to provide encapsulating material, nylon cloth coated with titanium dioxide pigmented Hypalon paint was selected for the outer cover. This paint provides a rubberized film on the nylon cloth for gas tightness, and the nylon cloth provides a satisfactory surface for bonding the flexible foam to the gas-tight barrier.

The prototype tunnel design final assembly is shown in Figure 31.

2. Prototype Tunnel Fabrication

a. General. The first step in the fabrication procedure was the assembly of a fabrication tool. The tool used was a rigid polyurethane foam mandrel machined to the interior contour of the expanded tunnel and mounted on a movable steel framework fixture. The prototype tunnel mandrel mounted on the fabrication support fixture is shown in Figure 32. The completed sandwich floor structure is also mounted on the support fixture and becomes a part of the fabrication tool. The floor mounted on the fixture is shown in Figure 8. The mandrel was sprayed with a separating agent to prevent adhesion of the pressure bladder to the mandrel.

The composite wall structure was then built up on the mandrel in layers using appropriate patterns. When the pressure bladder was completed, the floor was lowered against the mandrel with the bladder bonded to the floor. This is shown in Figure 33. When the remainder of the composite wall was completed, the complete structure was removed from the fabrication support fixture and placed upright on a wooden stand contoured to match the tunnel floor. While in this position, the rigid foam mandrel was removed from the tunnel interior by chipping it out in chunks. The prototype tunnel with the mandrel removed is shown in Figure 34.

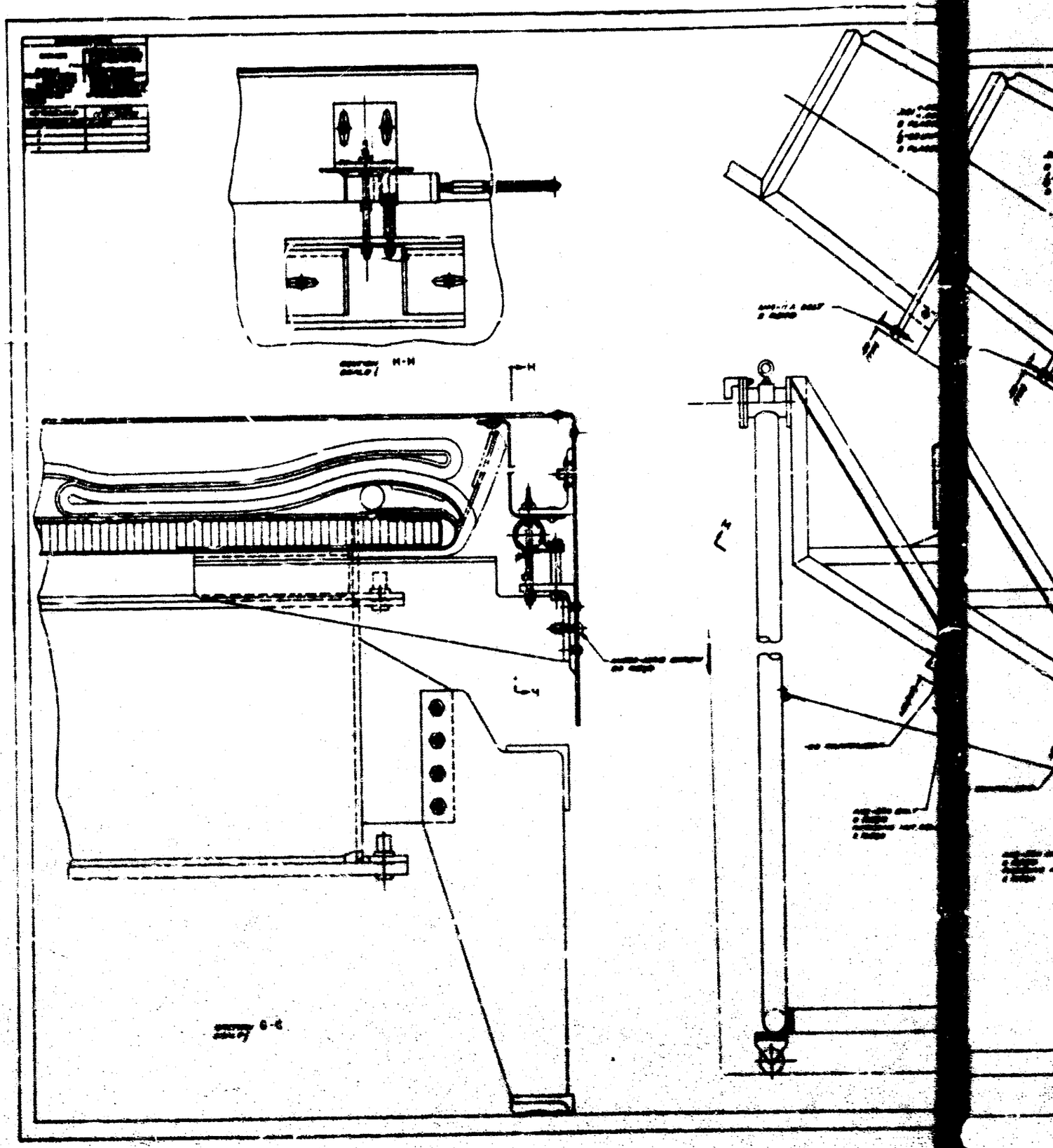

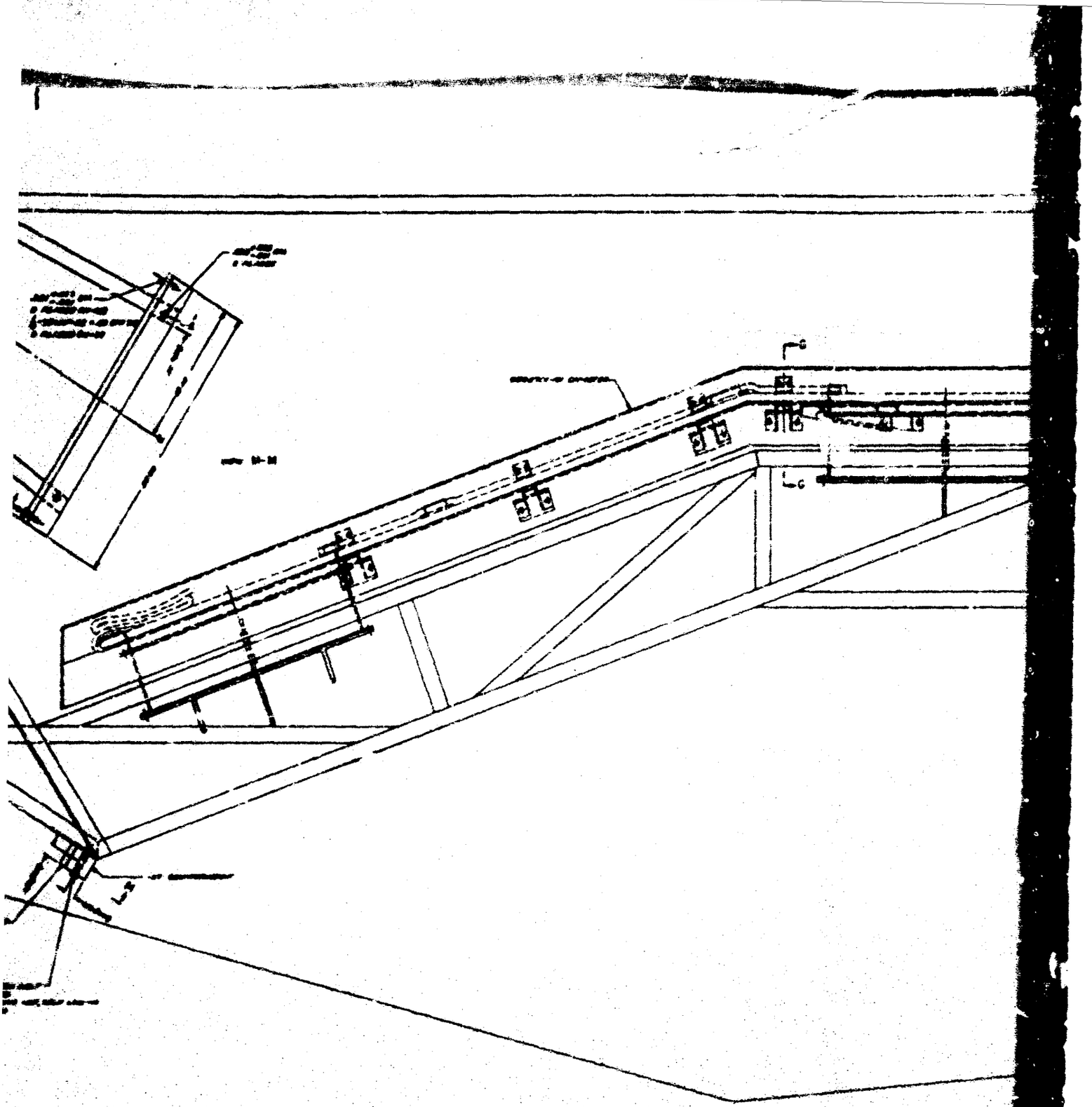

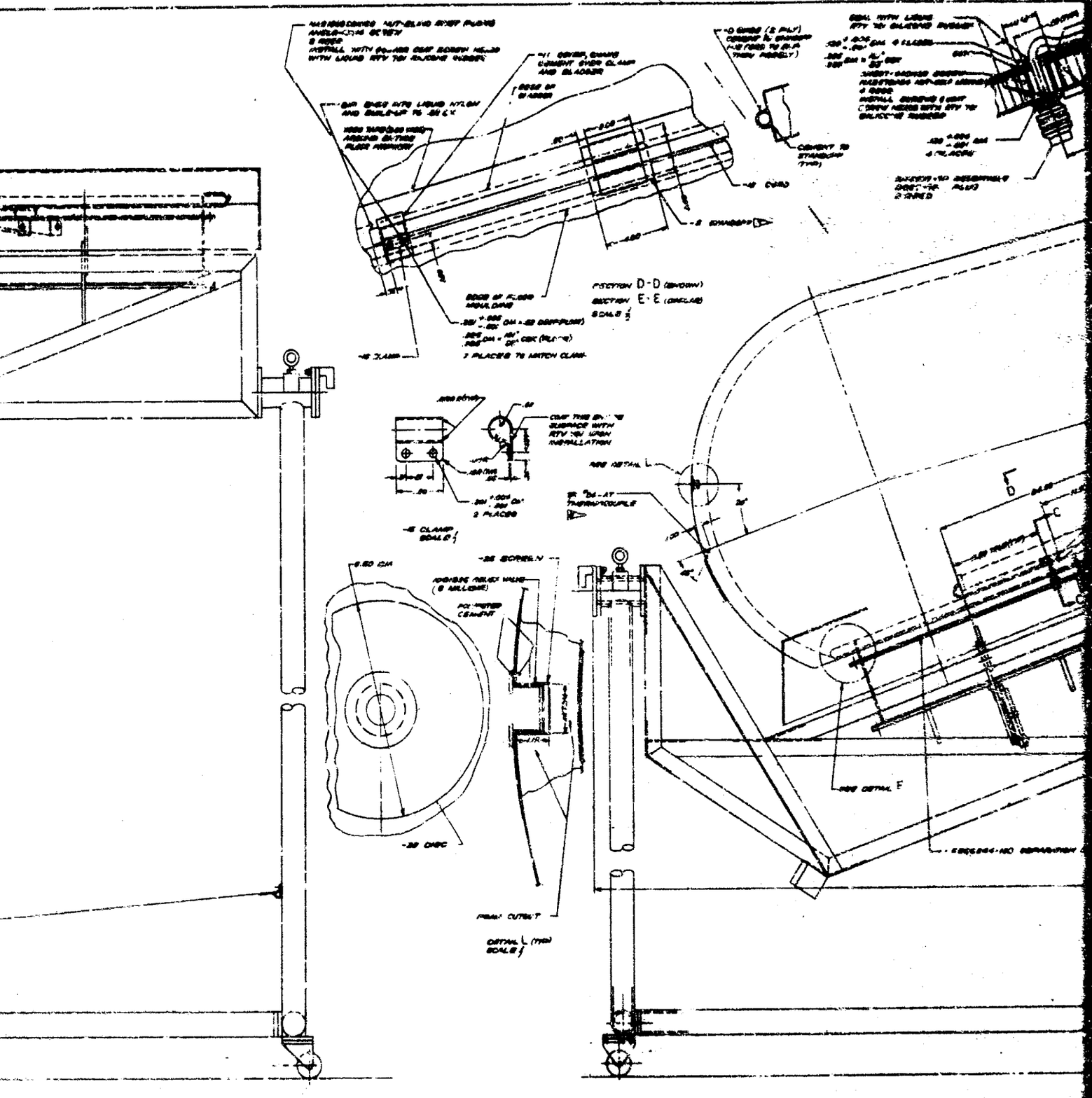

Figure 31. Prototype Tunnel Final Assembly

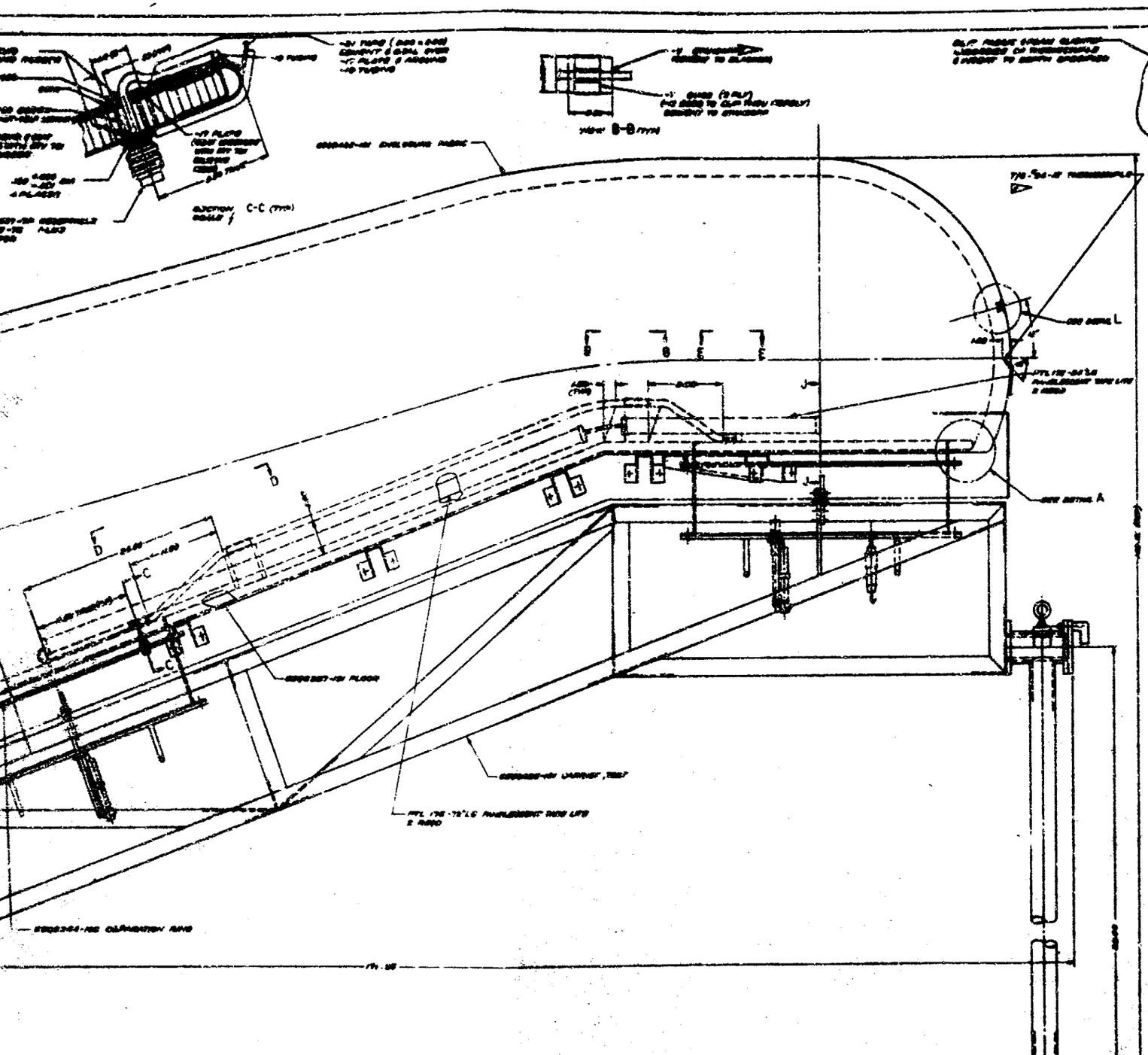

3

4

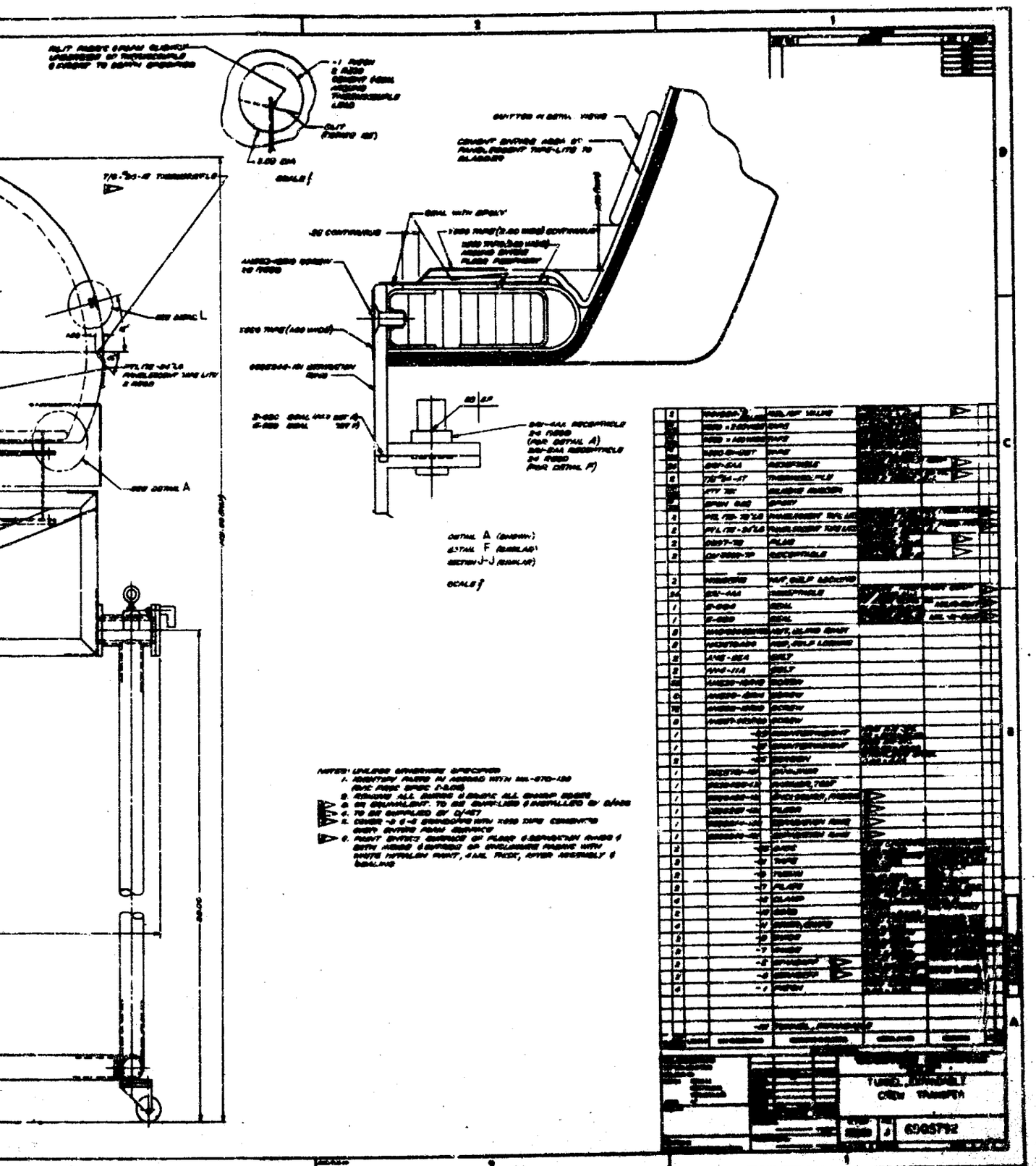

4

5

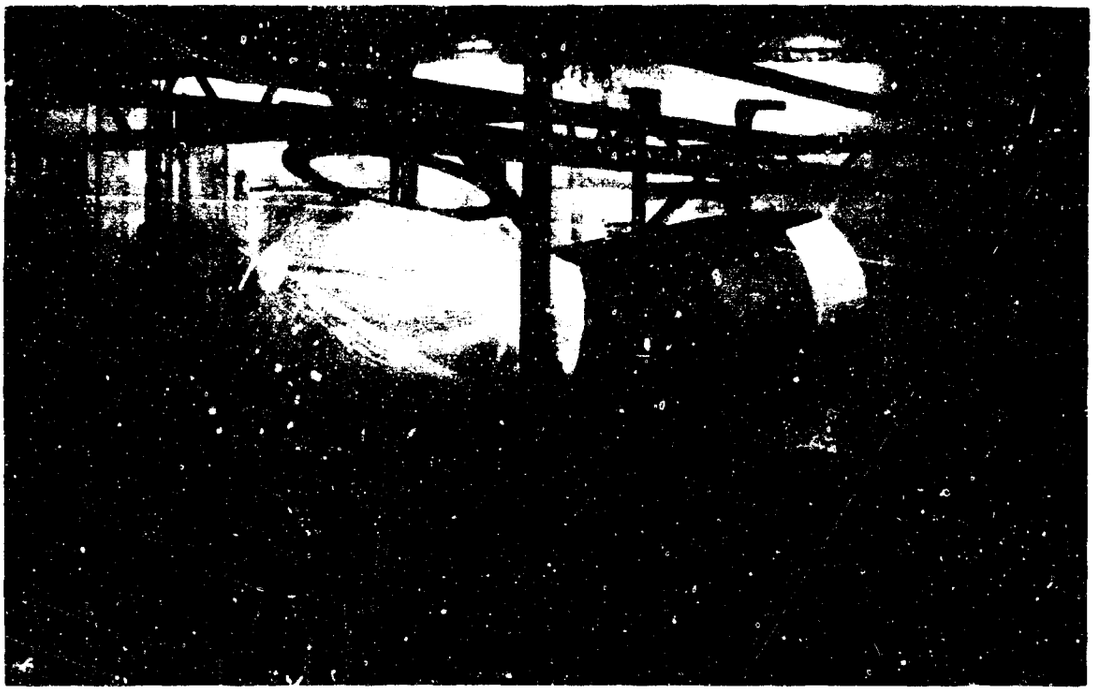

Figure 32. Rigid Foam Mandrel Mounted on Support Fixture

Figure 33. Complete Pressure Bladder with Floor Attached

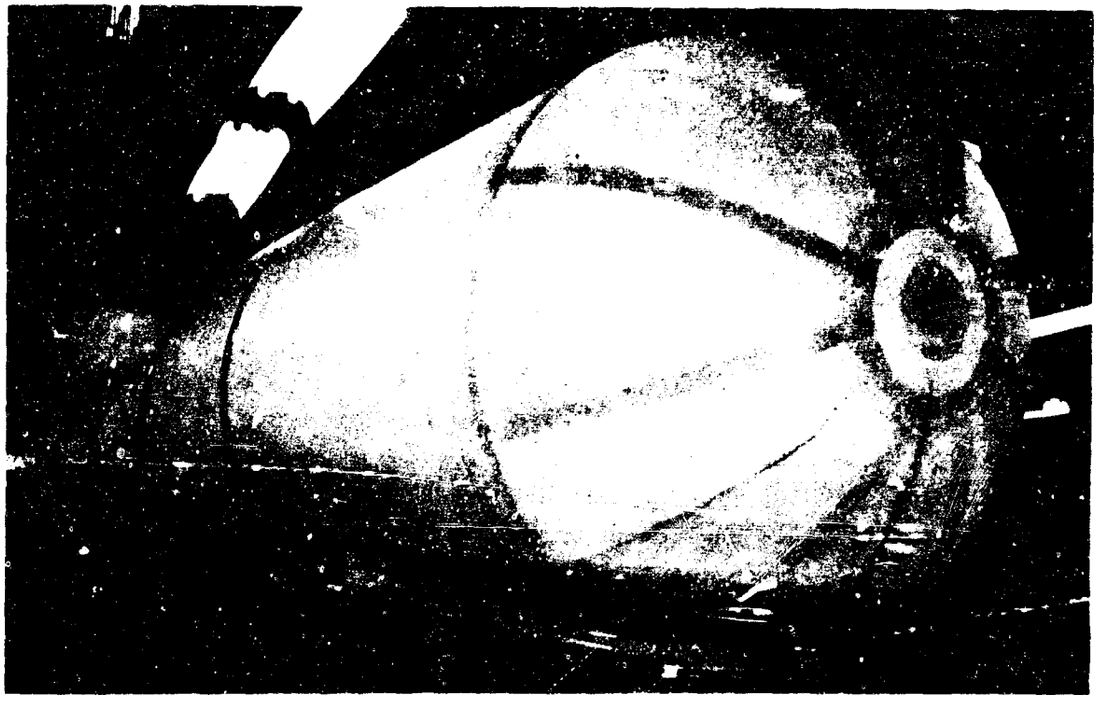

Figure 34. Mandrel Removed from Prototype Tunnel

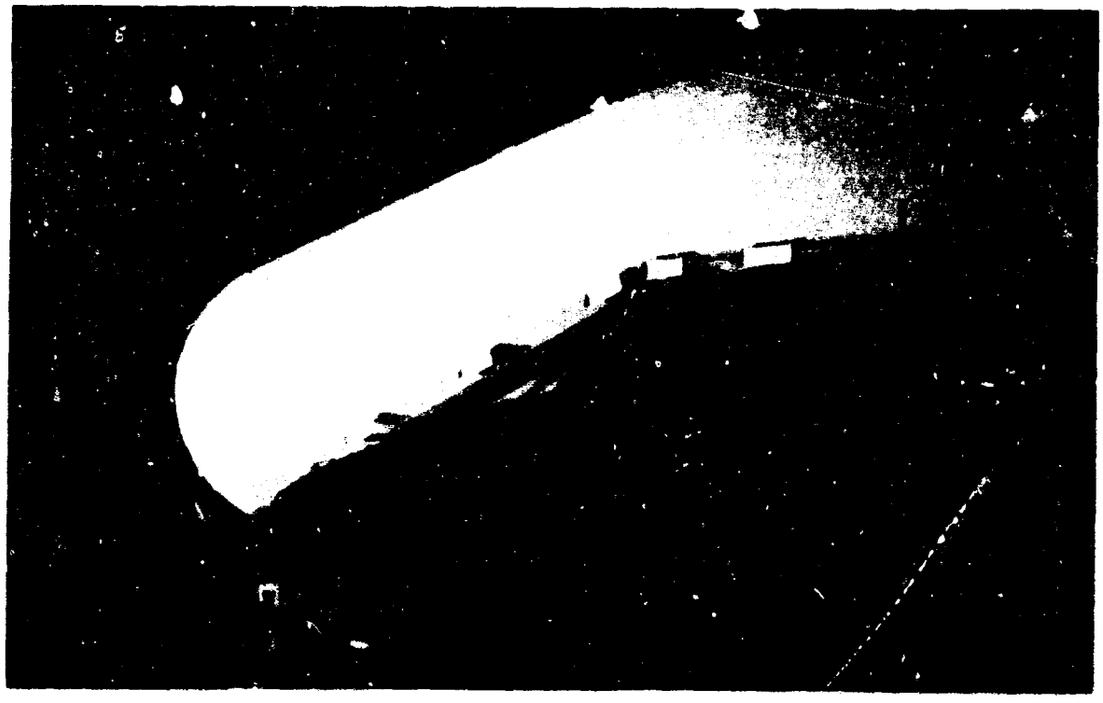

Figure 35. Completed Prototype Tunnel Unpressurized

After interior lighting and crew locomotion aids were evaluated by the human factors engineers, their locations were masked and the tunnel was painted inside and outside. The hand ropes and lighting strips were then installed on the tunnel interior, and the canister support brackets were installed on the floor. The tunnel was then complete. The completed tunnel is shown in Figure 35.

The canister was fabricated by riveting together a series of aluminum honeycomb sandwich panels and installing the appropriate bracketry. The completed canister is shown in Figure 15.

At various stages of fabrication, when practicable, the fabricated parts were weighed. The weights are given in Table II.

b. Sandwich Floor Structure. The prototype floor design is an exact reproduction of the modular design. The floor design is shown in Figure 36. The construction was described earlier in this section. The design of the hatch attachment separation rings and the canister support brackets that are attached to the floor structure are shown in Figure 37. The prototype separation rings differ from the actual tunnel design rings in that the flanges are flat and there is no provision for the FLSC separation system. These discrepancies were discussed earlier in this section. The feasibility of the tunnel design or the evaluation of test results are not affected by these changes. The completed floor is shown in Figure 38.

c. Composite Wall Fabrication. The triple-barrier pressure bladder and the flexible foam micrometeoroid barrier used in the fabrication of the prototype tunnel are identical with those of the actual tunnel design. The use of substitute cloth for the structural layer and the use of substitute cloth and thermal coating for the outer cover were discussed earlier in this section. All adhesive systems and fabrication techniques applying to the actual design were stringently followed in the construction of the prototype composite wall and the attachment of the structural layer to the floor. The prototype tunnel composite wall design is shown in Figure 39.

(1) Pressure Bladder. The pressure bladder is fabricated from subassemblies. The inner layer is a subassembly laminated by bonding a layer of Capran film between two layers of lightweight nylon cloth with polyester adhesive. The middle and outer layers of the pressure bladder, the closed cell vinyl foam layer and the polyester resin-coated nylon cloth layer, are laminated into a subassembly by bonding them together with polyester adhesive.

To prevent wrinkles in the pressure bladder when the patterns were placed over the hemispherical ends of the mandrel, the patterns were heat set to the proper curvature by clamping the patterns in a contouring fixture and pulling them tight against the fixture contour by a vacuum bagging technique. With the vacuum maintained, the fixture was placed in a curing oven and heated. When removed from the fixture, the pressure bladder patterns retained the proper contour. One of the contouring fixtures is shown in Figure 40.

The film-cloth inner laminate was placed on the mandrel first, using the appropriate design patterns. Then the outer foam-cloth laminate was placed on the mandrel, using the proper patterns to prevent any pressure bladder seams from becoming coincidental with the seams in the adjacent layer. The floor with its foam-cloth laminate "rug" in place was coated with polyester adhesive and lowered into place against the mandrel and the lapped pressure bladder. The entire assembly was then vacuum bagged and cured in an oven.

(2) Structural Layer. The patterns for the structural cloth layer were placed on the mandrel over the pressure bladder with each of the four plies coated with polyester adhesive for interply adhesion. The patterns are different for each ply so that no two plies have coincidental seams. As a result of this fabrication technique, there are three continuous plies over the seam in the remaining ply, which offers an effectively seamless construction. That is, a failure in a seam of any one ply would not prove catastrophic, but would only reduce the strength of the entire structural layer by 25 percent.

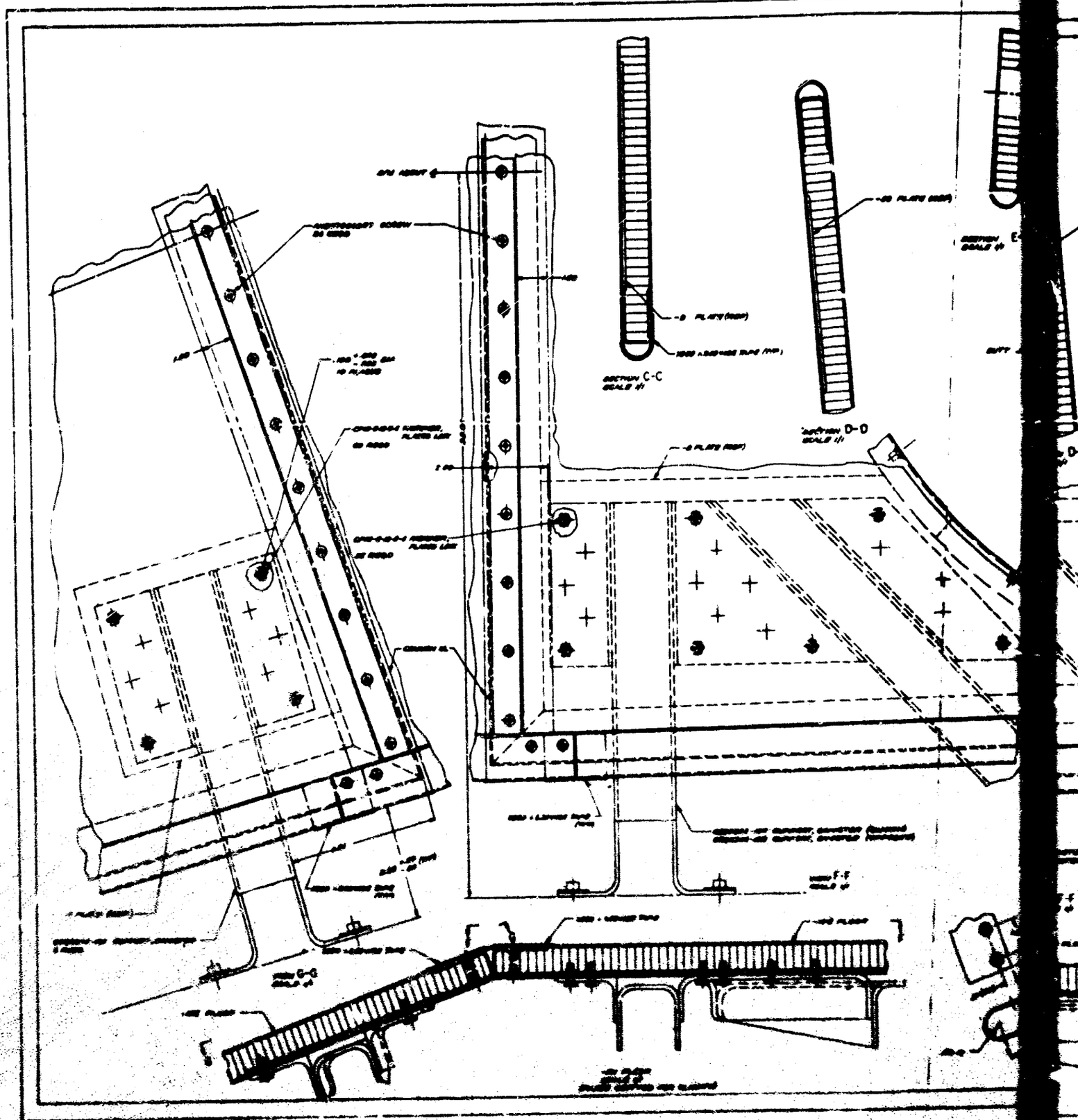

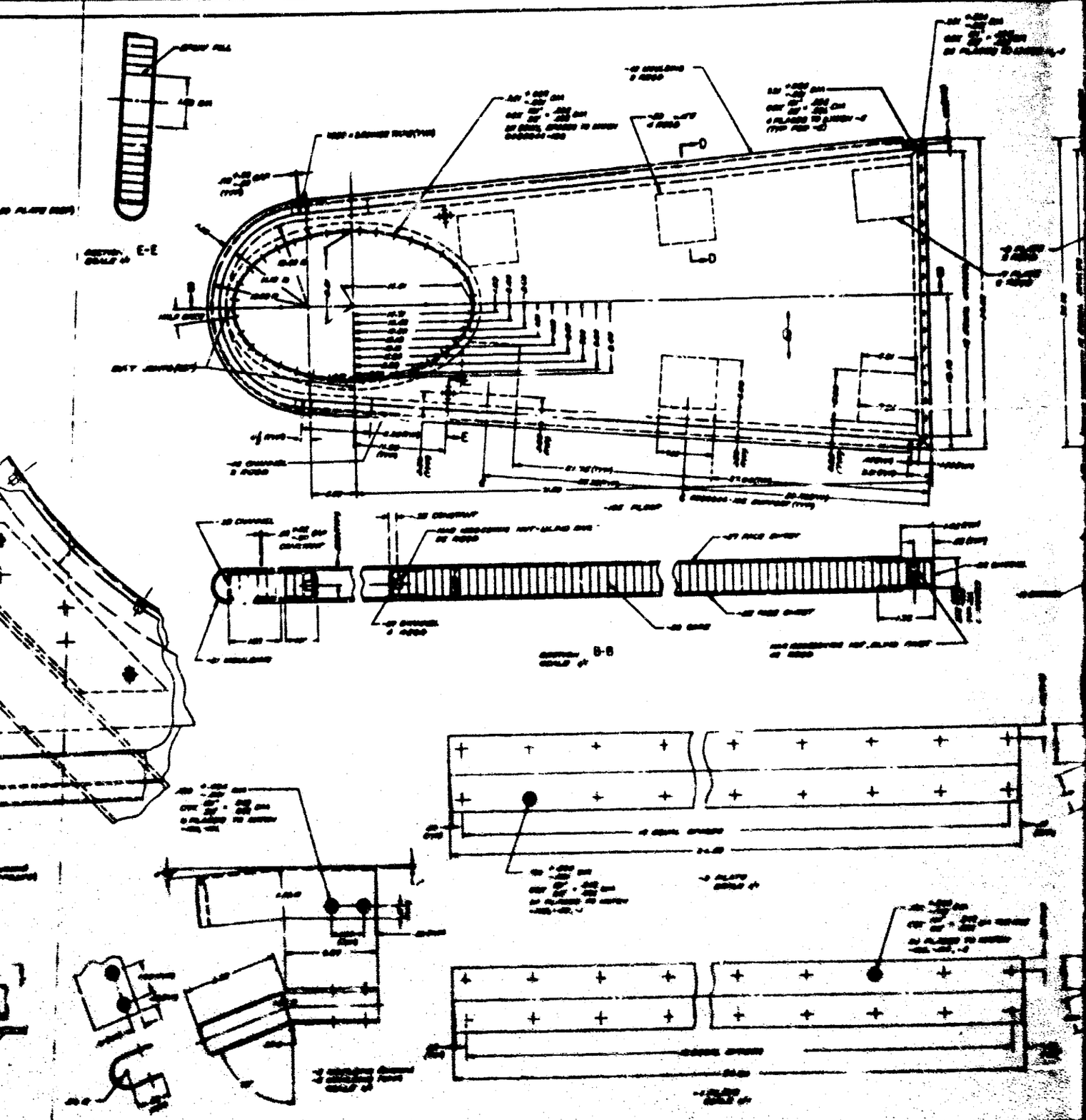

Figure 36. Prototype Tunnel Floor Design

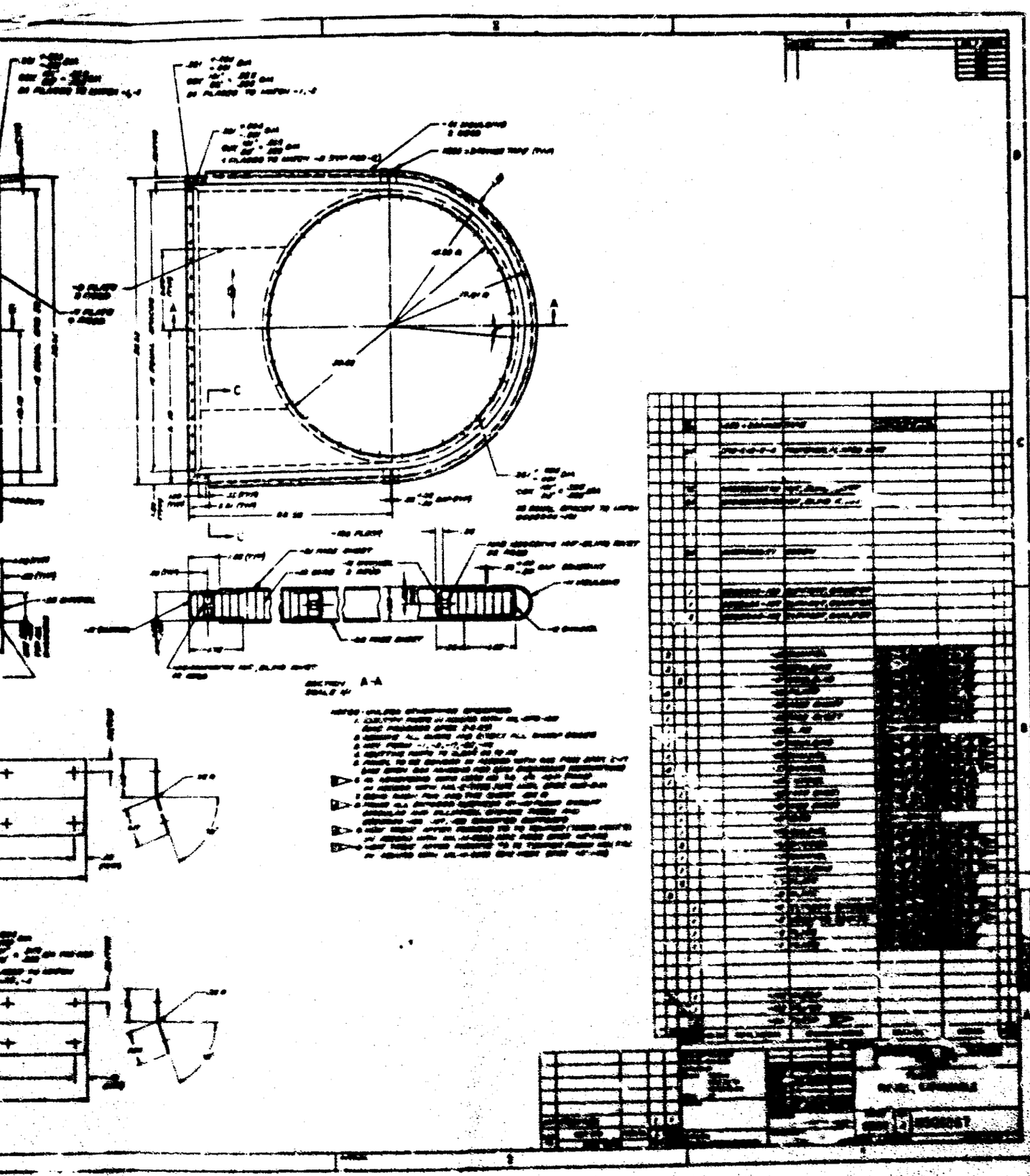

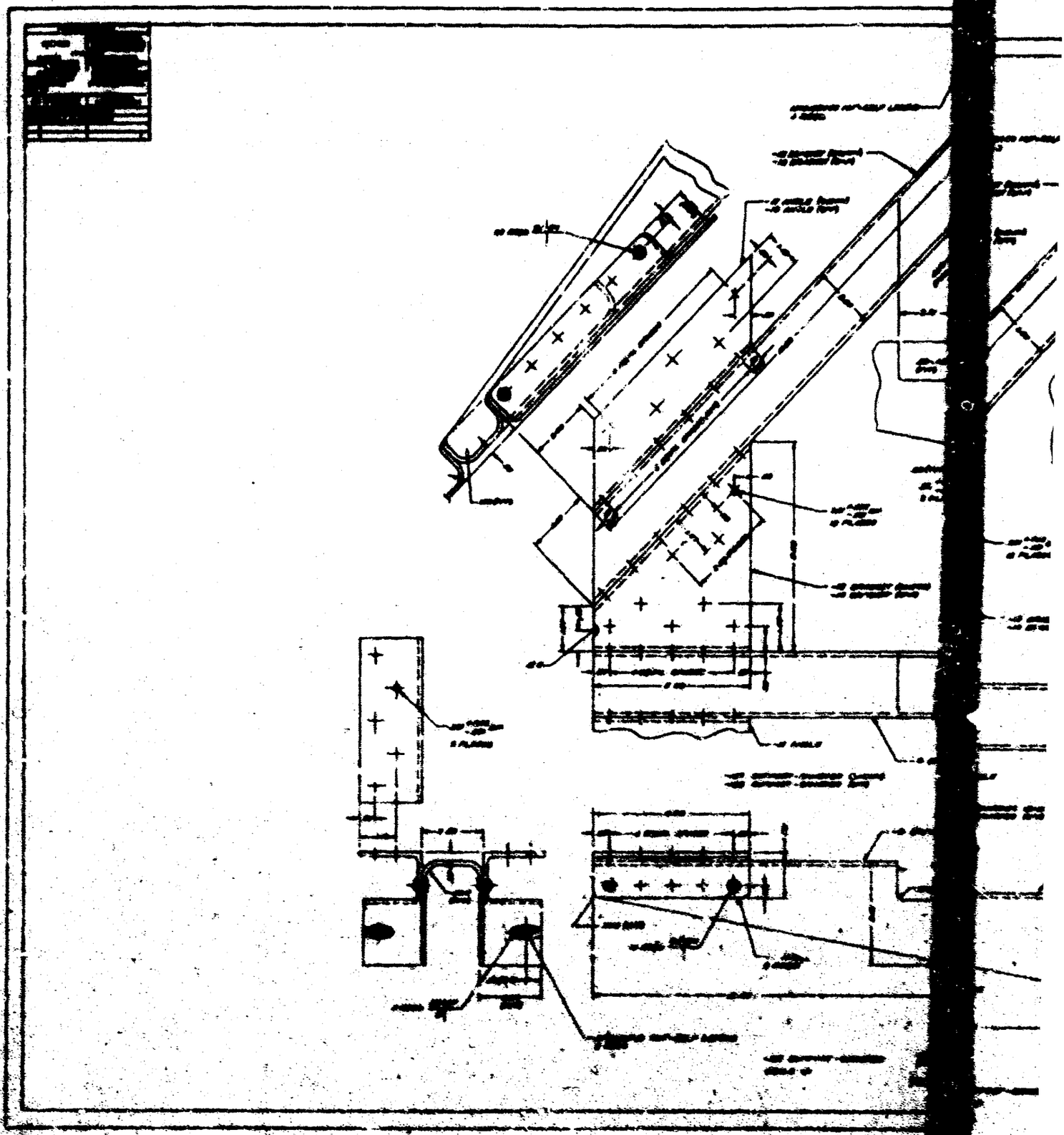

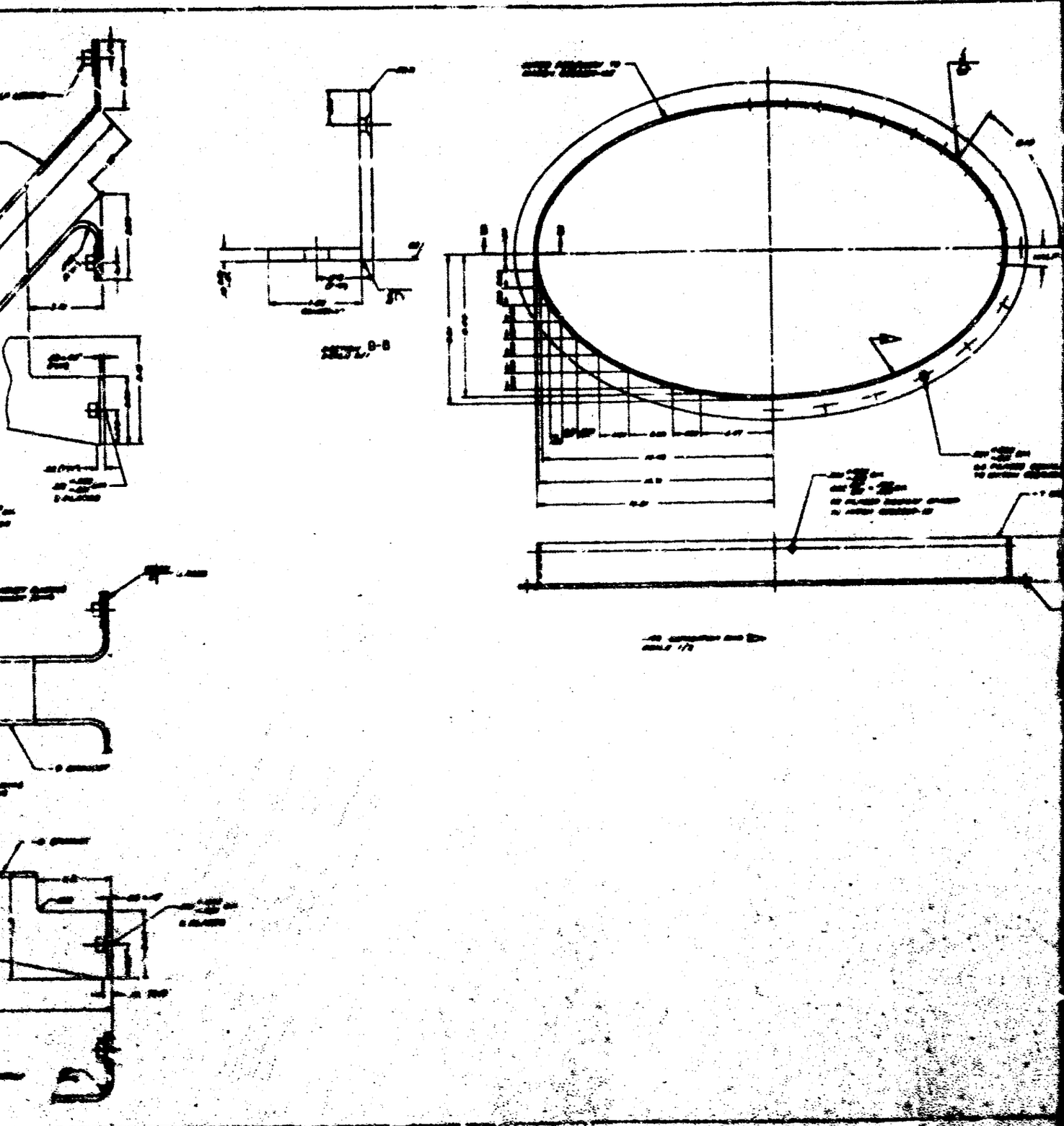

Figure 31. [illegible]

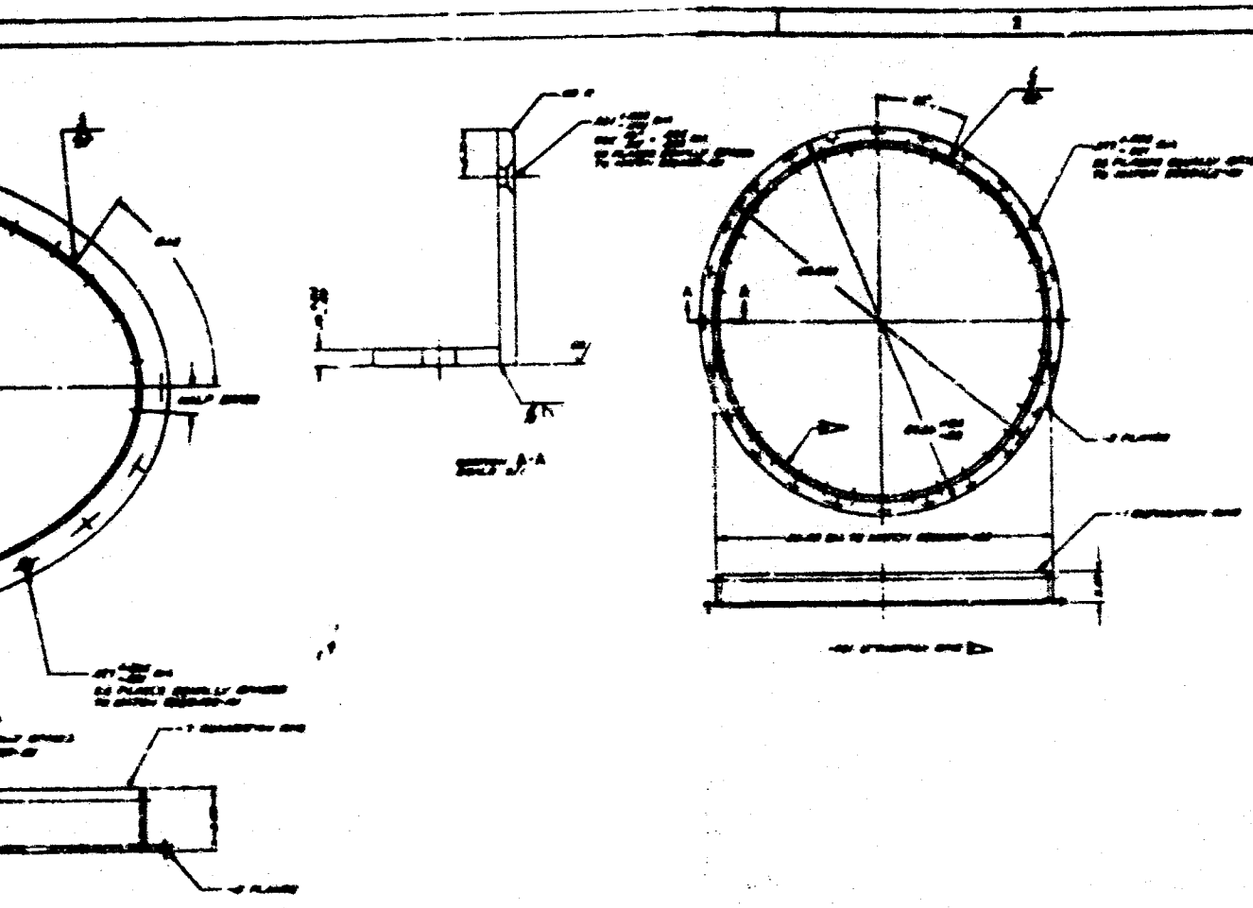

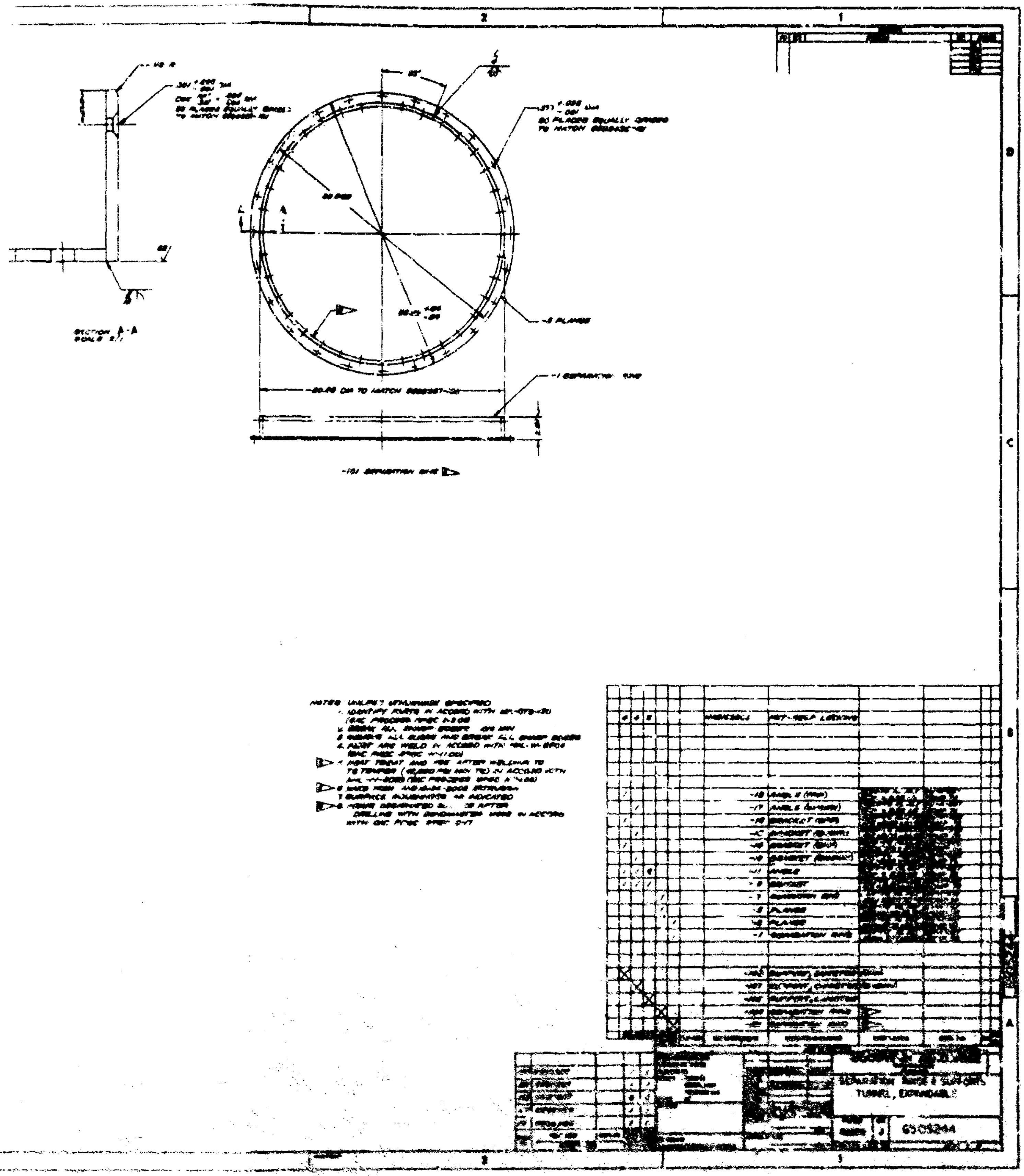

4

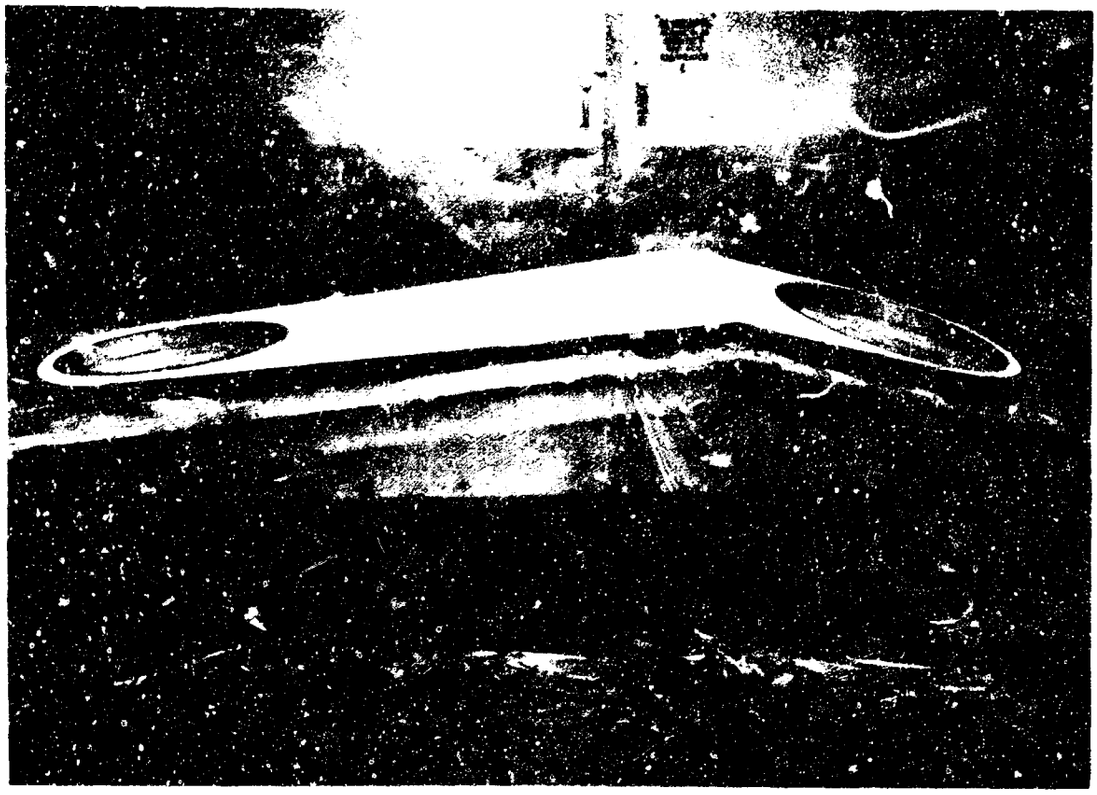

Figure 38. Prototype Tunnel Floor

During the lamination of the structural layer, separator strips were placed between each adjacent ply in the area of the floor joint. When all four plies had been placed on the mandrel, the four plies of reinforcing strips were inserted in place of the separator strips and bonded with polyester adhesive. The rigid epoxy bond was then fabricated to attach the composite wall structural layer to the rigid floor structure with an eight-ply splice. The entire assembly was again vacuum bagged and oven cured. The completed prototype tunnel four-ply Dacron cloth structural layer with the completed wall-floor epoxy joint is shown in Figure 41.

(3) Micrometeoroid Barrier. While the individual plies of the pressure bladder and the structural cloth layer were fabricated on the mandrel with lap seams, the 2-inch thick, 1.2-pcf density, flexible polyether foam micrometeoroid barrier was placed on the mandrel in patterns that formed butt joints. The reason for this procedure is obvious. Polyester adhesive was used to bond the foam to the structural layer. The completed foam layer is shown in Figure 42.

(4) Outer Cover and Thermal Coating. As previously discussed in this section, a nylon cloth outer cover was substituted for the film-cloth laminate of the actual tunnel design. The nylon cloth patterns were placed over the foam barrier on the mandrel with lap seams. Again, polyester adhesive was used for the interlaminar bond. The entire assembly was then vacuum bagged and oven cured for the final time. The complete outer cover is shown in Figure 43.

The tunnel with the enclosed mandrel was removed from the fabrication support fixture,

and the rigid foam mandrel was chipped from the tunnel interior. The Topolic tapes were installed on the bladder seams, and the film-cloth tapes were installed at the pressure bladder to floor joints. After the interior lighting and hand rope standoff locations were masked, both the interior and exterior surfaces of the tunnel were painted with titanium dioxide pigmented Hypalon paint. The use of this substitute thermal coating was discussed earlier in this section. The completed tunnel is shown in Figure 35.

d. Packaging Canister and Separation System. The prototype packaging canister design is shown in Figure 44. It was fabricated by riveting lightweight aluminum honeycomb sandwich panels together at the edges. For simplification in fabrication, a flat leading edge surface was used rather than the curved aerodynamic surface required for a flight hardware canister. The deviation from required materials was discussed earlier in this section. There was no deviation in the installation of the canister separation system for deployment, however. All brackets with separation screws and pyrotechnic guillotines were properly installed.

The lightweight prototype canister proved to be too flexible for proper handling, so the reinforcing panels and stiffeners shown in Figure 44 were added to the fabricated canister and incorporated in the design as revision A.

e. Locomotion Aids and Interior Lighting. The crew locomotion aids and tunnel interior lighting specified for the tunnel design were installed in the prototype tunnel. They were initially installed with double-backed tape in several locations while being evaluated by the human factors engineers. When final locations had been determined, the Sylvania flexible strip lighting was cemented in place along each side of the tunnel wall. The hand rope standoffs were cemented to the floor, and the cords with their end clamps were installed.

3. Weight Statement

The weight statement given in Table II is the actual weight of the prototype tunnel and its components.

Table II. Weight Statement

Transfer Tunnel		212 lb
Expandable Wall	101.8 lb	
Sandwich Floor	88.2	
Hatch Attachment-Separation Rings	13.6	
Lighting and Locomotion Aids	8.4	
Packaging Canister		102 lb
Sandwich Cover	81.1 lb	
Pyrotechnic Separation System	20.9	
Total Weight		314 lb

The expandable wall weight includes the wall-floor attachment weight. Based on sample weights, the expandable wall alone should weigh 85 pounds, which would leave 16.8 pounds for the wall-floor attachment weight. The estimate for this attachment weight is 16.1 pounds.

4. Tunnel Mounting Adapters

Provisions are necessary for supporting the tunnel hatch attachment rings during shipping and during the zero-G flights. Accordingly, adapters were designed and fabricated to attach to the tunnel rings and provide a separate row of mounting holes for attachment to a shipping crate or to some support in the KC-135 aircraft. The adapter designs are shown in Figure 45.

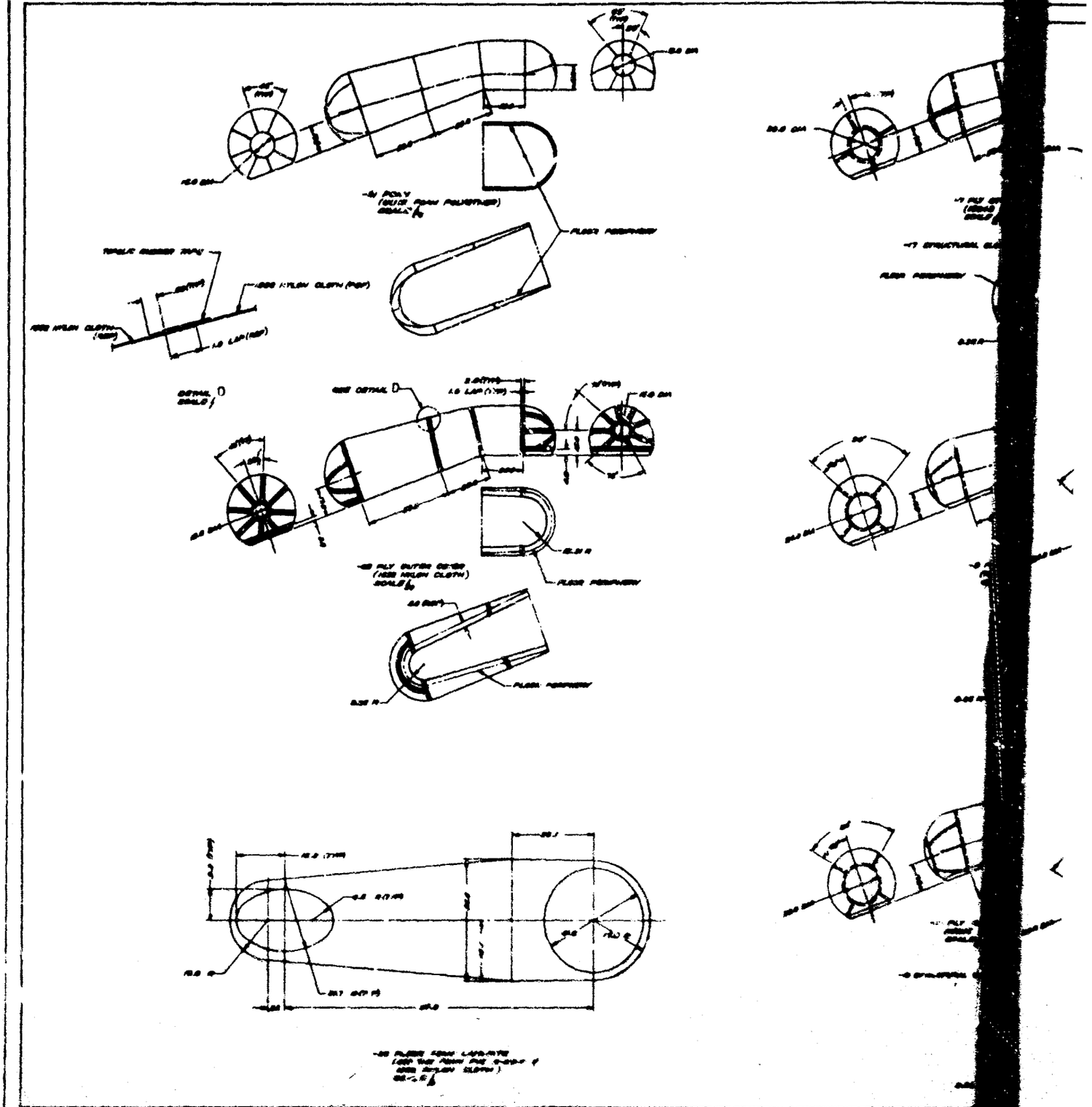

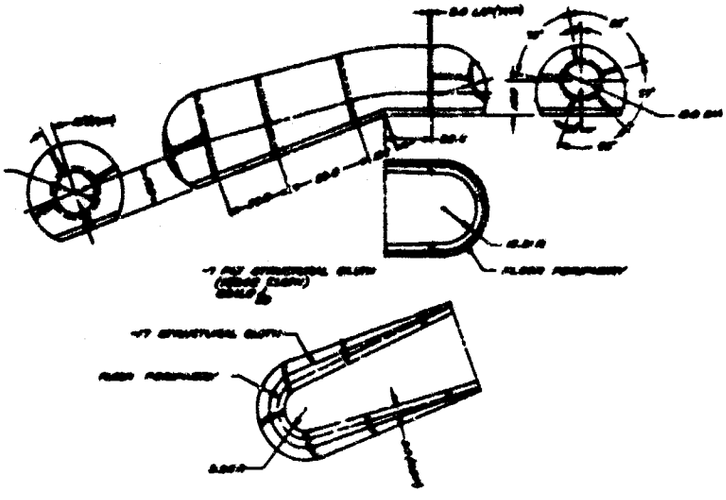

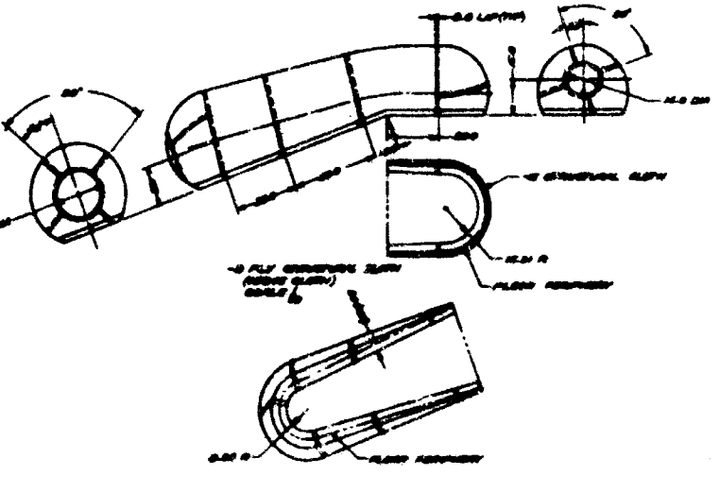

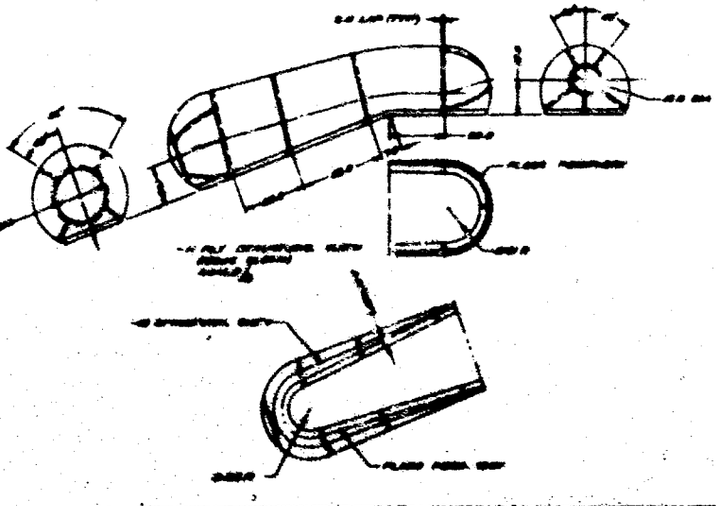

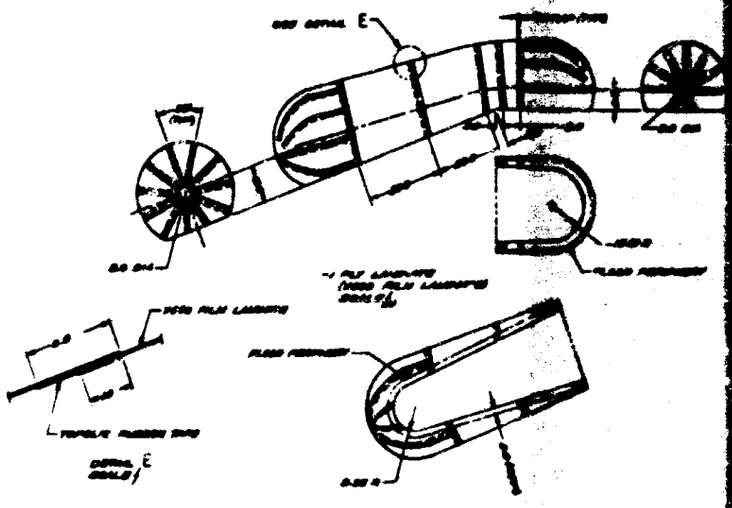

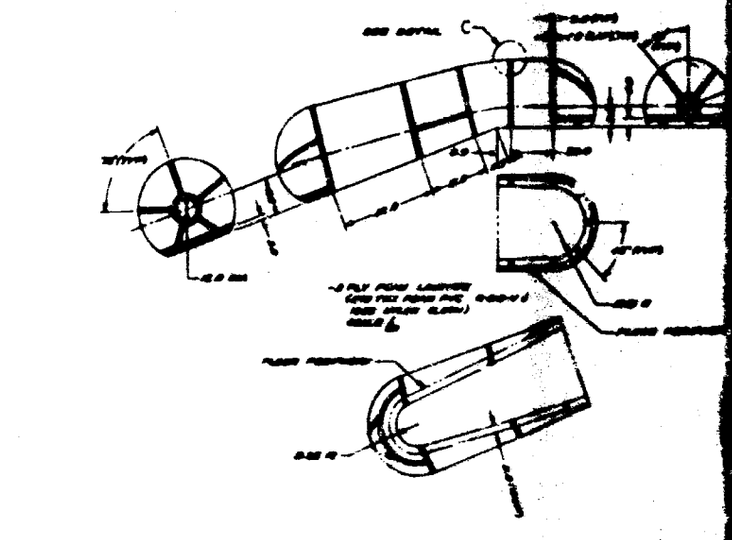

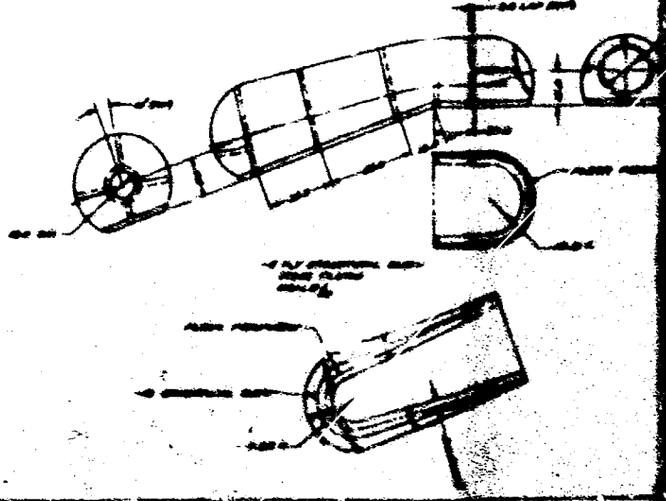

Figure 3A. Prototype

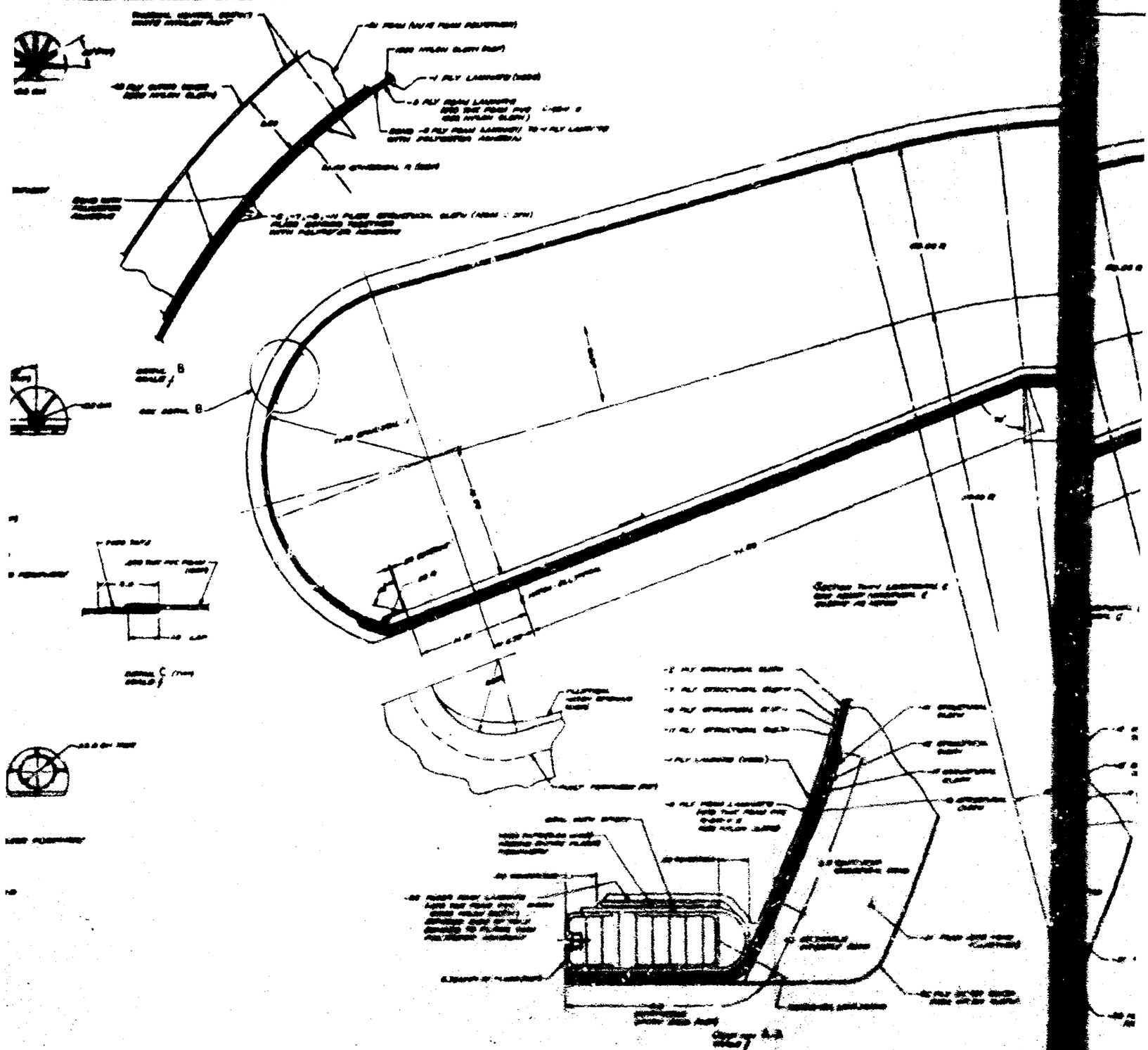

rototype Tunnel Composite Wall

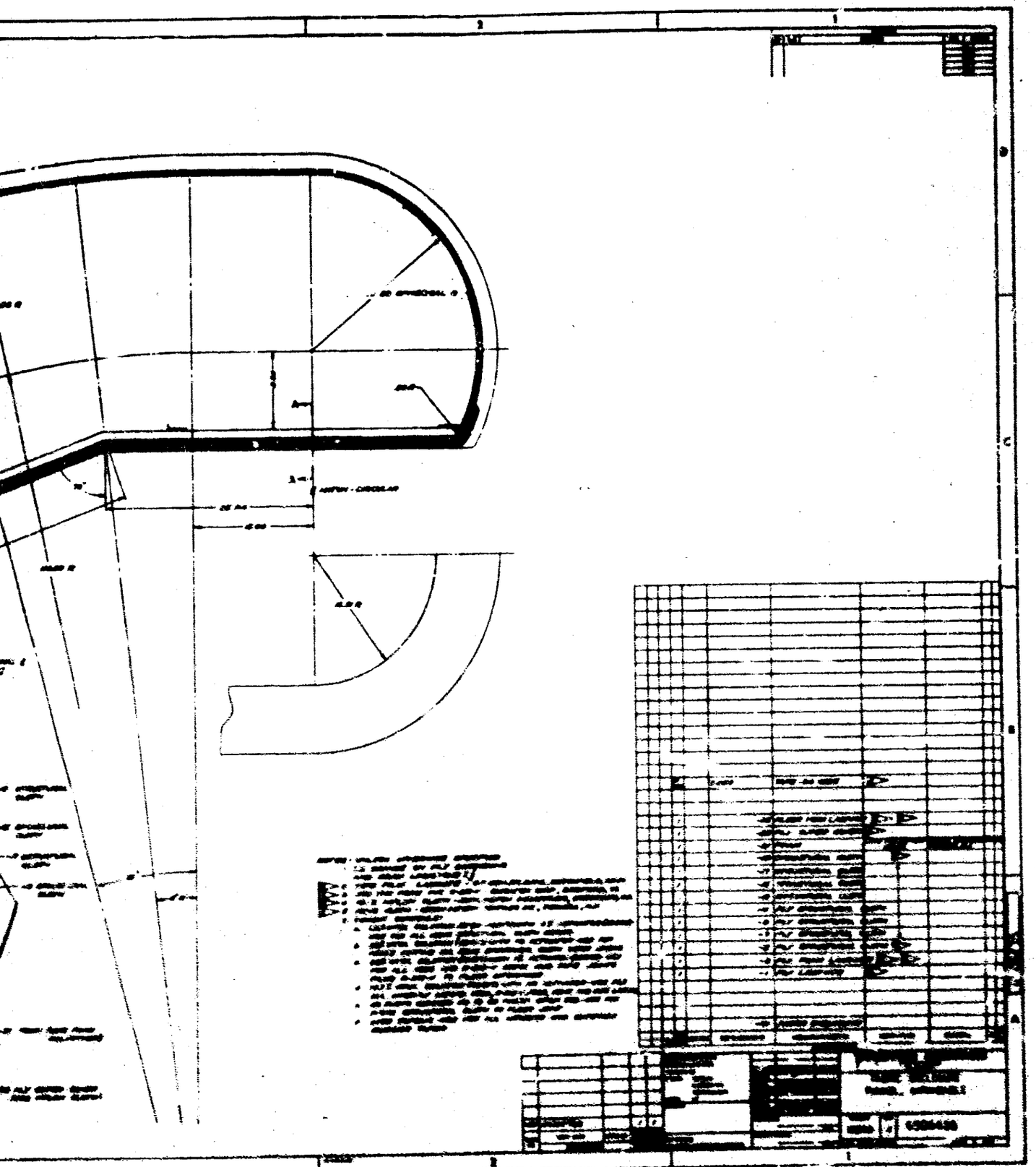

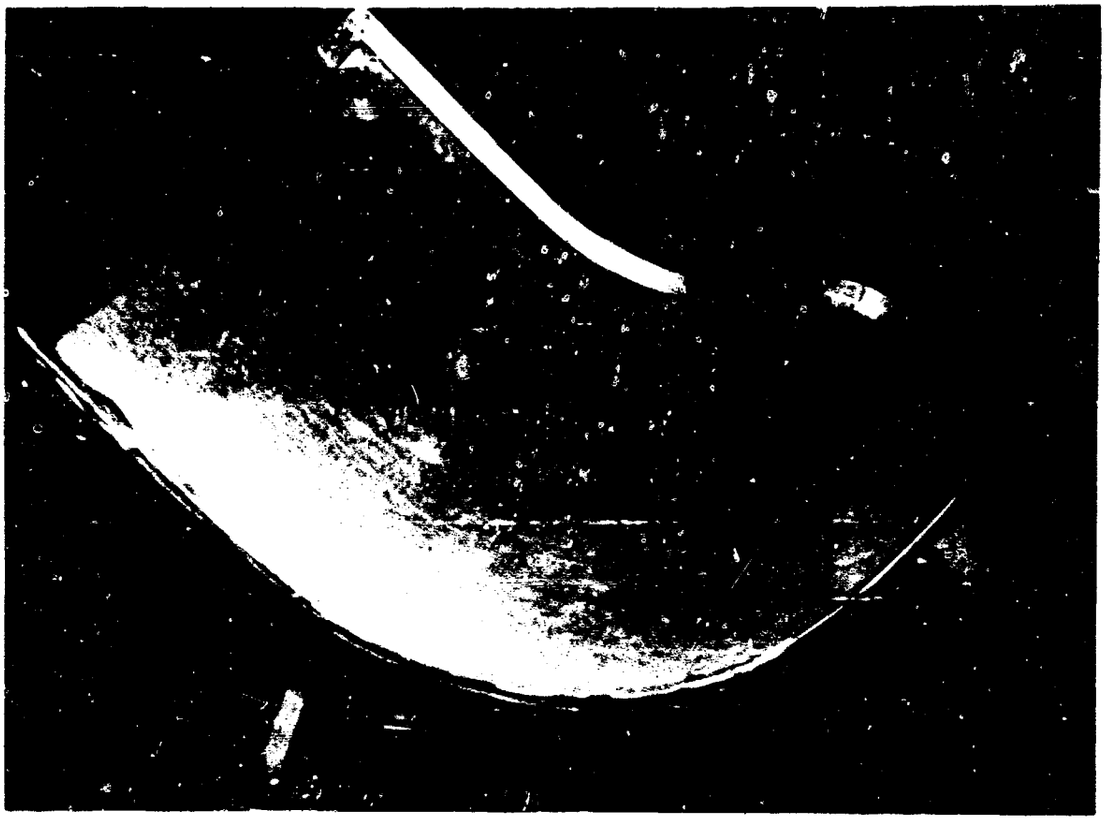

Figure 40. Pressure Bladder Contouring Fixture

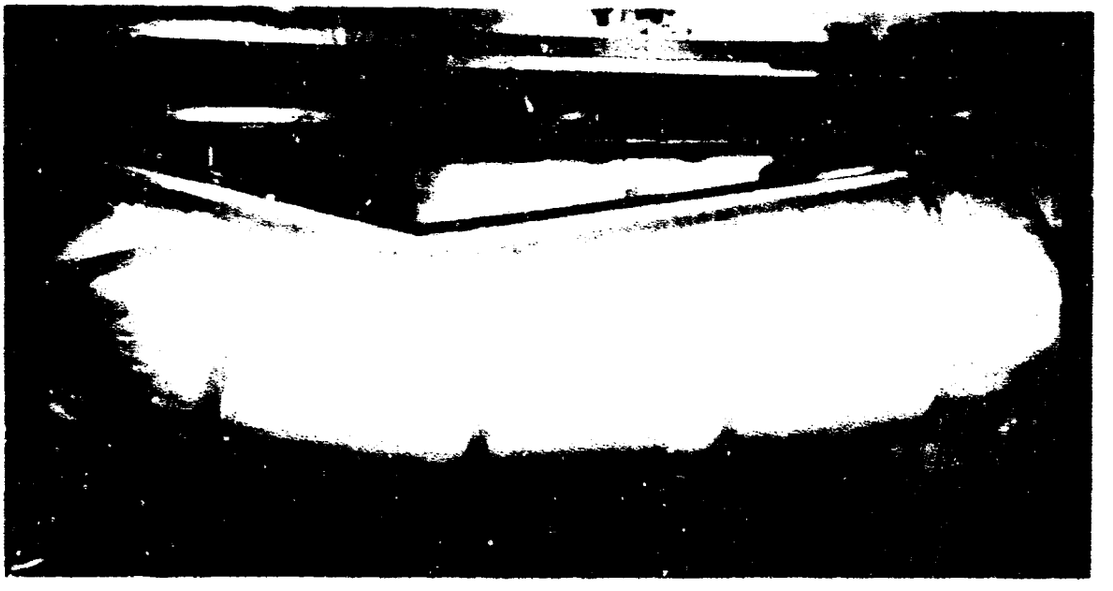

Figure 41. Structural Layer with Completed Wall-Floor Joint

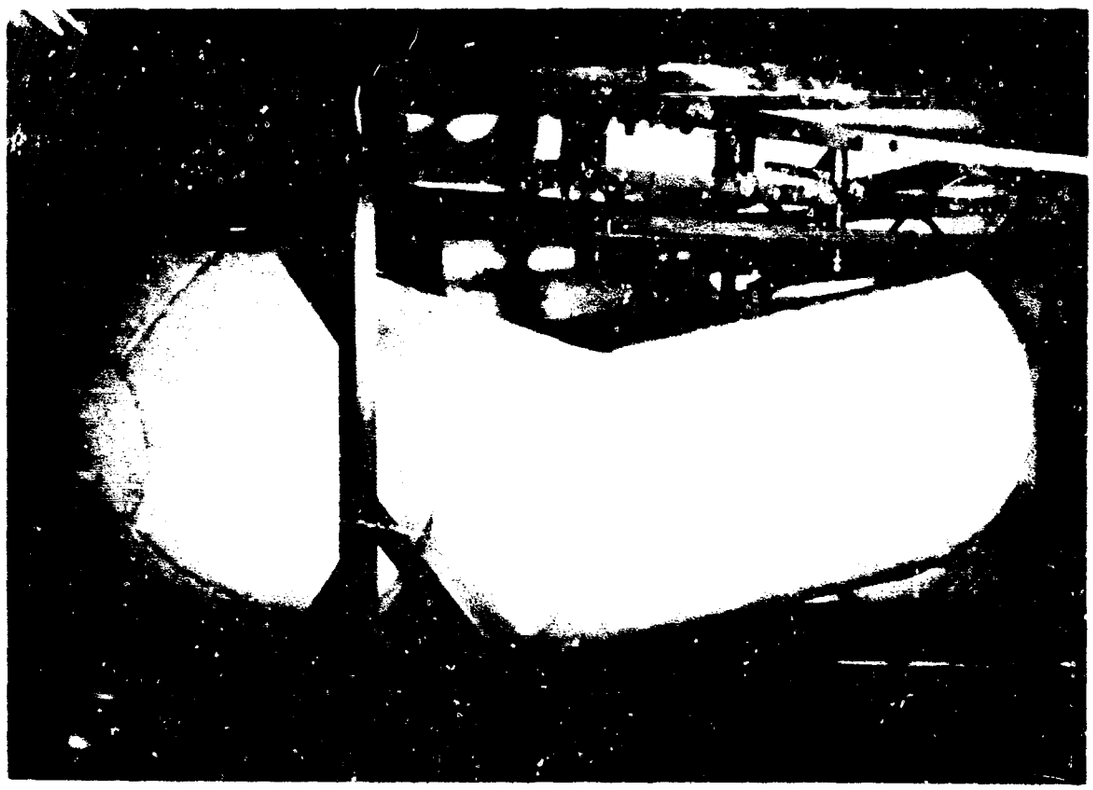

Figure 42. Prototype Flexible Foam Layer

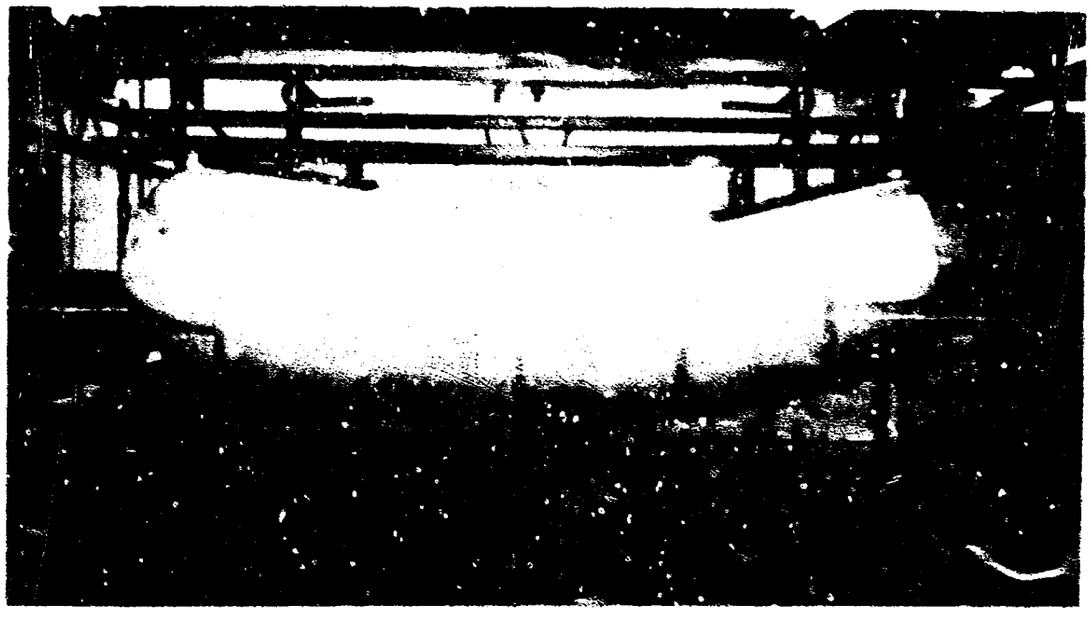

Figure 43. Completed Outer Cover

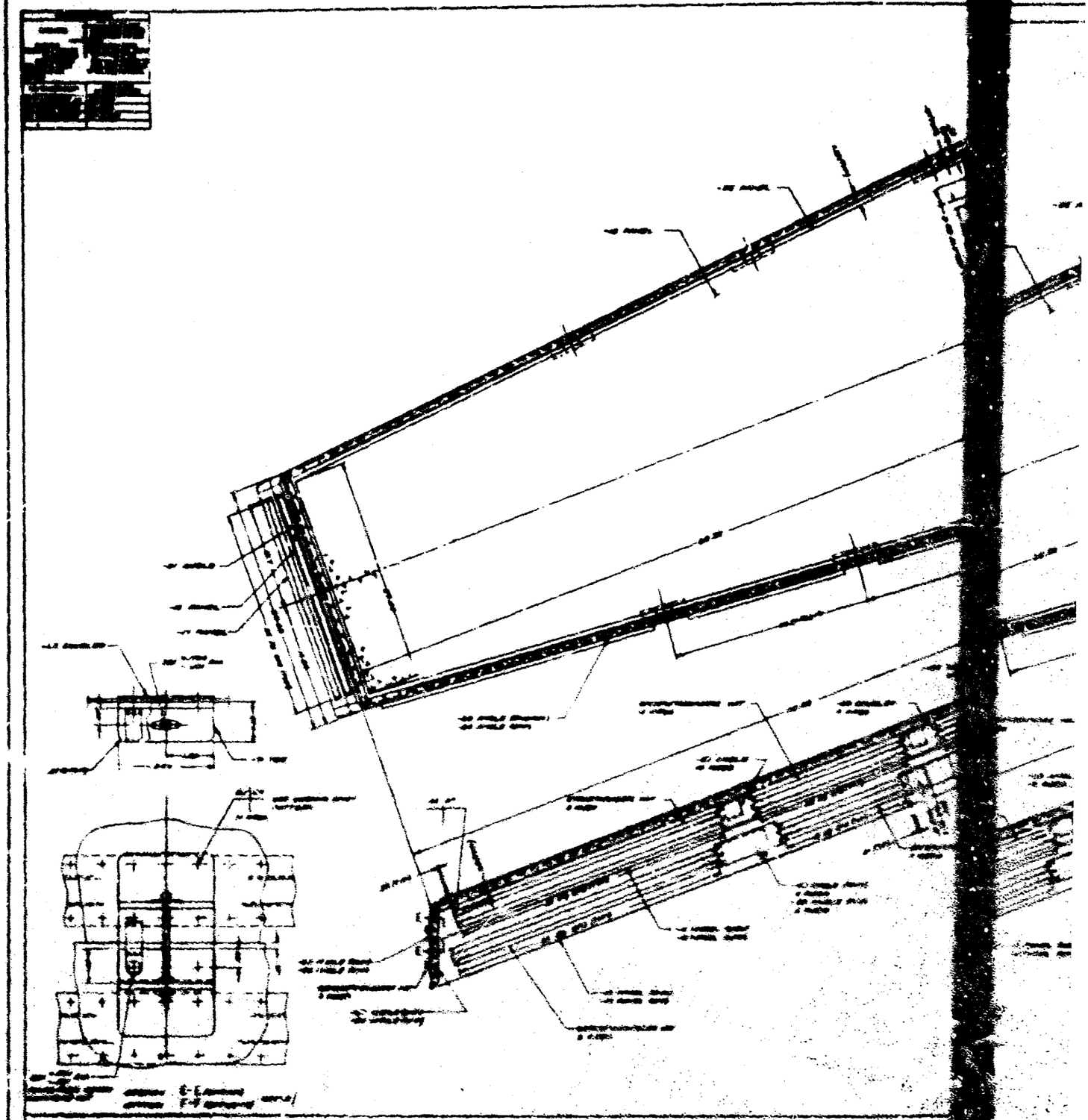

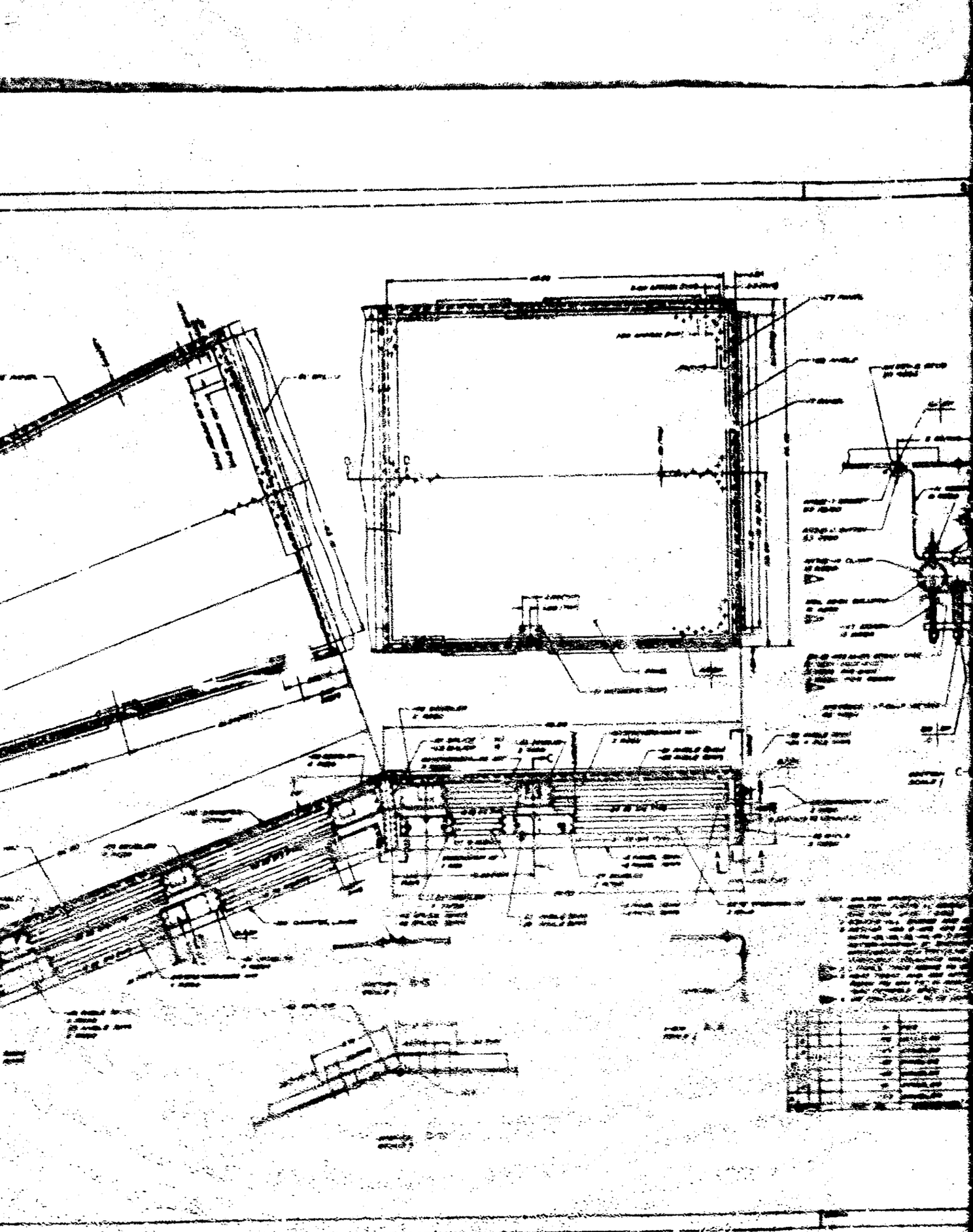

Figure 44. Prototype Thermal Packaging Container (Sheet 1 of 2)

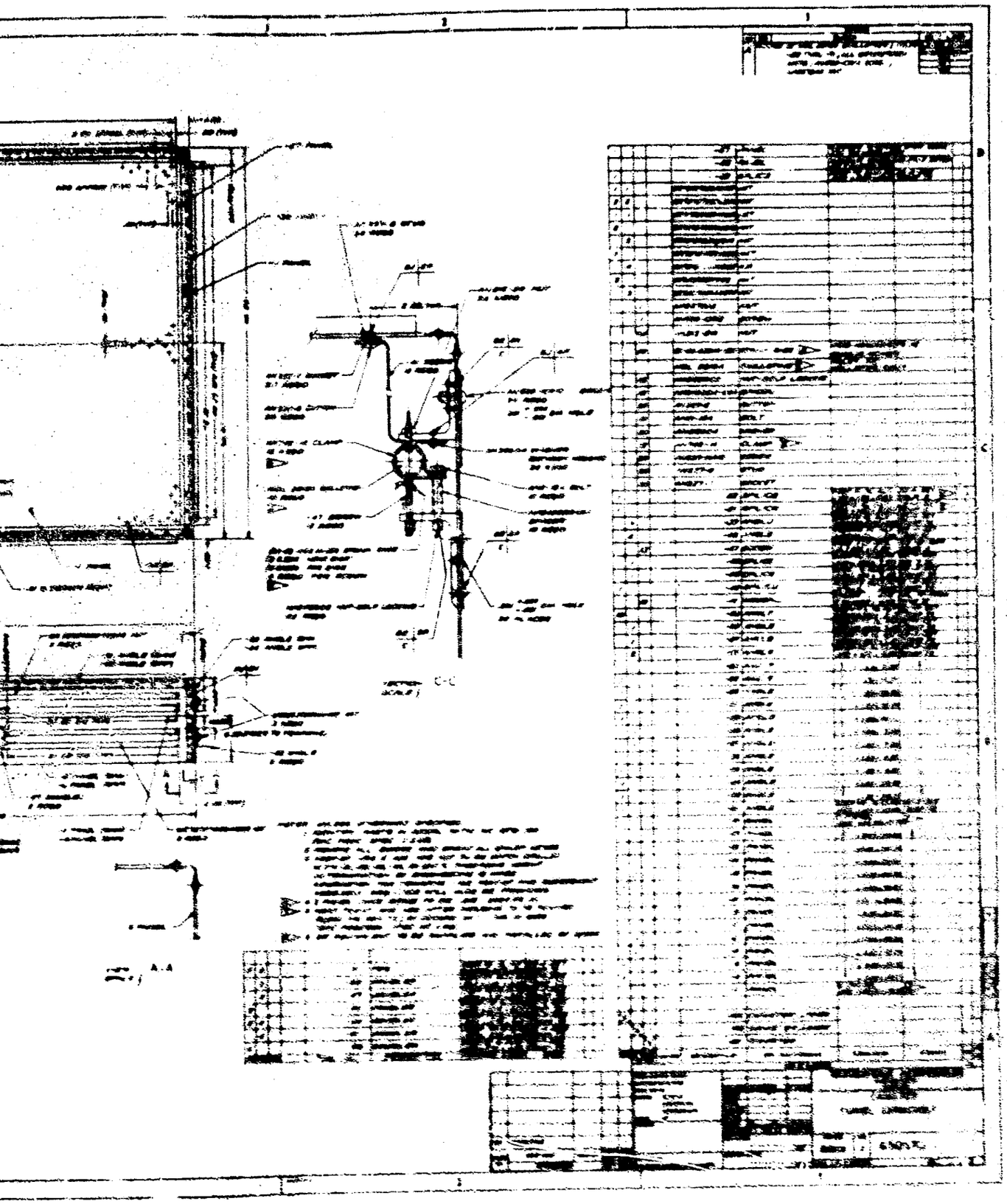

Sheet 1 of 2)

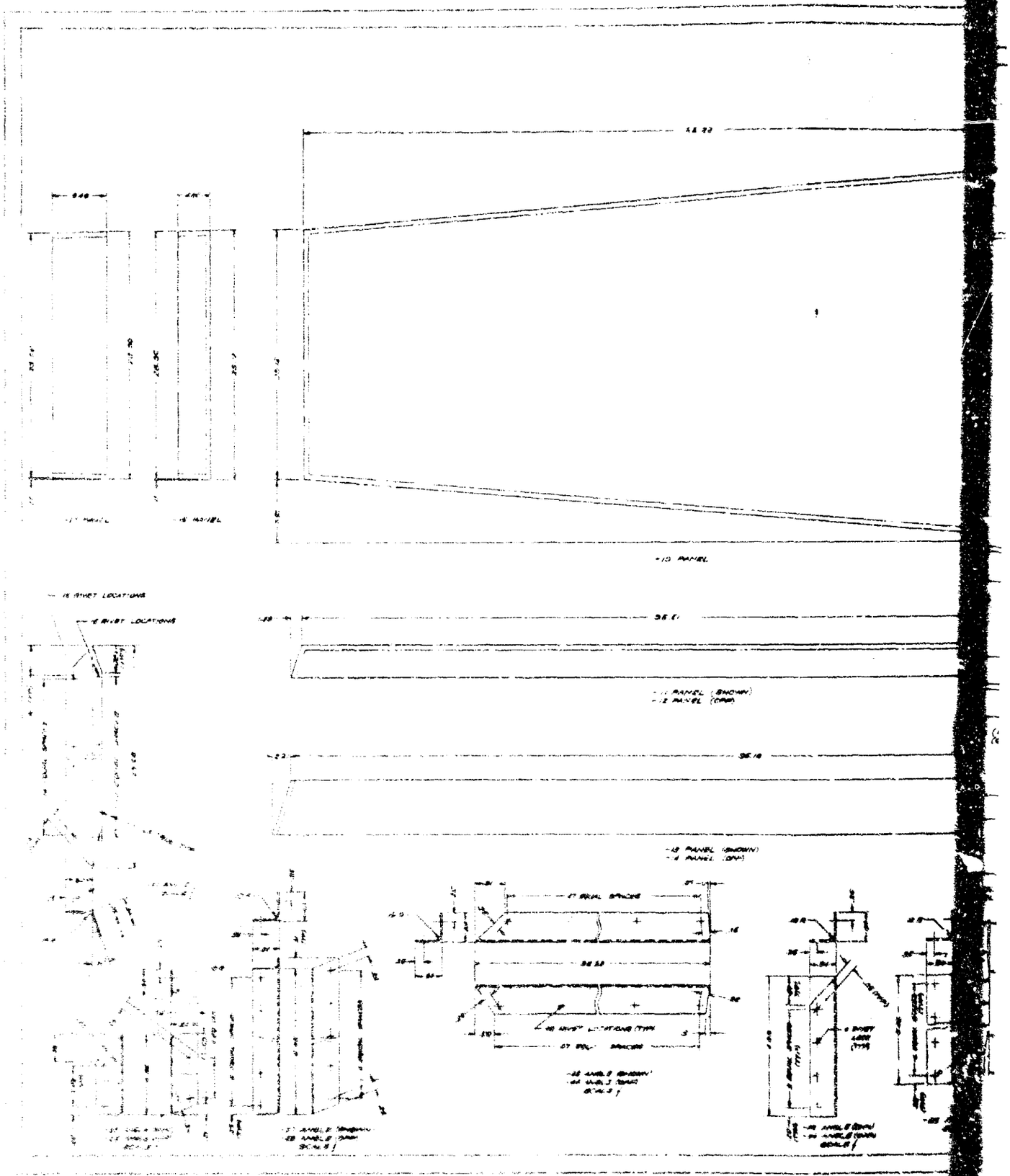

Figur

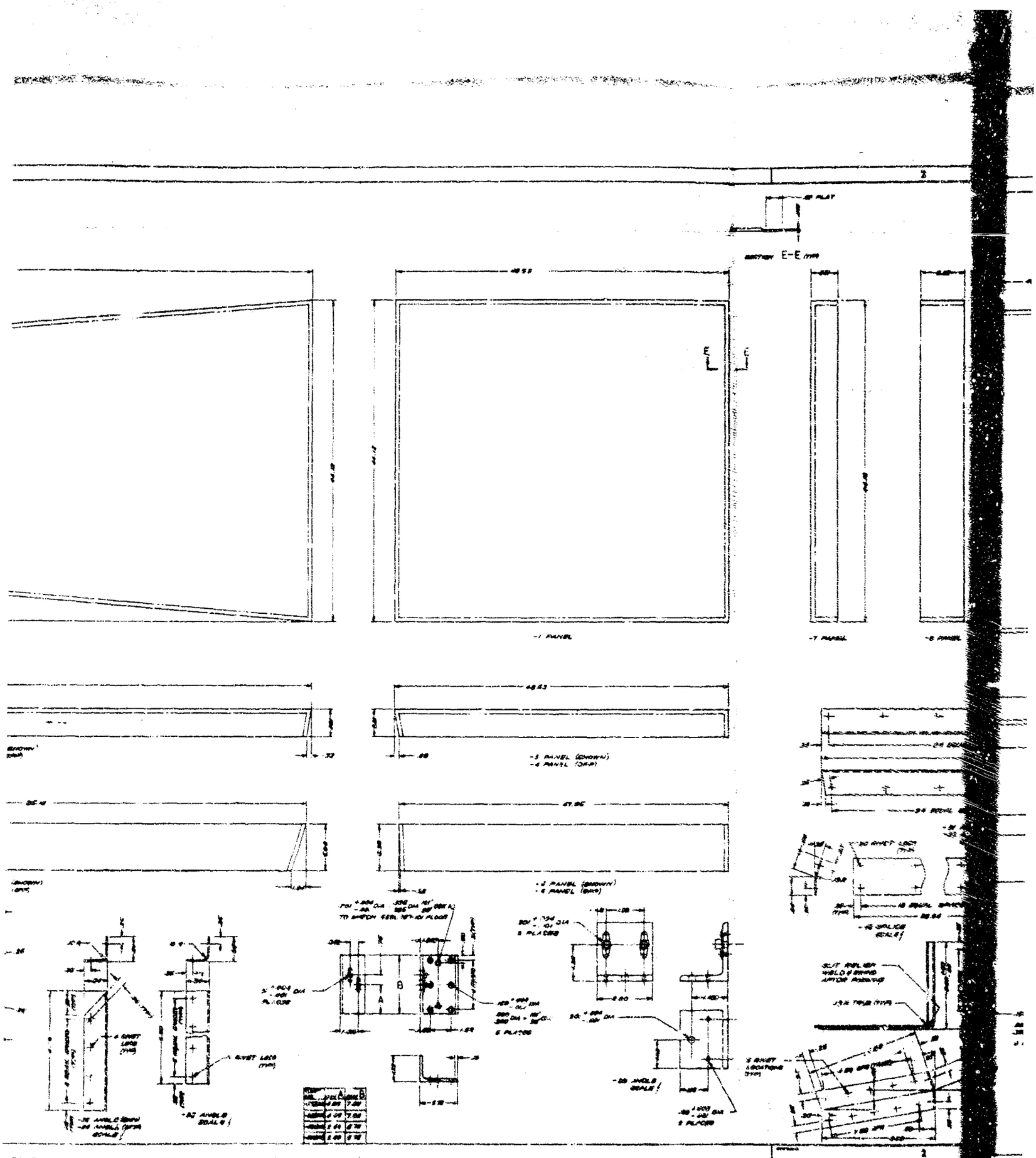

Figure 44. Prototype Tunnel Packaging Canister (Sheet 2 of 3)

3

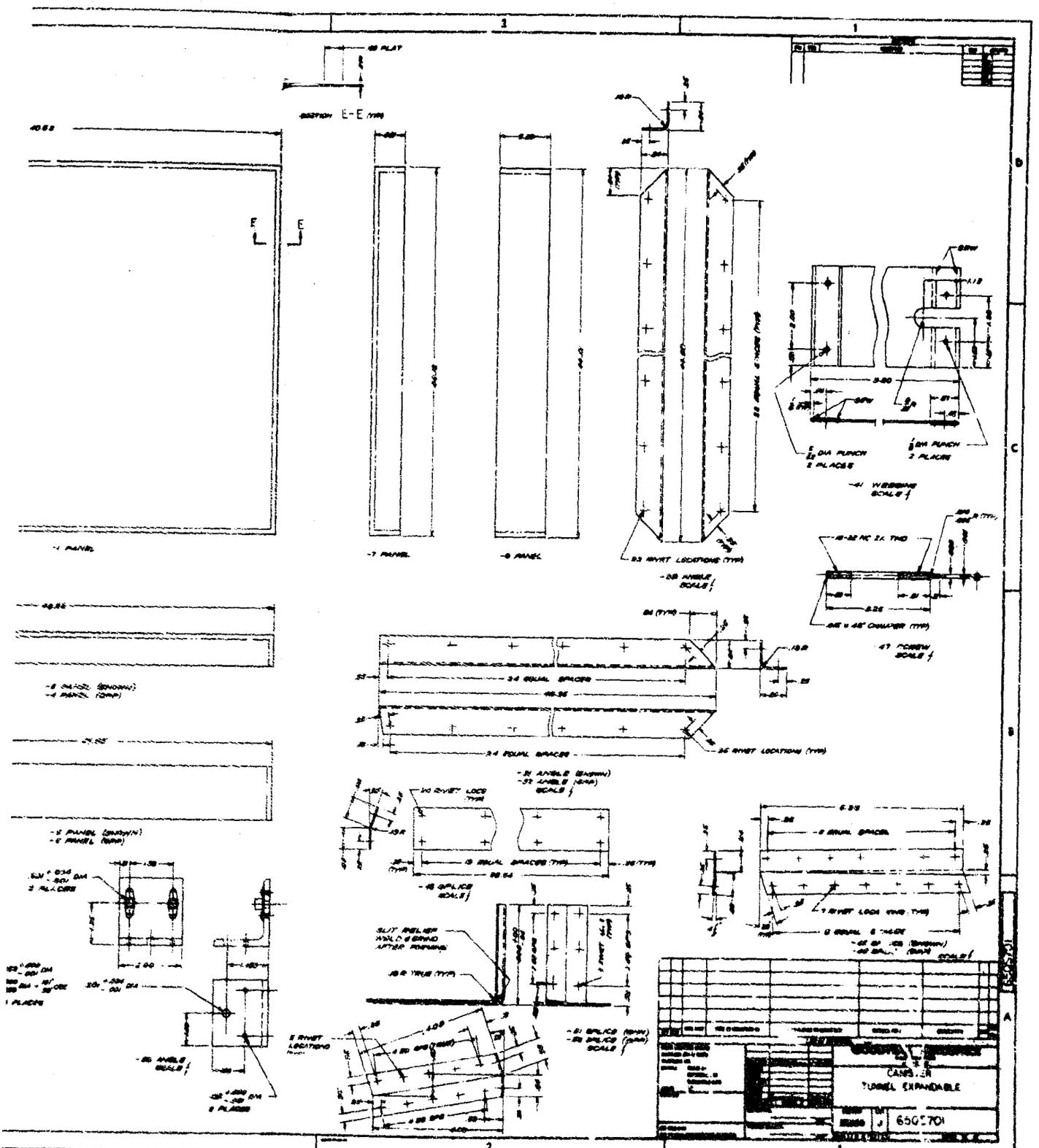

te: (Sheet 2 of 2)

3

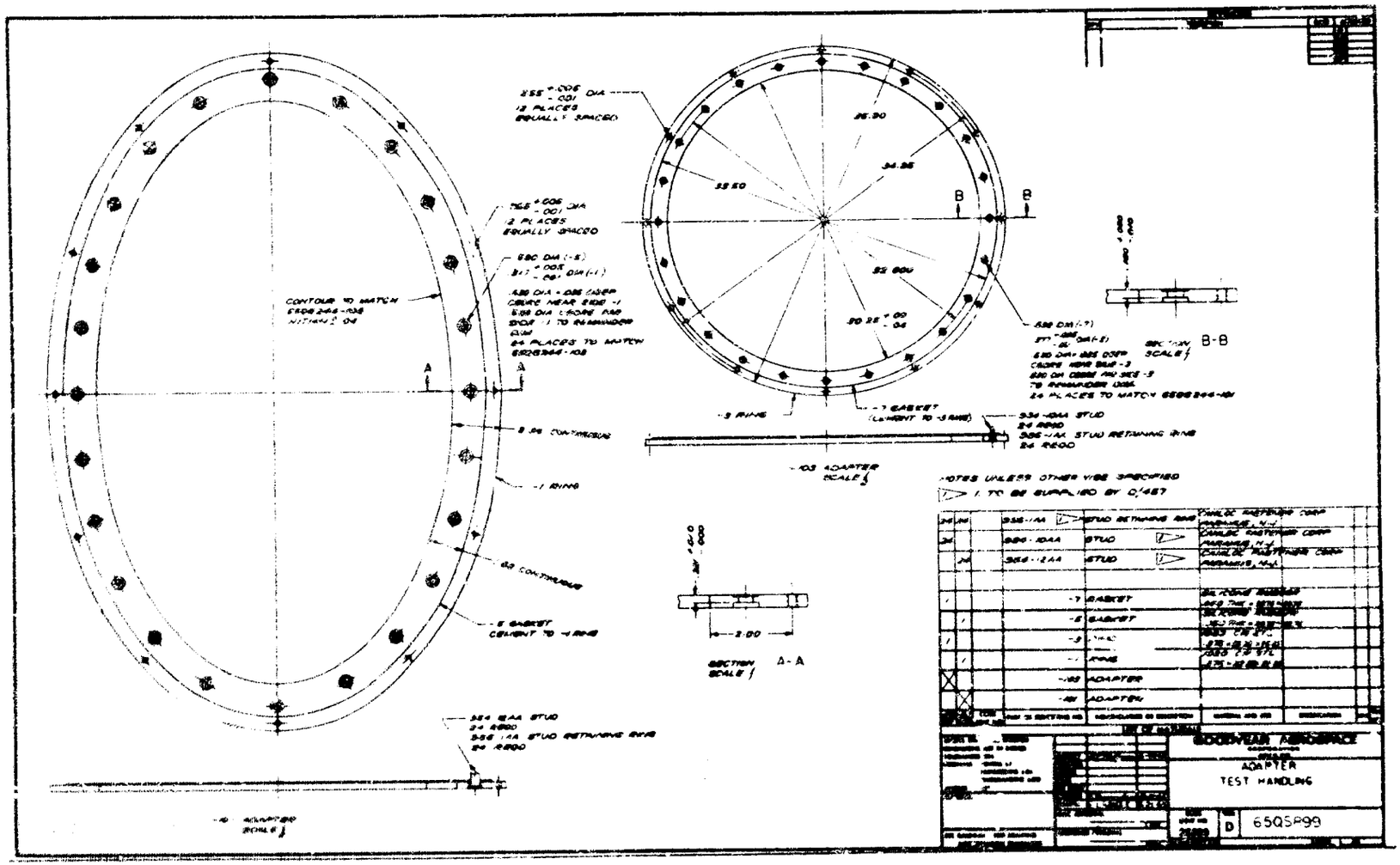

Figure 45. Tunnel Mounting Adapters

SECTION V

SUPPORTING ANALYSES

A. GENERAL

The following analyses were performed to support the tunnel design:

(1) Thermal Analysis

(2) Structural Analysis

(3) Environmental Hazards

(4) Materials Selection

The subsection on materials selection is a documentation of GAC-funded development programs specifically applicable to the tunnel design as well as a documentation of the materials qualification program conducted specifically for the tunnel design.

B. THERMAL ANALYSIS

1. Introduction

The expandable crew transfer tunnel will achieve a thermal balance dependent upon, but not completely established by, the Gemini-MSS vehicle thermal design, and the vehicle thermal design may be slightly influenced by the presence of the tunnel. The primary objective of the tunnel thermal design, preferably passive, is to maintain the interior at comfortable temperatures for astronaut transfer (75 (±25)°F) while limiting the external surface hot-spot and cold-spot temperatures to values within material capabilities (-100 to 225°F).

Thermal design optimization of the packaging canister and the tunnel itself will depend upon Gemini-MSS system parameters that have not yet been specified, and is considered beyond the scope of this study. The study will consider and define the effects on tunnel temperatures of the following parameters:

(1) Thermal coatings on the external surface of the tunnel.

(2) Thermal coatings on the internal surface of the tunnel.

(3) Thermal coatings on the Gemini-MSS surfaces adjacent to the tunnel.

(4) Tunnel orientation in relation to the earth and sun.

(5) Orbital inclination with respect to the ecliptic equator.

(6) Depressurization of the polyether foam due to micrometeoroid penetration of the outer cover.

The thermal problems and considerations of the tunnel will be defined along with the necessary corrective action. An IBM 7040 electronic computer has been utilized throughout this analysis; the resultant programs are identified as GAC program Z-0511.

2. Proposed Thermal Systems

The only major difficulty involved in the thermal design is passively maintaining the required internal temperature of 75 (±25)°F. A reasonably good match with this requirement may be made for any orbit with most tunnel orientations if the orbit and orientation are specified before the thermal coatings are selected. Allowance must be made for degradation of the thermal coatings; tolerances and degradation of the vehicle, tunnel, and coating thermal parameters as well as computational accuracy; and other system variables that affect the 50°F temperature tolerance.

As an illustration of the results of this analysis, three possible tunnel thermal designs, summarized in Table III, are presented in the following paragraphs. Common features are addition of thermal insulation to the floor and application of a low solar absorptance/emittance (α/ϵ) ratio white paint to the tunnel interior.

(1) For a day-night orbit passing through the earth-sun line with unknown tunnel orientation, the tunnel would be uniformly covered with stripes of aluminized silicone white paint on an aluminized film substrate. The average ratio of α/ϵ would be approximately 2; to prevent excessive hot-spot temperatures on the outer surface, copper drop threads would be woven through the polyether foam to obtain a conductivity of 0.5 Btu-in./hr-ft^2-°F. Neglecting material, system, and computation uncertainties, the internal temperature would be 60 (±50)°F.

(2) For a day-night orbit with an optimum tunnel orientation, a horizontal tunnel orientation may be specified. The above thermal coatings would be utilized with the quantity of painted stripes varied locally to alleviate hot spots and eliminate the requirement for drop threads. Again neglecting material, system, and computation uncertainties, the internal temperature would be 75 (±20)°F.

(3) For a twilight orbit over the dawn-dusk areas of the earth with an optimum tunnel orientation, a tunnel orientation away from the earth may be selected. Thermal coatings would be an aluminized film substrate with thin layers of silicon monoxide applied in some locations and stripes of aluminized silicone white paint applied unevenly over the entire surface. No drop threads would be required, and again neglecting material, system, and computation uncertainties, the internal temperatures would be 75 (±20)°F.

Table III. Proposed Thermal Systems

Type of Orbit	Tunnel Orientation	Thermal Coatings	Copper Drop Threads	Internal[d] Temperature (°F)
Day-Night	Any	a, b	Yes	60 (±50)
Day-Night	Optimum	a, b	No	75 (±20)
Twilight	Optimum	a, b, c	No	75 (±20)

[a] Aluminized film substrate.
[b] Aluminized silicone white paint.
[c] Silicon monoxide on aluminized film substrate.
[d] Tolerances include thermal transients and variation in thermal parameters only. External surface temperatures are -100 to 225°F.

3. Technical Discussion

a. Effect of Thermal Coating on Temperature. One of the many parameters that will affect expandable crew transfer tunnel temperatures is the orbit. A 165-mile altitude circular orbit (90-minute orbital period) is presumed as a typical condition. The position of the orbital plane with respect to the earth-sun line is much more critical and depends not only upon the orbital inclination to the equator but also upon the time of day and date of launch. Two extreme orbits are a day-night orbit passing through the earth-sun line and a twilight orbit over the dawn-dusk areas of the earth; temperatures in any orbit will generally fall within the limits set by these two orbits. The day-night orbit is possible with equatorial or polar orbits; the twilight orbit is possible only with a polar orbit. The former is considered the more likely.

The tunnel may be roughly approximated as a cylinder with spherical ends. Several conclusions may be attained by computing the temperature of an isothermal longitudinally oriented cylinder and sphere in orbit. Taking the albedo of the earth as 0.36, the energy balance on a sphere in a twilight orbit is

$$0.25\,\bar{C}\,\alpha + 0.16\,\bar{C}\,F_{S\text{-}E}\,\epsilon = \epsilon\sigma T^4 \tag{1}$$

where the first term is solar heating, the second is earth radiation heating, and the third is reradiation. Equation 1 reduces to

$$\sigma T^4 = 25.48 + 110.60\,\alpha/\epsilon. \tag{2}$$

The average temperature of a sphere in a day-night orbit is

$$\frac{0.25\,\bar{C}\,\alpha\int_{0^\circ}^{105^\circ} d\beta}{\int_{0^\circ}^{180^\circ} d\beta} + 0.16\,\bar{C}\,F_{S\text{-}E}\,\epsilon + \frac{0.36\,\bar{C}\,F_{S\text{-}E}\,\alpha\int_{0^\circ}^{90^\circ}\cos\beta\,d\beta}{\int_{0^\circ}^{180^\circ} d\beta} = \epsilon\sigma T^4, \tag{3}$$

since the sphere enters the umbra at $\beta = 105$ degrees. The added term is albedo heating. Equation 3 reduces to

$$\sigma T^4 = 25.48 + 82.77\,\alpha/\epsilon. \tag{4}$$

For a cylinder in a twilight orbit,

$$\bar{C}\,\alpha\,z + 0.16\,\bar{C}\,F_{C\text{-}E}\,\epsilon = \epsilon\sigma T^4 \tag{5}$$

or

$$\sigma T^4 = 27.09 + 140.82\,\alpha/\epsilon. \tag{6}$$

For a cylinder in a day-night orbit,

$$\frac{\bar{C}\,\alpha\int_{0^\circ}^{105^\circ}\cos^2\beta\,d\beta}{\pi\int_{0^\circ}^{180^\circ} d\beta} + 0.16\,\bar{C}\,F_{C\text{-}E}\,\epsilon + \frac{0.36\,\bar{C}\,F_{C\text{-}E}\,\alpha\int_{0^\circ}^{90^\circ}\cos\beta\,d\beta}{\int_{0^\circ}^{180^\circ} d\beta} = \epsilon\sigma T^4 \tag{7}$$

or

$$\sigma T^4 = 27.09 + 65.76\,\alpha/\epsilon. \tag{8}$$

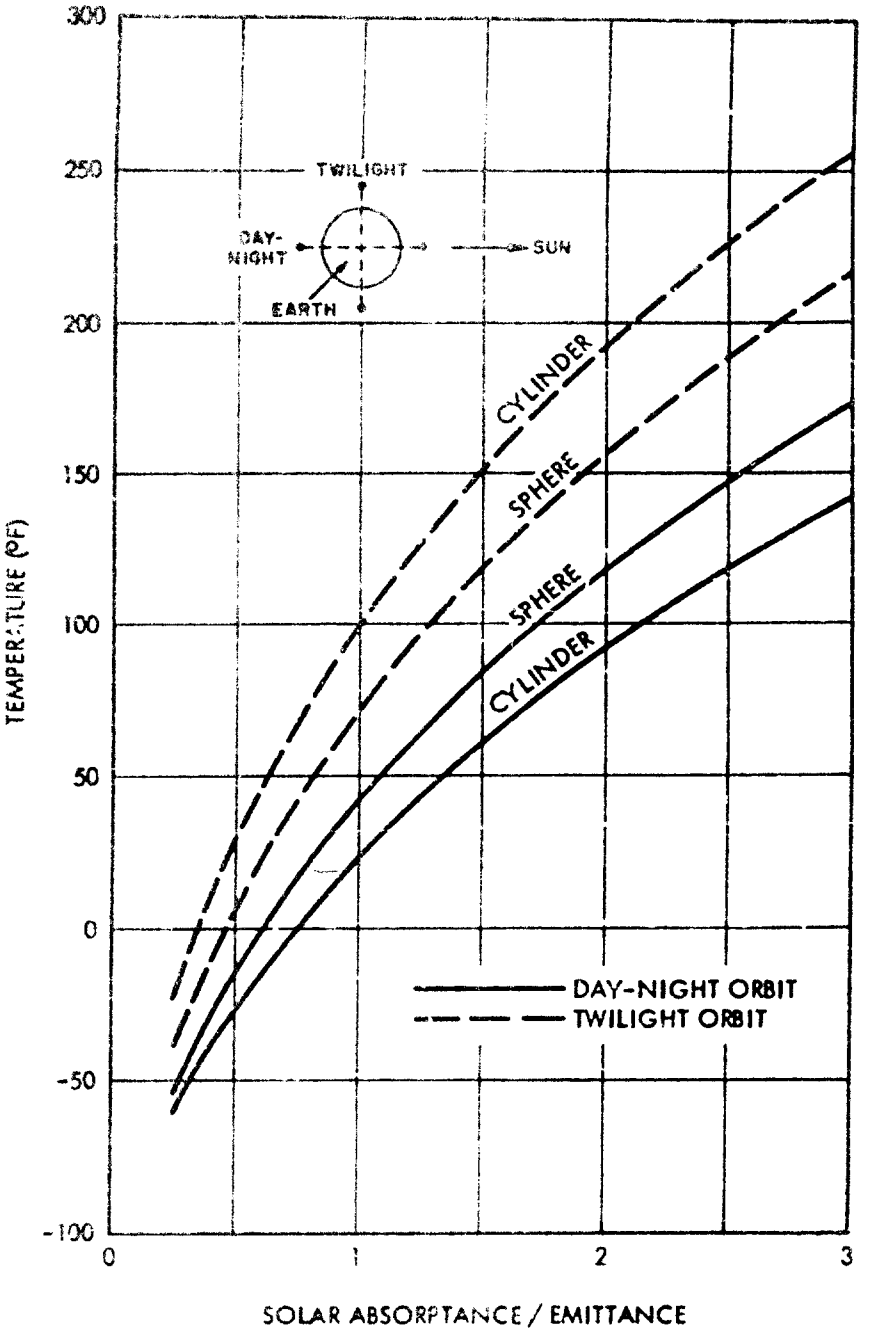

Figure 46. Sphere and Cylinder Isothermal Temperatures in Near-Earth Orbit

The temperatures are seen to be a function of the ratio α/ϵ, which is established by the thermal control coating. A plot of equations 2, 4, 6, and 8 is presented in Figure 46. The cylinder temperatures are more extreme than the sphere temperatures, so that a somewhat conservative anlysis of the tunnel may be obtained by neglecting the spherical ends. For comfortable temperatures, an α/ϵ ratio between 1 and 3 appears desirable for a day-night orbit. These α/ϵ ratios may be easily attained by a surface of an aluminized film substrate (α = 0.15, ϵ = 0.05, α/ϵ = 3) covered in part with an aluminized silicone white paint ($\alpha = \epsilon$ = 0.25, α/ϵ = 1). Spacings between the paint stripes or patterns would permit average ratios any-

where between 1 and 3. An α/ϵ ratio of 1 or slightly less appears desirable for a twilight orbit. These ratios may be obtained by applying the above white paint to a surface of silicon monoxide on an aluminized film substrate ($\alpha = 0.15, \epsilon = 0.5$, $\alpha/\epsilon = 0.3$).

Temperature differentials across the tunnel interior will exist due to uneven heating of the external surfaces. In order to minimize these differentials, the internal heat transfer should be maximized. In the absence of forced convection, the primary mode of heat transfer will be thermal radiation. A thermal coating on the interior surface with a high emittance is therefore desired, but the solar absorptance should be low (white surface) to improve lighting. A number of white paints having a low α/ϵ ratio are available, including the zinc oxide pigmented paint developed by GAC for the lunar shelter project. Stability should not be a problem, since the internal surface is not exposed to ultraviolet radiation or vacuum.

b. Hot- and Cold-Spot Temperatures. The tunnel configuration used for this study was preliminary in nature and is not reflected in the final design drawings. Thermal construction and properties of the tunnel walls are presumed as follows from the exterior surface to the interior surface:

(1) Outer cover consisting of a thermal control coating, nylon cloth, a layer of polyester adhesive, Capran film, adhesive, nylon cloth laminate, and adhesive. This composite has a mass of 0.095 psf, a thickness of 0.017 inch, specific heat of 0.25 Btu/lb-^{o}F, and a conductivity of 1.4 Btu-in./hr-ft^2-^{o}F.

(2) Two inches of polyether foam. This foam has a mass of 0.200 psf, specific heat of 0.23 Btu/lb-^{o}F, and a conductivity of 0.25 Btu-in./hr-ft^2-^{o}F. When the outer cover is pierced by micrometeorites, the entrapped gas will escape from the foam, reducing the conductivity to approximately 0.04 Btu-in./hr-ft^2-^{o}F.

(3) Structural layer consisting of a layer of adhesive, four layers of Dacron cloth and one of nylon joined by adhesive, and an inner layer of adhesive. This composite has a mass of 0.353 psf, a thickness of 0.062 inch, specific heat of 0.25 Btu/lb-^{o}F, and a conductivity of 1.4 Btu-in./hr-ft^2-^{o}F.

(4) PVC foam 0.070 inch thick. This foam has a mass of 0.058 psf, specific heat of 0.23 Btu/lb-^{o}F, and a conductivity of 0.25 Btu-in./hr-ft^2-^{o}F.

(5) An inner laminate that resembles the outer cover in reverse order of construction.

The inner radius of the tunnel varies from 20.8 inches at the MSS end to 21.4 inches at the Gemini end; the former is used throughout this analysis. Conduction takes place through the tunnel wall and around the tunnel wall, but due to the relatively large radius of curvature, the latter effect is negligible.

Since the polyether foam has a temperature limit of approximately 225^{o}F, a discussion of hot-spot temperatures on the external surface appears in order. In the day-night orbit, transient or variable heating occurs on the external surface. This heat is transferred through the tunnel wall by conduction and stored in the thermal mass of the wall, thereby changing its temperature. A thermal model of a slab of the wall was constructed by considering it as five nodes, located in order as (1) the internal surface, (2) center of the structural layer, (3) 1.5 inches from the external surface of the polyether foam, (4) 0.6 inch from the external surface of the polyether foam, and (5) the external surface. Node boundaries occur midway through the PVC foam, 0.05 and 0.95 inch from the inner surface of the polyether foam, and 0.15 inch from the external surface of the polyether foam. For the wall slab away from the earth on which the hot-spot temperature occurs, the differential energy equations on the five nodes are as follows:

$$
\left.
\begin{aligned}
U_{0-1}(T_0 - T_1) + U_{1-2}(T_2 - T_1) &= (WC)_1\, dT_1/d\theta \\
U_{1-2}(T_1 - T_2) + U_{2-3}(T_3 - T_2) &= (WC)_2\, dT_2/d\theta \\
U_{2-3}(T_2 - T_3) + U_{3-4}(T_4 - T_3) &= (WC)_3\, dT_3/d\theta \\
U_{3-4}(T_3 - T_4) + U_{4-5}(T_5 - T_4) &= (WC)_4\, dT_4/d\theta \\
U_{4-5}(T_4 - T_5) + C' A\alpha - \epsilon A\sigma T_5^4 &= (WC)_5\, dT_5/d\theta
\end{aligned}
\right\} \qquad (9)
$$

where

$C' = \bar{C} \cos\beta$ when $0 < \cos\beta \leq 1$,

$C' = 0$ when $-1 \leq \cos\beta \leq 0$.

With U_{0-1} based on a value of U which includes an internal surface coefficient of 1 Btu/hr-ft^2-$^\circ$F, these equations (Equation 9) are solved numerically using the backward difference method for the transient equilibrium conditions. Figure 47 presents the results of this study. The temperatures plotted are the maximum surface (node 5) temperatures. A hot-spot temperature problem is observed to exist which could be alleviated by increasing the thermal conductivity of the polyether foam, possibly by use of copper drop threads. A similar study has been accomplished for a twilight orbit by setting all derivatives in Equation 9 equal to zero and taking C' equal to $\bar{C}$. These results are presented in Figure 48.

Hot-spot temperatures may generally be alleviated by two methods other than increased thermal conductivity for a fixed α/ϵ ratio. One method would be to decrease the values of α and ϵ without changing the ratio, which dampens the day-night temperature cycle and increases the effect of conduction. The white paint and aluminized film previously presumed present the practical limit for this method. A second method, applicable only to the day-night orbit, would be to increase the external surface mass of the wall to dampen the day-night temperature cycle. This method is also evaluated using Equation 9 and is presented in Figure 49 with a polyether foam conductivity of 0.04 Btu-in./hr-ft^2-$^\circ$F. Lowering the α/ϵ ratio will of course decrease the hot-spot temperature but reduces the internal temperature below desired levels.

Cold-spot temperatures are most severe in a twilight orbit for a portion of the tunnel receiving no external heating. Such a study is obtained by setting all derivatives in Equation 9 equal to zero and taking C' equal to zero. Results are presented in Figure 50. Since the foam can withstand temperatures of approximately -300°F with an expected minimum greater than -200°F, no low temperature problem will be encountered.

c. Insulated Cylinder Internal Temperatures. Since the conductivity of the polyether foam has a significant effect on external surface temperatures, it is informative to determine the effect of conductivity on internal temperatures. A complete cylinder is presumed with the wall structure previously described and with an inner radius of 20.8 inches. A steady-state analysis is performed by considering the external surface as eight nodes, each of which covers 45 degrees of arc. A ninth node represents the interior of the tunnel as shown in Figure 51. The energy equation on each node is

$$
\left.
\begin{aligned}
&(C_i + Q_i)\alpha + E_i\epsilon + U'(T_9 - T_i) = \epsilon\sigma T_i^4 \text{ where } 1 \leq i \leq 8 \\
&T_9 = 0.125 \sum_{i=1}^{8} T_i
\end{aligned}
\right\} \qquad (10)
$$

where U' includes an internal surface coefficient of 1 Btu/hr-ft^2-$^\circ$F.

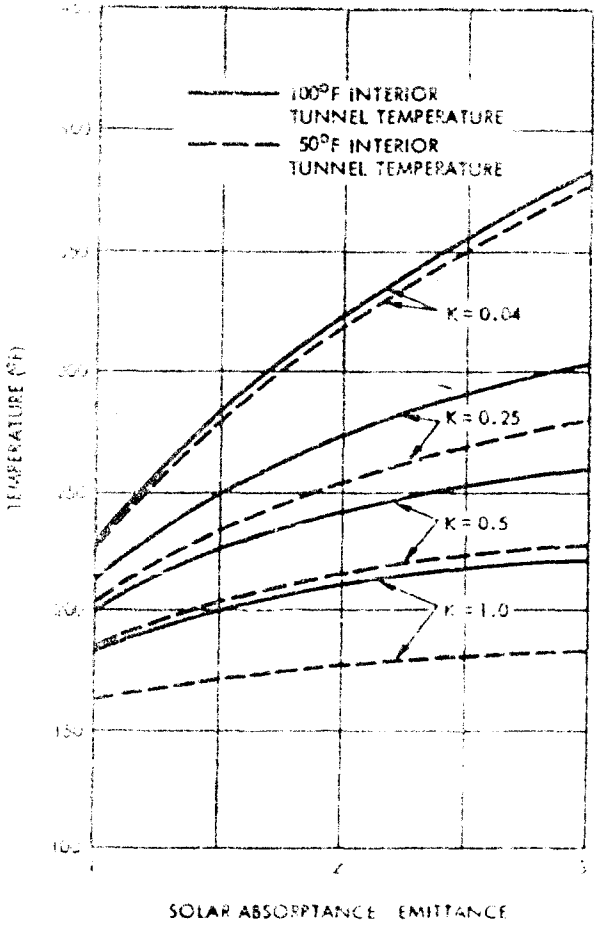

Figure 47. Effect of Foam Conductivity on Hot-Spot Temperatures in Day-Night Orbit

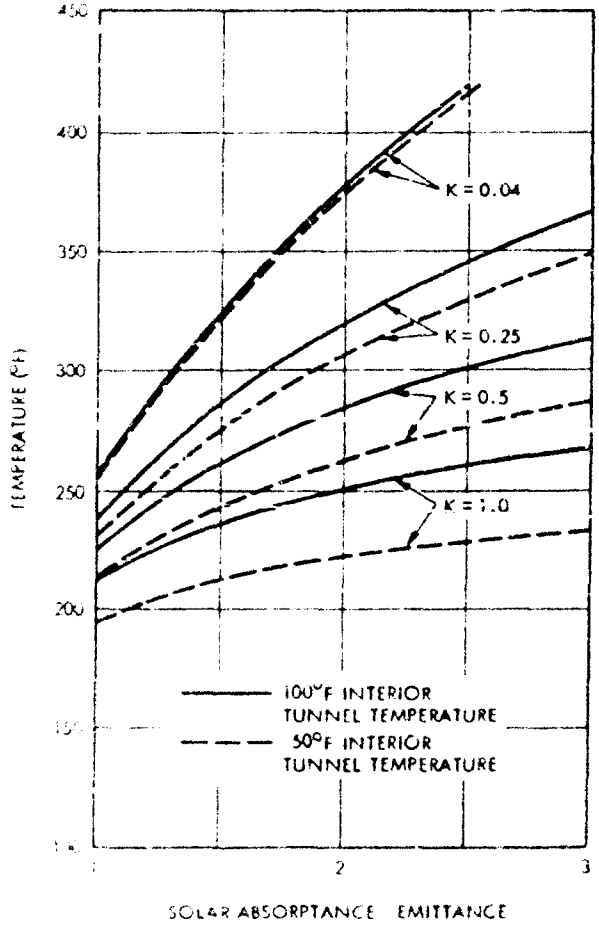

Figure 48. Effect of Foam Conductivity on Hot-Spot Temperatures in Twilight Orbit

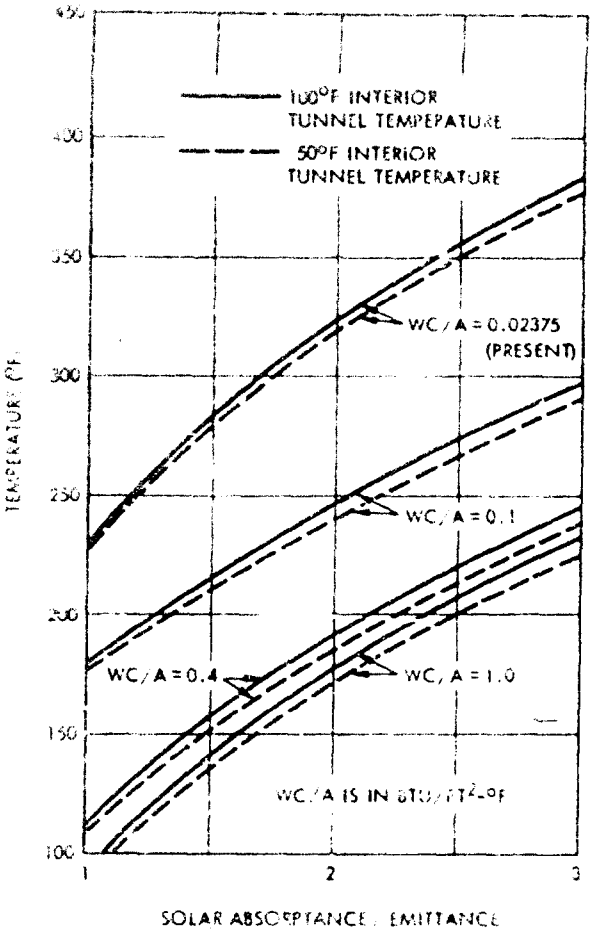

Figure 49. Effect of Surface Mass on Hot-Spot Temperatures in Day-Night Orbit

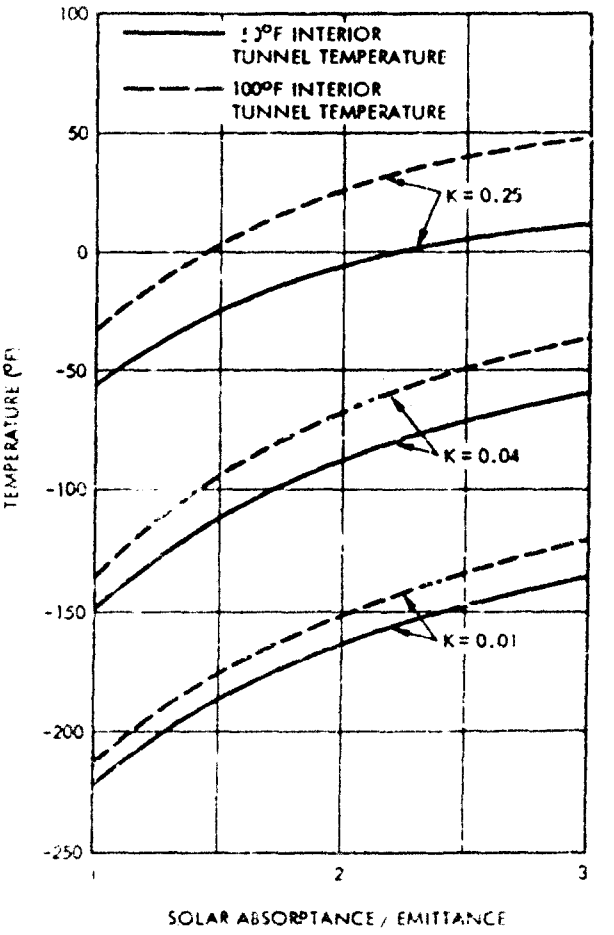

Figure 50. Effect of Foam Conductivity on Cold-Spot Temperatures in Twilight Orbit

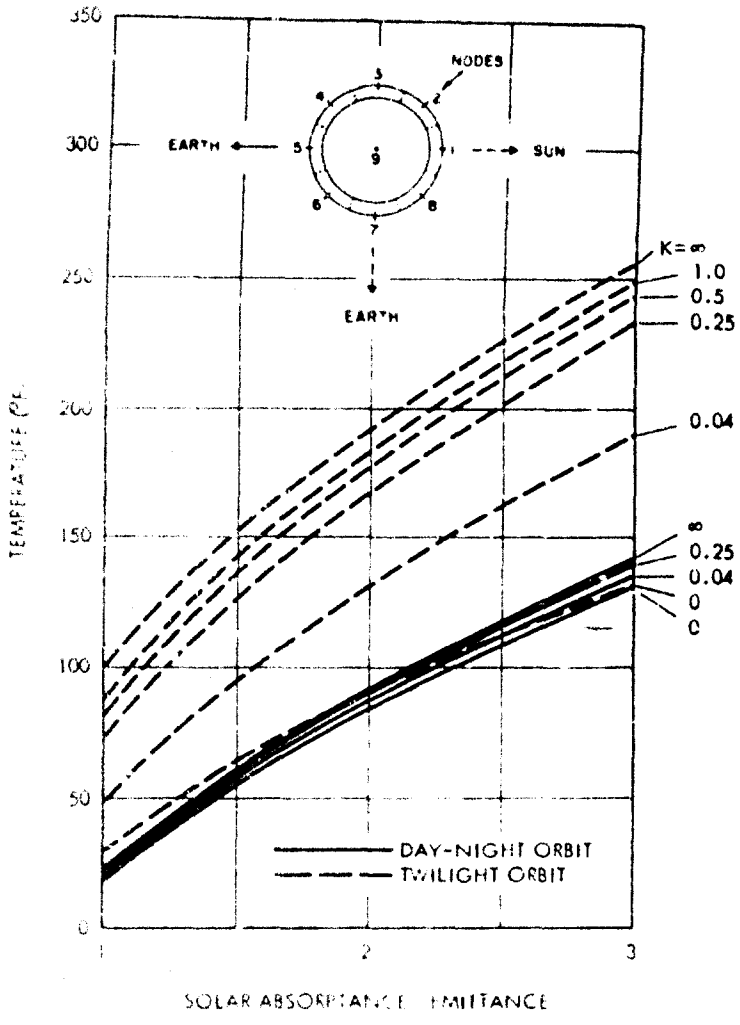

Figure 51. Effect of Foam Conductivity on Internal Temperature of an Unshielded Cylinder

For a twilight orbit,

$$\left.\begin{aligned} C_1 &= \frac{\bar{C}\int_{0^o}^{22.5^o} \cos\delta \, d\delta}{\int_{0^o}^{22.5^o} d\delta} \\ C_2 = C_3 &= \frac{\bar{C}\int_{22.5^o}^{67.5^o} \cos\delta \, d\delta}{\int_{22.5^o}^{67.5^o} d\delta} \end{aligned}\right\} \qquad (11)$$

(Continued)

$$C_3 = C_8 = \frac{\bar{C}\int_{67.5^\circ}^{90^\circ} \cos\delta \, d\delta}{\int_{67.5^\circ}^{112.5^\circ} d\delta}$$

$$C_4 = C_5 = C_6 = 0$$

$$E_i = 0.16\,\bar{C}F_{i-E} \text{ where } 1 \leqq i \leqq 8$$

$$Q_i = 0 \text{ where } 1 \leqq i \leqq 8$$

(11 cont)

For a day-night orbit,

$$E_i = 0.16\,\bar{C}F_{i-E} \text{ where } 1 \leqq i \leqq 8$$

$$Q_i = \frac{0.36\,\bar{C}F_{i-E}\int_{0^\circ}^{90^\circ} \cos\beta \, d\beta}{\int_{0^\circ}^{180^\circ} d\beta} \text{ where } 1 \leqq i \leqq 8$$

$$C_1 = \frac{\bar{C}\int_{\delta=0^\circ}^{22.5^\circ}\int_{\beta=0^\circ}^{90^\circ} \cos\delta \, d\delta \cos\beta \, d\beta}{\int_{\delta=0^\circ}^{22.5^\circ}\int_{\beta=0^\circ}^{180^\circ} d\delta \, d\beta}$$

$$C_2 = C_8 = \frac{\bar{C}\int_{\delta=22.5^\circ}^{67.5^\circ}\int_{\beta=0^\circ}^{90^\circ} \cos\delta \, d\delta \cos\beta \, d\beta}{\int_{\delta=22.5^\circ}^{67.5^\circ}\int_{\beta=0^\circ}^{180^\circ} d\delta \, d\beta}$$

(12)

$$C_3 = C_7 = \frac{\bar{C}\int_{\delta=67.5^\circ}^{90^\circ}\int_{\beta=0^\circ}^{105^\circ} \cos\delta \, d\delta \sqrt{\cos^2\beta} \, d\beta}{\int_{\delta=67.5^\circ}^{112.5^\circ}\int_{\beta=0^\circ}^{180^\circ} d\delta \, d\beta}$$

$$C_4 = C_6 = \frac{\bar{C}\int_{\delta=22.5^\circ}^{67.5^\circ}\int_{\beta=90^\circ}^{105^\circ} \cos\delta \, d\delta \sqrt{\cos^2\beta} \, d\beta}{\int_{\delta=22.5^\circ}^{67.5^\circ}\int_{\beta=0^\circ}^{180^\circ} d\delta \, d\beta}$$

(Continued)

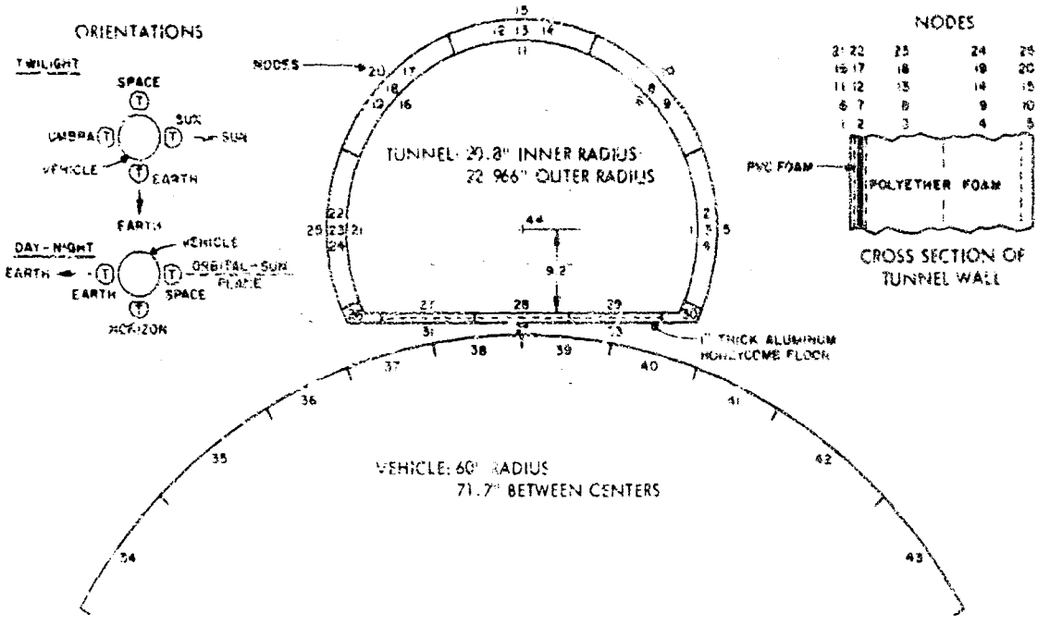

Figure 52. Thermal Schematic of Crew Transfer Tunnel

$$C_5 = \frac{\bar{C}\int_{\delta=0^\circ}^{22.5^\circ}\int_{\beta=90^\circ}^{105^\circ} \cos\delta \, d\delta \sqrt{\cos^2\beta} \, d\beta}{\int_{\delta=0^\circ}^{22.5^\circ}\int_{\beta=0^\circ}^{180^\circ} d\delta \, d\beta} \qquad \text{(12 cont)}$$

Radiation view factors of the earth are obtained by numerical integration around the node, utilizing Reference 1. Figure 51 presents the results of this study. It may be seen that an increase in the conductivity of the polyether foam raises the internal temperature, particularly for a twilight orbit. This effect is due to radiation interchange being proportional to the fourth power of temperature, while conduction is directly proportional to the temperature. When the conductivity approaches infinity, the isothermal case of Figure 46 is attained. The day-night temperature cycle for the day-night orbit may slightly reduce the internal temperatures for the same reason; this effect is not shown in Figure 51.

d. Tunnel Internal Temperatures. A thermal model of the crew transfer tunnel is shown in Figure 52. This schematic represents the MSS end of the tunnel with the junction of the honeycomb floor and walls geometrically simplified. For simplicity and a slightly conservative analysis, the model is presumed to be infinite in length perpendicular to the plane of the figure. The tunnel model is divided into 34 nodes as shown; the adjacent vehicle is represented as 10 nodes. For the Gemini end of the tunnel, the tunnel more closely approaches a complete cylinder with less shielding from the vehicle and may be presumed to lie between the models shown in Figures 51 and 52.

As may be deduced from the model, the uninsulated honeycomb floor provides the primary means of heat transfer to or from the tunnel interior and strongly affects internal temperatures. The floor temperature is greatly influenced by the vehicle thermal parameters

Table IV. Thermal Parameters for Model

SURFACE AREAS AND THERMAL MASSES[a]

Nodes	Thermal Masses (Btu/°F)	Areas (ft^2)
1, 6, 11, 16, 21	0.04144	1.36136
2, 7, 12, 17, 22	0.13151	
3, 8, 13, 18, 23	0.02906	
4, 9, 14, 19, 24	0.03028	
5, 10, 15, 20, 25	0.04085	1.50312
26, 30	0.2731	0.29507 (Int)
		0.46892 (Ext)
27, 29	0.2195	0.91667
28, 32	0.2156	0.91667
31, 33	0.2365	0.91667
34, 35, 42, 43	As specified	1.30899
36, 37, 38, 39, 40, 41	As specified	0.87266

THERMAL CONDUCTANCE[b]

Nodes	Conductance (Btu/hr-°F)	Nodes	Conductance (Btu/hr-°F)
1-2, 6-7, 11-12, 16-17, 21-22	4.336	26-27, 26-31, 30-29, 30-33	0.0072
2-3, 7-8, 12-13, 17-18, 22-23	0.1108 (K = 0.04)[a] 0.6860 (K = 0.25) 2.6556 (K = 1)	27-28, 28-29, 31-32, 32-33	0.5536
		27-31, 28-32, 29-33	7.3
3-4, 8-9, 13-14, 18-19, 23-24	0.06369 (K = 0.04) 0.3981 (K = 0.25) 1.5923 (K = 1)	34-35, 35-36, 36-37, 37-38, 38-39, 39-40, 40-41, 41-42, 42-43	As specified
4-5, 9-10, 14-15, 19-20, 24-25	0.1312 (K = 0.04) 0.8153 (K = 0.25) 3.1978 (K = 1)		

[a] Polyether foam conductivity in Btu-in./hr-ft^2-°F. [b] Based on model length of 1 foot.

directly beneath the floor, such as the quantity of insulation within the vehicle skin, which are unknown at this time. It is anticipated that the vehicle thermal control coating will be a low α/ϵ ratio white paint ($\alpha = 0.2$, $\epsilon = 0.8$) to achieve a low temperature surface from which some internal heat may be dissipated.

The model thermal parameters have been estimated and are presented in Table IV. Radiation view factors for the tunnel interior and for the energy exchange between the tunnel and vehicle are obtained by numerical or mathematical integration around the nodes. External heat fluxes (solar, albedo, and earth reradiation) on each external node are evaluated by numerical integration around the node for a given tunnel orientation and orbital position and include the effect of shielding from other nodes. These external fluxes have been evaluated for a day-night orbit with the tunnel facing (1) space, (2) horizon, and (3) earth, as well as a twilight orbit with

Table V. External Heat Fluxes[a] Incident on External Model Nodes

Node	Day-Night Orbit[b]						Twilight Orbit							
	Horizon		Earth		Space		Sun		Earth		Space		Umbra	
	Solar[c]	Earth	Solar[c]	Earth	Solar[c]	Earth	Solar[c]	Earth	Solar[c]	Earth	Solar[c]	Earth	Solar[c]	Earth
5	46.13	57.86	17.12	23.25	24.59	15.28	42.88	57.86	0	23.25	431.11	15.28	0	0
10	38.50	49.12	38.51	49.14	100.02	4.16	304.65	49.12	0	49.14	304.85	4.16	0	4.19
15	30.77	23.25	59.23	63.58	137.23	0	431.11	23.25	42.88	63.58	42.88	0	0	23.25
20	100.04	4.19	38.51	49.14	100.02	4.16	304.85	4.19	304.85	49.14	0	4.16	0	49.12
25	137.23	0	17.12	23.25	24.59	15.28	42.88	0	431.11	23.25	0	15.28	0	57.86
26	35.37	0.07	2.08	2.90	5.28	7.37	0	0.07	110.95	2.90	0	7.37	0	17.81
30	13.96	17.81	2.08	2.90	5.28	7.37	0	17.81	0	2.90	110.95	7.37	0	0.07
31	0.15	0.21	0	0	1.23	1.72	0	0.21	0	0	0	1.72	0	3.76
32	0.67	0.94	0	0	0	0	0	0.94	0	0	0	0	0	0.94
33	2.69	3.76	0	0	1.23	1.72	0	3.76	0	0	0	1.72	0	0.21
34	111.40	0	35.06	44.87	89.54	5.66	268.55	0	349.98	44.87	0	5.66	0	53.46
35	85.48	0	38.93	49.04	112.73	1.85	349.98	0	268.55	49.04	0	1.85	0	45.26
36	59.43	0	33.43	42.16	94.78	0.27	297.15	0	186.71	42.16	0	0.27	0	37.86
37	36.41	0	7.13	9.96	0	0	0	0	114.37	9.96	0	0	0	10.73
38	12.28	0.04	0	0	0	0	0	0.04	38.50	0	0	0	0	0.65
39	0.88	0.65	0	0	0	0	0	0.65	0	0	38.50	0	0	0.04
40	8.93	10.73	7.13	9.96	0	0	0	10.73	0	9.96	114.37	0	0	0
41	29.14	37.86	33.43	42.16	94.78	0.27	297.15	37.86	0	42.16	186.71	0.27	0	0
42	34.34	45.26	38.93	49.04	112.73	1.85	349.98	45.26	0	49.04	268.55	1.85	0	0
43	42.09	53.46	35.06	44.87	89.54	5.66	268.55	53.46	0	44.98	349.98	5.66	0	0

[a] Fluxes in Btu/hr-ft^2 without reflections. [b] Orbital averages. [c] Solar fluxes include albedo.

the tunnel facing (1) sun, (2) space, (3) umbra of earth, and (4) earth, without vehicle rotation. A summary of these fluxes is presented in Table V. Radiation interchanges including the reflections of external fluxes are handled by the Oppenheim method (Reference 2).

Transient solutions for the day-night orbit require a large amount of computer time due to the slow response rate of the tunnel. Considerably quicker stabilized solutions may be achieved by using the Gauss-Seidel method for the twilight orbit conditions and by using average external fluxes for the day-night orbit conditions. For these stabilized solutions, the internal surface coefficient is taken as 1 Btu/hr-ft^2-$^\circ$F and the foam conductivity as 0.94 Btu-in./hr-ft^2-$^\circ$F. The external surface of the honeycomb floor is presumed to be uncoated bare metal ($\alpha = 0.15$, $\epsilon = 0.05$), while the vehicle is presumed to have the likely coating ($\alpha = 0.2$, $\epsilon = 0.8$) with no internal heating. The conductance of the vehicle skin between nodes 36 and 37 is 0.1 Btu/hr-$^\circ$F for a 1-ft length, and was obtained by presuming a René 41 skin.

It is noted from Figure 53 that the temperatures are considerably higher within the tunnel when the tunnel is turned sideways to the sun, such as the horizon orientation in the day-night orbit and the earth and space orientations in the twilight orbit. This phenomenon is due to the high α/ϵ ratio of the floor reacting to vehicle-reflected sunlight. Revised tunnel schematics indicate that this effect will not occur, since the tunnel canister will prevent sunlight from entering this area. A more realistic estimate of temperatures with the floor shielded may be obtained by presuming no solar or albedo heating of nodes 31, 32, 33, 37, 38, 39, and 40. Figure 54 presents the results of this presumption while retaining other Figure 53 conditions. The honeycomb and vehicle α and ϵ values are the same for Figures 53 and 54.

A significant feature of Figure 54 is the effect of tunnel orientation on internal temperatures. A rather wide band of temperatures results for a given orbit according to the orientation. Vehicle surface temperatures are cool, attaining a maximum value of -21°F for the day-night orbit, although somewhat higher local temperatures are obtained in the twilight orbit. Since "shirt-sleeve" temperatures are desired within the tunnel with the lowest possible value of α/ϵ on the tunnel (to alleviate hot-spot temperatures), the tunnel floor should be thermally isolated from the vehicle. This may be partially accomplished by a low emittance coating on the external surface of the floor, such as was presumed in Figure 54, or by thermal insulation,

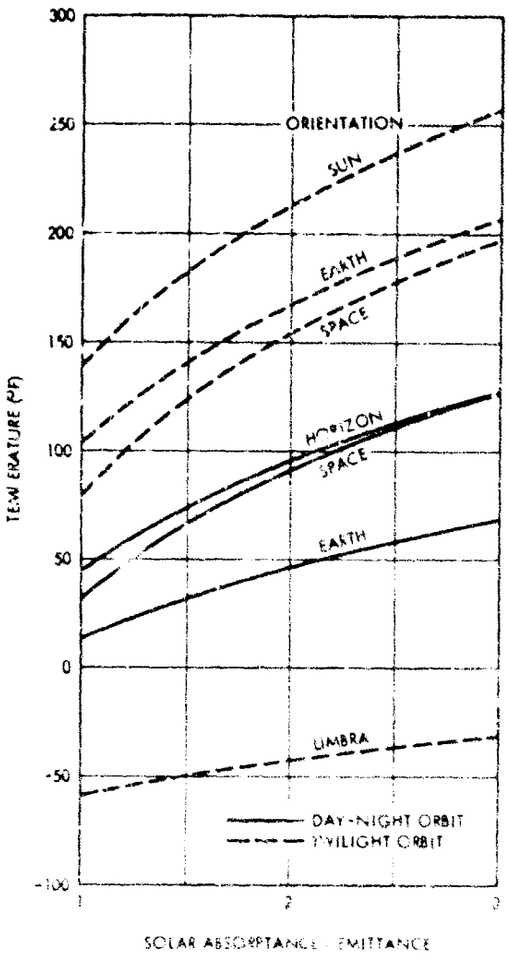

Figure 55. Tunnel Internal Temperatures with 50°F Internal Vehicle Heating and Floor Shielded (K = 0.25)

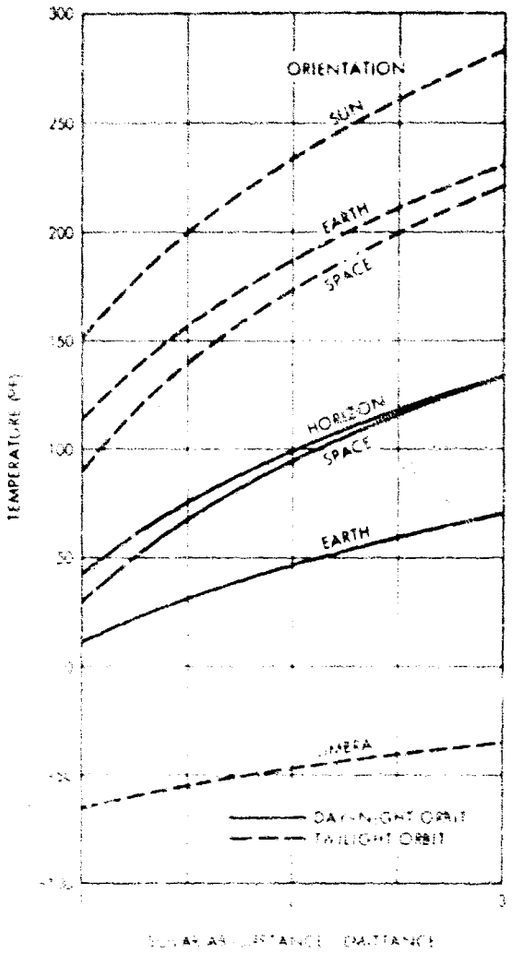

Figure 56. Tunnel Internal Temperatures with 50°F Internal Vehicle Heating and Floor Shielded (K = 1.0)

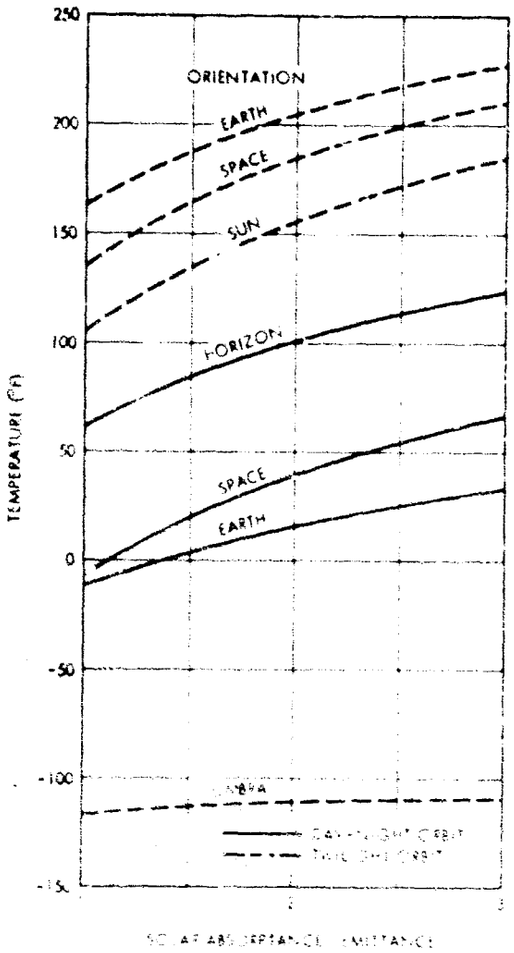

Figure 53. Tunnel Internal Temperatures with No Internal Vehicle Heating

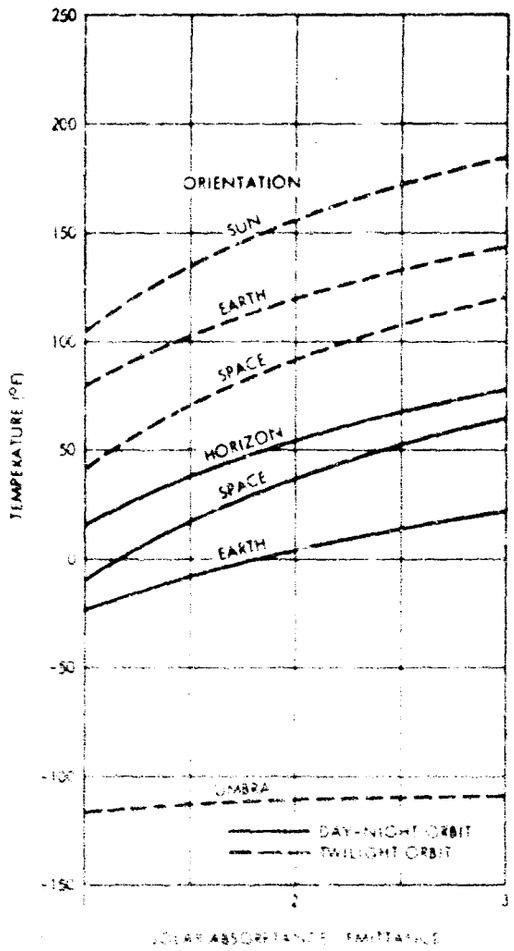

Figure 54. Tunnel Internal Temperatures with No Internal Vehicle Heating and Floor Shielded

Vehicle thermal coatings would also have some slight effect on tunnel temperatures. With no internal heating, the total heat flux leaving the vehicle consists of reflections of solar, albedo, and earth radiation as well as reradiation from the vehicle and is essentially constant. Since the tunnel α/ϵ ratio is greater than unity, it is desirable to have the largest portion of the heat flux leaving the vehicle consist of reflected solar and albedo radiation, which is obtained by a low α coating on the vehicle. A high ϵ coating on the vehicle will maximize the effect of internal heating on the tunnel temperatures. The presumed vehicle coating appears to be optimum in regard to tunnel temperatures.

Higher thermal conductivities in the polyether foam and vehicle internal heating should increase tunnel temperatures. Figure 55 shows the tunnel temperature when the foam conductivity is 0.25 Btu-in./hr-ft^2-^{o}F and the vehicle temperature is maintained at 50^{o}F by internal heating. Addition of copper drop threads to increase the foam conductivity to 1.0 Btu-in./hr-ft^2-^{o}F produces results as shown in Figure 56. As may be anticipated from Figure 51, the increased foam conductivity has a slight effect on day-night orbit temperatures and a significant effect on twilight orbit temperatures. Vehicle internal heating has a large effect on tunnel temperatures. The honeycomb and vehicle α and ϵ values are the same for Figures 55 and 56.

For the data shown in Figures 53 through 56 the internal tunnel surface temperatures vary locally from the average internal temperature by less than 10^{o}F in the day-night orbit and as much as 40^{o}F in the twilight orbit. Structural layer temperatures vary from the average internal temperature by approximately the same values for foam conductivities of 0.25 Btu-in./hr-ft^2-^{o}F or less; with copper drop threads the values become 15 and 55^{o}F respectively.

e. Temperature Distribution on Tunnel. While the interior and maximum surface temperatures are of primary concern, temperature distributions around the tunnel may also prove interesting. Figure 57 presents a typical temperature distribution for a twilight orbit and represents a Figure 54 condition with a foam conductivity of 0.04 Btu-in./hr-ft^2-^{o}F.

For a day-night orbit, the temperatures will vary with time due to variable external heating. Transient solutions may be obtained by use of a quasi-backward-difference numerical integration technique. This method utilizes forward-difference radiation interchange incident fluxes, backward-difference for conduction interchange and radiation emissions, and mid-difference external heating (solar, albedo, and earth radiation). A typical transient equilibrium solution is shown in Figure 58 with an interior surface emittance of 0.9. The Figure 58 conditions corresponds to the Figure 55 conditions with a foam conductivity of 0.25 Btu-in./hr-ft^2-^{o}F, permitting a comparison of results. The average internal temperature per Figure 58 is within 3^{o}F of the Figure 55 value, proving the validity of using orbital average fluxes for a stabilized solution. As shown, the internal temperature varies ±7^{o}F from the average value.

4. Conclusions

The following pertinent conclusions are attained as a result of the thermal analysis on the crew transfer tunnel:

(1) To passively maintain comfortable internal temperatures, the tunnel external surface generally requires a thermal coating with a ratio of α to ϵ between 1 and 3. The values of α and ϵ should be minimized to dampen the day-night temperature cycle and the hot-spot and cold-spot temperatures on the external surface. These criteria may be satisfied by using a coating of an aluminized film substrate (α = 0.15, ϵ = 0.05, α/ϵ = 3) covered in part by an aluminized silicone paint (α = ϵ = 0.25, α/ϵ = 1). By varying the quantity of painted surface, the effective α/ϵ ratio may be established at any desired value between 1 and 3. Ratios of α/ϵ less than 1 may be desired in a twilight orbit or locally for other orbits. These ratios may be obtained by adding a thin layer of silicon monoxide to the aluminized film substrate (α = 0.15, ϵ = 0.5, α/ϵ = 0.3).

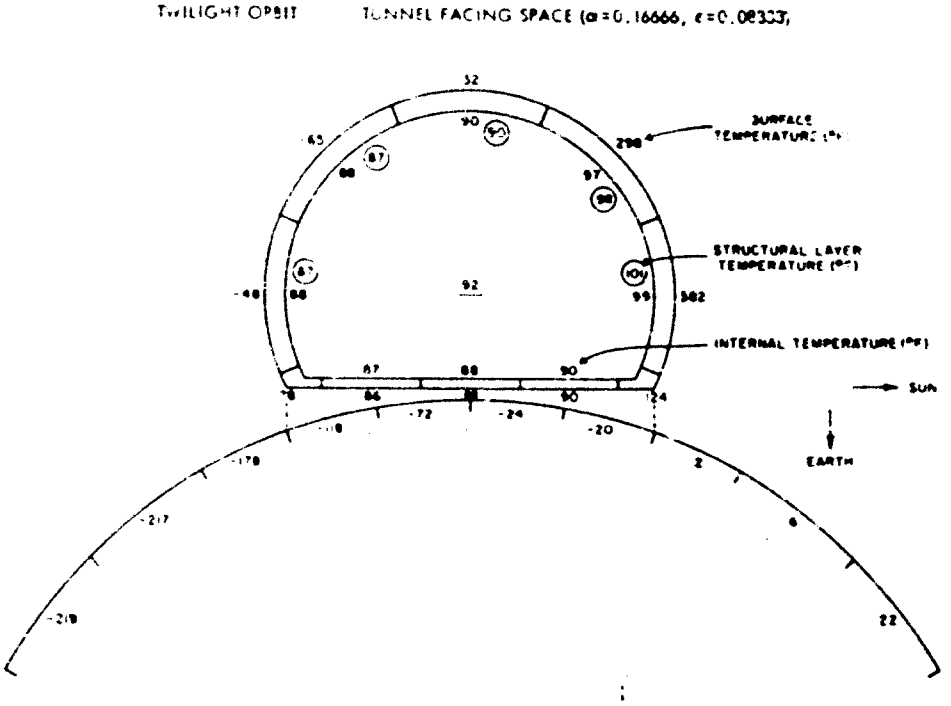

Figure 57. Typical Tunnel Temperatures with No Internal Vehicle Heating and Floor Shielded

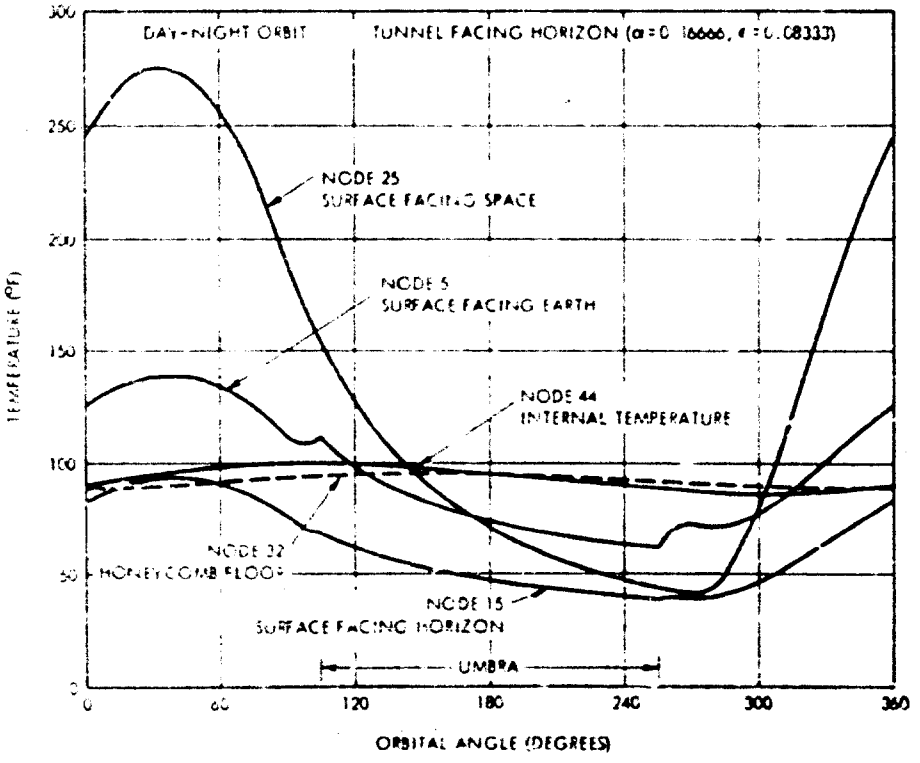

Figure 58. Typical Tunnel Temperatures with 50°F Internal Vehicle Heating and Floor Shielded

All thermal coatings described above are currently state of the art, with the possible exception of the aluminized silicone white paint. The latter has not been proved for inflated structures; since the elastomer base is very similar to that of a proven zinc oxide pigmented paint, no difficulties are anticipated. Development and testing of this aluminized silicone white paint on inflated surfaces should be accomplished at the earliest opportunity.

(2) With the external surface thermal coating specified above for comfortable internal temperatures, the external surface hot-spot temperatures are excessive. This problem is aggravated by outgassing of the polyether foam following micrometeoroid penetration of the outer cover, with hot-spot temperatures approaching 300°F before penetration and 350°F following penetration. Possible solutions to the problem are as follows:

(a) Installation of copper drop threads through the polyether foam to increase the conductivity. This approach was previously accomplished for the lunar shelter program; conductivities of approximately 0.5 to 1.0 Btu-in./hr-ft^2-°F would be desired.

(b) Increasing the mass of the external surface by additional layers of cloth or film. A surface layer mass of 1 psf appears desirable, although a mass of 0.5 psf would greatly reduce hot-spot temperatures. It should be noted that increased weight is undesirable from standpoints other than thermal. This solution would not apply to a twilight orbit.

(c) Rotating the system. A continuous system rotation of one revolution every 5 or 10 minutes would eliminate the problem.

(d) Use of a thermal control coating with an α/ϵ ratio less than 1 would eliminate the hot-spot problem but require heat addition to the tunnel for comfortable internal temperatures.

(e) Selective use of thermal control coatings. Portions of the tunnel that experience severe solar heating would have a low α/ϵ ratio coating, while other portions of the tunnel would have a high α/ϵ ratio coating. This method would require definition of the orbital and orientation parameters prior to coating selection.

(3) The tunnel orientation and the type of orbit selected have a significant effect on internal temperatures. For a given orbit, the orientation will vary the internal temperature through a band considerably wider than the ±25°F tolerance required. In orbits approaching a twilight orbit, there are orientations wherein the interior cannot be passively maintained at comfortable temperatures. Possible solutions to maintain a reasonably tight tolerance on internal temperatures are as follows:

(a) Selected orientation as required.

(b) System rotation as previously discussed.

(c) Heat addition to the tunnel as required.

(d) Forced convection of the Gemini-MSS atmosphere through the tunnel prior to use.

(e) Reconsideration of the need for a closely controlled tunnel internal temperature.

(4) Tunnel internal temperatures are considerably affected by the tunnel-vehicle interface area since the uninsulated floor represents the primary means of heat transfer into or from the tunnel. Since the vehicle surface will probably be cooler than room

temperature, the tunnel should be insulated from the vehicle by thermal insulation on the floor external surface. The two hatches are presumably near room temperature and should cause no problems. Final decisions on the interface thermal design must logically await details of the vehicle thermal design.

(5) Thermal coatings on the Gemini-MSS vehicle appear to have only slight effect on the tunnel thermal design, unless a highly specular reflective coating such as polished metal is used. A slight advantage is realized with low α/ϵ ratio vehicle coatings, but this advantage is not sufficient to justify alteration of the vehicle coatings.

(6) A low α/ϵ ratio white paint should be applied to the tunnel interior surface to expedite internal heat transfer and minimize temperature gradients while improving the lighting. The zinc oxide pigmented paint developed by GAC for the lunar shelter project would be suitable for this application.

(7) Cold-spot temperatures on the external surface do not present any difficulties. Except for a twilight orbit, the minimum temperature should be within the $-100^{\circ}F$ value desired.

It is recommended that the thermal study be refined in coordination with or subsequent to the Gemini-MSS thermal designs. The optimum solutions to the problems stated above may be selected on the basis of system or operational requirements. From a thermal viewpoint, the expandable crew transfer tunnel concept is definitely feasible and within the state of the art.

C. STRUCTURAL ANALYSIS

1. General

The crew transfer tunnel consists of the expandable structure, which is the nonmetal part of the tunnel, and the hard structure, which is the floor with all the necessary attachments to the Gemini and MSS. Attached to the outer surface of the floor by means of 10 brackets is the canister, within which the tunnel is packaged during ascent of the vehicle.

This analysis considers the stresses produced in the expandable structure, specifically the structural layer of the composite wall, the floor, and the separation rings, due to inflation pressure. The canister support brackets are also analyzed, but the load used is arbitrarily selected from preliminary aerodynamic considerations. The canister itself is not analyzed, since aerodynamic loads and temperatures depend on the launch profile, which is not specified.

2. Definition of Load Factors

The expandable structure should have a safety factor of 5 when inflated to an internal pressure of 7.5 psi. The metal structrue should have a safety factor of 2 on yield strength and a factor of 3 on ultimate strength for the internal pressure of 7.5 psi.

Limit load is defined as the load produced by an inflation pressure of 7.5 psi. For the metal structure, load factors based on limit load are used to determine yield loads and ultimate loads for the determination of margins of safety relative to allowable yield and ultimate stresses. Yield and ultimate load factors are defined for metal members as follows:

(1) Yield Load Factors
   (a) Members in Compression - 3
   (b) Members in Tension - 2
(2) Ultimate Load Factors
   (a) Members in Compression - 3
   (b) Members in Tension - 3

Yield loads are determined by multiplying limit loads by the yield load factors, and ultimate loads are determined by multiplying limit loads by the ultimate load factors. The compression yield load factor is based on the fact that compression yield is considered failure.

3. Expandable Structure

Geometrically, the expandable structure is a series of surfaces (parts of), which from the Gemini to MSS are as follows (see Figure 39):

(1) Sphere: R = 21.40 inches (on Gemini).

(2) Frustum of Cone: R = 21.40 inches, R' = 20.80 inches (on Gemini).

(3) Torus: R'' = 110 inches, r = R' = 20.80 inches (transition).

(4) Cylinder: R' = 20.80 inches (on MSS).

(5) Sphere: R' = 20.80 inches (on MSS).

The maximum stress occurs at the connection of the transition torus to the floor in the meridional direction of the torus while pressurized in orbit under zero G. Let b, shown in Figure 59, be the floor narrowest half width under the torus. Then b = 16.75 inches. The maximum meridional stress in the torus is

$$f''_{max} = \frac{pr}{2}\left(1 + \frac{R''}{R'' - \sqrt{r^2 - b^2}}\right) \text{lb/in.} \qquad (13)$$

where p is the inflation pressure (Reference 3, p 274). Substituting numerical values in Equation 13 yields

$$f''_{max} = \frac{p(20.80)}{2}\left(1 + \frac{110.0}{110.0 - \sqrt{20.8^2 - 16.75^2}}\right)$$

$$22.11p \text{ lb/in.} \qquad (14)$$

For p = 7.5 psi, f''_{max} = 165.8 lb/in.

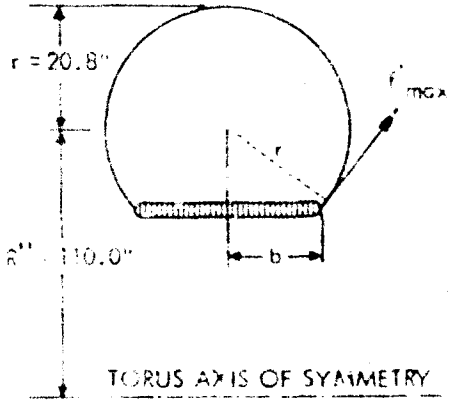

Figure 59. Torus Meridian Section

The materials used in the expandable wall of the tunnel are described in subsection E of this section. The design ultimate strength of the four-ply structural layer is given as 831 lb/in. including degradation for plying and seaming efficiency, and creep-rupture effects (Reference 4, p 132). With this ultimate strength and an applied stress of 165.8 lb/in., the factor of safety for the structural layer is 831/165.8 = 5.0 for an inflation pressure of 7.5 psi.

4. Hard Structure

a. Sandwich Floor. The floor consists of two plane surfaces subjected to normal uniformly distributed load (pressure) reacted by the membrane pull around its outer boundary and the forces between the tunnel and the Gemini-MSS vehicle around the elliptical and circular hatches where the floor is attached to the Gemini capsule and the MSS respectively. Since the membrane forces acting around the outer edge of the floor have some inclination relative to the floor, the floor is subjected to bending stresses created by the normal components of the above forces as well as distributed in-plane forces around the outer boundary created by the in-plane components. The in-plane load can be considered as a uniform "hydrostatic" tension equal to

the in-plane component of f'_{max} in Figure 59; i.e.,

$$f' = f'_{max} \frac{\sqrt{r^2 - b^2}}{r} = 22.11\ p\ \frac{12.33}{20.80} = 13.11\ p\ lb/in. \tag{15}$$

This force is taken by the two faces of the sandwich floor and has a relieving effect on the floor deflection. The floor is analyzed as a simply supported plate (beam) loaded uniformly by the inflation pressure, p. The maximum width of the floor is 36.36 inches.

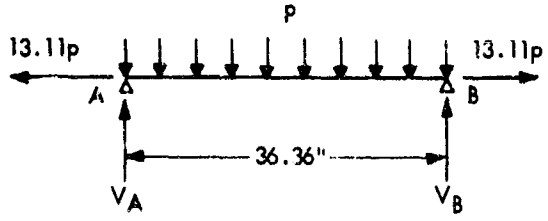

$$V_A = V_B = \frac{pL}{2} = 18.18p\ lb/in. \tag{16}$$

$$M_{max} = \frac{pL^2}{8} = 165.3p\ in.\text{-}lb/in. \tag{17}$$

The relieving effect of the axial tension, 13.11p lb/in., on the floor maximum deflection and compressive bending stress is neglected.

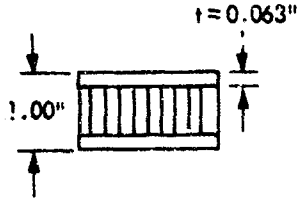

$$I = 2\left[\frac{t^3}{12} + t\left(0.5 - \frac{t}{2}\right)^2\right]. \tag{18}$$

$$I = 2\left[\frac{0.063^3}{12} + 0.063\ (0.4685)^2\right] = 0.02770\ in.^4/in.$$

For the yield and ultimate strengths of the 7075-T6 aluminum sandwich faces, see Reference 5, p 3.2.7.0(b). The limit compression stress is

$$f_c = \frac{165.3 \times 7.5 \times 0.5}{0.0277} = 22,380\ psi.$$

$$\text{Margin of safety (MS)} = \frac{68,000}{3 \times 22,380} - 1 = +0.01.$$

The limit tension stress is

$$f_t = 22,380 + \frac{13.11 \times 7.5}{2 \times 0.063} = 22,380 + 780 = 23,160\ psi.$$

$$MS = \frac{77,000}{3 \times 23,160} - 1 = +0.11.$$

The maximum floor deflection occurs at the midspan.

$$\delta_{max} = \frac{5}{384}\ \frac{pL^4}{EI} = \frac{5}{384}\ \frac{7.5 \times (36.36)^4}{10 \times 10^6 \times (0.02770)} = 0.62\ in. = 0.017L \tag{19}$$

For the core material chosen, the flexural shear strength in the longitudinal direction is 540 psi. From Equation 16, the maximum core shear is 18.18p. The core shear stress is

$$f_s = 18.18 \times 7.5 \times 3 = 409\ psi\ (yield).$$

$$MS = \frac{540}{409} - 1 = +0.32.$$

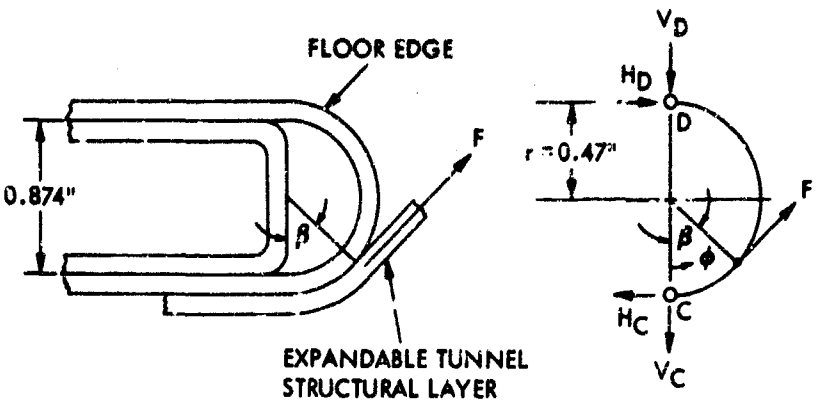

Figure 60. Floor Edge Molding Loading

The load applied to the floor edge molding is shown in Figure 60 as the load F, which is equivalent to the load f'_{max} shown in Figure 59.

$$F = 22.11p \text{ lb/in.} \tag{20}$$

From Figure 59,

$$\sin \beta = \frac{16.75}{20.80} = 0.8053$$

$$\beta = 53^{\circ}38'.$$

The reaction (see Figure 60) necessary for determining bending moments is determined from statics as follows:

$$H_C = \frac{F}{2} (1 + \cos \beta) = 0.7965F \text{ lb/in.} \tag{21}$$

The edge molding bending moments are as follows:

$$\text{When } \phi \leq \beta, \; M_\phi = V_C r \sin \phi - 0.7965Fr (1 - \cos \phi) \text{ in.-lb/in.} \tag{22}$$

$$\text{When } \phi > \beta, \; M_\phi = M_{(\phi < \beta)} - Fr \left[1 - \cos (\phi - \beta)\right] \text{ in.-lb/in.} \tag{23}$$

Using energy methods,

$$U = \frac{1}{2EI} \int M_\phi^2 \, ds \text{ in.-lb/in.} \tag{24}$$

Partial differentiation of Equations 22 and 23 yields

$$\frac{\partial M_\phi}{\partial V_C} = r \sin \phi \text{ in.-lb/in.} \tag{25}$$

Since $\frac{\partial U}{\partial V_C} = 0$,

partial differentiation of Equation 24 and the substitution of Equations 22, 23, and 25 give

$$\int_0^{\pi} \left| V_C\, r \sin\phi - 0.7965 Fr\,(1-\cos\phi) \right| r \sin\phi\, r\, d\phi +$$

$$\int_{\beta}^{\pi} Fr \left| 1-\cos(\phi-\beta) \right| r \sin\phi\, r\, d\phi = 0. \qquad (26)$$

Solving this equation for V_C yields

$$V_C = 0.5653F \text{ lb/in.} \qquad (27)$$

Then Equations 22 and 23 are as follows:

When $\phi \leqq \beta$, $M_\phi/Fr = 0.5653 \sin\phi - 0.7965\,(1-\cos\phi)$. (28)

When $\phi \geqq \beta$, $M_\phi/Fr = 0.5653 \sin\phi - 0.7965\,(1-\cos\phi) + 1-\cos(\phi - 53^\circ 38')$. (29)

Using equation 20 and Table VI with p = 7.5 psi, the maximum moment is

$$M_{max} \cong 0.18\ Fr = 0.18 \times 22.11 \times 7.5 \times 0.47 = 14.03 \text{ in.-lb/in.}$$

The floor edge section modulus is

$$\frac{I}{c} = \frac{t^2}{6} = \frac{(0.063)^2}{6} = 0.0006615 \text{ in.}^3/\text{in.}$$

The ultimate tensile stress is

$$f_{tu} = \left(\frac{14.03}{0.0006615} + \frac{22.11 \times 7.5}{0.063} \right) 3 = 71,526 \text{ psi.}$$

For the straight molding,

$$MS = \frac{77,000}{71,526} - 1 = +0.07.$$

The maximum compressive stress at about ϕ = 126 degrees (see Table VI), which would be multiplied by a load factor of 3 to be checked against the allowable yield strength of 68,000 psi, is

Table VI. Values of M_ϕ/Fr for Several Values of ϕ

ϕ (degrees)	sin ϕ	cos ϕ	cos $(\phi-\beta)$	1- cos ϕ	1- cos $(\phi-\beta)$	0.5653 x sin ϕ	0.7965 x (1- cos ϕ)	M_ϕ/Fr
0	0	1.000	-	0	-	0	0	0
18	0.3090	0.9511	-	0.0489	-	0.1747	0.0389	0.1358
36	0.5878	0.8090	-	0.1910	-	0.3323	0.1521	0.1802
$53^\circ 38'$	0.8052	0.5930	1.000	0.4070	0.000	0.4552	0.3242	0.1310
72	0.9511	0.3090	0.9491	0.6910	0.0509	0.5377	0.5504	0.0382
90	1.000	0	0.8052	1.0000	0.1948	0.5653	0.7965	-0.0364
108	0.9511	-0.3090	0.5826	1.3090	0.4174	0.5377	1.0426	-0.0875
126	0.8090	-0.5878	0.3029	1.5878	0.6971	0.4573	1.2647	-0.1103
144	0.5878	-0.8090	-0.0064	1.8090	1.0064	0.3323	1.4409	-0.1022
162	0.3090	-0.9511	-0.3151	1.9511	1.3151	0.1747	1.5541	-0.0643
180	0	-1.000	-0.5930	2.000	1.5930	0	1.5930	0

much lower than the tensile stress of 71,526 psi; hence the margin of safety is positive throughout. Around the curved portions of the floor, however, the maximum stress is about half the above stress, because the tunnel there is spherical. Therefore, the curved molding which is 6061-T6 aluminum with an ultimate tensile strength of 42,000 psi, exhibits a positive margin of safety throughout.

The bond stress between the molding and the channel is also checked.

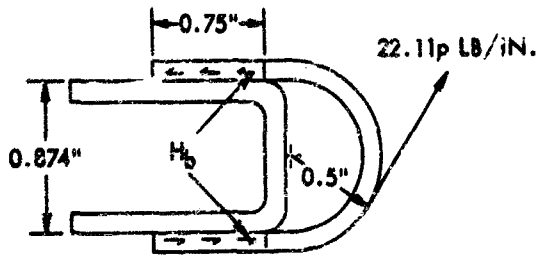

$$22.11p\,(0.50) = 0.874H_b$$

$$H_b = \frac{22.11(0.50)p}{0.874} = 12.66p \text{ lb/in.} \qquad (30)$$

The ultimate shear stress is

$$f_{su} = \frac{12.66 \times 7.5 \times 3}{0.75} = 380 \text{ psi.}$$

The allowable bond shear stress is 2500 psi.

$$MS = \frac{2500}{380} - 1 = + \text{ (high).}$$

Two floor section splice plates (7075-T6 aluminum) connect the two portions of the floor. The primary loads to which they are subjected are the bearing of the connecting rivets. These rivets are subjected to shear whose maximum value from Equation 16 and geometry is

$$1.13 \times 2.1 \times 18.18p = 43.14p \text{ lb} \qquad (31)$$

where the plate spacing is 1.13 inches and the rivet spacing is 2.1 inches. The bearing stress is

$$f_{br} = \frac{43.14 \times 7.5 \times 3}{0.221 \times 0.063} = 69,720 \text{ psi.}$$

$$MS = \frac{116,600}{69,720} - 1 = +0.66.$$

Thirty-four blind rivets, NAS 1330, No. 10, are used to attach the splice plates. The allowable rivet single shear strength is 1220 pounds.

$$MS = \frac{1220}{43.14 \times 7.5 \times 3} - 1 = +0.25.$$

b. Separation Rings. The circular ring is analyzed because it is larger and hence more critically loaded than the elliptical ring. The ring is subject to loads p and w acting on the cylindrical portion of the ring. The load w is the axial stress in the cylinder inflated to a pressure p. Using ultimate loads, p = 22.5 psi and w = 0.5 (22.5)(15.12) = 170.1 lb/in. The ring is fastened at 24 places (point C in Figure 61) evenly spaced on the flange. Three different cases might describe the way the flange responds to the load w, which comes from the cylindrical part of the ring. Reference 5 and 6 notations are used. These cases are as follows:

Case I - w' applied at point A, w" equals zero.

Case II - w' applied at point C, w" equals zero.

Case III - w' applied at point C, w" applied at point B.

For w" = 0,

$$w'_A = \frac{c}{a} w = \frac{15.12}{17.00} \times 170.1 = 151.3 \text{ lb/in.}$$

$$w'_C = \frac{c}{b} w = \frac{15.12}{16} \times 170.1 = 160.7 \text{ lb/in.}$$

For w'' at point B,

$$w'' = \frac{c}{a+e}\left[\frac{3}{4}w\ \frac{e-c-t}{d-e}\right]$$

$$= \frac{15.12}{16.67}(0.75)(170.1)\frac{0.69}{1.00} = 79.8 \text{ lb/in.}$$

$$w'_C = \frac{c}{b}w + \frac{a+e}{b}w'' = \frac{15.12\,(170.1)}{16} +$$

$$\frac{16.67\,(79.8)}{16} = 243.9 \text{ lb/in.}$$

In all cases the rotation of the cylinder and the flange at their intersection should be equal for compatibility. It is clear that case I is unrealistic, because it assumes that the flange is supported at point A instead of point C, and case III assumes that the flange is infinitely stiff from point C to point A. This infinite rigidity is no structural advantage to the ring, since with no contact between the flange and the underlying frame as in Case II, the flange is sufficiently strong, as is proved below, to withstand the applied loads w and p shown in Figure 61.

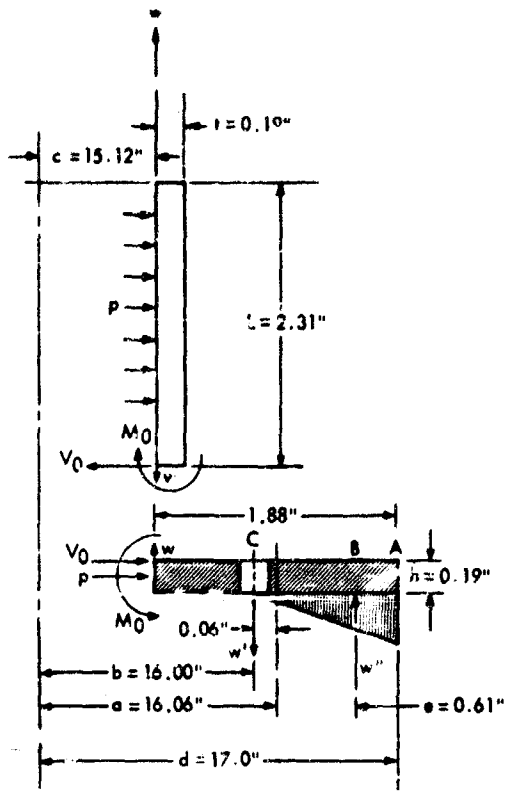

Figure 61. Separation Ring Cross Section

The cylinder deflection and rotation where δ_C and θ_C are the total deflection and rotation of the cylindrical portion of the ring (Reference 3, Table XIII), are determined as follows:

$$\lambda = \sqrt[4]{\frac{3(1-\mu^2)}{c^2t^2}} = \sqrt[4]{\frac{3\left[1-0.3^2\right]}{(15.12 \times 0.19)^2}} = 0.7584 \text{ in.}^{-1}$$

$$\lambda L = 0.7584 \times 2\ 31 = 1.75.$$

$$\frac{1.75 - 1.7}{2 - 1.7} = \frac{0.05}{0.3} = 0.167.$$

The following coefficients are used with the corresponding deflections and rotations for the total values:

$$C'_3 = 1.28 - 0.167\,(1.28 - 1.14) = 1.24 \sim (\delta_V).$$

$$C'_4 = 1.36 - 0.167\,(1.36 - 1.21) = 1.33 \sim (\theta_V).$$

$$C'_5 = 1.40 - 0.167\,(1.40 - 1.18) = 1.36 \sim (\delta_M).$$

$$C'_6 = 1.22 - 0.167\,(1.22 - 1.08) = 1.20 \sim (\theta_M).$$

The flexural rigidity is

$$D' = \frac{Et^3}{12\,(1-\mu^2)} = \frac{10 \times 10^6 \times (0.19)^3}{12\,(1 - 0.3^2)} = 6.281 \times 10^3 \text{ in.-lb.}$$

The cylinder deflection due to p is

$$\delta_{CP} = \frac{c}{E}\left(\frac{pc}{t} - \mu\frac{pc}{2t}\right) = \frac{(6.12)^2 p}{10 \times 10^6 \times 0.19}\left(1 - \frac{0.3}{2}\right) = 0.10227 \times 10^{-3}\ p \text{ in.} \quad (32)$$

The cylinder deflection and rotation due to V_0 are

$$\delta_{CV} = -\frac{V_0}{2D'\lambda^3} = -\frac{V_0}{2(6.281)\ 10^3 \times (7.584)^3 \times 10^{-3}} = -0.1825 \times 10^{-3} V_0 \text{ in.} \quad (33)$$

$$\theta_{CV} = \frac{V_0}{2D'\lambda^2} = -\lambda\delta_{CV} = -0.7584(-0.1825)\ 10^{-3} V_0 = 0.1384 \times 10^{-3}\ V_0 \text{ rad.} \quad (34)$$

The cylinder deflection and rotation due to M_0 are

$$\delta_{CM} = -\frac{M_0}{2D'\lambda^2} = -\frac{M_0}{V_0} \quad \theta_{CV} = -M_0\ (0.1384)\ 10^{-3} \text{ in.} \quad (35)$$

$$\theta_{CM} = \frac{M_0}{\lambda D'} = \frac{M_0}{0.7584 \times 6.281 \times 10^3} = 0.2099\ (10^{-3})\ M_0 \text{ rad.} \quad (36)$$

The flange deflection and rotation for Case II, where δ_F and θ_F are the total deflection and rotation of the flange portion of the ring (Reference 6, p179), are discussed as follows. The twisting moment on the flange due to w is

$$M_{Tw} = \frac{c}{a} w \left(\frac{d - c}{2}\right) - \frac{b}{a} w' (a - b) = \frac{c}{a} w (a - c) - w (a - b) = \frac{cw}{a}(b - c) \text{ in.-lb/in.} \quad (37)$$

The total twisting moment on the flange due to w, V_0, and M_0 is

$$M_T = M_{Tw} + \frac{c}{a} V_0 \frac{h}{2} - \frac{c}{a} M_0 = \frac{c}{a}\left[w(b - c) + 0.5hV_0 - M_0\right]$$

$$M_T = \frac{15.12}{16.06}\left[\frac{15.12}{2}(16 - 15.12) + 0.5\ (0.19)\ V_0 - M_0\right]$$

$$= 6.26341p + 0.08944\ V_0 - 0.94147\ M_0 \text{ in.-lb/in.} \quad (38)$$

The flange rotation due to V_0 and M_0 is

$$\theta_{FVM} = \frac{12M_T a}{Eh^3 \ln\frac{d}{c}} = M_T \frac{12\ (16.06)}{10 \times 10^6\ (0.19)^3 \ln\left(\frac{17}{15.12}\right)} = 23.98417 \times 10^{-3} M_T$$

$$\theta_{FVM} = 23.98417 \times 10^{-3}\ (6.26341p + 0.08944\ V_0 - 0.94147\ M_0)$$

$$\theta_{FVM} = 150.2269 \times 10^{-3} p + 2.14514 \times 10^{-3}\ V_0 - 22.58038 \times 10^{-3}\ M_0 \text{ rad.} \quad (39)$$

The flange deflection due to V_0 and M_0 is

$$\delta_{FVM} = \frac{\theta_{FVM}}{a}\frac{h}{2} c = \frac{0.19\theta_{FVM}}{2}(0.94147) = 0.08944\theta_{FVM}$$

$$\delta_{FVM} = 13.43592 \times 10^{-3}\ p + 0.19186 \times 10^{-3}\ V_0 - 2.01959 \times 10^{-3}\ M_0 \text{ in.} \quad (40)$$

The flange deflection due to p is

$$\delta_{FP} = \frac{pc}{E}\left[\frac{d^2 + c^2}{d^2 - c^2} - \mu\left(\frac{c^2}{d^2 - c^2} - 1\right)\right] = \frac{15.12p}{10 \times 10^6}\left\{\frac{(17)^2 + (15.12)^2}{(17)^2 - (15.12)^2}\right.$$

$$\left. - 0.3\left[\frac{(15.12)^2}{(17)^2 - (15.12)^2} - 1\right]\right\} = 0.01170(10)^{-3}\ p \text{ in.} \qquad (41)$$

For compatibility, $\delta_C = \delta_F$ and $\theta_C = \theta_F$ (42)

where

$$\delta_C = \delta_{CP} + C_3' \delta_{CV} + C_5' \delta_{CM} \text{ and } \theta_C = C_4' \theta_{CV} + C_6' \theta_{CM},$$

$$\delta_F = \delta_{FP} + \delta_{FVM} \text{ and } \theta_F = \theta_{FVM}. \qquad (43)$$

Using Equations 32 through 36 and 39 through 42 in conjunction with Equations 43, the first of the compatibility equations (42) becomes

$$0.10227 \times 10^{-3} p + 1.24\ (-0.1825) \times 10^{-3}\ V_0 + 1.36\ (-0.1384) \times 10^{-3}\ M_0 =$$

$$0.01170 \times 10^{-3} p + 13.43592 \times 10^{-3}\ p + 0.19166 \times 10^{-3}\ V_0 - 2.01959 \times 10^{-3}\ M_0$$

$$-0.41816\ V_0 + 1.83137\ M_0 = 13.34535\ p = 300.27 \qquad (44)$$

and the second compatibility equation becomes

$$1.33\ (0.1384) \times 10^{-3}\ V_0 + 1.20 \times 0.2099 \times 10^{-3}\ M_0 = 150.22269 \times 10^{-3}\ p$$

$$+ 2.14514 \times 10^{-3}\ V_0 - 22.58038 \times 10^{-3}\ M_0$$

$$-1.98107\ V_0 + 22.83226\ M_0 = 150.22269\ p = 3380.01. \qquad (45)$$

Solving Equations 44 and 45 simultaneously for V_0 and M_0 yields

$V_0 = -111.768$ lb/in., $M_0 = 138.44$ in-lb/in.

(1) Cylindrical Portion Stresses. In the following equations, the subscript 1 refers to meridional or axial stresses, the subscript 2 refers to hoop stresses.

$$f_1 = S_{1P} \pm S_{1V}' \pm S_{1M}' = \frac{pc}{2t} \pm 0 \pm \left(-\frac{6}{t^2}\right)(-M_0) = \frac{22.5\ (15.12)}{2\ (0.19)} \pm \frac{6\ (138.4)}{(0.19)^2}$$

$$= 895 \pm 23{,}003 \text{ psi.}$$

f_1 = 23,900-psi tension
f_1 = -22,110-psi compression
(ultimate).

$$f_2 = S_{2P} + S_{2V} + S_{2M} \pm S_{2V}' \pm S_{2M}' = \frac{pc}{t} - \frac{2\lambda c V_0}{t} + \frac{2\lambda^2 c}{t}(-M_0) \pm 0 \pm \mu\left(-\frac{6}{t^2}\right)(-M_0)$$

$$= \frac{22.5 \times 15.12}{0.19} - \frac{2\ (0.7584)\ (15.12)\ (-111.5)}{0.19} \qquad \text{(cont)}$$

$$+ \frac{2\,(0.7584)^2}{t^3}\,(15.12)\,(-138.4) \pm \frac{0.3\,(6)\,(138.4)}{(0.19)^2} = 1790 + 13,459 - 12,670 \pm 6901$$

$$= 2579 \pm 6901 \text{ psi}$$

f_2 = 9480-psi tension
f_2 = -4322-psi compression
(ultimate).

(2) Flange Stresses. In the following equations, the subscript 2 refers to hoop stresses.

$$M_T = \left(\frac{c}{a}\right) M_0 - \frac{c}{a} V_0 \frac{h}{2} - \frac{c}{a} w\,(a-c) + \frac{b}{a} w'\,(a-b)$$

$$= \frac{c}{a}\left[M_0 - \frac{hV_0}{2} - w\,(b-c)\right] \text{ in.-lb/in.} \qquad (46)$$

$$f_2 = S_{2p} \pm S_2' = p\left(\frac{d^2 + c^2}{d^2 - c^2}\right) \pm \frac{12 M_T a h}{2c\,h^3 \ln\left(\frac{d}{c}\right)} = p\left(\frac{d^2 + c^2}{d^2 - c^2}\right) \pm \frac{6a\,M_T}{ch^2 \ln\left(\frac{d}{c}\right)} \text{ psi} \qquad (47)$$

From equations 46 and 47,

$$f_2 = 22.5\left[\frac{17^2 + 15.12^2}{17^2 - 15.12^2}\right] \pm \frac{6 \times 16.06 \times 15.12}{15.12\,(0.19)^2\,(0.11715)\,(16.06)}$$

$$\left[138.4 - \frac{0.19\,(-111.5)}{2} - 170.1\,(16 - 15.12)\right] = 193 \pm 976 \text{ psi}$$

f_2 = 1150-psi tension
f_2 = -803-psi compression
(ultimate).

The above discussion shows clearly that ultimate stresses in all cases are far below the ultimate strength of 42,000 psi for the ring material.

c. Floor-Ring Attachments. The floor is attached to both rings (circular and elliptical) by means of 36 fasteners per ring. The fasteners are subject to single shear by virtue of the tunnel inflation, which tends to detach the floor from the Gemini capsule and the MSS. Also, the fasteners are subject to tension, if the ring effect of the floor around the hatches is conservatively neglected, due to the tension in the floor from the in-plane component of the structural layer stresses.

Because the circular hole is larger than the elliptical hole, the analysis is done for the circular ring fasteners and the result is applied to both.

The shear force taken by each fastener is 1/36 of the pressure load acting normal to the plane of the hatch; i.e.,

$$P_s = \frac{\pi(15)^2\,(7.5)\,(3)}{36} = 442 \text{ lb (ultimate).}$$

The allowable ultimate shear strength per fastener is 1220 pounds.

$$MS = \frac{1220}{442} - 1 = 1.76 \text{ (high).}$$

The tension to which each fastener is subjected can be found from

$$P_t = (13.11p)\,\frac{2\pi\,(15)}{36} = \frac{15\pi}{18}\,(13.11p) \text{ lb.} \qquad (48)$$

With p = 7.5 psi and a load factor of 3, from Equation 48,

$$P_t = \frac{15\pi}{18} \times 13.11 \times 7.5 \times 3 = 772 \text{ lb (ultimate)}.$$

The allowable ultimate tensile strength per fastener is 1,470 pounds.

$$MS = \frac{1470}{772} - 1 = 0.90.$$

Each separation ring is fastened to the vehicle with 24 Camloc fasteners. The total applied load is $W = 3(7.5) \pi (15.12)^2 = 16,160$ pounds (ultimate tension). The load per fastener is

$$\frac{16,160}{24} = 673 \text{ pounds (ultimate tension)}.$$

The allowable ultimate tensile strength per fastener is 3840 pounds.

$$MS = \frac{3840}{673} - 1 = +4.70 \text{ (high)}.$$

d. Canister Support Brackets. The arbitrarily assumed ultimate load on each of the 10 canister support brackets is assumed to be taken by a bracket as a concentrated tip load, P. The maximum bending moment is determined from the sketch on the right to be

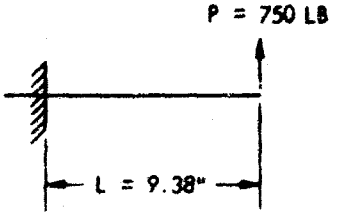

$$M'_{max} = 750 \times 9.38 = 7040 \text{ in.-lb}.$$

A typical 7075-T6 aluminum bracket cross section is shown in Figure 52. The cross section element properties are given in the following table.

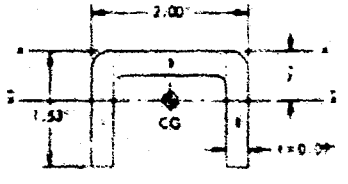

Figure 52. 7075-T6 Aluminum Bracket Cross Section (Typical)

Element	b	t	$A' = bt$	y	$A'y$	$A'y^2$
1	1.53	0.09	0.1377	0.765	0.1053	0.08055
2	1.53	0.09	0.1377	0.765	0.1053	0.08055
3	1.82	0.09	0.1638	0.045	0.0074	0.00033
Σ			0.4392		0.2180	0.16143

The cross section centroid location is given by

$$\bar{y} = \frac{\Sigma A'y}{\Sigma A'} = \frac{0.2180}{0.4392} = 0.496 \text{ in.}$$

The cross section moment of inertia is given by

$$I'_{\bar{x}} = I'_x - (\Sigma A')\bar{y}^2$$

$$I'_{\bar{x}} = \Sigma I'_0 + \Sigma A'y^2 - (\Sigma A')\bar{y}^2$$

$$= 2 \times \frac{0.09 \times 1.53^3}{12} + \frac{1.82 \times 0.09^3}{12} + 0.16143 - 0.4392 \times 0.496^2$$

$$= 0.05372 + 0.00011 + 0.16143 - 0.10805 = 0.10721 \text{ in}^4$$

The maximum bracket bending stress is

$$f_{max} = \frac{M c}{I_x} = \frac{7040\ (1.53 - 0.406)}{0.10721} = 67,800 \text{ psi (ultimate tension).}$$

The allowable tension strength of 7075-T6 aluminum is given in Reference 5, p 3.2.7.0(b) as 77,000 psi.

$$MS = \frac{77,000}{67,800} - 1 = 0.13.$$

D. ENVIRONMENTAL HAZARDS

1. Introduction

The two environmental hazards that are of concern to the tunnel design effort are the possibility of expandable wall punctures due to micrometeoroids and the materials and biological implications of space radiation. The wall puncture hazard due to micrometeoroids is assessed in terms of a probability of zero penetrations of 0.995. This probability depends upon the surface area, the exposure time, and the micrometeoroid flux relative to the shielding effectiveness of the tunnel wall. The radiation dosage necessary to cause material degradation or to endanger the welfare of the astronauts depends upon the radiation environment and the exposure time. Proton, alpha particle, and electron radiation are considered.

2. Micrometeoroid Hazard

a. General. The micrometeoroid protection afforded by the selected foam material is not optimized (maximum protection afforded versus weight of material, etc), since the micrometeoroid protection is only one of numerous factors that determine the selection of the material. Therefore, the test program was conducted to verify the fact that the proposed barrier concept would provide adequate micrometeoroid protection for the desired application. Some of the hypervelocity impact tests were conducted while this material was being subjected to the various conditions that are likely to be encountered in its Gemini-MSC crew transfer tunnel application in space. The results of the hypervelocity impact tests conducted indicate that this foam material would be adequate to ensure a probability greater than 0.995 of no penetrations in space for orbital missions of 60 days.

b. Micrometeoroid Environment. The [illegible] micrometeoroid environment used in the following hazard assessment is the standardized meteoroid environment recently proposed by a Meteoroid Specialists Subcommittee to the Aerospace Research and Testing Committee of the Aerospace Industries Association (Reference 7) and is the environment shown in Reference 8.

The yearly average sporadic environment can be represented by the following equation (Reference 8):

$$\log N = -1.34 \log m - 10.432 \qquad (4)$$

where

m, particle mass (grams) $\geq 10^{-7}$

N = number of particles of mass m or larger/ft^2-day.

This environment is illustrated in Figure 63.

For particles smaller than 10^{-7} g, a slightly different expression would be requir

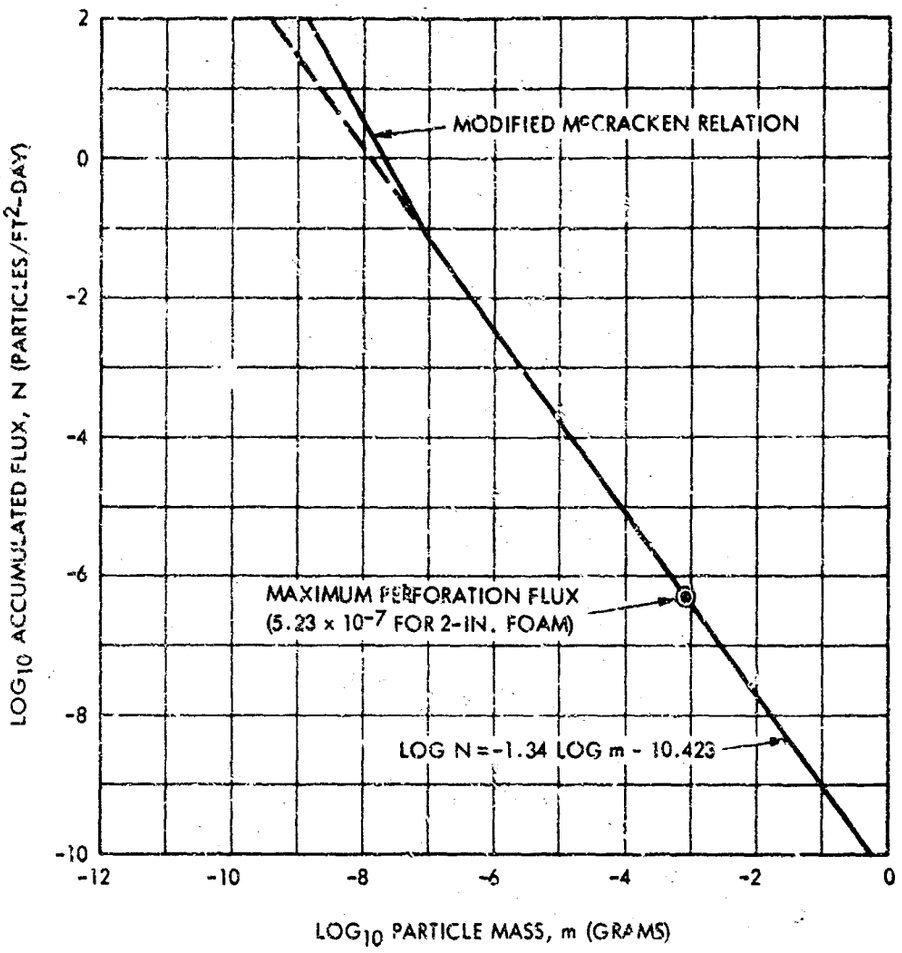

Figure 63. Near-Earth Micrometeoroid Environment

The sporadic environment is considered to be omnidirectional; therefore, a vehicle in a near-earth orbit is partially shielded by the earth from this environment at all times. In addition to the earth shielding, when impacts on only a certain part of a space vehicle are concerned, specifically the crew transfer tunnel attached to the Gemini-MSS vehicle, vehicle interference may provide additional shielding. The interference factor is designated S_I, and the earth shielding factor is S_E. The total shielding factor is then the product of these two and is expressed as S_F.

$$S_F = S_E S_I. \tag{50}$$

There is a noticeable change in sporadic environment at different times of the year; therefore, for short-term missions, a factor K is introduced to account for differences between the environment for these missions and the yearly average environment. The total number of sporadic meteoroid impacts, N'_{SP}, for a mission duration of τ days can be written as follows (Reference 8):

$$N'_{SP} = S_F N K A_B \tau \tag{51}$$

where

A_s = vehicle surface area exposed (ft^2)

S_F = total shielding factor.

The shower meteoroid flux density can be represented by an expression of the form FN, where F is the ratio of shower meteoroids to sporadic meteoroids. The shower meteoroids are considered to be unidirectional; hence, in a near-earth orbit, both the earth and the vehicle interference itself act as a periodic shield.

The number of shower meteoroid impacts is dependent on the projected area presented to the meteoroid shower stream as well as the amount of shielding. The number of shower meteoroid impacts, N'_{SH}, can be written as follows (Reference 8):

$$N'_{SH} = S_F F A_p N \tau \tag{52}$$

where

A_p = projected area (ft^2).

The total number of meteoroid impacts is then

$$U = N'_{SH} + N'_{SF}. \tag{53}$$

Combining Equations 51 through 53,

$$U = S_E N \tau (F A_p + K A_s). \tag{54}$$

For particles of mass 10^{-7} g or larger, from Equation 49,

$$N = m^{-1.34} \times 10^{-10.432} \ (ft^{-2}\text{-day}^{-1}). \tag{55}$$

From Equations 54 and 55, the total number of meteoroid impacts of particles of mass 10^{-7} g or larger is

$$U = S_E \tau (F A_p + K A_s)\ m^{-1.34} \times 10^{-10.432}. \tag{56}$$

For the Gemini-MSS crew transfer tunnel, the following values are used:

A_p = 46.0 ft^2 (maximum projected area),

A_s = 115.0 ft^2 (exposed surface area),

F = 0.62,

K = 1.73 (maximum),

τ = 60 days,

S_I = 1.00 (conservative),

S_E = 0.70 (for 300-nmi orbital height),

$S_F = S_I S_E = 0.70$.

Upon substituting these values into Equation 56, the total number of meteoroid impacts of particles of mass 10^{-7} g or larger is

$$U = 9.54 \times 10^{-7.432}\ m^{-1.34} \tag{57}$$

If U is much less than one, it can be considered the probability of impact of particles of mass 10^{-7} g or larger.

The probability of impacts, U, added to the probability of no impacts, $P_{x=0}$, must be 1; i.e.

$$U = 1 - P_{x=0} \tag{58}$$

Therefore, from Equations 57 and 58,

$$1 - P_{x=0} = 9.54 \times 10^{-7.432\ m^{-1.34}}. \tag{59}$$

Since the probability of no penetrations is to exceed 0.995, Equation 59 indicates that the barrier material must be capable of stopping all particles for which the probability of no impacts, $P_{x=0}$, is less than 0.995. Substituting $P_{x=0} = 0.995$ in Equation 59 results in a critical mass of 8.12×10^{-4} g, which is the largest projectile the barrier material must be capable of stopping to ensure a 0.995 probability of zero penetrations.

c. Micrometeoroid Penetrations. The micrometeoroid barrier capability of various materials is measured by comparing the resistance of these materials to micrometeoroid penetration as opposed to the resistance offered by a single sheet of aluminum.

The perforation thickness of single-wall aluminum, t_{al}, can be calculated by using the following equation (Reference 8):

$$t_{al} = 2.18\ m^{1/3} \tag{60}$$

where

M = particle mass (grams).

The preceding paragraph showed that a critical mass of 8.12×10^{-4} g must be stopped by the Gemini-MSS crew transfer tunnel barrier material if the probability of zero penetrations is to be 0.995 or greater. This mass would require a barrier of single sheet aluminum with a thickness of

$$t_{al} = 2.18\ (8.12 \times 10^{-4})^{1/3} = 0.2034 \text{ in.} \tag{61}$$

Polyurethane foam has been shown by company-funded hypervelocity impact tests (Reference 9) to be at least 15 times as effective by weight as single-sheet aluminum. Therefore, the required thickness of polyurethane foam for this application to achieve $P_{x=0} = 0.995$ for a two-month mission is

$$t_{foam} = 0.2034 \text{ in. al } \frac{172.8 \text{ pcf}}{15 \times 1.2 \text{ pcf}} = 1.95 \text{ in.} \tag{62}$$

The material developed for the Gemini-MSS crew transfer tunnel was therefore composed of a thin-cloth bumper wall followed by 2 inches of 1.2-pcf polyether foam. Figure 64 shows the probability of zero penetrations versus time for this material when used in the Gemini-MSS crew transfer tunnel application.

A hypervelocity particle upon striking the bumper wall is shattered. From tests conducted on this program as well as on other programs, it has been shown that projectiles of glass or plastic at velocities in excess of 20,000 fps are very easily shattered. In fact, they shatter so easily that the bumper wall can be omitted and the low-density barrier material will adequately shatter the particles. Higher velocity particles (in excess of 30,000 fps) should be shattered even more effectively; therefore, it is felt that the bumper wall would have little significance in this protection concept at very high velocities. The bumper wall becomes more and more critical as the velocity is

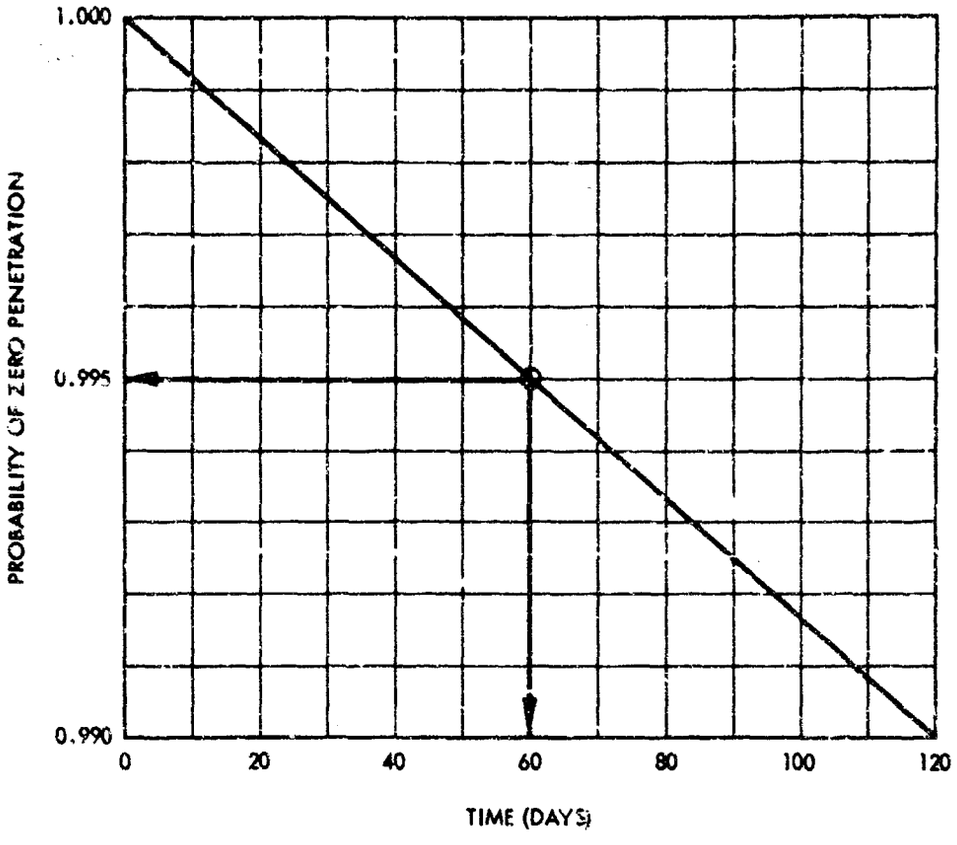

Figure 64. Probability of Zero Penetration for Tunnel Barrier Material

lowered. From other test programs, expecially Contract NAS 8-11747, GAC has shown that a bumper wall that is more than adequate at 20,000 fps may not adequately shatter the projectiles for velocities of 13,000 to 16,000 fps. Therefore, the choice of bumper wall becomes critical at low velocities. The probability of collision with a slow particle is very slight and therefore is neglected.

The barrier has to be a low-density material and of such a nature that the pieces of the shattered projectile can spread transversely to the direction of penetration. The penetration effects in the barrier as a function of mass and velocity of the projectile are affected so strongly by changing bumper wall effects as these parameters are varied that it is very difficult to analyze how barrier damage changes with these parameters.

The data that GAC has from this program and from other programs indicates that no change in barrier damage can be noted in the velocity range of 20,000 to 30,000 fps. Velocities above 30,000 fps cannot be consistently obtained; therefore, at the present time very little can be said about the velocity dependence of the barrier damage experienced.

d. Hypervelocity Impact Test Program

(1) General. The test program was conducted to verify that the material proposed by GAC for the Gemini-MSS crew transfer tunnel would be an adequate micrometeoroid barrier so that a probability of no penetrations of 0.995, using the best available estimate of the space environment, could be assured.

The calculation in paragraph "b" shows that to assure this 0.995 probability of no penetrations, the material must show a capability of stopping particles of mass 8.12×10^{-4} g or larger. The test program was carried out using projectiles of mass of approximately 5×10^{-3} g and maximum obtainable velocities of 25,000 to 30,000 fps.

(2) Test Facilities. The hypervelocity impact tests for this program were conducted at the Air Force Materials Laboratory (AFML), Wright-Patterson Air Force Base, Dayton, Ohio.

The AFML hypervelocity facility consists of an electronically triggered, high-energy storage system together with high-speed streak and framing photographic instrumentation for measuring particle velocity, size, shape, and momentum. Electronic instrumentation is provided for measuring capacitor bank discharge characteristics and the energy input to the exploding-foil gun.

Essentially, the gun consists of an electrically exploded thin foil contained in a solid plastic breech, using a plastic tube as a barrel. A schematic diagram of one arrangement of an early experimental gun is shown in Figure 65.

The electrical explosion is separated from the gun barrel and vacuum chamber by a Mylar diaphragm (rupture disk) that confines the explosion for a short time interval during which the foil melts, vaporizes, and begins to expand. In approximately 2 *usec* the diaphragm ruptures, forming a disk-shaped particle. During this time, energy is deposited at a very high rate in the propellant gas or plasma, which expands behind the particle, propelling it down the accelerator tube into an evacuated target chamber. With proper coupling, the particle is accelerated to meteoric velocities.

Since the gun completely disintegrates when it is fired, a special room houses the evacuated gun chamber and exploding-foil gun to protect equipment and operating personnel. Also provided is an air-conditioned area containing a shielded control room, a dark room, and a data analysis area.

The entire experimental area is covered with a ground plane of 0.005-inch thick copper foil soldered into a continuous sheet and connected to ground by eight copper rods driven into the earth. The copper sheet is covered with a protective layer of vinyl asbestos tile.

A camera using a double-pulsed Kerr cell electro-optical shutter for taking two frames superimposed on the same film was developed for obtaining high-resolution photographs of the particle in flight. The interframe time, which is very accurately known, and the distance traveled between frames as measured on the film with the microprojector provide the necessary data for precise calculation of particle velocity.

A schematic diagram of the high-voltage double-pulse generator used for actuating the Kerr cell shutter and the double-pulsed backlighting source are shown in Figure 66. Figure 67 shows two films taken with this Kerr cell arrangement. Each film contains two superimposed pictures of the same projectiles at slightly different times. The velocity can be determined from the distance traveled in this time interval.

The projectiles that were chosen to be fired in this test program were Mylar disks. The projectile velocities ranged from 20,000 to 30,000 fps. The mass of the projectiles upon impact were $4.81(\pm 1.38) \times 10^{-3}$ g, which was determined by firing a large number of these projectiles into lead targets and measuring the depth of penetration.

The AFML facilities were modified so that stressed specimens could be used as projectile targets. The apparatus that GAC constructed to fit the AFML facility is shown in Figures 68, 69, and 70.

(3) Test Results. The tests that were conducted to verify the micrometeoroid protection capability of the proposed barrier material can be placed into three distinct categories as follows:

(a) Seven tests were conducted in which the composite wall specimens were left at their full natural thickness of 2 inches and no stress was applied to the structural layer of the wall. The results of these tests, shown in Figures 71, 72, and 73, indicate that

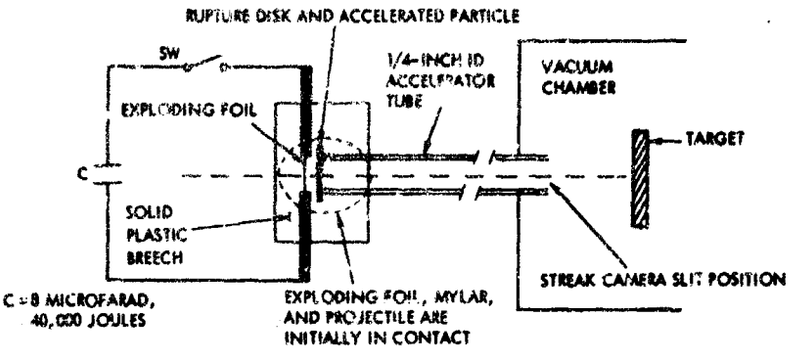

Figure 65. Schematic Diagram of Early Exploding-Foil Gun

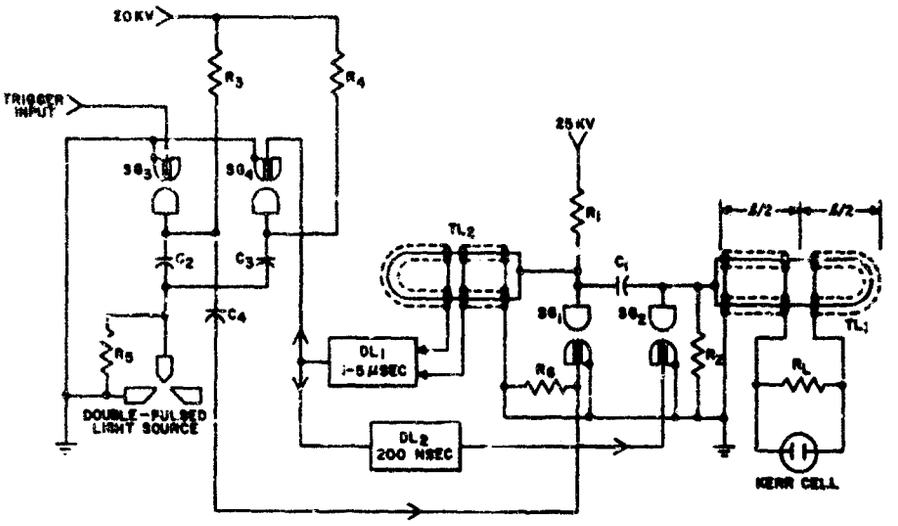

Figure 66. Schematic Diagram of Electrical Circuit for Double-Pulse Generator and Backlighting Source

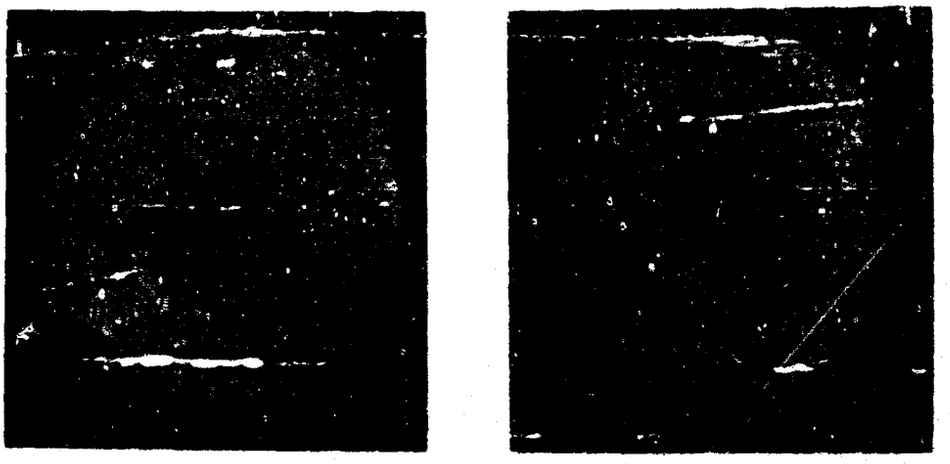

Figure 67. Projectile Films

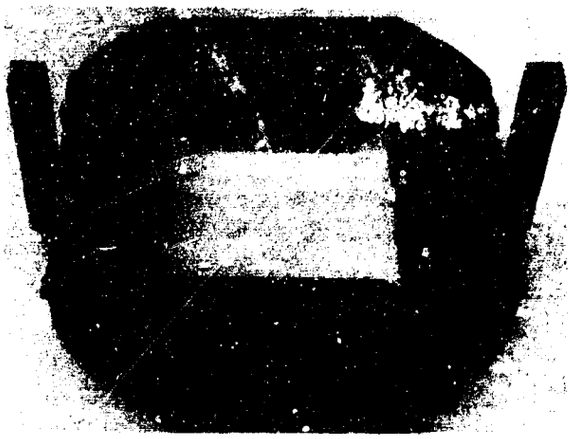

Figure 68. Test Fixture Stressing Frame

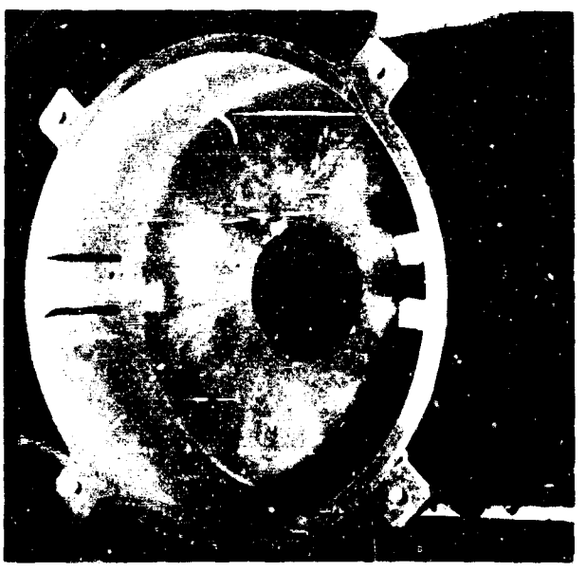

Figure 69. Test Fixture Vacuum Chamber

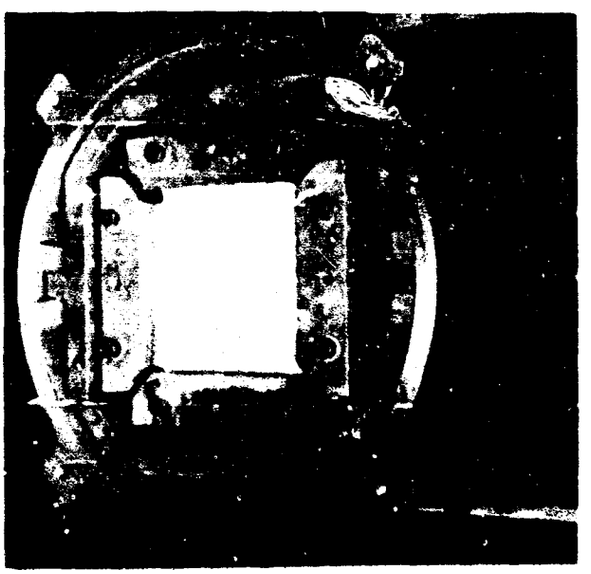

Figure 70. Test Fixture Containing Stressed Specimen

Figure 71. Hypervelocity Impact Test Specimens

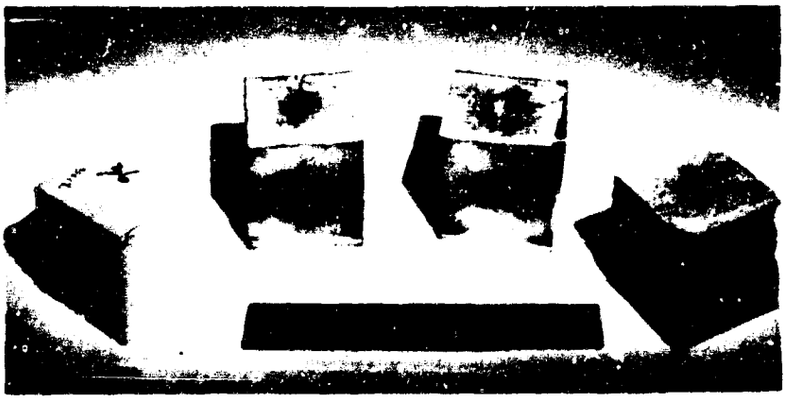

Figure 72. Typical Particle Entry Effects

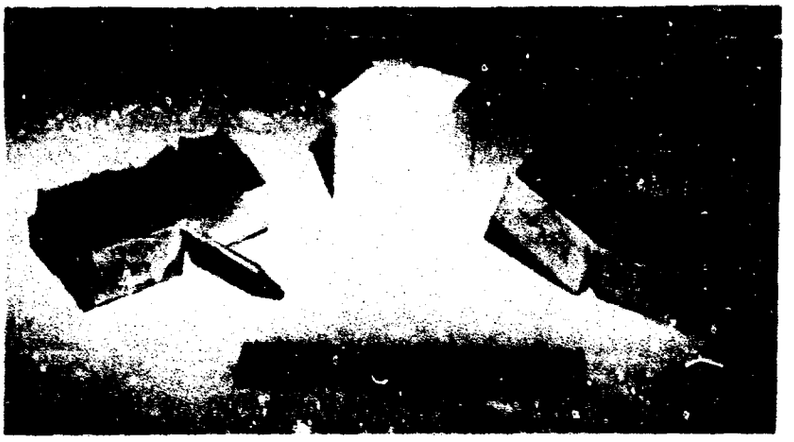

Figure 73. Typical Micrometeoroid Barrier Effects

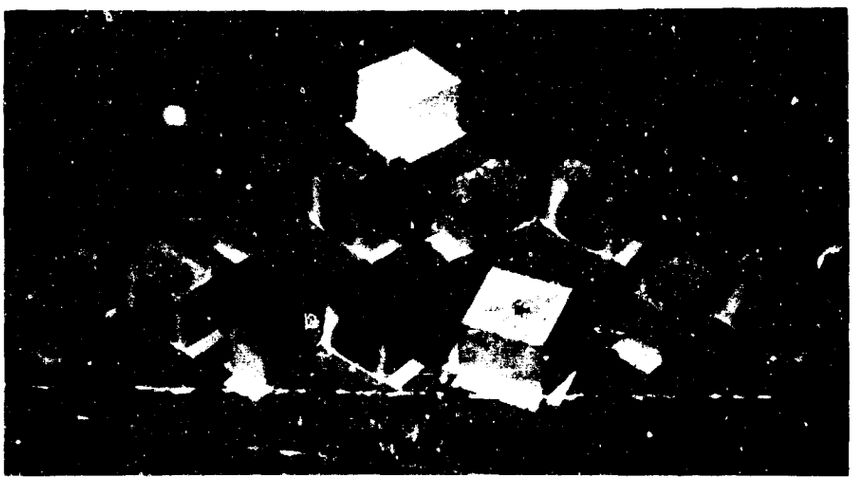

Figure 74. Stressed Specimens

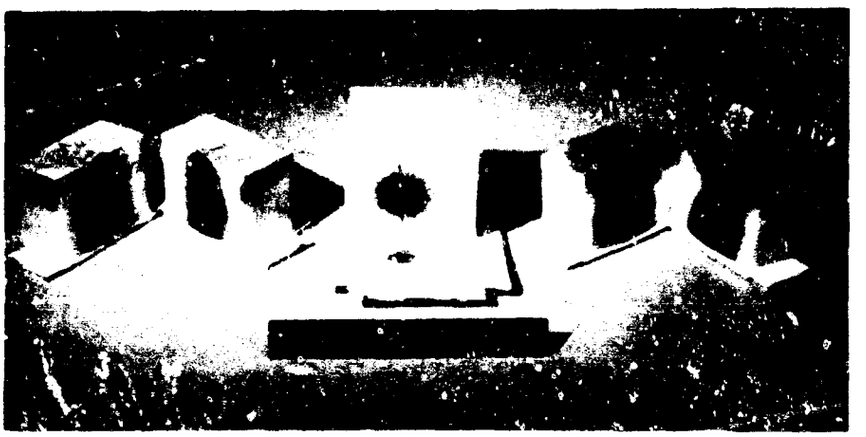

Figure 75. Specimen Comparison with Bumper Wall Removed

even though the projectile velocities varied from 25,000 to 29,000 fps, with an average of 27,000 fps, and the projectile masses varied considerably as explained earlier, the impact effects on the bumper and barrier materials were nearly identical in all cases. Typical results were the penetration of all the foam with absolutely no damage to the structural layer of the composite wall specimens. It should be noted that the nominal density of the polyether foam is 1.2 pcf, but the actual density of the foam received by GAC and used for the specimens is 1.0 pcf.

(b) The second category of tests conducted were those in which a stress was applied to the structural layer of the composite wall specimens. The stress applied was equivalent to a tunnel design pressure stress obtained by an inflation pressure of 7.5 psi. A strain was applied to the specimens equivalent to the material strain at 20 percent of the breaking strength. Six specimens with bumper walls and one specimen with the bumper wall removed were stressed and impacted. The results on all seven tests, shown in Figures 74 and 75, were very similar to the results of the tests conducted on the unstressed

specimens. The foam barrier was again penetrated, but there was absolutely no damage to the stressed structural layer. The specimen with the bumper wall removed showed barrier penetration similar to the specimens with bumper walls. If it were not necessary for other purposes, it is questionable whether or not the bumper wall would be necessary from a micrometeoroid protection standpoint. The comparison between specimens with and without bumper walls is shown in Figure 75. The middle specimen shows the foam barrier adjacent to the structural layer. The structural layer shows discoloration from the test debris, but absolutely no damage to the threads of the structural cloth is indicated.

(c) All the tests in the first two categories were conducted on specimens at their full natural thickness of 2 inches. In actual application, due to bending and folding, there is a good chance that the material may be slightly thinner than 2 inches at some points. Tests were conducted in which the thickness of unstressed specimens was varied to determine the ballistic limit of the material. The ballistic limit of the material was found to be 1.50 inches, when either foam was removed or the specimen was compressed to obtain this thickness. Specimens that had a thickness of 1.25 inches had consistent damage and/or penetration of the structural layer. Specimens that were 1.50 inches thick were never completely penetrated, although damage occurred.

Figure 76 shows unstressed specimens compressed to 1 inch with a small penetration and to 0.5 inch with major penetration. Figure 77 shows unstressed specimens 1.25, 1.5, and 1.75 inches thick respectively. The 1.25-inch specimen exhibits structural damage but no penetration. The 1.5- and 1.75-inch specimens exhibit no damage.

Tests were then conducted on 1.5-inch thick specimens in which varying stresses were applied to the structural layer. Damage with near penetration resulted in some cases, but in no case did complete penetration occur, and in no case did any tearing of the structural layer result, even when a stress equivalent to 40 percent of the layer breaking strength was applied.

To determine the effects of complete penetration on a stressed layer, a 12-inch diameter cylinder was fabricated with only a pressure bladder and a single-ply structural layer. To apply a stress in the structural layer equivalent to the tunnel structural layer design stress, the cylinder was pressurized to 8 psi. While pressurized, the cylinder was penetrated by a .22 caliber rifle bullet at a velocity of 1365 fps, so that the bullet entered on one side and exited on the other side at a point almost diametrically opposite the entry point. There was no explosive decompression or tearing. The only damage to the structural layer was the cutting of the individual cloth threads in an area approximately equivalent to the area of the bullet. This test indicates that the only damage to be expected from a penetration is a hole roughly the size of the penetrating particle.

e. Conclusions. The material proposed by GAC for the Gemini-MSS crew transfer tunnel is an adequate micrometeroid barrier to assure a probability of no penetrations of at least 0.995 during a 2-month mission using the environment given in Reference 8. The hypervelocity particle impact tests conducted at AFML showed that the material was capable of stopping particles in the mass range of $4.81(\pm 1.38) \times 10^{-3}$ g (3.5 to 6.0 g) with velocities ranging from 20,000 to 30,000 fps. The average test velocity was 27,000 fps. The following formula, obtained in Equation 59, can be used to calculate the probability of zero penetrations, using the largest mass projectiles that impacted (6 g) and were stopped by the material during the tests.

$$P_{x=0} = 1 - 9.54 \times 10^{-7.432} \times m^{-1.34}$$

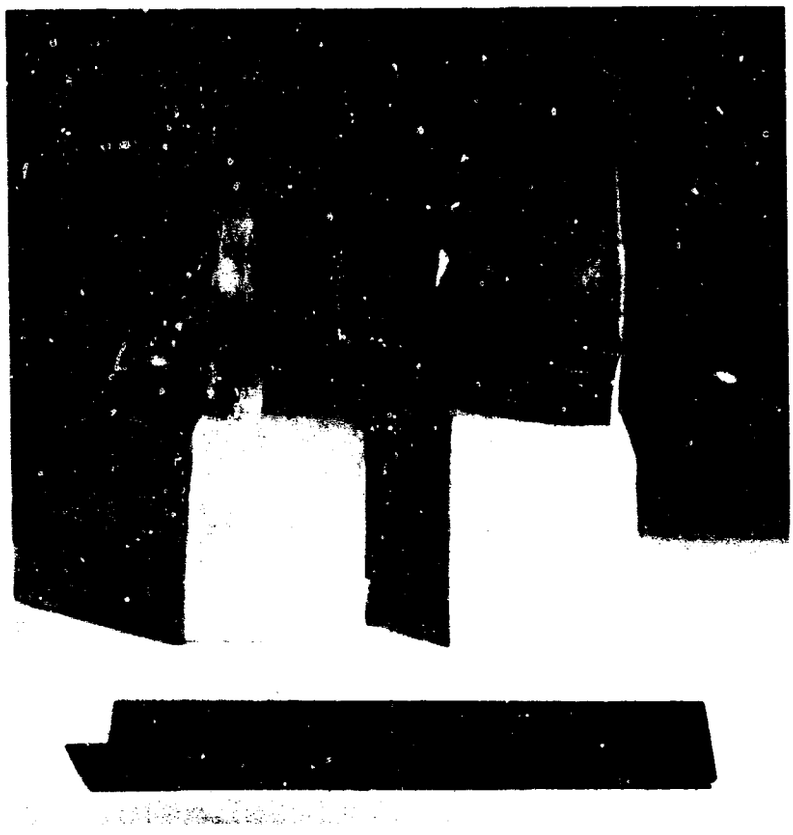

Figure 76. Unstressed Compressed Specimens

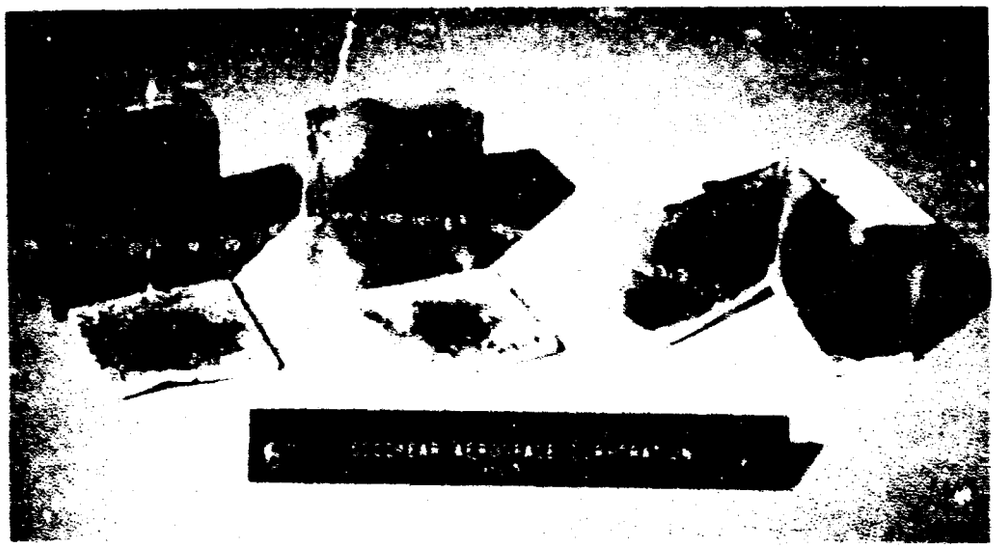

Figure 77. Specimens with Varying Thicknesses

Using $m = 6 \times 10^{-3}$ g for the particle mass, the probability of zero penetrations is

$$P_{X=0} = 0.9997.$$

Tests conducted by AFML indicate that the projectiles that were stopped by the GAC barrier material would penetrate a 3/16-inch sheet of aluminum but would not penetrate a 1/4-inch aluminum plate. Using the 3/16-inch plate for comparison, the foam has an efficiency on a weight per unit area basis of at least 16 times that of single-sheet aluminum; i.e., a sheet of aluminum having the same barrier capability would weigh 16 times as much as the foam.

The tests that were conducted at the ballistic limit of the barrier material on specimens with a stressed structural layer indicate that the structural material when penetrated does not exhibit any tearing tendencies.

3. Radiation Hazard

a. Space Radiation Environment. The orbit of the Gemini-MSS vehicle has yet to be defined; therefore, it is necessary to consider the radiation environment of all possible near-earth orbits (100 to 300 nmi) that could be used. A space vehicle can encounter high energy proton, electron, and alpha particle radiation, depending on its orbit. The major sources of proton and alpha particle radiation are solar flares and the Van Allen belts. At low latitudes, near-earth orbits are shielded by the earth's magnetic field; however, at the high latitudes, the magnetic field lines bend into the earth, and therefore both Van Allen belt radiation and solar flare radiation can extend down to a much lower altitude in these regions. This effect is discussed in References 10 and 11. The effect that the earth's magnetic field would have on the directional characteristics, shielding effects, etc in the high latitude regions would be very difficult, if not impossible, to obtain. Therefore, the assumption is made that at latitudes below 60 degrees, no high energy protons or alpha particles get through the earth's magnetic field, and at latitudes above 60 degrees, no solar flare protons or alpha particles are stopped by the earth's magnetic field. In a polar orbit a vehicle would be subject to proton and alpha particle bombardment for approximately half of the orbit, which would be divided into two periods of approximately 22 minutes of radiation and two periods of approximately 22 minutes of no radiation, while no proton or alpha particle radiation would be encountered in orbits that did not extend above the 60-degree latitude. The Gemini-MSS crew transfer tunnel is to be used only to transfer astronauts, and it is felt that this transfer could take place during periods of no radiation if the radiation level were excessive. Hence no consideration is given to the proton or alpha particle radiation dosage an astronaut inside the tunnel might recieve, but only the radiation dosage received by the tunnel wall itself is considered.

The probability per day, P, of having a solar flare with a total flux of protons larger than N is given by the following equation (see Reference 12):

$$P[N] = 0.0022 (10 - \log_{10} N) \tag{63}$$

where

N, the total solar flare event number of protons with energy above 30 mev, $\geq 10^{10}$ protons cm^2.

This is shown in Figure 78.

For any mission duration, the probability, P_τ, of encountering a solar flare with a total flux of protons larger than N is given by

$$P_\tau[N] = 0.0022 (10 - \log_{10} N)\tau \tag{64}$$

where

τ is the mission duration (days).

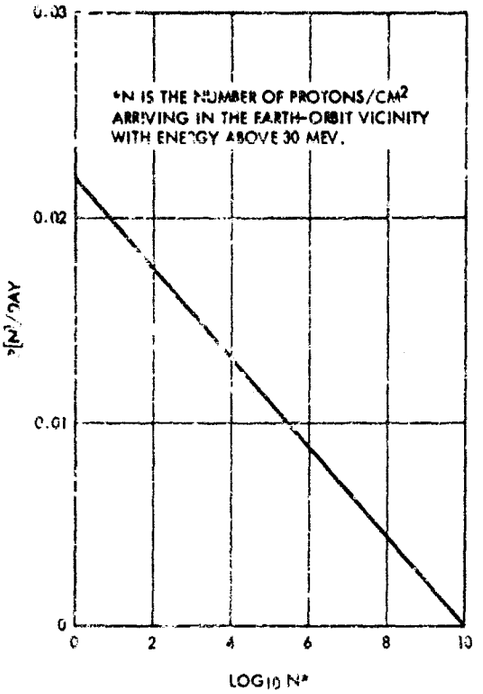

Figure 78. Probability per Day for the Occurrence of an Event Having a Size Greater Than N

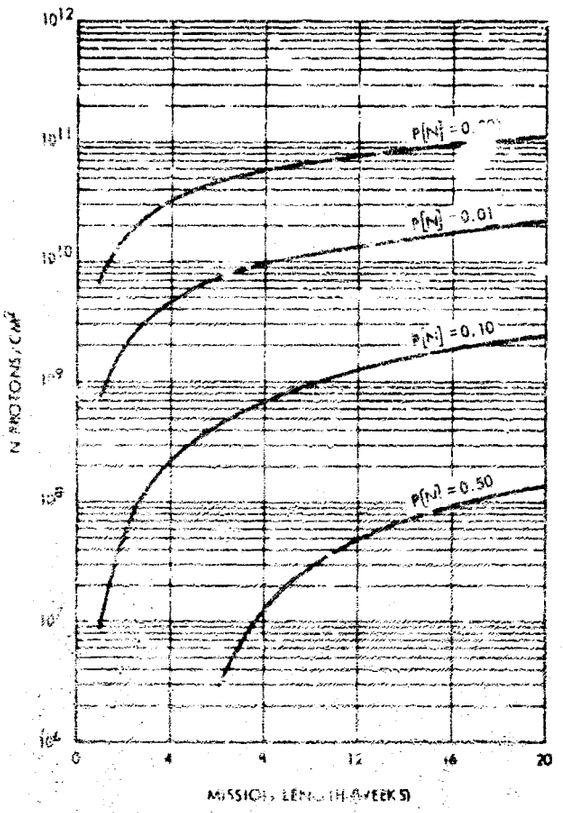

Figure 79. Variation of Number of Protons/Cm^2 with Mission Lengths at Four Probability Levels

$N \leq 10^{10}$ protons/cm^2.

This is shown in Figure 79, which is taken from Reference 13. The mission duration is to be 60 days, and the probability of encountering any event during this mission, $P_M[N]$, would be, using $\tau = 60$ days in Equation 64,

$$P_M[N] = 0.1320\,(10 - \log_{10} N)$$

where

$$N \leq 10^{10} \text{ protons/cm}^2. \tag{65}$$

This expression shows that small solar flares occur much more frequently than large solar flares. By using this expression or Figure 79, it is possible to show that the probability of not receiving a total flux greater than 10^{10} protons/cm^2 from all sized solar flares is greater than 0.990.

The spectrum for alpha particles and protons, which a space vehicle can be expected to encounter in a near-earth polar orbit as a result of one complete 10^{10} total flux solar flare, can be written in the following form (see Reference 12):

$$N[>R] = 6 \times 10^{10}\ e^{-R/80} \tag{66}$$

where

$N[>R]$ = the number of isotropic particles/cm^2 with magnetic rigidity $> R$,

$$R = \frac{pc}{Z\epsilon}, \text{ particle rigidity (million volts)}, \tag{67}$$

where

p = particle momentum (mev-sec/cm),

c = velocity of light (cm/sec),

$Z\epsilon$ = the nuclear charge of the particle (electron charges).

Equation 66 is illustrated graphically in Figure 80.

Relativistic expressions can be used to obtain magnetic rigidity, R, as a function of kinetic energy.

$$T^2 = p^2c^2 + m_0{}^2c^4 \tag{68}$$

where

$T = E + m_0c^2$ (mev),

where

E = kinetic energy (mev),

m_0 = particle rest mass (g),

m_0c^2 = rest energy (mev).

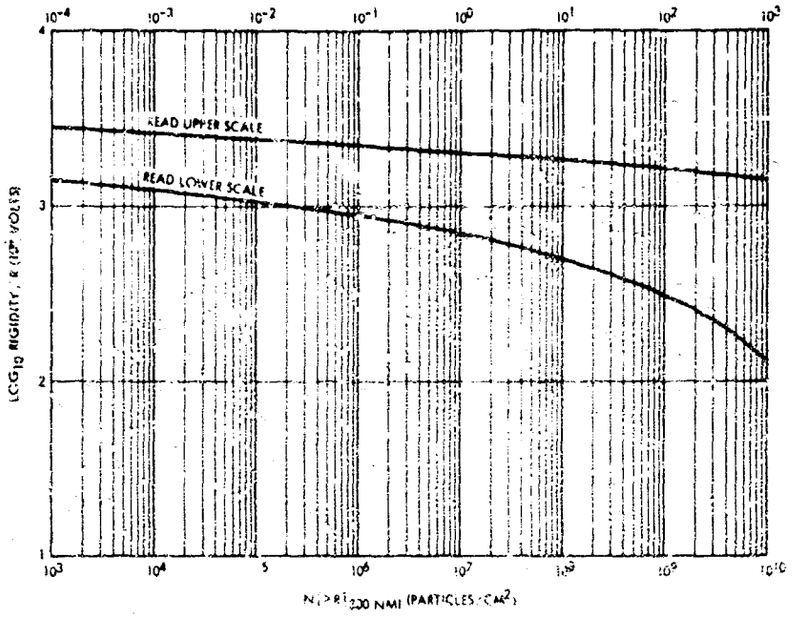

Figure 80. Flux of Protons and Alpha Particles with Rigidity > R from Model Solar Flare for a 300-NMi Altitude Earth Orbit

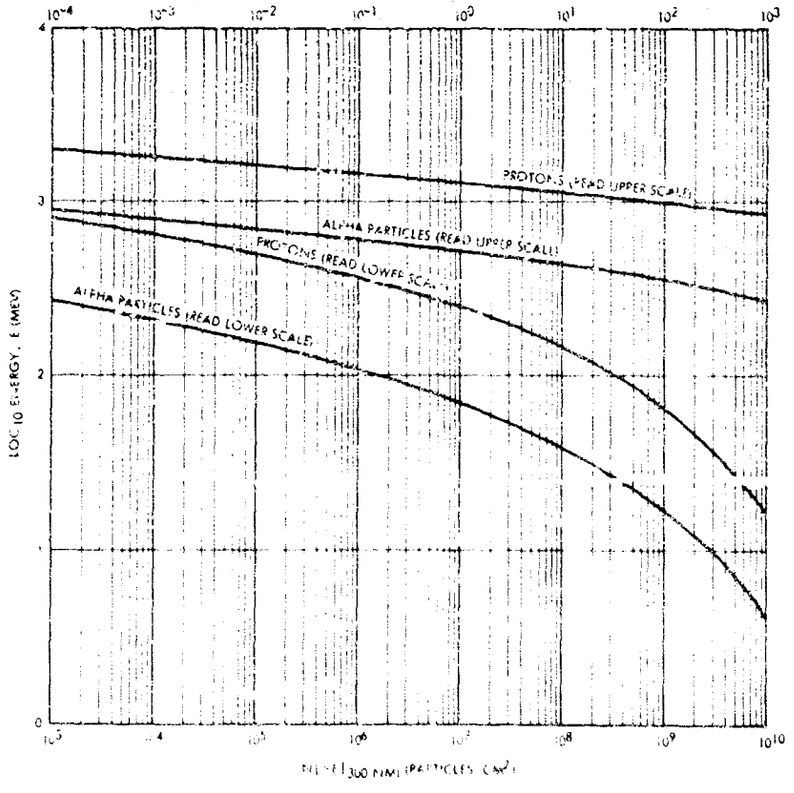

Figure 81. Flux versus Energy of Proton and Alpha Particle Radiation for a 300-NMi Altitude Earth Orbit

From Equation 68, the rigidity is

$$\frac{pc}{Ze} = \frac{\sqrt{T^2 - m_0^2 c^4}}{Ze} \tag{69}$$

Substituting $T = E + m_0 c^2$ into Equation 69 gives

$$\frac{pc}{Ze} = \frac{\sqrt{\left(E + m_0 c^2\right)^2 - m_0^2 c^4}}{Ze} = \frac{\sqrt{E^2 + 2Em_0 c^2}}{Ze}. \tag{70}$$

Using this rigidity-energy relationship, fluxes of protons and alpha particles with energy greater than E for a 300 nautical mile orbit, $N[>E]_{300\ nmi}$, may be obtained from Equation 66 for fluxes with magnetic rigidity greater than P, $N[>R]_{300\ nmi}$. The flux versus energy relationship is shown in Figure 81.

b. Proton and Alpha Particle Radiation Damage Effects. The radiation damage to a material is measured in terms of the amount of energy absorbed from incident radiation per unit weight of absorbing material. The most commonly used unit is the rad, which is the amount of incident radiation on any material necessary to cause that material to absorb 100 ergs of energy for each gram of material present. The energy absorbed in rads by a material due to both protons and alpha particles from a single solar flare having a total flux of 10^{10} particles/cm^2 is calculated by numerically integrating the relationship (see Reference 14)

$$\Delta D = \frac{\Delta N\left(\bar{E} - E'\right)}{r_{\bar{E}}\left(6.25 \times 10^7\ \text{mev/g-rad}\right)} \tag{71}$$

where

ΔD = the energy absorbed per unit mass of the material from ΔN particles (rads),

$\Delta N = (dN/dE)\ 2\Delta E \approx N[E + \Delta E] - N[E - \Delta E]$, the number of particles/cm^2 from a single 10^{10} particles/cm^2 total flux solar flare with incident energy in the energy range of $E + \Delta E$ to $E - \Delta E$,

where

ΔE = the energy increment small enough for the derivative dN/dE to be replaced by $\frac{N[E + \Delta E] - N[E - \Delta E]}{2\Delta E}$ and maintain the desired calculation accuracy (mev),

$N[E + \Delta E]$ = the number of particles/cm^2 from a single 10^{10} particles/cm^2 total flux solar flare with energy greater than $E + \Delta E$,

$N[E - \Delta E]$ = the number of particles/cm^2 from a single 10^{10} particles/cm^2 total flux solar flare with energy greater than $E - \Delta E$,

and where

$\bar{E}$ = average incident energy of particles in the range of $E + \Delta E$ to $E - \Delta E$ (mev),

E' = average energy with which the particles leave after they have penetrated the material (mev),

$r_{\bar{E}}$ = average range of particles for energy $\bar{E}$ (g/cm^2).

A plot of proton range in water versus proton energy is given in Figure 82, and a plot of alpha particle range in water versus alpha particle energy is given in Figure 83. These curves are from Reference 15. The material used in the Gemini MSS crew transfer tunnel has an areal density of about 0.34 g/cm^2.

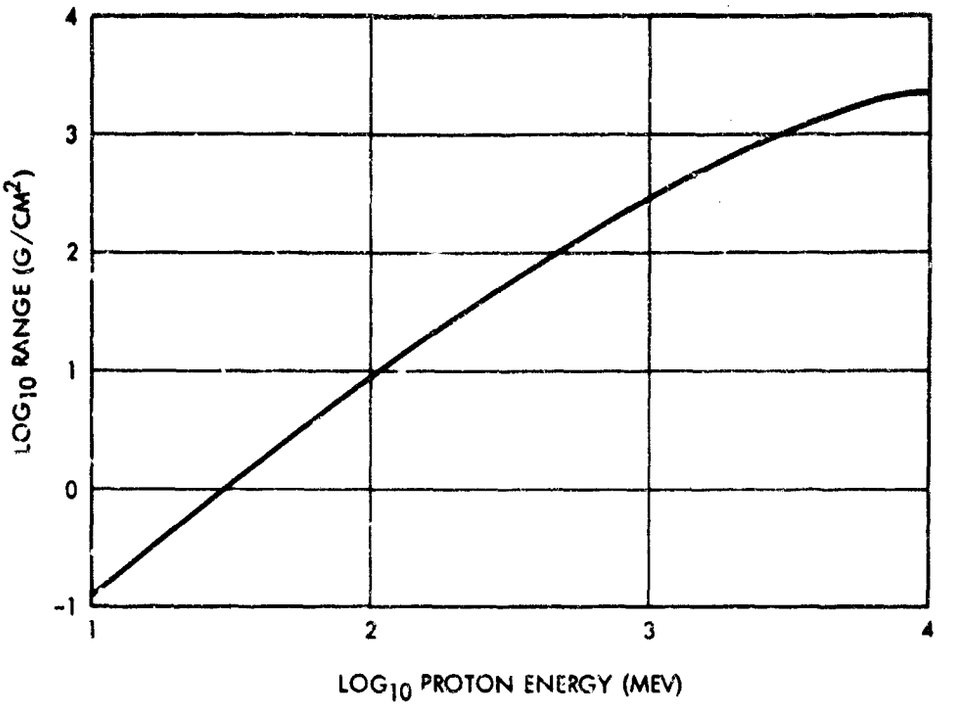

Figure 82. Proton Range in H_2O versus Proton Energy

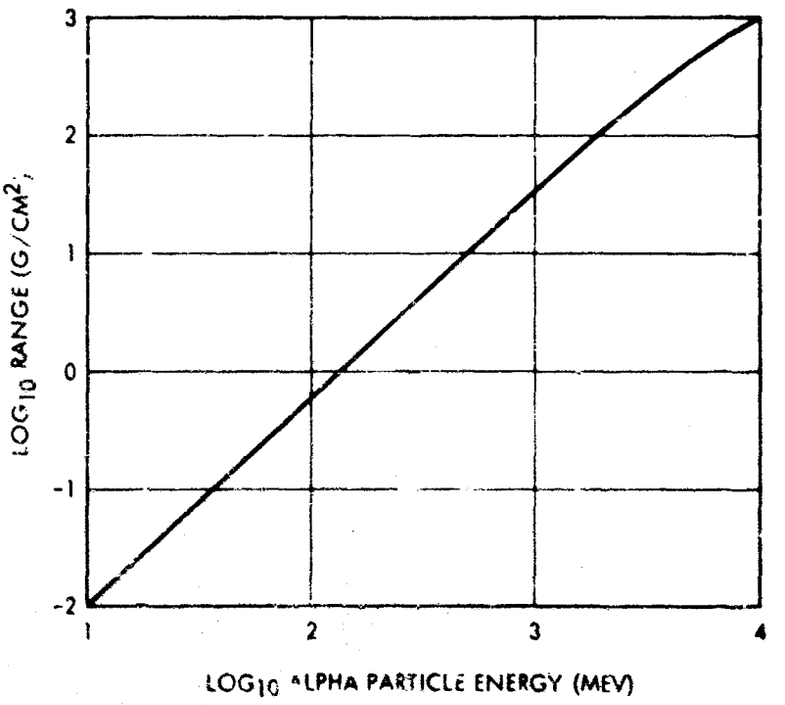

Figure 83. Alpha Particle Range in H_2O versus Alpha Particle Energy

Using the above relationship, Equation 71, in conjunction with Figures 81, 82, and 83, it is possible to obtain the radiation dose received by the tunnel material. The calculations are shown in Tables VII and VIII.

The maximum high energy proton and alpha particle radiation dose received by any part of the tunnel wall is the sum of the total dosage given in Tables VII and VIII, which is about 2×10^5 rads for a 10^{10} particles/cm^2 total flux (i.e., time integrated flux) solar flare. The largest portion of this radiation is due to relatively low energy alpha particles that are absorbed by the thin outer fabric layer containing the thermal coating (areal density 2.3×10^{-2} g/cm^2). All radiation with a range less than 2.3×10^{-2} g/cm^2 will be absorbed by the outer layer fabric, which can be seen from Tables VII and VIII to include all particles with energy less than 20 mev. The maximum radiation dose received by any of the material inside the outer fabric layer is the sum of all the dosages associated with particle energies above 20 mev.

The summation of these terms from Tables VII and VIII yields a number less than 2×10^4 rads for the maximum dose received by any of the foam or structural wall materials. GAC has conducted tests and shown that no measurable damage occurs to plastic-type materials subjected to radiation dosages in excess of 10^6 rads. Other data, Reference 11, indicates that no significant damage would occur to material similar to that used on the tunnel with dosages of 10^8 rads. Therefore, one can confidently say that no damage would result to the tunnel material due to proton and alpha particle radiation regardless of which near-earth orbit was chosen.

c. Electron Radiation. In addition to the proton and alpha particle radiation, which would only be encountered in polar orbits, the Gemini-MSS vehicle would be subjected to electron radiation in any near-earth orbit. The electron radiation environment encountered varies somewhat with orbit; however, from data given in Reference 16, as can be seen in Figure 84, a conservative estimate would be a flux of 10^7 electrons/cm^2-sec with energies above 40 kev for any near-earth orbit. The range of electrons in aluminum (which does not vary more than a factor of 2 for other materials) in g/cm^2 is given by the following expression (see Reference 14):

$$r_e = 0.407\, E_e^{1.38} \tag{72}$$

where

$$E_e < 0.8 \text{ mev.}$$

For the electron energy spectrum that is being considered, it can be seen that the electrons have a very small range. Therefore, most of these electrons would be absorbed in the outer fabric layer, which has an areal density of approximately 2.3×10^{-2} g/cm^2. The number of particles with energies $\geq$ 40 kev drops off very rapidly, and therefore the assumption is made that the average particle encountered has an energy of about 50 kev. The following expression can be used to calculate the radiation dose (in rads) due to electrons:

$$\text{radiation dose} = \frac{\text{incident flux x mission time x energy per particle}}{\text{areal density} \times 6.25 \times 10^7 \text{ mev/g rad}} . \tag{73}$$

Substituting the appropriate values for the Gemini-MSS crew transfer tunnel mission into Equation 73 gives

$$\text{radiation dose} = \frac{8.64 \times 10^{11} \text{ electrons/cm}^2\text{-day} \times 60 \text{ days} \times 50 \times 10^{-3} \text{ mev}}{2.3 \times 10^{-2} \text{ g/cm}^2 \times 6.25 \times 10^7 \text{ mev/g rad}}$$

$$= 1.8 \times 10^6 \text{ rads.}$$

Even this radiation dose would prove to be no hazard to the tunnel material, and this number is very conservative.

Table VII. Proton Radiation Dose Received by Gemini-MSS Crew Transfer Tunnel from a 10^{10} Particles/Cm^2 Total Flux Solar Flare

E (mev)	$N[>E]_{300\ nmi}$ (particles/cm^2)	ΔN (particles/cm^2)	$\bar{N}$[a] (particles/cm^2)	$\bar{E}$ (mev)	$r_{\bar{E}}$ (g/cm^2)	$r_{E'}$[b] (g/cm^2)	E' (mev)	$\bar{E} - E'$ (mev)	ΔD[c] (rads)
500	9.0×10^4	2.8×10^7	1.4×10^7	235	33.0	32.66	233.7	1.3	0.0176
200	2.8×10^7	3.0×10^8	1.8×10^8	121	10.7	10.36	118.5	2.5	1.121
100	3.3×10^8	1.4×10^9	1.0×10^9	64.6	3.45	3.11	60.8	3.8	24.700
50	1.7×10^9	2.6×10^9	3.0×10^9	37.2	1.26	0.92	31.0	6.2	200.00
30	4.3×10^9	3.7×10^9	6.15×10^9	23.4	0.55	0.21	14.0	9.4	1010.00
20	8.0×10^9	2.0×10^9	9.0×10^9	17.5	0.32	--	--	17.5	1750.00
17	1.0×10^{11}	$\Sigma = 10^{10}$							$\Sigma = 2985$

[a] $\bar{N}$ = average $N[>E]$, the number of particles/cm^2 with incident energy greater than $\bar{E}$.

[b] $r_{E'} = r_{\bar{E}} - t'$, average range of particles for energy E' (g/cm^2) where t', material thickness (areal density), = 0.34 g/cm^2 for the tunnel composite wall.

[c] $\Delta D = \dfrac{\Delta N (\bar{E} - E')}{r_{\bar{E}} (6.25 \times 10^7\ mev/g\text{-}rad)}$ rads (see Equation 71).

Table VIII. Alpha Particle Radiation Dose Received by Gemini-MSS Crew Transfer Tunnel from a 10^{10} Particles/Cm^2 Total Flux Solar Flare

E (mev)	$N[>E]_{300\ nmi}$ (particles/cm^2)	ΔN (particles/cm^2)	$\bar{N}$[a] (particles/cm^2)	$\bar{E}$ (mev)	$r_{\bar{E}}$ (g/cm^2)	$r_{E'}$[b] (g/cm^2)	E' (mev)	E - E' (mev)	ΔD[c] (rads)
500	1.4	1.3×10^4	6.5×10^3	218	3.0	2.66	212	6.0	0.0004
200	1.3×10^4	1.5×10^6	7.5×10^5	112	0.8	0.46	82	30.0	0.822
100	1.5×10^6	3.55×10^7	1.92×10^7	59.0	0.24	--	0	59.0	140.0
50	3.7×10^7	1.63×10^8	1.19×10^8	36.4	0.11	--	0	36.4	865.0
30	2×10^8	4.5×10^8	4.25×10^8	23.4	0.047	--	0	23.4	3580
20	6.5×10^8	1.15×10^9	1.22×10^9	14.7	0.017	--	0	14.7	15.970
10	1.8×10^9	6.2×10^9	4.9×10^9	7.08	0.0042	--	0	7.08	97.500
5	8×10^9	2.0×10^9	9.0×10^9	4.37	0.0020	--	0	4.37	70.000
3.98	1.0×10^{10}	$\Sigma = 10^{10}$							$\Sigma = 188.000$

[a] $\bar{N}$ = average $N[>E]$, the number of particles/cm^2 with incident energy greater than $\bar{E}$.

[b] $r_{E'} = r_{\bar{E}} - t'$, average range of particles for energy E' (g/cm^2) where t', material thickness (areal density), = 0.34 g/cm^2 for the tunnel composite wall.

[c] $\Delta D = \dfrac{\Delta N (\bar{E} - E')}{r_{\bar{E}} (6.25 \times 10^7\ mev/g\text{-}rad)}$ rads (see Equation 71).

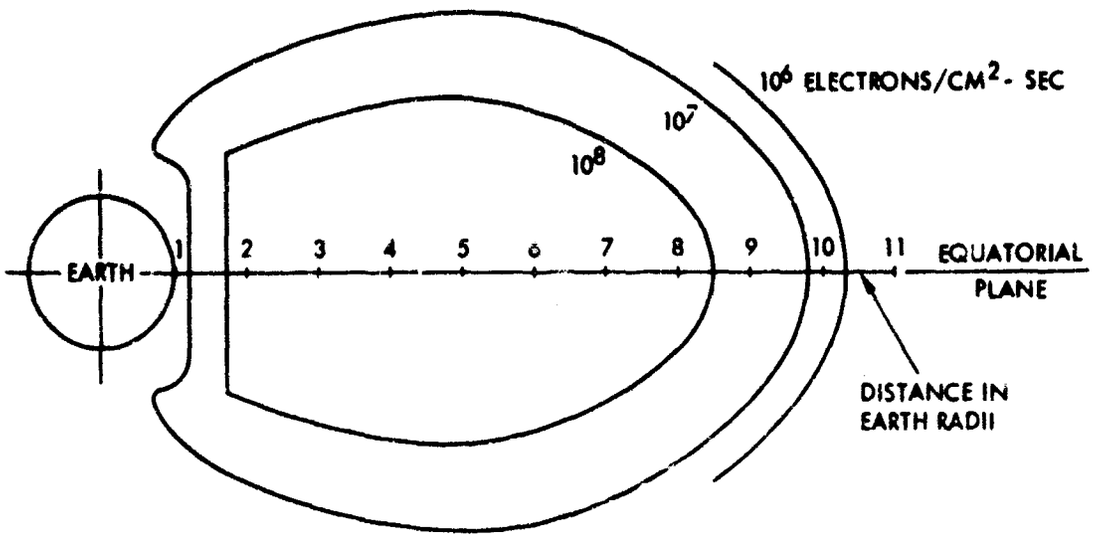

Figure 84. Flux of Electrons with Energy Greater Than 40 KeV Trapped in the Earth's Magnetic Field

It was shown earlier that most of the electrons would be absorbed in the outer layer of fabric. The rest of the electrons would be absorbed by the wall material, and virtually no electron radiation would get through the tunnel wall to bombard astronauts in the tunnel.

d. Conclusions. The Gemini-MSS crew transfer tunnel will be subjected to electron radiation in any near-earth orbit and to high energy proton and alpha particle radiation for approximately half the time in a polar orbit. Since it is felt that astronaut transfer could take place during periods of no radiation during a polar orbit, no consideration is given to the proton and alpha particle radiation dosage an astronaut inside the tunnel might receive.

The maximum high energy proton and alpha particle radiation dose received by any part of the tunnel wall is 2×10^5 rads for a 10^{10} particles/cm^2 total flux solar flare, most of which is absorbed by the outer cover of the tunnel wall, which supports the thermal coating. Only particles with energies above 20 mev will penetrate the outer cover, and the radiation dose received by the foam barrier and structural layer of the tunnel wall is less than 2×10^4 rads.

A very conservative value for the electron radiation dose is less than 2×10^6 rads, most of which is absorbed by the outer cover. The remainder is mostly absorbed by the inner layers of the tunnel wall, and virtually no electron radiation will penetrate to the tunnel interior.

Since test data indicates that the tunnel wall material can withstand radiation dosages of 10^8 rads with no measurable damage, the radiation dose received by the tunnel presents no problem with regard to damage to the tunnel materials.

E. MATERIALS SELECTION

1. General

A composite material structure was selected as the best approach to meet the overall requirements of the transfer tunnel design. This composite structure was developed on in-house, company-funded development programs. The results of the development programs that are applicable to this contract effort are discussed in this subsection. Figure 85 depicts the composite, which comprises four distinct layers bonded into a homogenous structure. The inner layer, an unstressed pressure bladder, maintains pressure tightness and transmits pressure loads to an adjacent structural layer. The structural layer carries structural loads resulting from internal pressure. The flexible foam layer acts as a micrometeoroid barrier, protecting the pressure bladder from penetration. The outer cover performs a dual function. It is used as a smooth base for the application of a thermal coating, and it encapsulates the total composite for evacuation and compression prior to packaging for launch.

2. Composite Wall Description

a. Pressure Bladder. The pressure bladder is a laminate of three individual sealant layers (see Figure 86). The inner layer is a laminate of Capran film (Allied Chemical Type 77-C) bonded with polyester adhesive (Schjeldahl Type GT-201) between two layers of lightweight nylon cloth (Travis Style 5096). This layer is bonded with polyester adhesive (Goodyear PE-207) to a second layer of closed-cell polyvinyl chloride foam 0.070 inch thick (Great American Industries Rubatex R-313-V). The outer sealant is a close-weave nylon cloth (Burlington Style 1632) coated with a polyester resin (Goodyear PE-207). Qualification testing of the pressure bladder components demonstrated the basic material to be suitable for the design requirements. Tests were conducted on the pressure bladder to determine permeability rate, possible toxicity, abrasion characteristics with respect to the astronaut's space suit, and weight loss and possible delamination due to off-gassing in a vacuum environment. Excellent flexibility is imparted to the laminate with the use of low modulus Capran film, while the closed cell vinyl foam provides a cushioned layer for puncture protection. Physical properties of the pressure bladder component materials are shown in Table IX.

b. Structural Layer. The structural layer is a four-ply laminate of Dacron cloth bonded with a polyester adhesive (Goodyear PE-207). Although a design pressure of 7.5 psia with a safety factor of 5 requires a load capability of 829 lb/in., further allowance for degradation in strength due to creep rupture and ply lamination produces a required original strength of approximately 1300 lb/in. . This load is carried entirely by the structural layer which due to the multiple ply technique of staggering joints in the individual plies, offers an essentially seamless construction. This strength requirement can be satisfied by four plies of Stern and Stern Style 15292 Dacron cloth having a single-ply strength of 329 lb/in. Due to the unavailability of the desired style 15292 Dacron cloth, all qualification test samples and the prototype tunnel structural layer were constructed with Stern and Stern Style 15246 Dacron cloth. The same percentage changes under test conditions as compared to original values for Style 15246 cloth are applied to Style 15292 cloth for evaluation purposes.

Structural material qualification testing conducted to investigate environmental effects due to temperature extremes, vacuum, high energy radiation, and creasing and flexing indicated that the full load capability of 829 lb/in. could be carried by both the four-ply structural layer and joints. Physical properties of the Dacron structural ply cloths are shown in Table X.

c. Micrometeoroid Barrier. To provide the penetration resistance required by the micrometeoroid hazard assessment (see subsection D), a 2-inch thick layer of flexible polyether foam of 1.2-pcf density was selected. Shelf life tests indicate that the polyether foam provides good elastic recovery characteristics for the exposure conditions required before and after deployment. Also, good ply adhesion strength is obtained in bonding the polyether foam layer to the other layers. Qualification tests conducted to determine effects of off-gassing, temperature extremes, and radiation exposure determined the polyether foam to be compatible with environmental requirements.

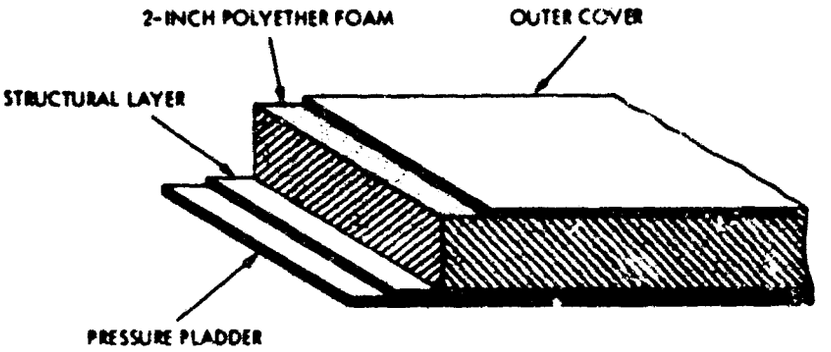

ITEM	WEIGHT (PSF)
INNER REFLECTIVE COATING	0.032
PRESSURE BLADDER	0.126
STRUCTURAL LAYER	0.210
2-INCH FOAM LAYER (1.2 PCF)	0.200
OUTER COVER	0.041
INTERLAYER POLYESTER ADHESIVE	0.081
TOTAL	0.690

Figure 85. Tunnel Design Composite Wall

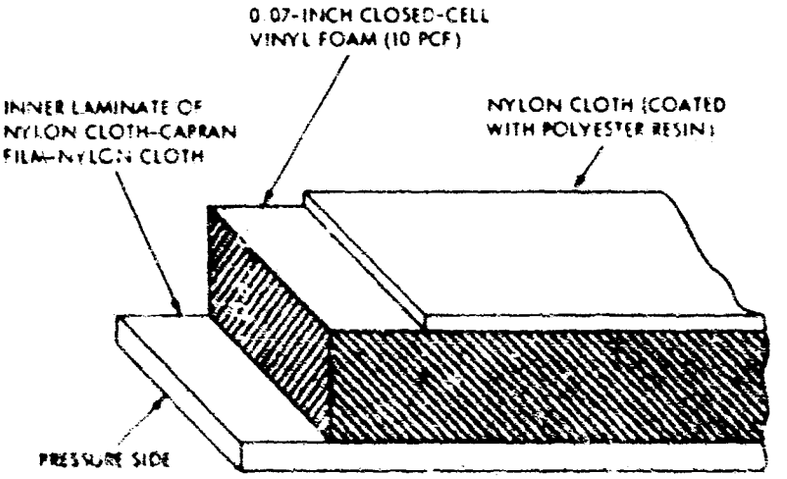

ITEM	WEIGHT (PSF)
INNER LAMINATE	0.015
POLYESTER ADHESIVE	0.027
CLOSED-CELL VINYL FOAM	0.042
POLYESTER ADHESIVE	0.027
OUTER NYLON CLOTH	0.015
TOTAL	0.126

Figure 88. Pressure Bladder

Table IX. Physical Properties of Pressure Bladder Components

Nylon Cloth (Travis 5096)	
Weight (psf)	0.0063
Breaking strength, warp/fill (lb/in.)	40/40
Thickness (mils)	2.5
Capran Film (Allied Chemical 77-C)	
Specific gravity	1.13
Thickness (mils)	0.75
Ultimate tensile, longitudinal (psi)	8500 - 11,500
Ultimate tensile, transverse (psi)	7000 - 11,000
Elongation, longitudinal/transverse (percent)	300 - 400
Tensile modulus, longitudinal (psi)	90,000 - 110,000
Tensile modulus, transverse (psi)	105,000 - 125,000
Nylon-Capran-Nylon Laminate	
Weight (psf)	0.015 (avg)
Breaking strength, warp/fill (lb/in.)	72.0/60.0 (min)
Ply adhesion (lb/in.)	4.0 (avg)
Thickness (mils)	6.75
Nylon Cloth (Burlington 1632)	
Weight (psf)	0.015
Breaking strength, warp/fill (lb/in.)	140/91
Thickness (mils)	4.7
PVC Foam (Rubatex R-313-V)	
Density (pcf)	10.0 - 13.0
Temperature resistance (°F)	
Low	-10
High continuous	130
High intermittent	200
Compression set (ASTM method)	
Compressed 50 percent for 22 hours at 70°F	50 percent (max)
Thickness (inches)	0.070

Table X. Physical Properties of Dacron Cloth

Property	Dacron 15246	Dacron 15292
Width (inches)	44.0	44.0
Thread count, warp	65	51
Thread count, fill	65	46
Ultimate tensile strength, warp (lb/in.)	270	329
Ultimate tensile strength, fill (lb/in.)	277	293
Tongue tear strength, warp (lb)	43	18
Tongue tear strength, fill (lb)	35	17
Ultimate elongation, warp (percent)	27	36
Ultimate elongation, fill (percent)	31	35
Air porosity (cu ft/min)	63	9
Thickness (inches)	0.0136	0.0117
Weight (psf)	0.048	0.045
Cloth weave	Basket	Plain

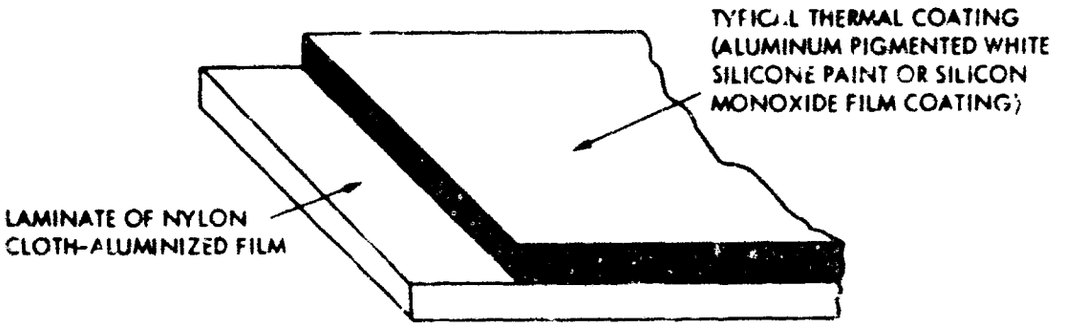

ITEM	WEIGHT (PSF)
FILM CLOTH LAMINATE	0.015
THERMAL COATING	0.026
TOTAL	0.041

Figure 87. Outer Cover of Composite Wall

d. Outer Cover and Thermal Control Coating. The outermost layer of the composite wall structure encapsulates the wall and provides a smooth base for the application of a thermal coating. The construction of this layer is shown in Figure 87.

Inasmuch as the outer cover encapsulates the composite wall, it serves as an aid in packaging the tunnel prior to launch. By a vacuum technique, the wall thickness can be compressed from the fully expanded 2 inches to about 3/8 inch, suitable for folding and subsequent packaging in the canister. Also, a certain amount of air will still be trapped in the composite wall, even after evacuation. This air can be used as a thickness recovery aid, augmenting the elastic recovery characteristics of the compressed foam. Thus, full recovery of the wall thickness, even under adverse temperatures, will be ensured.

The thermal control coating will be applied in two variations as follows:

(1) Aluminum coating vacuum deposited on a film substrate with striping of aluminum pigmented white silicone paint.

(2) Same as (1) but with the addition of a silicon monoxide overcoating in certain locations.

Measurements of thermal radiation properties before and after solar ultraviolet exposure under vacuum conditions substantiate the above coatings as space-stable. Also, the effects of off-gassing induced by vacuum testing were found to be negligible. For the interior surface of the tunnel design, a titanium dioxide pigmented silicone paint is specified because of its low solar absorptance for improved lighting and high emittance to minimize extreme temperature variations. For the prototype tunnel, a titanium dioxide pigmented Hypalon paint was used for both interior and exterior tunnel surfaces. Also, the same style nylon cloth (Burlington 1632) as used for the pressure bladder layer was used for the outer cover layer of the prototype tunnel.

3. Fabrication Techniques and Processes

a. Bonded Floor Structure. The tunnel rigid floor structure is metal sandwich construction consisting of 7.9-pcf density aluminum honeycomb core bonded between 7075-T6 aluminum face sheets 0.063 inch thick with Epon 934 epoxy adhesive. Shaped aluminum edge members are bonded around the floor periphery with the same adhesive. This fabrication technique has been proved by years of use. The use of Epon 934 epoxy adhesive was based on the original high strength of the adhesive and manufacturer's test data, indicating no strength loss after exposure to 10^9 rads of ionizing radiation from a Van deGraf electron beam. The sandwich floor structure adhesive cure was accomplished in an autoclave under pressure at a high temperature.

b. Composite Wall Bonding. In fabricating the tunnel composite wall structure, each component layer is built up layer by layer, starting with the pressure bladder, on a male mandrel fabricated of rigid foam. With the polyester adhesive (Goodyear PE-207) binder layers bonding the multiple-layer pressure bladder components together, bonding the outer cover to the 2-inch foam layer, bonding the multiple-ply structural layer together, and bonding the structural layer to its adjacent pressure bladder and flexible foam layers, the total composite wall structure is bonded together into an integral and homogenous structure. The joints of the individual plies in both pressure bladder and structural layers are staggered in such a way as to offer an essentially seamless construction.

At intermediate phases during the lay-up construction, the polyester adhesive layers are cured with heat and pressure by vacuum bagging techniques. (The foam mandrel is extracted from the completed structure after application of the outer cover.) A polyurethane elastomeric tape (Goodyear Topolic) is applied to all exposed lap seam joints on both interior and exterior tunnel surfaces. Physical properties of the bonding components are shown in Table XI.

c. Floor Joint Bonding. Particular emphasis was placed on the design and development of a structural joint between the rigid floor of the tunnel and the flexible structural layer. The technique that evolved from this investigation (see Figure 98) uses a blended polyamide-epoxy adhesive rigid bond. Strip tensile tests of this technique indicated a 50 percent load capability, as compared to that of the parent structural cloth. The degradation in strength is attributed to the locked-in crimp effect of the Dacron yarns embedded in the rigid adhesive bond. Attempts to improve joint efficiency by using a more elastic type epoxy bond were not successful and only resulted in shear failure of the joint. A polyester adhesive bond similar to that used in the structural wall seams was also tested but was wholly inadequate for the required bond strength. Consequently, the blended polyamide-epoxy rigid bond technique was adopted as the required design technique and resulted in an eight-ply bond to the structural floor joined to the four-ply structural layer with a polyester adhesive bond. Strip tensile tests of this overall joint design indicated that the full load capability of 829 lb/in. could be carried by both the joints and the basic four-ply structural layer. Qualification tests were conducted on the floor joint to investigate environmental effects due to temperature extremes, vacuum and radiation, and creasing. The tests indicated that the full load capability of 929 lb/in. could be carried by the floor joint.

Table XI. Physical Properties of Bonding Components

Property	Polyester	Polyurethane	Epoxy
Code	Goodyear PE-207	Goodyear Topolic	Epon 828, Versamid 140
Type	Thermoplastic	Thermoset	Thermoset
Tensile strength (psi)	7000	3000	2700
Ultimate elongation (percent)	100	480	7
Specific gravity	1.2	1.1	1.2

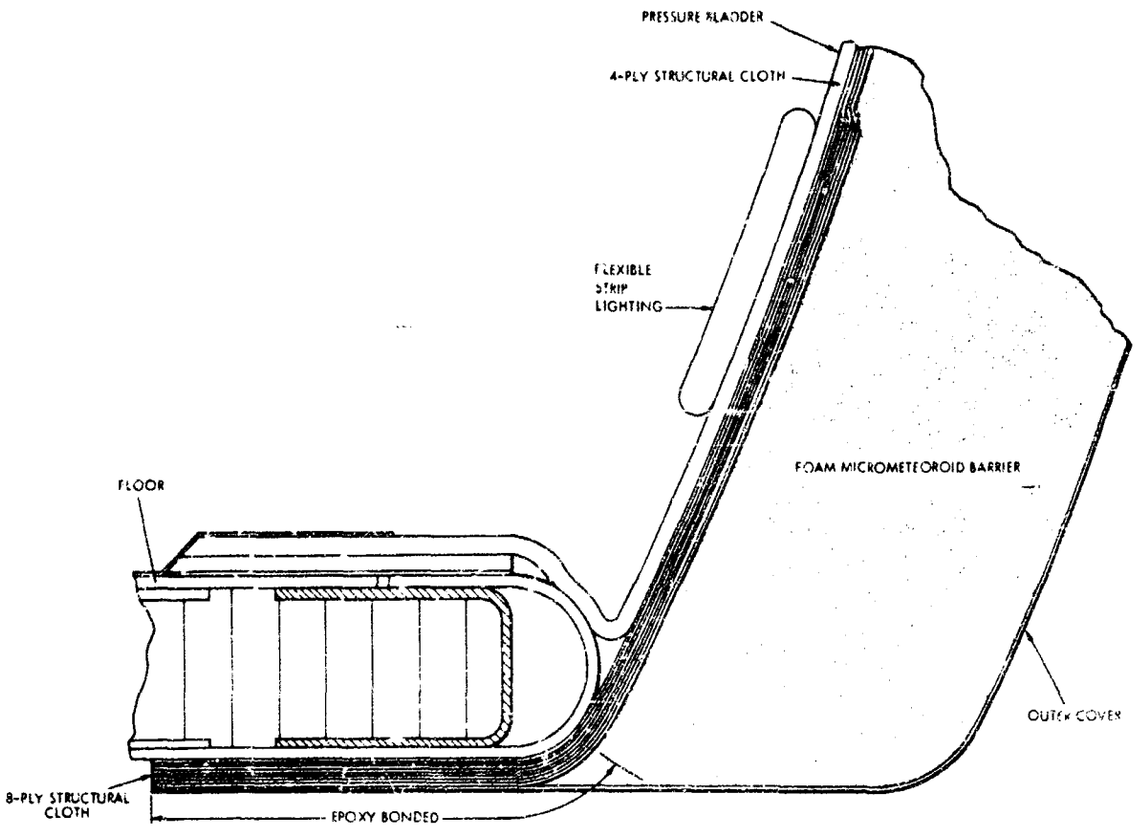

Figure 88. Structural Joint between Expandable Wall and Rigid Floor

4. Materials Test Results and Evaluation

a. General. Although the materials selected for fabrication of the transfer tunnel composite structure were based on GAC in-house development programs, sufficient material qualification testing was conducted on the selected materials to substantiate the environmental, human factors, and structural requirements.

b. Weight. Actual weighing of component material yielded average unit weights for the prototype tunnel (see Table XII). Estimated weights based on the use of material proposed for the tunnel design are also given in Table XII.

c. Pressure Tightness. To substantiate gas pressure tightness of the pressure bladder, permeability measurements of samples were made on Dow-type gas transmission cells in accordance with ASTM procedures. The tests were conducted at room temperature, 5-psia pressure differential across the sample, and gas atmosphere of 100 percent oxygen. The test results given in Table XIII show the permeability of original samples and the same samples after various exposure conditions. Relating the maximum rate of 2.0×10^{-4} psf/day to the tunnel expandable surface area (130 ft^2) indicates a gas loss of 0.026 lb/day, or substantially less than the maximum specified allowance of 1.0 pound per day.

Table XII. Composite Wall Weight Breakdown

Construction		Actual Wt (psf)	Est Wt (psf)
Outer Thermal Control Coating		0.045	0.026
Outer Cover		0.015	0.015
Polyester Adhesive		0.027	0.027
2-Inch Polyether Foam		0.200	0.200
Polyester Adhesive		0.027	0.027
4-Ply Structural Cloth (including adhesive)		0.222	0.210
Polyester Adhesive		0.027	0.027
Pressure Bladder		0.126	0.126
Nylon Cloth	0.015		
Polyester Adhesive	0.027		
0.070-Inch PVC Foam	0.042		
Polyester Adhesive	0.027		
Film-Cloth Laminate	0.015		
Inner Reflective Coating		0.032	0.032
	Total	0.721	0.690

Table XIII. Pressure Bladder Leak Rates

Sample Condition	Avg Leak Rate (psi/24 hr)
Original Sample	1.0×10^{-4}
High-Vacuum Soaked Sample	1.1×10^{-4}
Creased Sample	1.2×10^{-4}
One-Side Pin-Punctured Sample	2.0×10^{-4}

d. Structural Integrity. To demonstrate structural integrity of the flexible structural layer, test samples were made and tested for both the laminated four-ply Dacron structural layer and the termination floor joint. Strip tensile test specimens were fabricated with Stern and Stern Style 15246 Dacron cloth in 2-inch raveled widths (see Figures 89 and 90). Strip tensile tests were made in accordance with ASTM standard methods for testing woven fabrics. Test results on the effects of temperature extremes, vacuum, high energy radiation, and creasing are summarized in Table XIV. To substantiate the biaxial type of loading of the actual tunnel structure, cylinder burst test specimens of the four-ply structural layer were also fabricated with the Style 15246 Dacron cloth. Four cylinders 12 inches in diameter by 36 inches long were laminated in accordance with the actual tunnel construction methods. Three cylinders were tested for quick-break burst pressure, and one cylinder was cycled 60 times at pressures simulating inflation and deflation before application of quick-break pressure (see Figure 91).

Applying the percentage factor of loss in strength for ply efficiency (see cylinder burst test in Table XIV) and for creep rupture effects (see Reference 4) to the four-ply strength for Style 15292 Dacron cloth would indicate that the full design ultimate load capability of 829 lb/in. could be carried. The ply efficiency factor for the cylinder burst test is 81 percent (see Table XIV). The creep

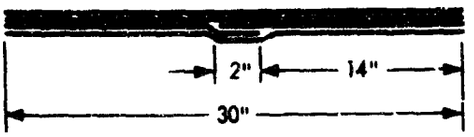

Figure 89. Typical Four-Ply Laminate Specimen

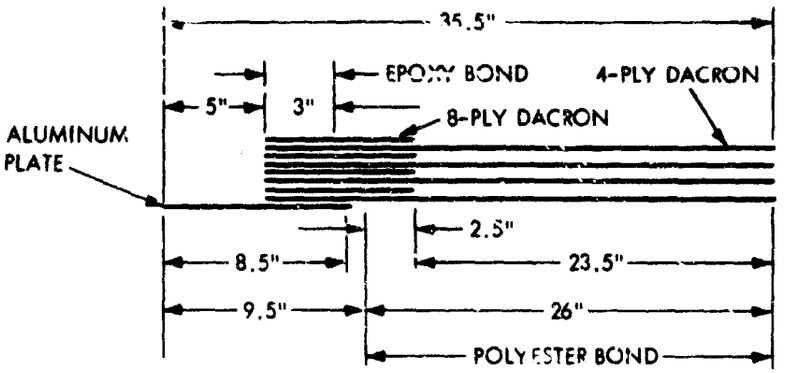

Figure 90. Typical Eight-Ply Dacron Floor Joint Specimen

rupture effect for a two-month load at room temperature has a factor of 78 percent (see Reference 4). Applying these reduction factors to the four-ply strength gives a tunnel design load carrying capability of 831 lb/in. This is shown by 4 x 329 x 0.81 x 0.78 = 831 lb/in. The design ultimate load was previously given as 829 lb/in.

It should be noted that the structural efficiencies below 100 percent in Table XIV are extreme cases not specified for the normal mission environment, where the thermal control coating is designed to maintain 75°F on the tunnel interior and the radiation exposure of the structural layer is calculated to be at least one order of magnitude lower than the test sample exposure.

e. Temperature Control. Both laboratory test data and space service data are available for thermal control coatings that would satisfy the requirements determined by the tunnel thermal analysis for space-stable thermal radiation properties of the thermal control layer. Measurements of solar absorptance (α) and emittance (ϵ) were made before and after ultraviolet exposure under vacuum conditions. GAC laboratory tests consisted of exposing the thermal control coating specimen to simulated solar radiation under vacuum at 10^{-7} torr or lower. Solar absorptance and thermal emittance of the laboratory specimens were measured using a dynamic thermal vacuum technique similar to that in Reference 19, p 192. A comparison of optical characteristics for the specified coatings is given in Table XV.

The tunnel thermal analysis indicates that the external surface should have a ratio of solar absorptance (α) to emittance (ϵ) between 1 and 3, with the absolute values of α and ϵ as low as possible. These criteria may be satisfied by using an external thermal control coating of aluminized film (α = 0.129, ϵ = 0.037, α/ϵ = 3.5) covered in part by aluminum powder in silicone paint (α = 0.24, ϵ = 0.25, α/ϵ = 0.96) and possibly covered with an overcoat of silicon monoxide (α = 0.138, ϵ = 0.512, α/ϵ = 0.27). By varying the quantity of the individual

Table XIV. Summary of Structural Cloth Tests

Type of Test	Condition	Avg Breaking Strength (lb/in.)			15246 Dacron (% Original Room Temp Amb Value)
		Room Temp	-100°F	110°F	
Strip Tensile (15246 Dacron Cloth)					
One Ply					
Ambient, Warp/Fill	Original	270/277			100
Ambient, Warp/Fill	After radiation (10^6 rads)	287/289			106
Four Ply (two seam)					
Ambient, Warp	Original	1098			% (4 x 270) = 102
Four Ply (One Ply Seamed)					
Ambient, Warp	Original		956		102
Ambient, Warp	Original	940			% (4 x 270) = 87
Ambient, Warp	Original			924	98
Ambient, Warp	After creasing	970			103
Ambient, Warp	After radiation (10^6 rads)	930			99
Vacuum (10^{-4} torr), Warp	Original		976		104
Vacuum (10^{-4} torr), Warp	Original	1038			110
Vacuum (10^{-4} torr), Warp	Original			968	103
Strip Tensile (15246 Dacron Cloth Floor Joint)					
Ambient, Warp	Original		974		90
Ambient, Warp	Original	1079			% (4 x 270) = 100
Ambient, Warp	Original			1008	93
Ambient, Warp	After radiation (10^6 rads)	998			92
Vacuum (10^{-4} torr), Warp	Original		1110		103
Vacuum (10^{-4} torr), Warp	Original	1088			101
Vacuum (10^{-4} torr), Warp	Original			956	88
Cylinder Burst (15246 Dacron Cloth)					
Four Ply					
Ambient, Warp	Original	872			% (4 x 270) = 81
Ambient, Warp	After cycling	916			% (4 x 270) = 85
Strip Tensile (15292 Dacron Cloth)					
One Ply					
Ambient, Warp/Fill	Original	329/293			

Table XV. Optical Characteristics of Thermal Control Coatings

Characteristic	Surface			
	Outer			Inner
	Aluminized Mylar	Silicon Monoxide on Al Mylar	Al Powder in Silicone	TiO_2 in Silicone
Type of surface	Evaporated film	Evaporated film	Leafing-type pigment	Air-cured white paint
Source	Ref 17, 18, and 19	Ref 19 and 20	Ref 19	Ref 19
Coating thickness	2000A	20,000A	0.001 in.	0.002 in.
α (initial)	0.100 - 0.129	0.138	0.24	0.24
α (final)	$\Delta\alpha$ = (+) 1%	$\Delta\alpha$ = (+) 10%	$\Delta\alpha$ = negligible	$\Delta\alpha$ = (+) 60%
ϵ (initial)	0.037 - 0.045	0.512	0.25	0.76
ϵ (final)	$\Delta\epsilon$ = negligible	$\Delta\epsilon$ = negligible	$\Delta\epsilon$ = negligible	$\Delta\epsilon$ = negligible
α/ϵ (initial)	3.5	0.270	0.96	0.32
α/ϵ (final)	$\Delta(\alpha/\epsilon)$ = (+) 1%	$\Delta(\alpha/\epsilon)$ = (+) 10%	$\Delta(\alpha/\epsilon)$ = negligible	$\Delta(\alpha/\epsilon)$ = (+) 60%
Exposure				
Laboratory	Initial	Initial	Initial	Initial
Orbital flight	1 year	200 days	125 days	60 days

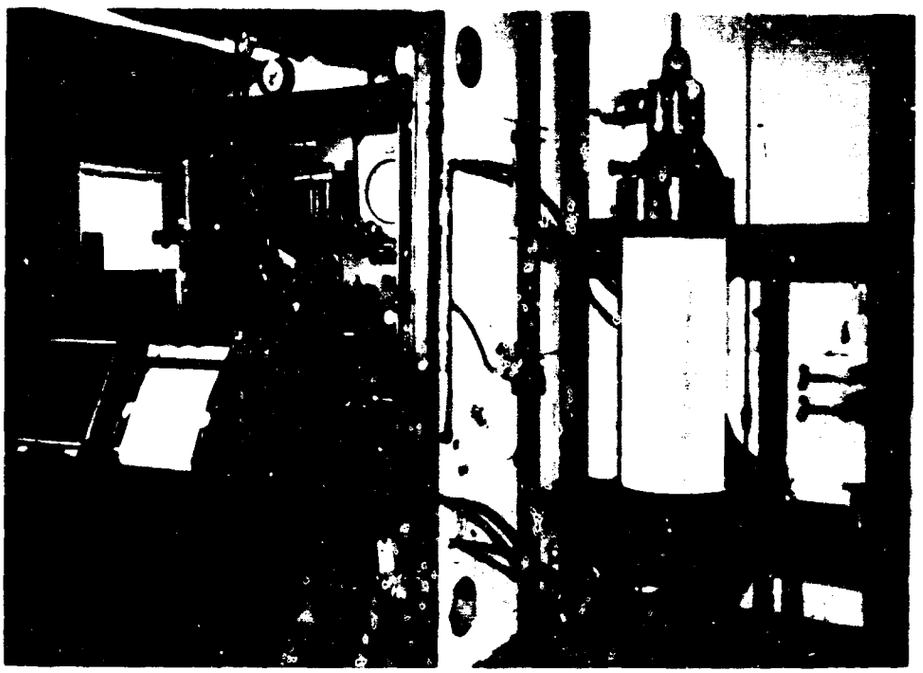

BEFORE APPLICATION OF QUICK-BREAK BURST PRESSURE

AFTER APPLICATION OF QUICK-BREAK BURST PRESSURE

Figure 91. Cylinder Burst Specimen

coating areas, the effective α/ϵ ratio may be established at any desired value between 1 and 3. The interior of the tunnel is designed to have a low value of solar absorptance (α = 0.24, white surface) for improved lighting and a high value of emittance (ϵ = 0.78) to minimize extreme temperature variations within the tunnel. For the interior coating on the tunnel design, a titanium dioxide pigmented silicone paint is selected. For the prototype model, a more economical titanium dioxide pigmented white Hypalon paint was used for the tunnel interior.

To correlate the interior and exterior tunnel wall surface temperatures as predicted by the thermal analysis, thermal conductivity tests were conducted on a sample of the tunnel composite wall material, utilizing the cryogenic guarded hot plate method. The test was in a vacuum of 10^{-6} mm Hg, and the measured data indicates a conductivity of 0.07 Btu-in./hr-ft^2-^{o}F; the major portion of the composite thermal resistance is attributed to the 2-inch thick polyether foam.

f. Elastic Recovery. To demonstrate shelf life characteristics of the tunnel wall, time-load tests were conducted on small samples of the micrometeoroid barrier foam layer to ascertain the maximum length of time that the tunnel can be packaged with a high reliability of elastic recovery when unpackaged. Figure 92 shows the recovery characteristics of the foam under vacuum conditions of 10^{-4} torr for varying temperatures and packaged durations. From Figure 92 it can be seen that the packaged structure must be insulated against extreme cold if full recovery is to be achieved.

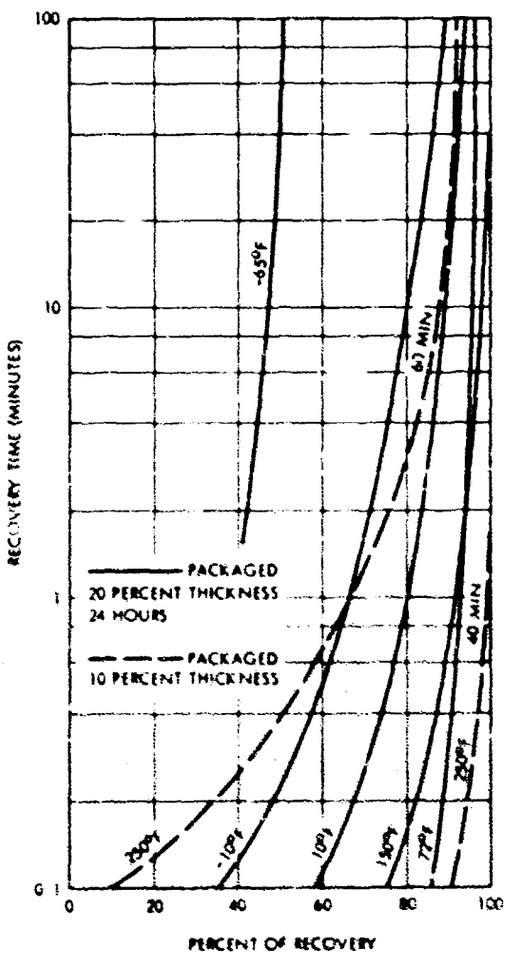

Figure 92. Foam Thickness Recovery versus Time

Table XVI. Vacuum Off-Gassing of Composite Wall Materials

Material	Percent Weight Loss	Time to Stabilize (hr)	Vacuum Level (torr)
Total Composite	2.63	40	10^{-6}
Outer Cover	0.36	1.5	4×10^{-6}
2-Inch Foam	0.39	1.5	4.8×10^{-6}
Structural Layer	0.12	1.0	10^{-6}
Pressure Bladder	6.3	96.0	10^{-6}

g. Environmental Effects. Environmental effects to be considered include combined vacuum and ultraviolet radiation, the thermal environment, and high energy radiation from VanAllen electrons. Only the thermal control coating is affected by the combined vacuum and ultraviolet radiation. This effect has already been discussed. Thermal effects relative to extremes in temperature combined with vacuum were evaluated in testing for structural integrity and elastic recovery. Also, strip tensile tests on the structural layer irradiated with 10^6 rads of gamma radiation were evaluated. The tolerance of the other composite layers to high-energy radiation is higher than the anticipated dose of approximately 10^6 rads. Finally, tests on the composite wall material and its component layers under vacuum conditions were used to evaluate off-gassing effects on the material physical properties (see Table XVI). An initial off-gassing is encountered, resulting from boil-off of plasticizers and volatile solvents, with a negligible weight loss, which subsequently levels off. The hard vacuum exposure also proved that the pressure bladder construction technique was successful in preventing delamination of the bladder composite. Curves of off-gassing versus time are shown in Figures 93 through 97.

h. Toxicity. Tests were made to assure that no toxic by-products, such as those used in the pressure bladder polymer type materials, are given off while under the deployment environment of 5-psia, 100 percent oxygen atmosphere. A survey of toxic materials known to be used in the pressure bladder material construction was made, and the materials were found to be toluene, xylene, methyl ethyl ketone and methylene chloride solvents, and toluene-diisocyanate (TDI). Although it was not known if carbon monoxide is present, tests for it were also included. The test procedure for collecting traces of any toxic gases was to place the test material in a pressure vessel that was evacuated and subsequently pressurized to 5 psig with 100 percent oxygen. The test material was exposed for 24 hours prior to chemical analysis of the toxic gases, and all were found to be below the threshold limit values for atmospheric contaminants established for occupational exposure. The values as determined by a calorimeter type of chemical tester or mass spectrometer are shown in Table XVII.

i. Abrasion Effects. Tests were conducted to determine the abrasion characteristics of the tunnel liner with respect to the outer layer of the astronaut's space suit - the Nomex white reflecting nylon. The test was conducted in accordance with Federal Specification CCC-T 191b, Method 5304-Abrasion Resistance of Cloth (Oscillatory Cylinder Method), except that the specimens were run for 600 cycles instead of 250 cycles. Strip tensile breaking strength before and after testing is used as the measure of abrasion resistance. Test results indicated less than 10 percent decrease in breaking strength after abrasion testing, with no change in visible appearance of the cloth.

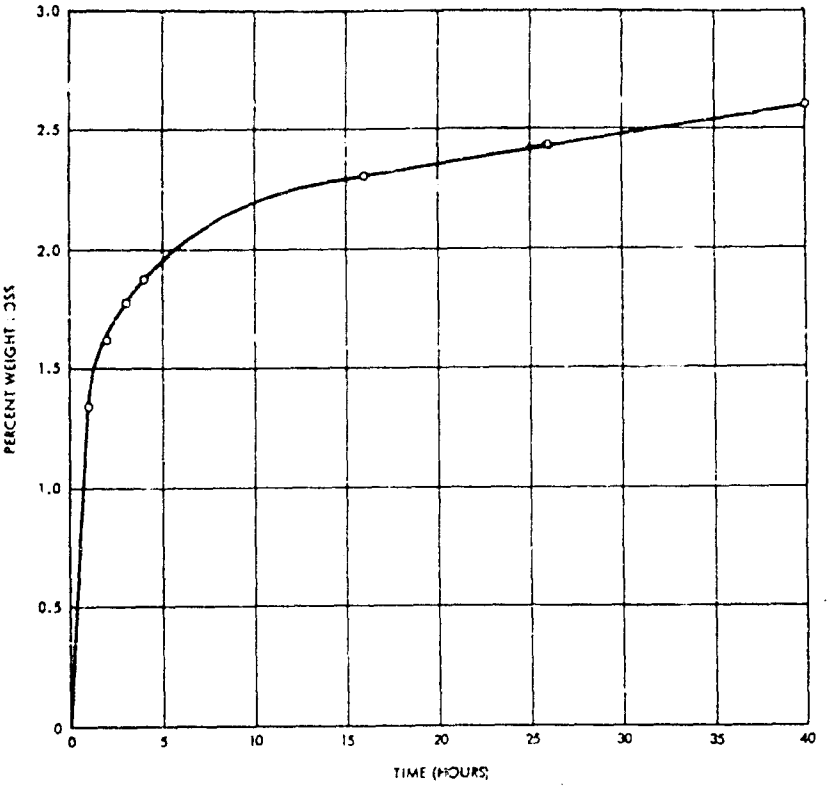

Figure 93. Composite Wall Weight Loss at 10^{-6} Mm Hg

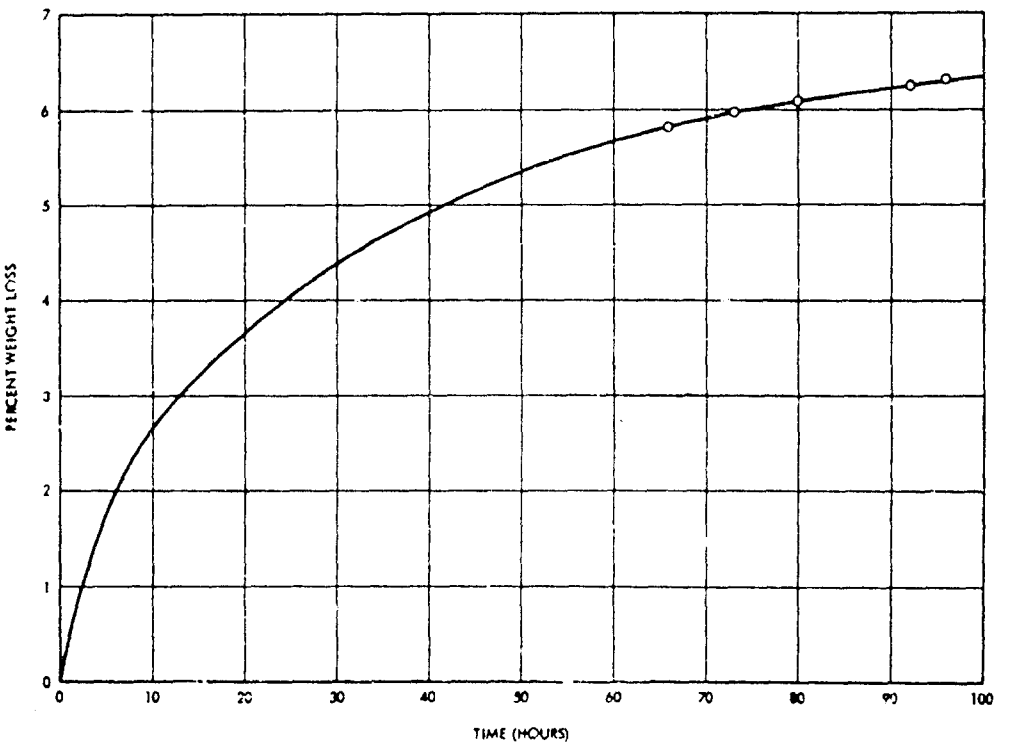

Figure 94. Pressure Bladder Weight Loss at 10^{-6} Mm Hg

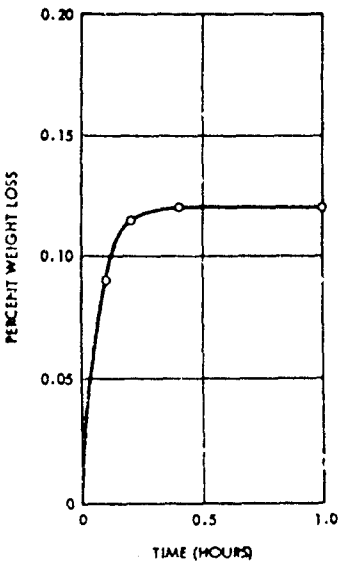

Figure 95. Dacron Structural Cloth Weight Loss at 10^{-6} Mm Hg

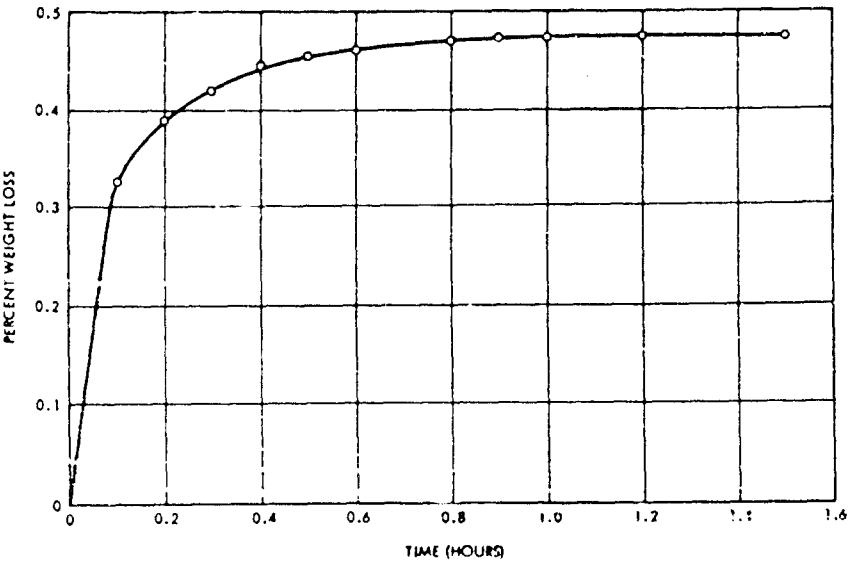

Figure 96. Two-Inch Foam Weight Loss at 10^{-6} Mm Hg

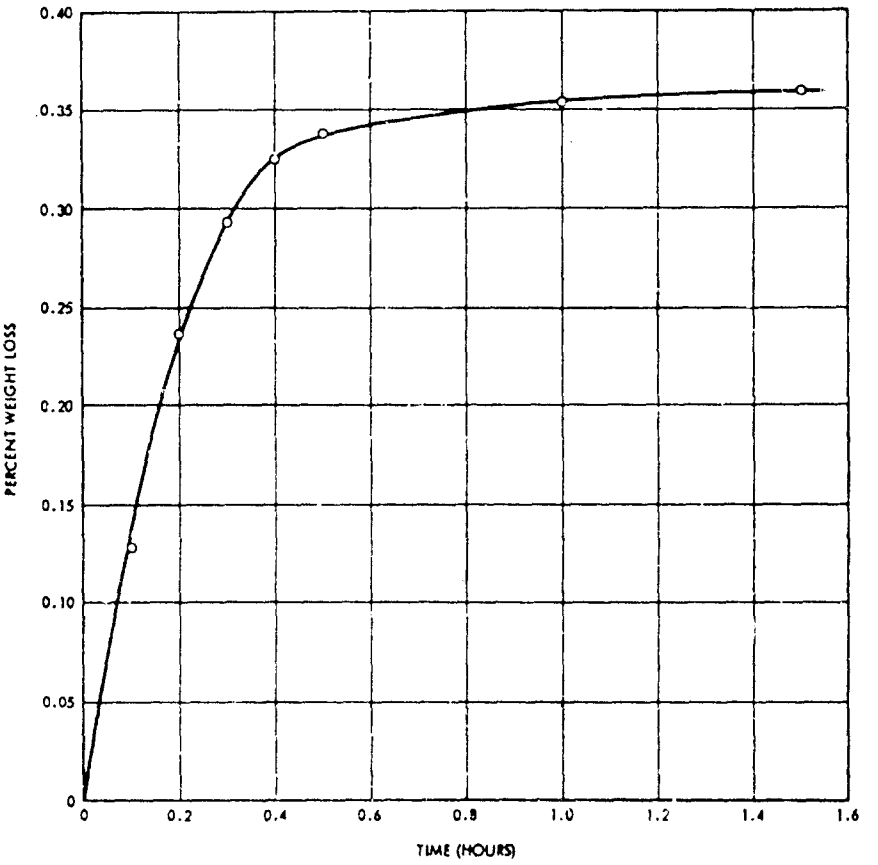

Figure 97. Outer Cover Weight Loss at 10^{-6} Mm Hg

Table XVII. Threshold Limits for Atmospheric Contaminants

Gases	Test Result Value[a] (PPM)	Threshold Limit Value[b] (PPM)
Toluene	200.0	200.0
Xylene	200.0	200.0
Methyl Ethyl Ketone	200.0	200.0
Methylene Chloride	200.0	500.0
Toluene-Diisocyanate	0.01	0.02
Carbon Monoxide	25.0	100.0

[a] Note that the values shown are minimum sensitivity values of the instruments used in testing. In all cases, no trace of the contaminants was found, therefore proving if there were minute traces of contaminants, the concentration is below the threshold limit value.

[b] American Conference of Governmental Industrial Hygienists, 1963, or National Bureau of Standards.

5. Repair Techniques

Repair materials were evaluated for repairing tears or known particle penetration locations in the inner pressure bladder layer of the composite wall structure. A cemented patch repair technique was selected as the most suitable for application to the damaged area. The patch was made from the same film-cloth laminate as was used for the pressure bladder component layer. The environmental effects on the patch are the same as the effects on the pressure bladder component material. Dow Corning 90-092 silicone rubber adhesive was used for the cement application. The 90-092 adhesive, a one-part, ready-to-use adhesive that is applied directly from squeeze tubes onto the desired surface, is cured upon exposure to moisture into a tough, rubbery solid. The moisture-curing mechanism of 90-092 adhesive does not liberate acetic acid, and therefore avoids the corrosion and toxicity problems that would be associated with acetic acid-evolving systems in space structures. Once extruded, the 90-092 adhesive stays where it is placed, and will not sag or slump from its own weight, which is especially significant in a zero-G application. The adhesive has a putty-like consistency and is easily tooled with a spatula to position the adhesive or to smooth its surface. Reference 21 reports that putty-type sealants with the consistency of the 90-092 adhesive will effectively seal holes up to 1/4 inch in diameter in space structures. The film-cloth laminated patch material is placed over the adhesive layer to prevent accidental displacement of the adhesive before complete cure. For small patch size areas, the adhesive line will cure in about 24 hours at ordinary room temperatures. Excellent peel strength is developed between the patch and repaired surface after adhesive cure. The repair materials will operate satisfactorily in the tunnel environmental conditions of vacuum and 100 percent oxygen atmosphere. Reference 22 reports a negligible weight loss rate for silicone rubbers, with the weight loss occuring in the first few hours at 10^{-7} torr range. Reference 23 reports silicone rubbers to have a radiation tolerance of 10^{7} to 10^{8} rads, well above the expected exposure.

SECTION VI

PRELIMINARY QUALIFICATION TESTING

A. GENERAL

The completed prototype tunnel was subjected to a series of preliminary qualification tests to substantiate the structural integrity, gas tightness, and some of the operational aspects of the design in order to evaluate the application of such structures to actual space missions. The test program included packaging, pressure proof and leak tests, cyclic pressure test, and a vacuum chamber deployment test. Zero-G flight tests are to be conducted on the KC-135 zero-G aircraft at Wright-Patterson AFB, and the results of these tests will be reported in Part III of this report.

A steel framework test carrier with hatch mock-ups simulating the Gemini and MSS access hatches was fabricated to support the prototype tunnel during the preliminary qualification testing. Each access hatch is fitted with a hatch cover utilizing an O-ring seal for pressure tightness. The test carrier is also equipped with a canvas catcher to catch the canister cover when it is jettisoned for deployment. The completed prototype tunnel mounted on the test carrier is shown in Figure 13. The test carrier design is shown in Figures 98 and 99.

B. PACKAGING TEST

1. General

The purpose of the packaging test was to establish the minimum height into which the expandable tunnel could be folded and packaged in the canister. The minimum attainable packaging height is desirable to reduce the effects of aerodynamic drag on the packaging canister during the launch phase.

2. Test Procedure

Air was evacuated from the foam meteoroid barrier of the composite wall via a vacuum line attached to one of the plastic pressure relief valves installed through the wall outer cover. When the expandable wall was compressed as much as possible, another vacuum line was attached to a fitting in the cover of the MSS access hatch for evacuation of the tunnel interior. As the tunnel interior was being evacuated, the fold pattern of the collapsing wall was controlled by a crew of technicians. The start of the interior evacuation is shown in Figure 14. In all cases, the folding procedure utilized a vertical accordion fold with the creases running lengthwise along the tunnel wall. Attaining the minimum packaging height became a matter of determining the most efficient method of folding the hemispherical tunnel ends. In all cases, the folded tunnel presented a fairly flat package with a base having approximately the same overall dimensions as the tunnel floor. One of the attempted folding patterns is shown in Figure 100.

After each of the end folding patterns was attempted, the canister was placed over the folded tunnel and strapped down tightly to the test carrier bed. The height of the canister relative to the test carrier was then measured. When the pattern that produced the minimum height had been determined, the tunnel was again folded in this most efficient pattern and the canister was strapped tightly in place. The canister attachment holes were then match drilled with the canister support brackets attached to the tunnel floor.

3. Test Results

The most efficient folding procedure utilized the vertical accordion fold with the creases

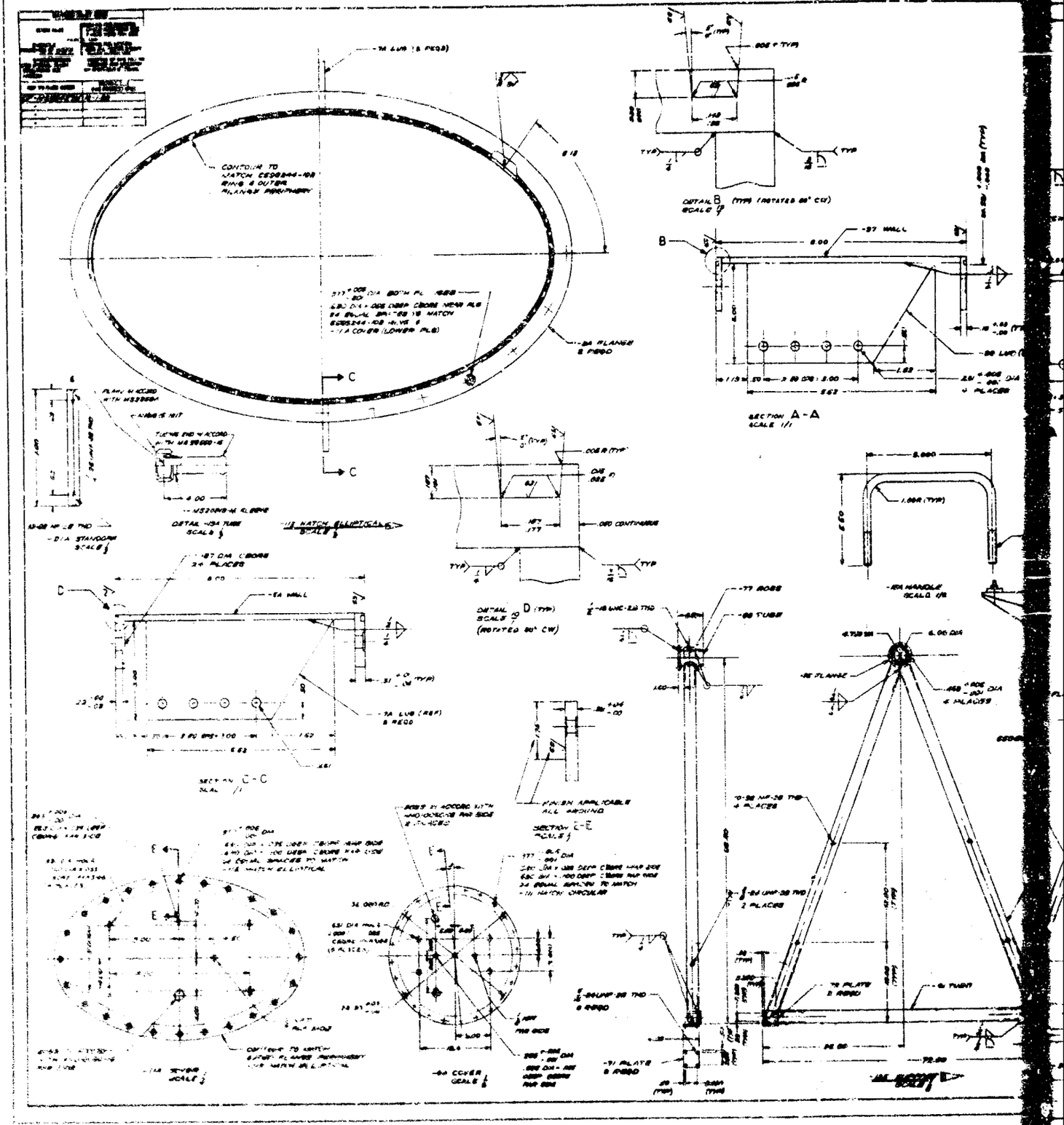

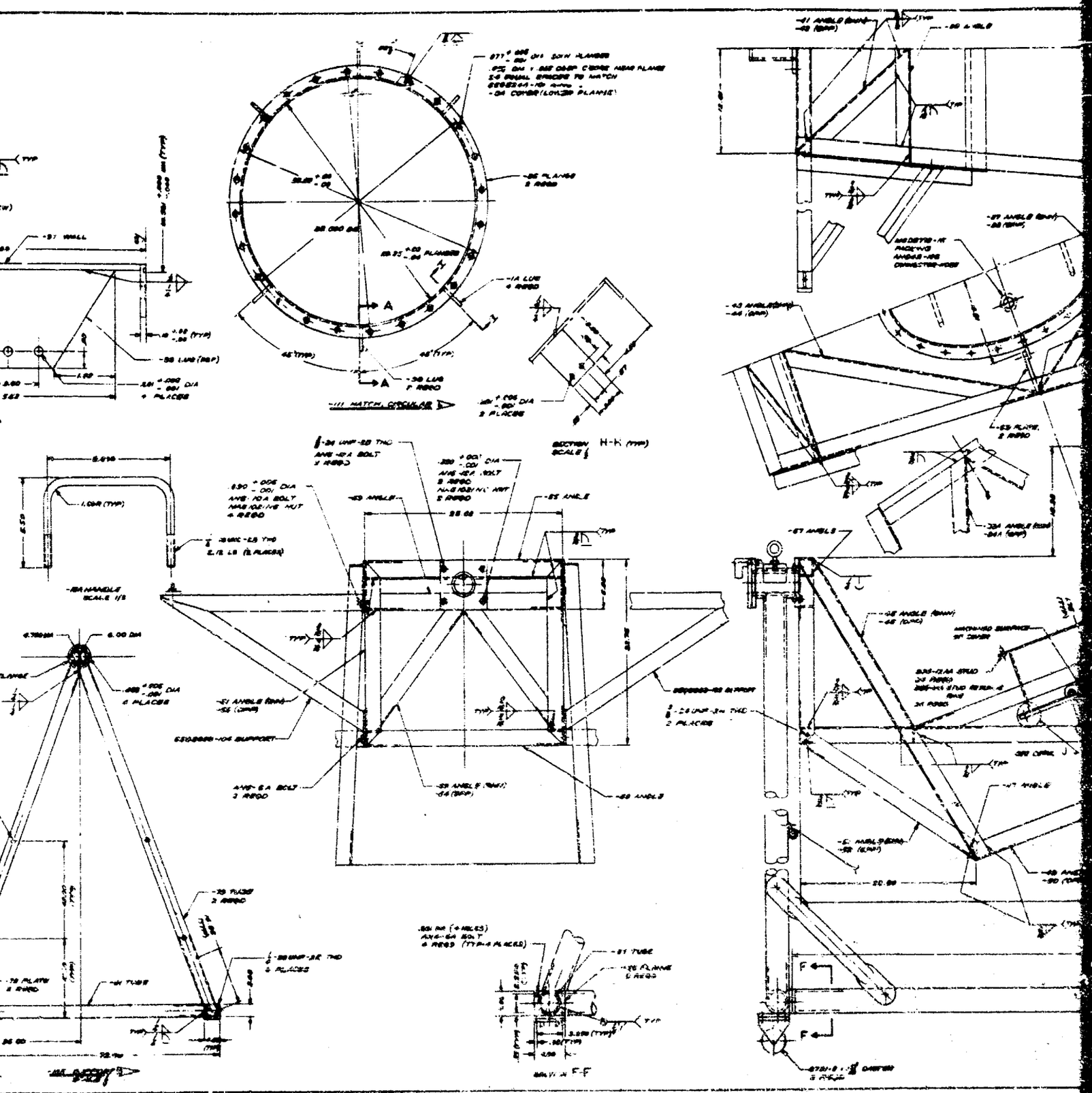

2b

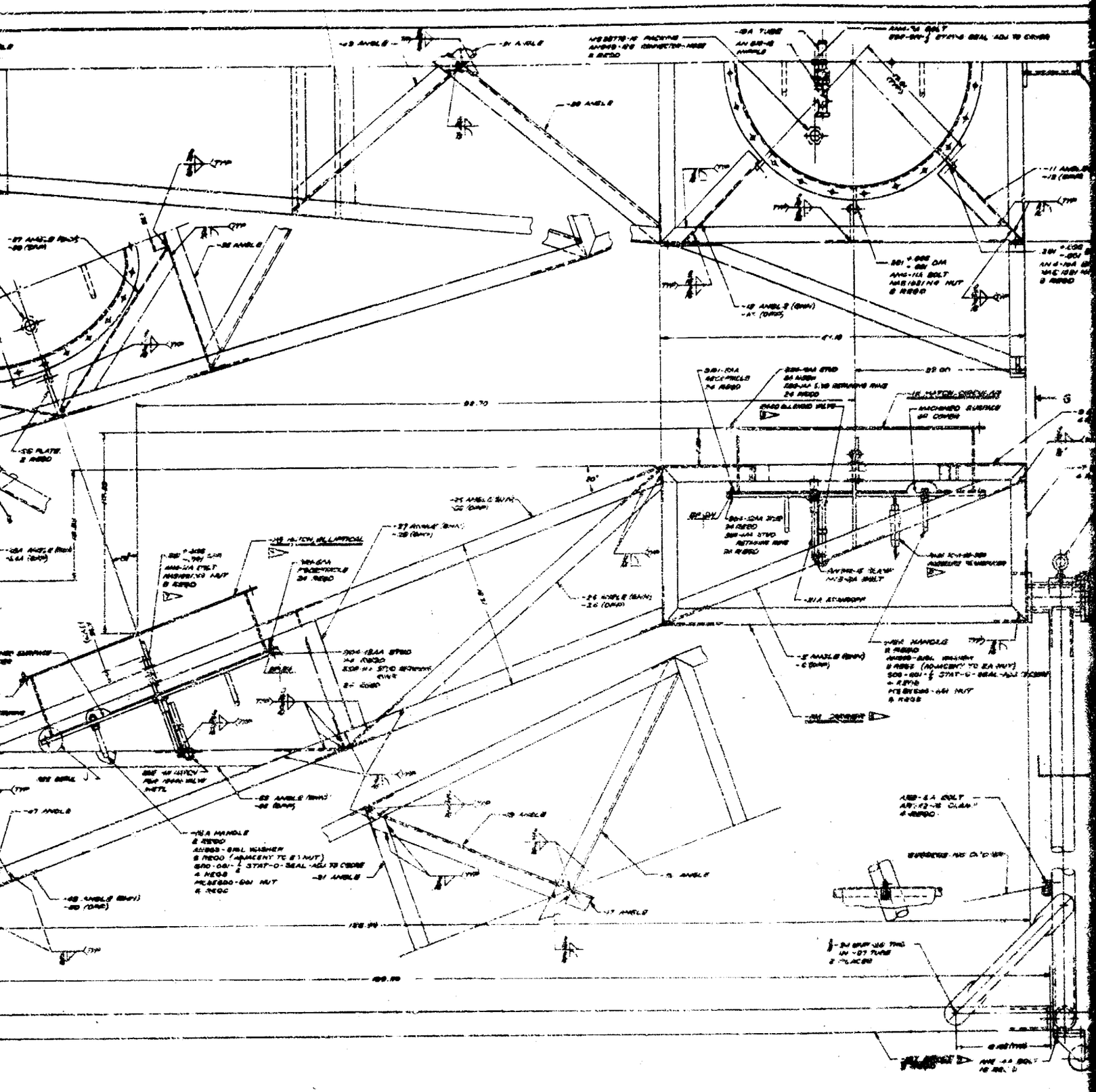

Figure 98. Test Carrier Design

3

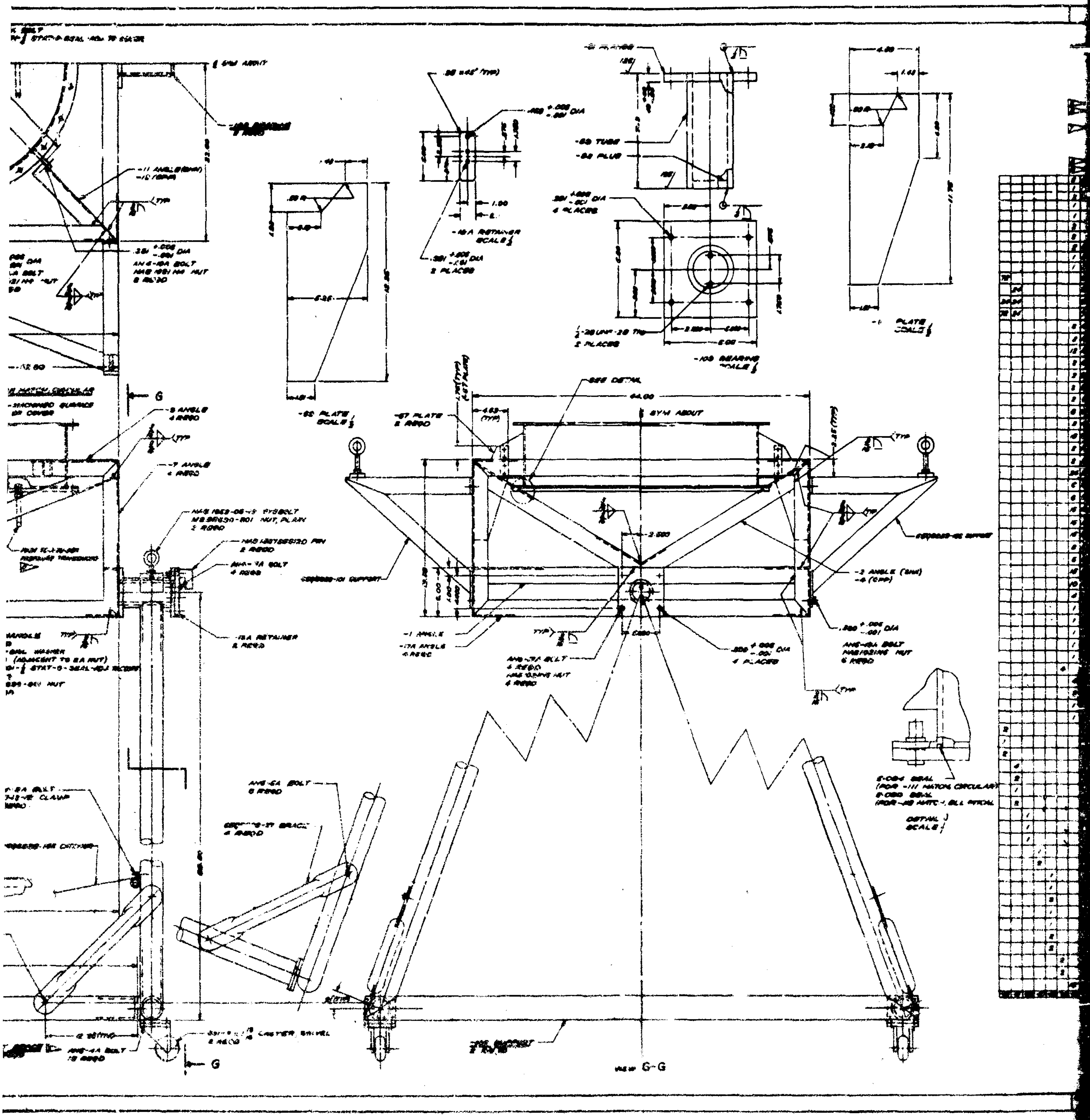
VIEW G-G
DETAIL J
SCALE 1
-1 PLATE
SCALE 1/4
-103 BEARING
SCALE 1/2
-60 PLATE
SCALE 1/4
64.00
SYM ABOUT
G
G

4

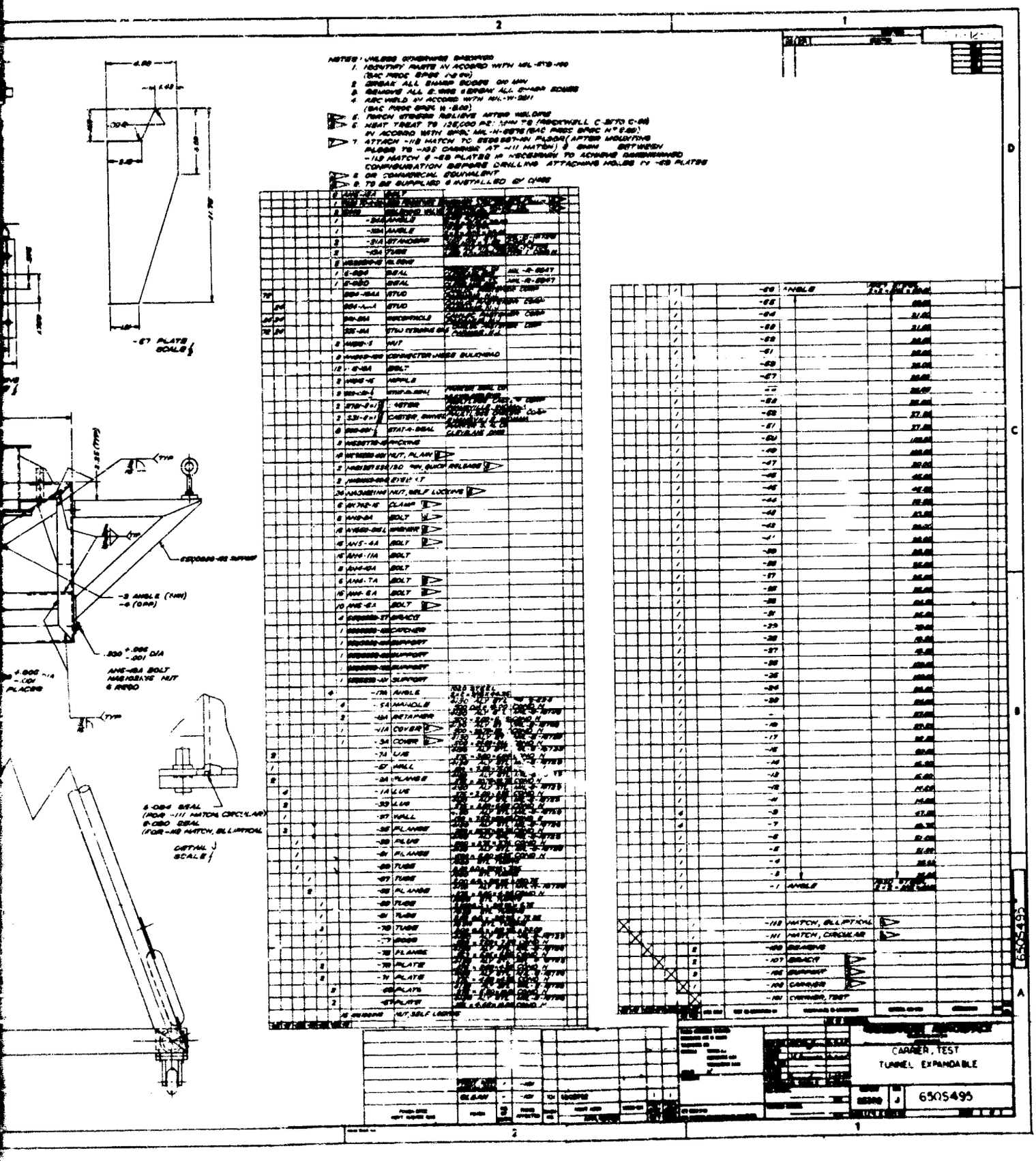

5

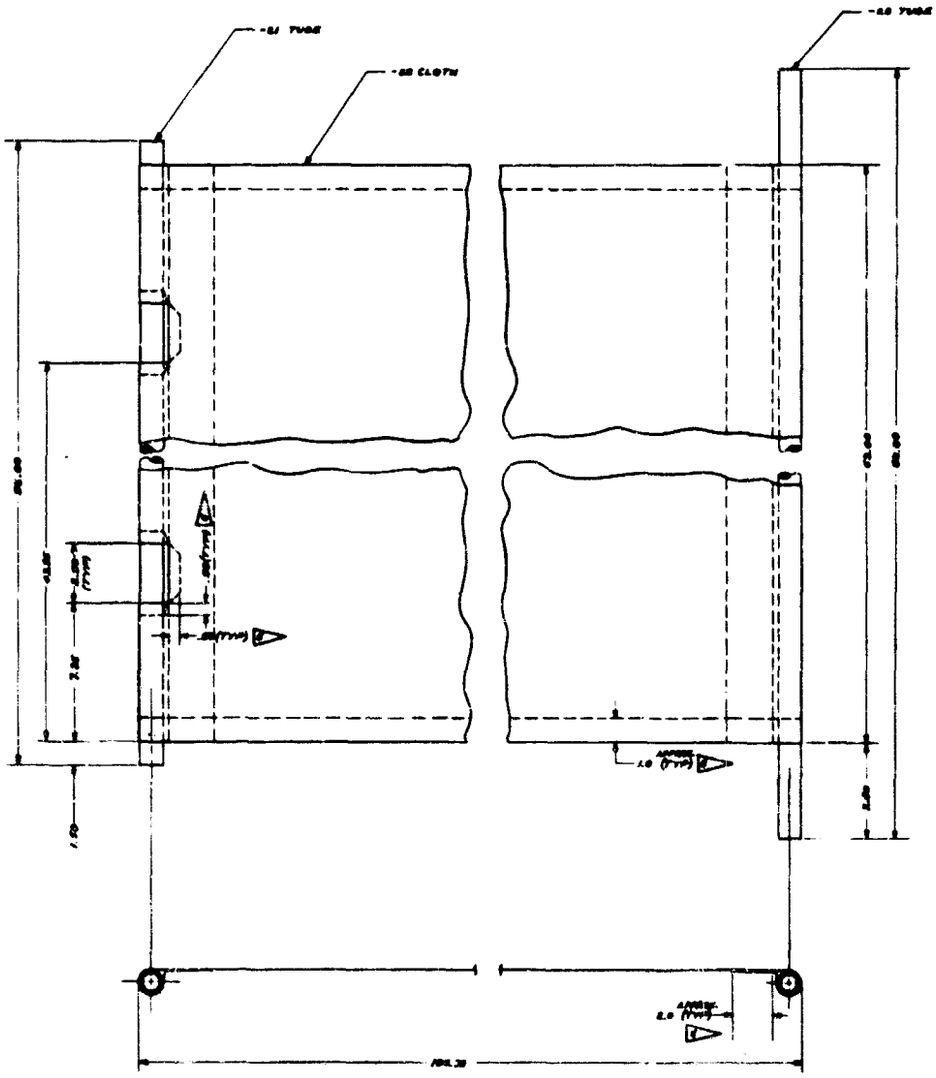

-105 CATCHER ASSY

65 QS 838

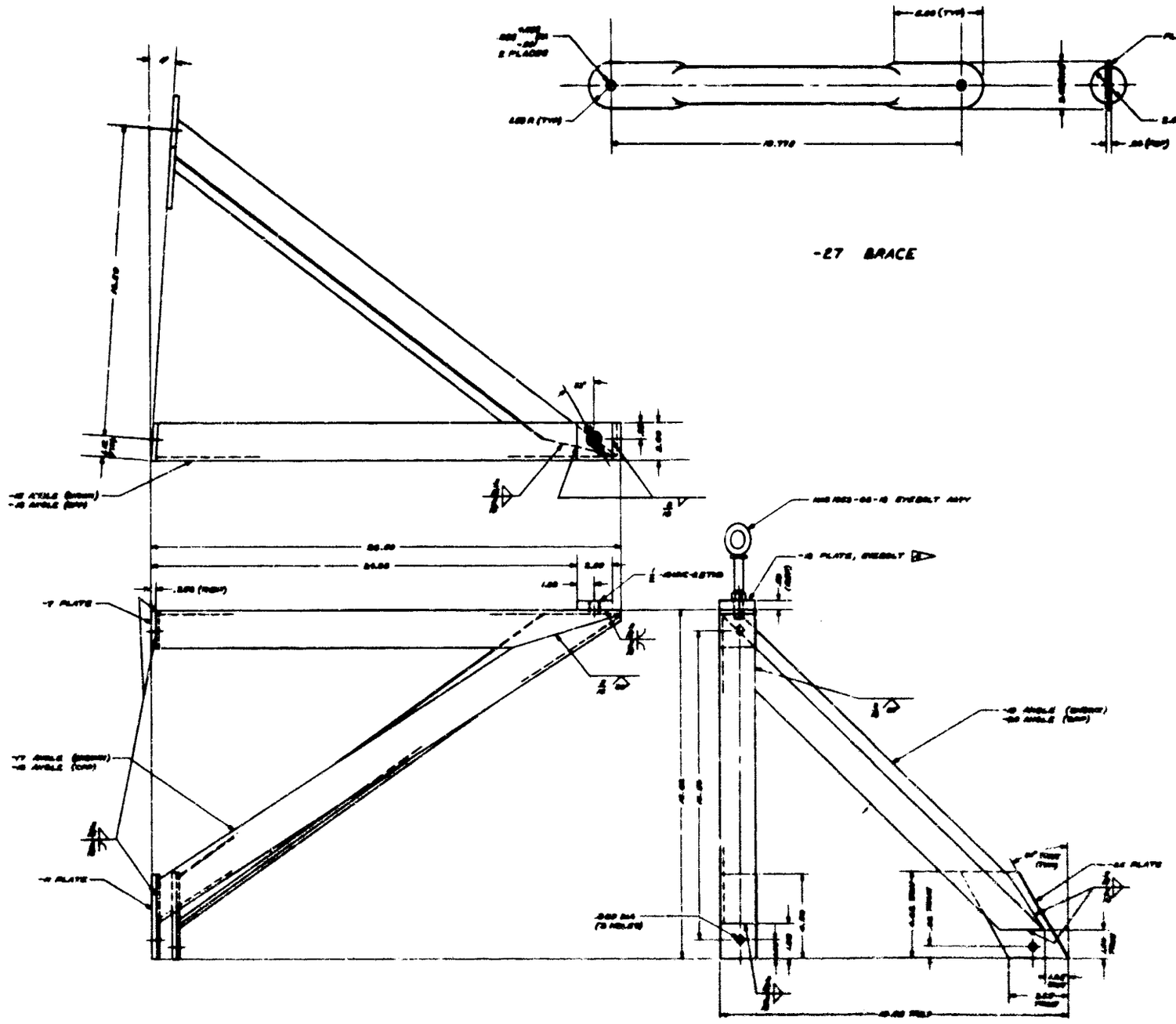

-27 BRACE

-103 SUPPORT ASSY (SHOWN)

-104 SUPPORT ASSY (OPP)

Figure 99. Outrigger

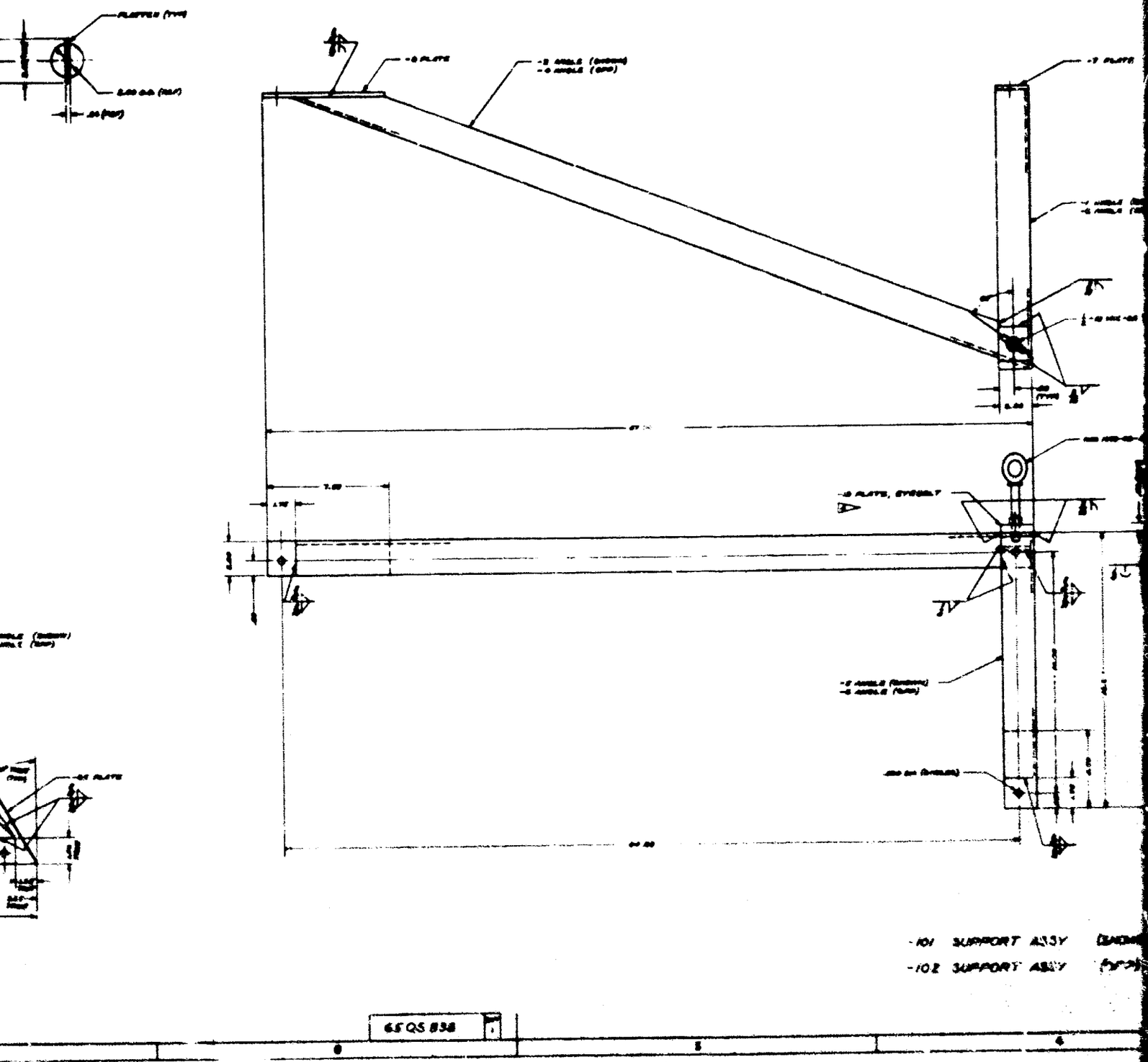

ure 99. Outrigger Supports and Canvas Catcher

3

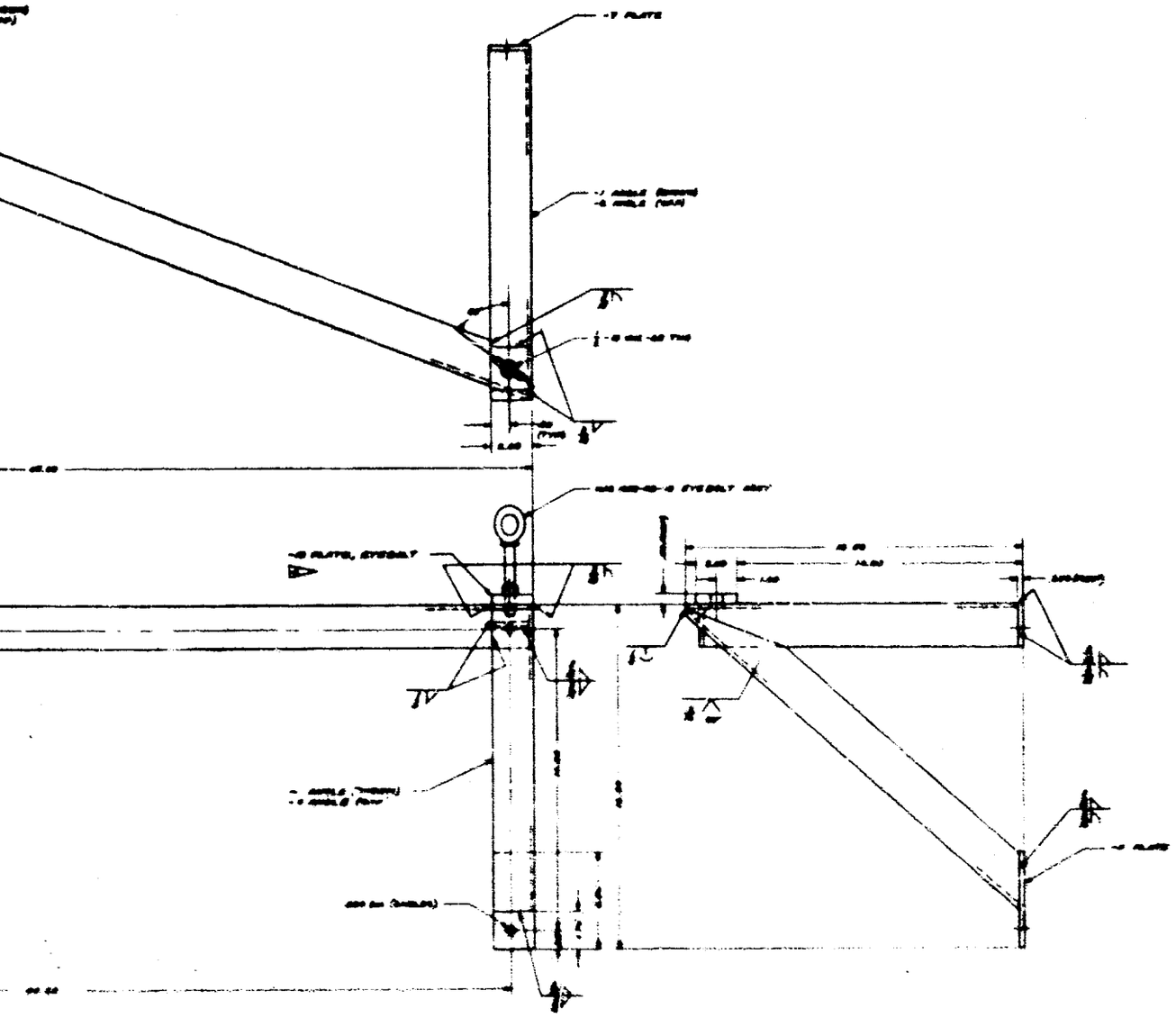

-101 SUPPORT ASSY (SHOWN)
-102 SUPPORT ASSY (OPP)

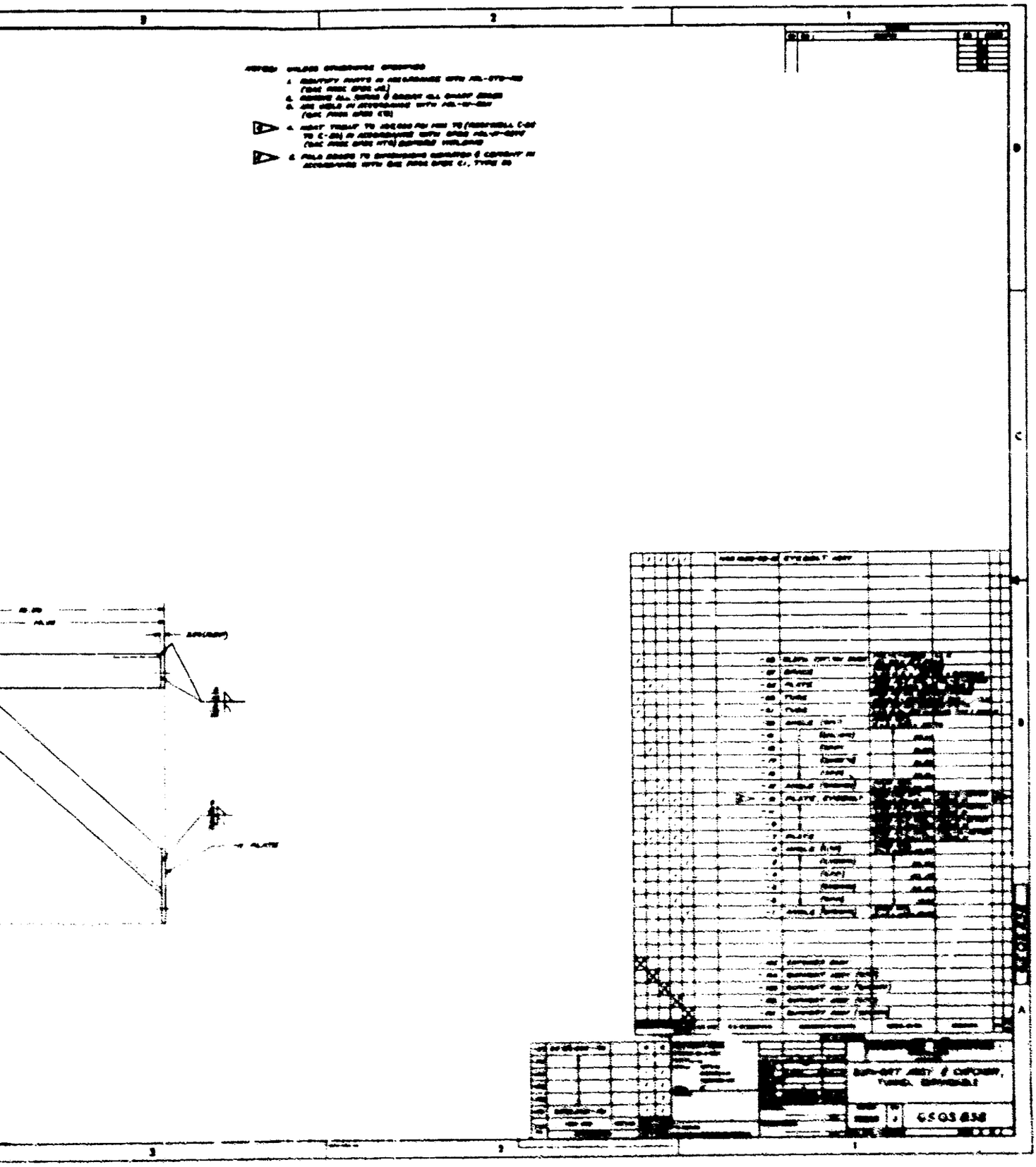

5

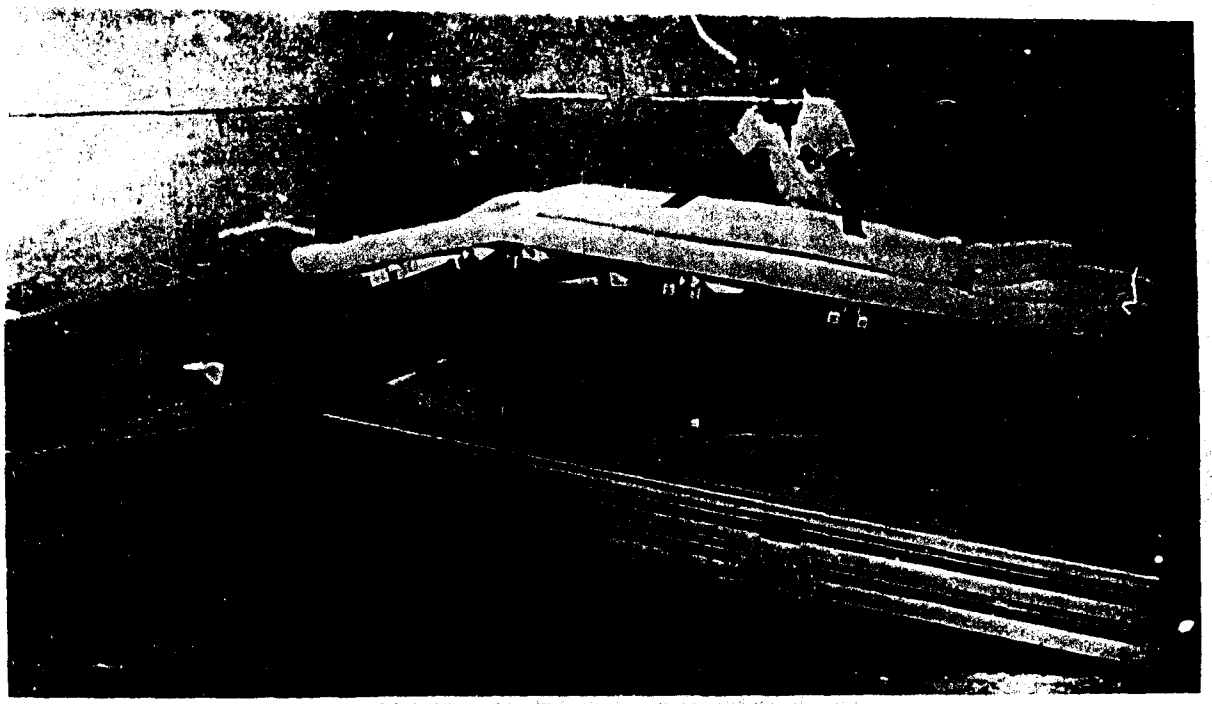

Figure 100. Tunnel Folded during Packaging Test

running lengthwise along the tunnel and had the hemispherical ends folded back across the tops of the lengthwise folds. The folded configuration is shown in Figure 5, and the packaged tunnel is shown in Figure 15. The minimum packaging height was established as 3-3/8 inches from the top of the tunnel floor to the inside surface of the canister. The packaging volume from the bottom surface of the floor to the inside surface of the canister is 14.8 cubic feet. With the tunnel floor, composite wall, lighting, and locomotion aids weighing 198.4 pounds, the packaging density is 13.4 pcf. The total packaging volume provided by the canister with the side fairings resting against the launch vehicle is 20.8 cubic feet. The volume contained below the floor except that occupied by the attachment rings and canister support brackets is wasted space, although necessary for the configuration enclosure. Based on the total volume and weight, the packaging density is 10.2 pcf.

C. PRESSURE PROOF TEST

1. General

The purpose of the pressure proof test was to establish the structural integrity of the tunnel by maintaining an inflation pressure of 10 psi, 1.33 times the design pressure of 7.5 psi, for a period of 7 days.

2. Test Procedure

After completion of the packaging test, the prototype tunnel mounted on the test carrier bed was placed in the GAC pressure test room for the pressure proof and leak tests and the cyclic pressure test. A temperature indicator was installed in the cover plate on the Gemini access hatch to monitor internal tunnel temperature. The tunnel with the temperature indicator installed so that it could be read in a mirror from the window of the pressure test room is shown in Figure 101. A dial mercury manometer and a filtered shop air supply line were attached to a port in the cover plate on the MSS access hatch. The air supply line was equipped

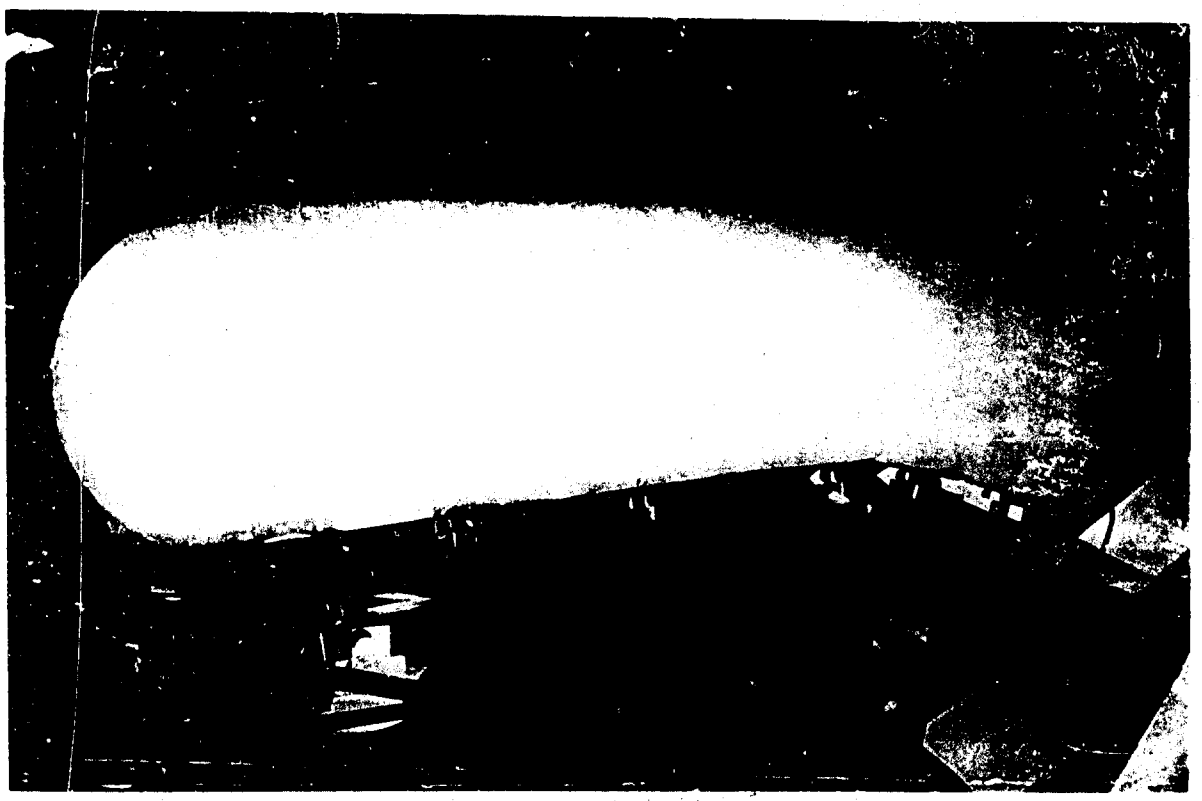

Figure 101. Tunnel in Pressure Test Room

with two pressure regulators in series, capable of maintaining pressure within ±0.2 inch of mercury, ±0.1 psi. The regulated side of the air supply line was equipped with a 21-inch maximum pressure (10.3 psi) U-tube mercury manometer to serve as a pressure relief device to guard against over-pressure due to thermal expansion or regulator malfunction. The regulators and manometers were located outside the room by the window. The test arrangement is shown in Figures 16 and 17.

The tunnel was pressurized to 10 psi (20.4 inches of mercury), and after the pressure and temperature had stabilized and were recorded, the test time period was started. The 10-psi pressure was maintained for a period of 7 days while pressure and temperature were monitored periodically.

3. Test Results

The prototype tunnel withstood the 10-psi proof pressure for 7 days with no visible change in configuration and with no visual signs of damage.

D PRESSURE LEAK TEST

1. General

The purpose of the pressure leak test was to establish the gas tightness of the prototype tunnel by determining the leak rate at the design pressure of 7.5 psi for a period of 7 days.

2. Test Procedure

The only change in the test arrangement from the proof test was changing the pressurization air supply from the shop air line to a bottle of compressed air, which was placed on a calibrated platform scale. The initial part of this test included determination of the tunnel volume when pressurized to 7.5 psi. The actual barometric pressure and the weight of the compressed air bottle were recorded, and the tunnel was pressurized to 7.5 psi (15.3 inches of mercury). The air supply was carefully regulated so that the pressure was 7.5 psi when the internal tunnel temperature was stabilized. The pressure, temperature, compressed air bottle weight, and actual barometric pressure were then recorded, and the test time period was started. The weight of air used to pressurize the tunnel was used to determine the inflated volume. The 7.5-psi pressure was maintained for a period of 7 days while pressure, temperature, and compressed air bottle weight were monitored periodically. At the end of the 7-day period, the pressure, temperature, compressed air bottle weight, and actual barometric pressure were again recorded.

3. Test Results

Prior to the packaging tests, a one-day (24-hour) leak test was conducted to establish a reference leak rate to be used for evaluating possible degrading effects of folding and packaging. The 24-hour leak test was conducted by pressurizing the tunnel to 10 psi, reading barometric pressure and temperature, and monitoring the pressure decrease for 24 hours. At the end of this time period, the temperature and barometric pressure were again recorded.

The equation of state of an ideal gas is used to determine the pressurized volume and the significant gas weights. This equation in other forms is used to convert the test leak rate to a leak rate of a gas mixture of 50 percent nitrogen and 50 percent oxygen under orbital conditions of an internal pressure of 7.5 psia and an external pressure of 0 for practical purposes. The absolute pressure used in determining the converted leak rate is based on a constant volume of gas at a reference temperature of 75°F.

The equation of state of an ideal gas is

$$144\, p_{AP}\, V = wRT' \tag{74}$$

where

p_{AP} = absolute pressure (psia),

V = volume (ft^3),

w = weight (lb),

R = specific gas constant (ft-lb/lb-°R),

T' = temperature (°R).

When the pressure, weight, and temperature are known, the volume of a specific gas can be found from Equation 74 in the form

$$V = \frac{wRT'}{144\, p_{AP}} \tag{75}$$

When the pressure, volume, and temperature are known, the weight of a specific gas can be found from Equation 74 in the form

$$w = \frac{144\, p_{AP}\, V}{RT'} \tag{76}$$

When the weight and volume of a specific gas are held constant, the ratio of the pressure to the temperature is constant. This is expressed as

$$\frac{p_{AP}}{T'} = \frac{wR}{144V} = \text{constant.} \tag{77}$$

From Equation 77,

$$\frac{p_1}{T_1'} = \frac{p_2}{T_2'} \text{ or } p_2 = \frac{p_1 T_2'}{T_1'} \tag{78}$$

where

p_1 = pressure (psia) at temperature T_1' (^{o}R),

p_2 = pressure (psia) at temperature T_2' (^{o}R).

When the volume and temperature of a specific gas are held constant, the ratio of the weight to the pressure is constant. This is expressed as

$$\frac{w}{p_{AP}} = \frac{144V}{RT'} = \text{constant.} \tag{79}$$

From Equation 79,

$$\frac{w_1}{p_1} = \frac{w_2}{p_2} \text{ or } w_2 = \frac{w_1 p_2}{p_1} \tag{80}$$

where

w_1 = weight (lb) at pressure p_1 (psia),

w_2 = weight (lb) at pressure p_2 (psia).

The equation of state of an ideal gas, Equation 74, can also be expressed in another system of units in the form

$$144\, p_{AP} V = \frac{w}{M} R' \overline{T} \tag{81}$$

where

$\overline{T}$ = temperature (^{o}K),

M = molecular weight (lb mole),

R' = universal gas constant having the same value for all gases (ft-lb/mole -^{o}K).

When the same pressure, volume, and temperature are held constant for any two gases, Equation 81 indicates that the ratios of the gas weight to the molecular weight of the two gases are equal. This is shown by

$$\frac{w_1}{M_1} = \frac{w_2}{M_2} = \frac{144\, p_{AP} V}{R' \overline{T}} = \text{constant} \tag{82}$$

where

w_1 = weight of gas (lb) with molecular weight M_1 (lb/mole),

w_2 = weight of gas (lb) with molecular weight M_2 (lb/mole).

It is also known that the weight of gas flowing through an orifice is proportional to the velocity of flow. Then, for a specified period of time,

$$w = Cv \tag{83}$$

where

w = weight flow (lb),

C = proportionality constant (lb/Mach number),

v = velocity (Mach number).

Equation 83 can then be expressed in the form

$$\frac{w_1}{v_1} = \frac{w_2}{v_2} = C = \text{constant} \tag{84}$$

where

w_1 = weight flow (lb) in a specified time at a velocity of v_1 (Mach number),

w_2 = weight flow (lb) in the same specified time at a velocity of v_2 (Mach number).

When the tunnel was initially pressurized from the compressed air bottle, the inflation pressure and the gas temperature and weight were recorded. Using the test data recorded in Table XVIII and Equation 75, with R = 53.30 ft-lb/lb-^{o}R for air and 0.072 pcf for the density of air at 29.15 inches of mercury and 77^{o}F, the expanded tunnel volume is determined:

$$V = \frac{wRT'}{144\, p_{AP}} = \frac{(w_c + \rho V)\, R\, (460 + T)}{144\, p_{AP}} = \frac{(3.88 + 0.072V)(53.30)(460 + 77)}{144\,(21.83)}$$

$$144(21.83)\, V = 53.30\,(537)\,(3.88 + 0.072V).$$

$$V = 103\ \text{ft}^3.$$

The leak rate is established for the one-day (24-hour) leak test and the seven-day leak test by determining the weight of air lost in leakage per day and converting this loss into an equivalent loss of a mixture of 50 percent nitrogen and 50 percent oxygen at a pressure of 7.5 psia at 75^{o}F leaking into a vacuum.

The weight of air lost is given by

$$w_{LT} = w_I - w_F + w_c \tag{85}$$

where

w_{LT} = weight of air lost during the test (lb),

w_I = initial weight of pressurized air (lb),

w_F = final weight of pressurized air (lb),

w_c = weight of air added due to cylinder weight decrease (lb).

From Equation 76 with V = 103 ft^3 and R = 53.30 ft-lb/lb-^{o}R for air,

$$w_I = \frac{144\, p_{API}\,(103)}{53.30\,(460 + T_I)} = \frac{278.3\, p_{API}}{460 + T_I} \tag{86}$$

where

p_{API} = initial pressure (psia),

T_I = initial temperature (^{O}F).

Also,

$$w_F = \frac{278.3\, p_{APF}}{460 + T_F} \tag{87}$$

where

p_{APF} = final pressure (psia),

T_F = final temperature (^{O}F).

The average pressure for the leak test is corrected to the value at the reference temperature of 75^{O}F by using Equation 78.

$$p_{\bar{A}T} = \frac{p_{ACI} + p_{ACF}}{2} \tag{88}$$

where

$p_{\bar{A}T}$ = average leak test pressure (psia),

p_{ACI} = initial corrected pressure (psia),

p_{ACF} = final corrected pressure (psia).

In converting the weight of air lost during the test to the weight that would have been lost in orbit at an inflation pressure of 7.5 psia, Equation 80 is used.

$$w_{Lp} = \frac{7.5\, w_{LT}}{p_{\bar{A}T}} \tag{89}$$

where

w_{Lp} = converted weight of air lost (lb) due to a different pressure.

The velocity of flow through an orifice is a function of both the absolute pressure and the pressure differential across the orifice. The velocity of flow (Mach number) as a function of absolute pressure and pressure differential is given in standard tables. From Equation 84,

$$w_{Lv} = \frac{w_{LT} v_O}{v_I} \tag{90}$$

where

w_{Lv} = converted weight of air lost (lb) due to a different flow velocity,

v_O = velocity of flow in orbital conditions (Mach number),

v_T = velocity of flow during the leak test (Mach number).

In converting the weight of air lost during the test to the weight of a gas mixture of 50 percent nitrogen and 50 percent oxygen, which would have been lost in orbit under identical conditions, Equation 82 is used.

$$w_{Lm} = \frac{w_{LT} M_N}{M_T} \tag{91}$$

where

w_{Lm} = converted weight loss (lb) of the mixture due to different molecular weights,

M_N = molecular weight of mixture (lb/mole),

M_T = molecular weight of test gas, air (lb/mole).

Thus, the factors that must be considered in converting the leak rate in terms of the weight loss of air during the test to the equivalent weight loss of a mixture of 50 percent nitrogen and 50 percent oxygen with a pressure of 7.5 psia at 75°F leaking into a vacuum are the absolute pressures involved, the velocities of the loss flow, and the molecular weights of the gases considered. The weight loss of the mixture under orbital conditions is then determined by combining Equations 89, 90, and 91 as follows:

$$w_{LO} = w_{LT} \left(\frac{7.5}{p_{\bar{A}1}}\right)\left(\frac{v_O}{v_T}\right)\left(\frac{M_N}{M_T}\right) \tag{92}$$

where

w_{LO} = converted equivalent weight loss of the nitrogen-oxygen mixture under orbital conditions (lb).

Since the weight of air lost during the test, w_{LT} in Equation 89, is determined for the total test time, it should be expressed in terms of a daily basis for determining the equivalent orbital leak rate. Therefore,

$$w_{LTD} = \frac{w_{LT}}{\tau} \tag{93}$$

where

w_{LTD} = daily weight of air lost during the test (lb day),

τ = total test time (days).

Equation 92 can then be expressed in terms of a daily weight loss by the use of Equation 93. Then

$$w_{LOD} = w_{LTD} \left(\frac{7.5}{p_{\bar{A}T}}\right)\left(\frac{v_O}{v_T}\right)\left(\frac{M_N}{M_T}\right) \tag{94}$$

where

w_{LOD} = converted equivalent daily weight loss of the nitrogen-oxygen mixture under orbital conditions (lb day).

Using Equations 85, 86, 87, 93, and 94 in conjunction with the data in Table XVIII, the leak rates are determined.

Table XVIII. Ambient Atmosphere Leak Test Data

Test	Reading Initial (I)	Reading Final (F)	τ (days)	T (^{O}F)	w_c (lb)	p_{BH} (in. Hg)	p_{GH} (in. Hg)	p_{GP}[a] (psi)	p_{AH}[b] (in. Hg)	p_{AP}[c] (psia)	p_{AC}[d] (psia)	$p_{\bar{A}T}$[e] (psia)
Volume Determination		X		77	3.88	29.15	15.30	7.51	44.45	21.83	--	--
One-Day Leak Test	X		0	77	--	29.30	20.40	10.02	49.70	24.41	24.32	23.06
		X	1	80	--	29.10	15.70	7.71	44.80	22.00	21.80	
Seven-Day Leak Test	X		0	72	0	28.83	15.40	7.56	44.23	21.72	21.84	21.88
		X	7	75	7.75	29.15	15.50	7.61	44.65	21.93	21.93	

[a] $p_{GP} = 0.4912\, p_{GH}$. [b] $p_{AH} = p_{BH} + p_{GH}$. [c] $p_{AP} = 0.4912\, p_{AH}$.

[d] $p_{AC} = \frac{p_{AP}(460 + 75)}{460 + T} = \frac{535 p_{AP}}{460 + T}$. (See Equation 78.) [e] $p_{\bar{A}T} = \frac{p_{ACI} + p_{ACF}}{2}$. (See Equation 88.)

The values in Table XVIII used in determining the leak rate for the one-day leak test are as follows:

p_{API} = 24.41 psia. τ = 1 day.

T_I = 77^{O}F. v_T = Mach 0.89 ($p' \cong$ 23 psia, $\Delta p' \cong$ 9 psia).

p_{APF} = 22.00 psia. v_O = Mach 1.00 (p' = 7.5 psia, $\Delta p'$ = 7.5 psia).

T_F = 80^{O}F M_T = 29 lb/mole (air).

$p_{\bar{A}T}$ = 23.06 psia. M_N = 30 lb mole (50% nitrogen, 50% oxygen).

w_c = 0.

From Equation 86,

$$w_I = \frac{278.3 p_{API}}{460 + T_I} = \frac{278.3\,(24.41)}{460 + 77} = 12.65 \text{ lb.}$$

From Equation 87,

$$w_F = \frac{278.3 p_{APF}}{460 + T_F} = \frac{278.3\,(22.00)}{460 + 80} = 11.34 \text{ lb.}$$

From Equation 85,

$$w_{LT} = w_I - w_F - w_c = 12.65 - 11.34 + 0 = 1.31 \text{ lb.}$$

From Equation 93,

$$w_{LTD} = \frac{w_{LT}}{\tau} = \frac{1.31}{1} = 1.31 \text{ lb/day.}$$

From Equation 94,

$$w_{LOD} = w_{LTD}\left(\frac{7.5}{p_{\bar{A}T}}\right)\left(\frac{v_O}{v_T}\right)\left(\frac{M_N}{M_T}\right) = 1.31\left(\frac{7.5}{23.06}\right)\left(\frac{1.00}{0.80}\right)\left(\frac{30}{29}\right) = 0.50 \text{ lb/day.}$$

The leak rate for the one-day leak test is therefore 1.31 lb/day for air under ambient conditions. The equivalent loss of the nitrogen-oxygen mixture under orbital conditions is 0.50 lb/day.

The values in Table XVIII used in determining the leak rate for the seven-day leak test are as follows:

p_{API} = 21.72 psia.
T_I = 72°F.
p_{APF} = 21.93 psia.
T_F = 75°F.
$p_{\bar{A}T}$ = 21.88 psia.
w_c = 7.75 lb.
τ = 7 days.
v_T = Mach 0.78 ($p' \cong 22$ psia, $\Delta p' \cong 7.5$ psia).
v_O = Mach 1.00 (p' = 7.5 psia, $\Delta p'$ = 7.5 psia).
M_T = 29 lb/mole (air).
M_N = 30 lb/mole (50% nitrogen, 50% oxygen).

From Equation 86,

$$w_I = \frac{278.3 p_{API}}{460 + T_I} = \frac{278.3\ (21.72)}{460 + 72} = 11.36 \text{ lb.}$$

From Equation 87,

$$w_F = \frac{278.3 p_{APF}}{460 + T_F} = \frac{278.3\ (21.93)}{460 + 75} = 11.41 \text{ lb.}$$

From Equation 85,

$$w_{LT} = w_I - w_F + w_c = 11.36 - 11.41 + 7.75 = 7.70 \text{ lb.}$$

From Equation 93,

$$w_{LTD} = \frac{w_{LT}}{\tau} = \frac{7.70}{7} = 1.10 \text{ lb/day.}$$

From Equation 94,

$$w_{LOD} = w_{LTD}\left(\frac{7.5}{p_{\bar{A}T}}\right)\left(\frac{v_O}{v_T}\right)\left(\frac{M_N}{M_T}\right) = 1.10\left(\frac{7.5}{21.88}\right)\left(\frac{1.00}{0.78}\right)\left(\frac{30}{29}\right) = 0.50 \text{ lb/day.}$$

The leak rate for the seven-day leak test is therefore 1.10 lb/day for air under ambient conditions. The equivalent loss of the nitrogen-oxygen mixture under orbital conditions is 0.50 lb/day. Thus the equivalent leak rates under orbital conditions are the same for the one-day leak test prior to folding and packaging as for the seven-day leak test subsequent to the packaging test. The conclusion is then drawn that folding and packaging have no degrading effects on the gas tightness of the composite tunnel wall, i.e., the pressure bladder.

From Equation 94,

$$w_{LOD} = w_{LTD}\left(\frac{7.5}{p_{\bar{A}T}}\right)\left(\frac{v_O}{v_T}\right)\left(\frac{M_N}{M_T}\right) = 1.31\left(\frac{7.5}{23.06}\right)\left(\frac{1.00}{0.89}\right)\left(\frac{30}{29}\right) = 0.50 \text{ lb/day.}$$

The leak rate for the one-day leak test is therefore 1.31 lb/day for air under ambient conditions. The equivalent loss of the nitrogen-oxygen mixture under orbital conditions is 0.50 lb/day.

The values in Table XVIII used in determining the leak rate for the seven-day leak test are as follows:

p_{API} = 21.72 psia.
T_I = 72°F.
p_{APF} = 21.93 psia.
T_F = 75°F.
$p_{\bar{A}T}$ = 21.88 psia.
w_c = 7.75 lb.
τ = 7 days.
v_T = Mach 0.78 ($p' \cong$ 22 psia, $\Delta p' \cong$ 7.5 psia).
v_O = Mach 1.00 (p' = 7.5 psia, $\Delta p'$ = 7.5 psia).
M_T = 29 lb/mole (air).
M_N = 30 lb/mole (50% nitrogen, 50% oxygen).

From Equation 86,

$$w_I = \frac{278.3 p_{API}}{460 + T_I} = \frac{278.3\ (21.72)}{460 + 72} = 11.36 \text{ lb.}$$

From Equation 87,

$$w_F = \frac{278.3 p_{APF}}{460 + T_F} = \frac{278.3\ (21.93)}{460 + 75} = 11.41 \text{ lb.}$$

From Equation 85,

$$w_{LT} = w_I - w_F + w_c = 11.36 - 11.41 + 7.75 = 7.70 \text{ lb.}$$

From Equation 93,

$$w_{LTD} = \frac{w_{LT}}{\tau} = \frac{7.70}{7} = 1.10 \text{ lb/day.}$$

From Equation 94,

$$w_{LOD} = w_{LTD}\left(\frac{7.5}{p_{\bar{A}T}}\right)\left(\frac{v_O}{v_T}\right)\left(\frac{M_N}{M_T}\right) = 1.10\left(\frac{7.5}{21.88}\right)\left(\frac{1.00}{0.78}\right)\left(\frac{30}{29}\right) = 0.50 \text{ lb/day.}$$

The leak rate for the seven-day leak test is therefore 1.10 lb/day for air under ambient conditions. The equivalent loss of the nitrogen-oxygen mixture under orbital conditions is 0.50 lb/day. Thus the equivalent leak rates under orbital conditions are the same for the one-day leak test prior to folding and packaging as for the seven-day leak test subsequent to the packaging test. The conclusion is then drawn that folding and packaging have no degrading effects on the gas tightness of the composite tunnel wall, i.e., the pressure bladder.

E. CYCLIC PRESSURE TEST

1. General

The purpose of the cyclic pressure test was to establish the structural integrity of the tunnel from the standpoint of durability with respect to cyclic loading intended to simulate possible pressurization and depressurization cycles in orbital applications. The test consisted of cycling the tunnel internal pressure from a vacuum to a pressure of 7.5 psig for 60 cycles in a short period of time while the structure was observed for possible deformations.

2. Test Procedure

The test arrangement was similar to the proof test with filtered inflation air supplied by a shop air line except that a vacuum line was also attached to the cover plate on the MSS access hatch. Starting the test with the tunnel internal pressure at ambient atmospheric pressure, the tunnel was rapidly pressurized to 7.5 psig in approximately 20 seconds. After the pressure was allowed to stabilize for a few seconds, the vacuum line was opened and the tunnel was evacuated until the expandable wall started to collapse. The vacuum line was then closed and the air supply line was opened to start the pressurization part of the next cycle. This procedure was repeated until the tunnel had been pressurized 60 times.

3. Test Results

The were no visual signs of rigid structure deformation during the test. At the completion of the test, no visible signs of any damage could be detected. The cyclic pressure test together with the pressure proof test demonstrated the structural integrity of the tunnel.

F. VACUUM CHAMBER DEPLOYMENT TEST

1. General

The purpose of the vacuum chamber deployment test was to demonstrate the operational aspects of the tunnel by a deployment and pressurization sequence performed under vacuum conditions of 10^{-4} torr and to establish the tunnel leak rate under the same conditions by a 24-hour leak test. The test was intended to simulate packaging, canister ejection, and subsequent tunnel deployment in orbit. The test was conducted in the Aerospace Environmental Facility (AEF) 40 by 80 foot Mark I vacuum chamber at the Arnold Engineering Development Center (AEDC), Tennessee.

2. Test Procedure

The detailed test plan is presented in Reference 24, which was submitted to AEDC for formal approval by ARO, Inc and the Air Force. The procedure discussed here is a resumé of the procedure presented in Reference 24.

The test carrier with the packaged tunnel attached was lowered into the vacuum chamber through the 22-foot diameter access port. This operation is shown in Figure 102. The packaged tunnel was rotated into an inverted position for deployment so that the canister cover could be jettisoned in the one-G environment. The instrumentation and controls were then connected to the tunnel and the instrumentation penetration flange in the chamber wall. The tunnel installation is shown in Figure 103, and the instrumentation flange is shown in Figure 104. After all of these connections were checked, the connections were made to the instrumentation control panel and the entire system was checked. The instrumentation control panel is shown in Figure 105. GAC-supplied equipment and instrumentation are shown in Figure 106. The chamber was then sealed, and pump-down was started.

During the pump-down to 3×10^{-5} torr, the solenoid valves mounted on the access hatch cover plates were actuated to allow the packaged tunnel internal pressure to decrease coincidentally with the chamber pressure. This was done so that the elastic recovery action of the

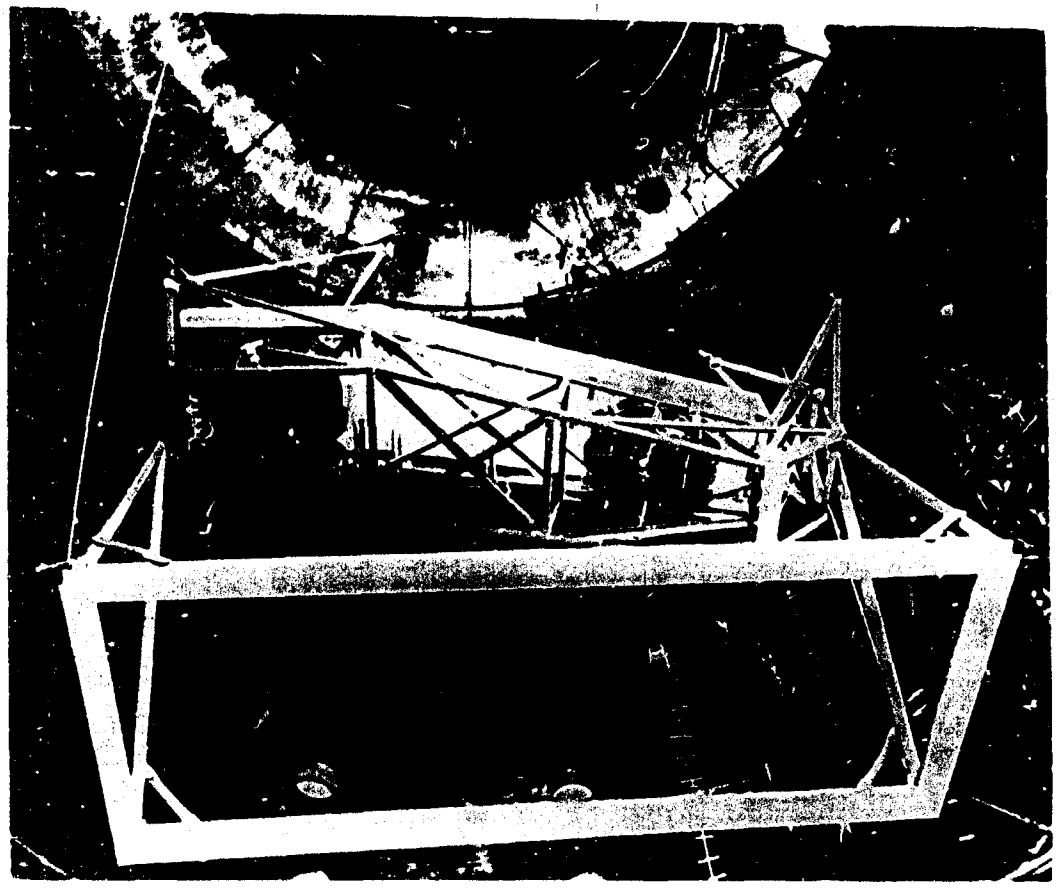

Figure 102. Tunnel Being Placed in the Mark I Chamber

meteoroid barrier foam as a deployment device could be evaluated. If the solenoid valves had not been opened, the pressure of the entrapped gas in the packaged tunnel would have increased sufficiently to deploy the tunnel to the desired configuration when the canister was ejected. When the chamber pressure was stabilized at 3×10^{-5} torr, the solenoid valves were closed. The pressure of the tunnel entrapped gas was 4 torr.

The canister cover was ejected by firing the pyrotechnic guillotines that cut the 12 canister separation screws, allowing the canister cover to fall into the canvas catcher. Canister separation and ejection occurred as planned, with the guillotines supplying enough separating force to actually hurl the canister cover away. However, the elastic recovery action of the foam was not sufficient to overcome the stiffness of the packaging folds and shape the tunnel. It was necessary to pressurize the tunnel to about 0.25 psia to completely expand it to the proper design configuration.

The tunnel was then further pressurized to 7.5 psia with carbon dioxide. After the pressure, temperature, and growth had been allowed to stabilize for almost two hours, the 24-hour leak check was started. During the test period, the tunnel pressure and temperature and the chamber pressure were monitored and recorded. At the end of the 24-hour test period, the chamber pressure was allowed to return to ambient. When the chamber pressure reached the internal tunnel pressure, the solenoid valves were again actuated to allow the tunnel internal pressure to increase with the chamber pressure. This was done to prevent the tunnel from being crushed against the test carrier and the lower canister part. When the Mark I chamber

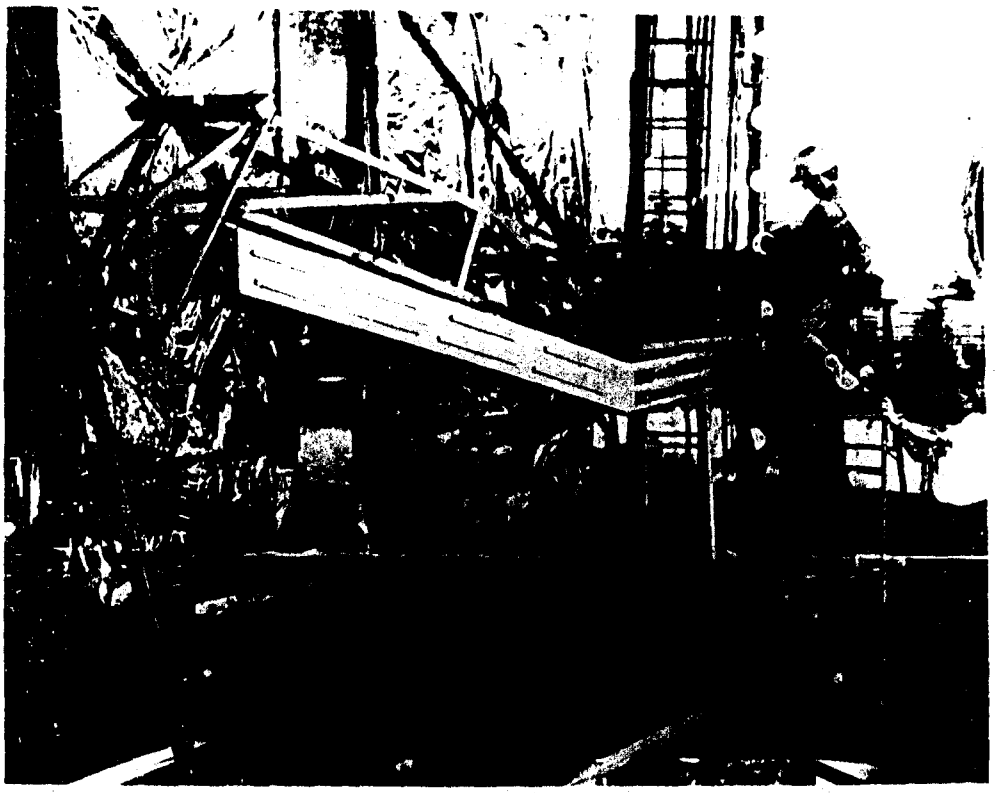

Figure 103. Packaged Tunnel Installation in Mark I Chamber

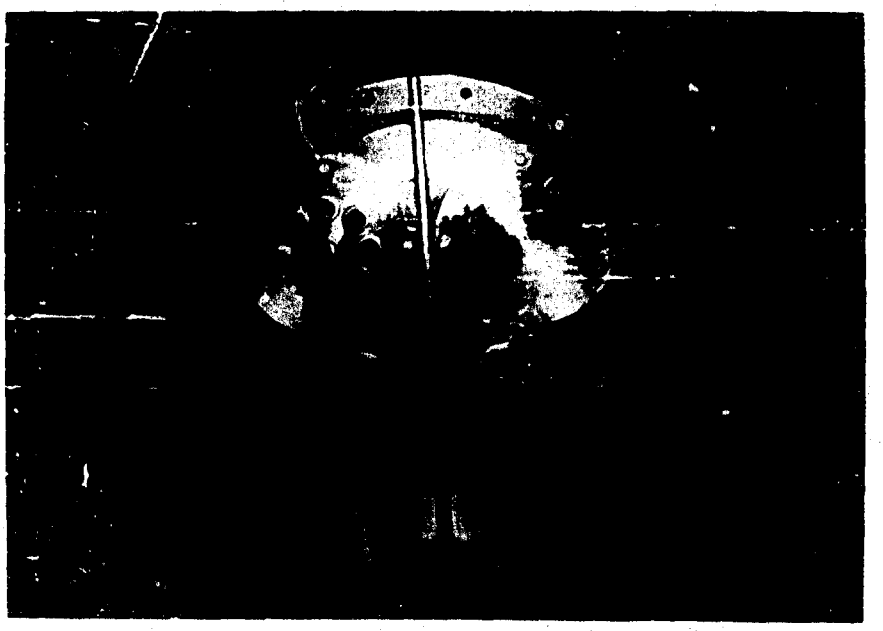

Figure 104. Instrumentation Flange

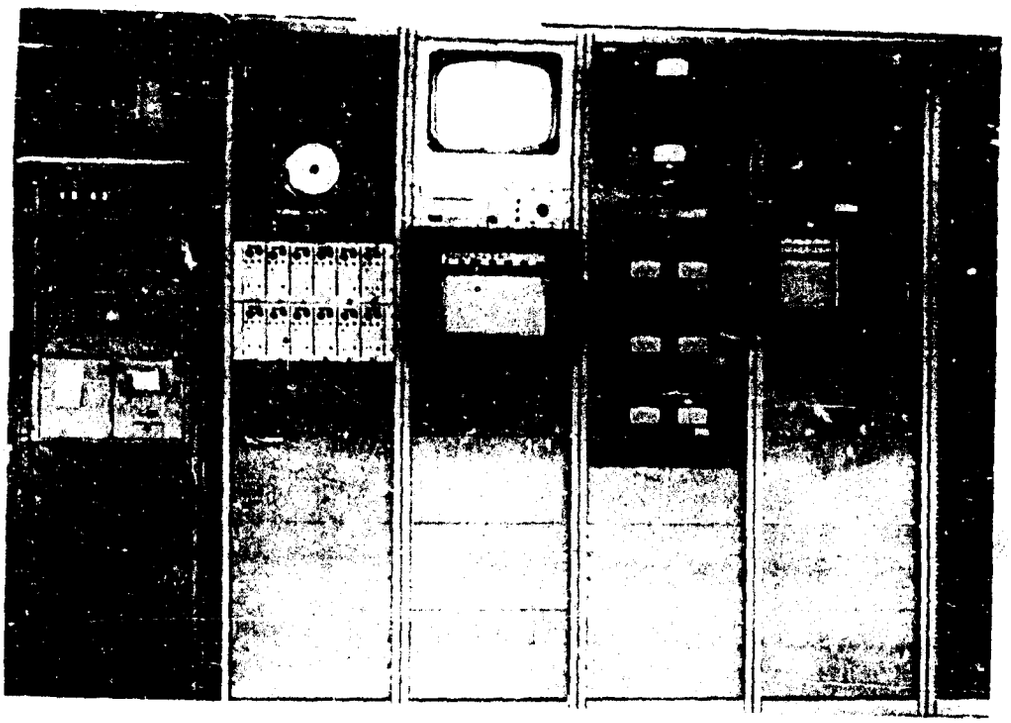

Figure 105. Instrumentation Control Panel

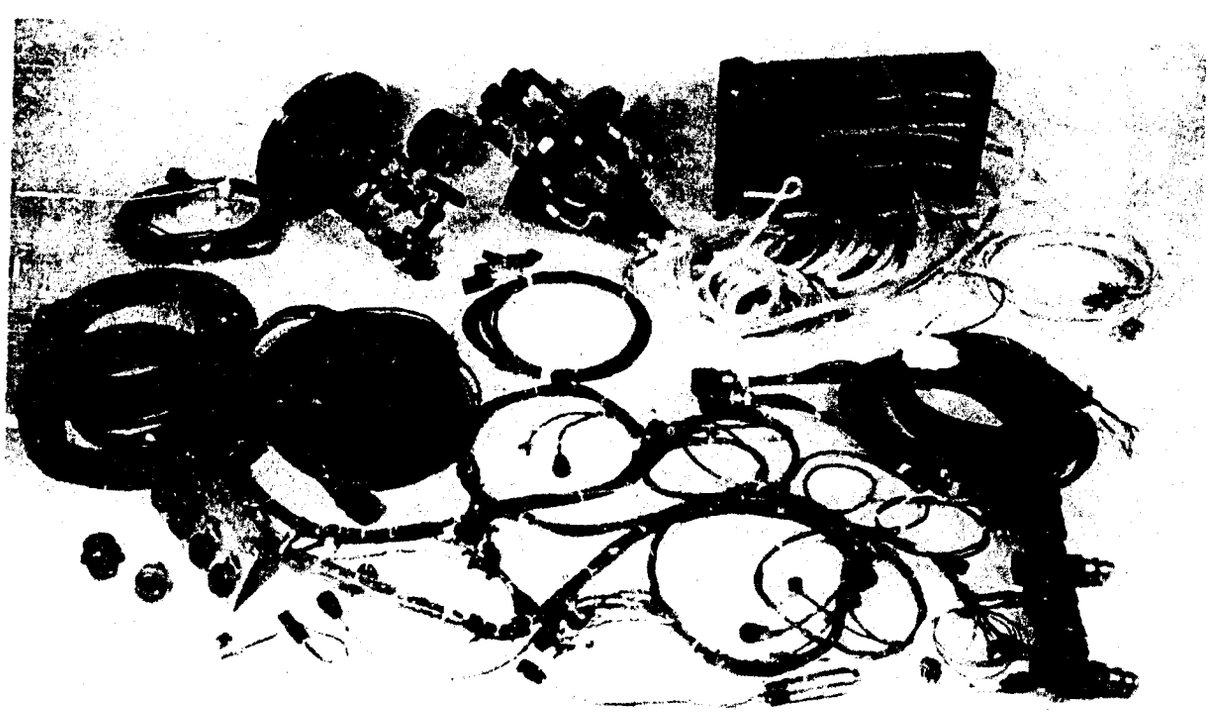

Figure 106. GAC-Supplied Test Equipment and Instrumentation

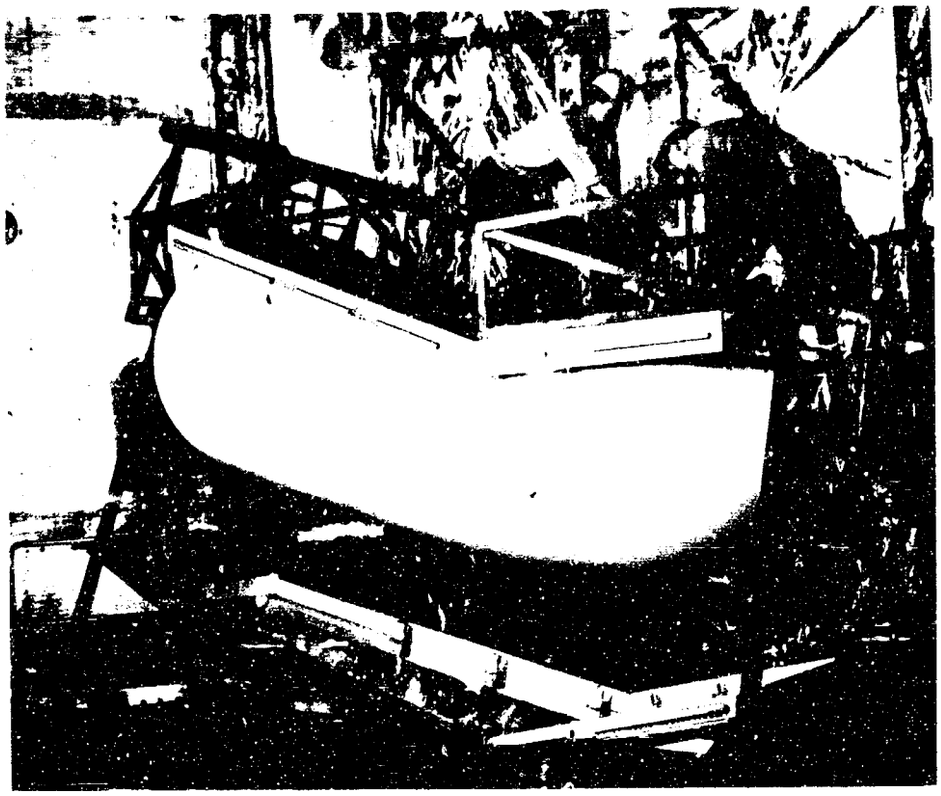

Figure 107. Tunnel Pressurized at 2 PSIG after Deployment Test

pressure reached ambient atmospheric pressure, the solenoid valves were closed, and the tunnel was pressurized to 2 psig with carbon dioxide. The chamber access hatch was then opened, and the tunnel was examined for damage. The tunnel pressurized to 2 psig after the leak test was completed is shown in Figure 107. There were no visible signs of damage to the tunnel as a result of the vacuum chamber deployment test.

3. Test Results

The packaged tunnel in the evacuated Mark I chamber just prior to deployment is shown in Figure 19. The chamber pressure was 3×10^{-5} torr, and the packaged tunnel internal pressure was 4 torr. Ten minutes before the deployment sequence was initiated, the lights were turned on in the chamber so that photo coverage of the test could be made. At that time, the chamber pressure was 1.2×10^{-5} torr. When the canister was jettisoned with a complete and very rapid separation, the elastic recovery action of the composite wall foam was not sufficient to shape the tunnel. The deployed unpressurized tunnel is shown in Figure 20. It was necessary to pressurize the tunnel to about 0.25 psia to completely expand it to the design configuration. Sequential pressurization is shown in Figures 21 through 23.

The 24-hour leak test was started after the tunnel pressure and temperature had been allowed to stabilize for almost 2 hours. The exact pressures and temperatures at the beginning and the completion of the test are given in Table XIX. The actual stabilized tunnel pressure at the beginning of the 24-hour period was about 7.7 psia. The pressure had decreased to 7 psia at the completion of the test. During the test period, the Mark I chamber pressure, which had risen to 5.5×10^{-5} torr during the tunnel pressurization with the lights on, decreased at a nearly linear rate to 2.4×10^{-5} torr.

Table XIX. Vacuum Chamber Leak Test Data

Reading								
Initial (I)	Final (F)	T (°F)	p_{AMV}[a] (torr)	p_{AM} (torr)	p_{AH}[b] (in. Hg)	p_{AP}[c] (psia)	p_{AC}[d] (psia)	$p_{\bar{A}T}$[e] (psia)
X		90	5.5×10^{-5}	397	15.63	7.68	7.47	7.12
	X	92	2.4×10^{-5}	362	14.25	7.00	6.78	

[a] p_{AMV} = the Mark I vacuum chamber pressure.

[b] $p_{AH} = 0.03937 p_{AM}$.

[c] $p_{AP} = 0.01934 p_{AM}$

$= 0.4912 p_{AH}$.

[d] p_{AC}, tunnel internal pressure corrected to a reference temp of 75°F,

$$= \frac{p_{AP}\,(460 + 75)}{460 + T} = \frac{535 p_{AP}}{460 + T}.$$ (See Equation 78.)

[e] $p_{\bar{A}T} = \frac{p_{ACI} + p_{ACF}}{2}$. (See Equation 88.)

The same procedure is used to determine the leak rate for the vacuum chamber test as was used for the ambient atmosphere leak tests. The weight of carbon dioxide gas in the pressurized tunnel at both the beginning and completion of the leak test is determined from the equation of state of an ideal gas. The weight of gas lost during the 24-hour period is then the daily leak rate. The test leak rate is converted to an equivalent leak rate of a mixture of 50 percent nitrogen and 50 percent oxygen at a pressure of 7.5 psia and a reference temperature of 75°F, simulating orbital conditions. The tunnel internal pressure used in converting the leak rate is the average test pressure corrected to the reference temperature of 75°F.

The leak rates are determined by using Equations 85, 86, 87, 93, and 94 modified by the use of R = 35.13 ft-lb/lb-°R for carbon dioxide instead of R = 53.30 ft-lb/lb-°R for air, and with $w_c = 0$.

The values in Table XIX used in determining the leak rate for the vacuum chamber leak test are as follows:

$p_{API} = 7.68$ psia.

$T_I = 90°F$.

$p_{APF} = 7.00$ psia.

$T_F = 92°F$.

$p_{\bar{A}T} = 7.12$ psia.

$\tau = 1$ day.

v_T = Mach 1.00 ($p' \cong 7$ psia, $\Delta p' \cong 7$ psia).

v_O = Mach 1.00 (p' = 7.5 psia, $\Delta p'$ = 7.5 psia).

M = 44 lb/mole (carbon dioxide).

M_N = 30 lb/mole (50% nitrogen, 50% oxygen).

From Equations 86 and 87 with R = 35.13 ft-lb/lb-^oR,

$$w_I = \frac{144\,(p_{API})(103)}{35.13\,(460 + T_I)} = \frac{422.2 p_{API}}{460 + T_I} = \frac{422.2\,(7.68)}{460 + 90} = 5.90 \text{ lb.}$$

$$w_F = \frac{422.2 p_{APF}}{460 + T_F} = \frac{422.2\,(7.00)}{460 + 92} = 5.35 \text{ lb.}$$

From Equations 85 and 93 with $w_c = 0$ and $\tau = 1$,

$$w_{LTD} = \frac{w_{LT}}{\tau} = w_I - w_F = 5.90 - 5.35 = 0.55 \text{ lb/day.}$$

From Equation 94,

$$w_{LOD} = w_{LTD}\left(\frac{7.5}{p_{\bar{A}T}}\right)\left(\frac{v_O}{v_T}\right)\left(\frac{M_N}{M_T}\right) = 0.55\left(\frac{7.5}{7.12}\right)\left(\frac{1.00}{1.00}\right)\left(\frac{30}{44}\right) = 0.40 \text{ lb/day.}$$

The leak rate for the 24-hour leak test is then 0.55 lb/day for carbon dioxide under vacuum chamber test conditions. The equivalent loss of the nitrogen-oxygen mixture under orbital conditions is 0.40 lb/day. This leak rate compares quite favorably with the leak rate of 0.50 lb/day established by the ambient atmosphere leak tests, being only 80 percent of the ambient atmosphere test value. The conclusion, therefore, is that the vacuum environment has no degrading effects on the gas tightness of the pressure bladder of the tunnel composite wall.

G. ZERO-G FLIGHT TEST

The purpose of the flight tests is tunnel evaluation and check-out from a human factors standpoint under conditions of no gravity (zero G). The flight tests will be conducted at Wright-Patterson AFB in the KC-135 zero-G aircraft, which is capable of simulating zero-G in multiple trajectories, each up to 30 seconds in duration. During these tests the tunnel will be unpressurized and will depend entirely on the inherent stiffness of the composite wall material to maintain the expanded tunnel geometry. Transfers will be conducted in both pressurized and nonpressurized space suits from both ends of the tunnel, simulating either exit from or return to either the MSS or the Gemini capsule. The astronaut will be encumbered by umbilical cables to determine their effect on transfer.

The objective of these flight tests will be to check out the tunnel geometry and the locomotion devices and interior lighting needed for effective transfer through the tunnel. In addition to ascertaining man's ability to transfer through the tunnel in zero G, the ability to transfer equipment will also be evaluated. In this respect, simulated equipment packages of approximately one cubic foot in volume will be used. In addition, tests will be conducted to determine whether or not an incapacitated astronaut can be transferred through the tunnel by another astronaut. The final area to be evaluated is man's ability to use the GAC repair kit in zero G to repair simulated tunnel damage.

Since the tunnel expanded geometry and locomotion aids were prescribed by the simulated tunnel mock-up previously used successfully to demonstrate zero-G transfers, no major problems are anticipated in regard to the test flights. The results of the flight tests will be reported in Part III of this report.

SECTION VII

CONCLUSIONS AND RECOMMENDATIONS

A. CONCLUSIONS

Under this contract, the design aspects of an expandable modular crew transfer tunnel were investigated, and practical solutions were evolved. A preliminary detailed design within the current state of the art was then executed, and a prototype tunnel was fabricated. Preliminary qualification testing was conducted on the prototype tunnel to establish the feasibility of the design for application to actual space missions. The testing program involved determination of the structural integrity and gas tightness of the structure and evaluation of operational aspects of the design.

The design was oriented specifically toward operational and packaging integration with the Gemini-MSS vehicle, with a minimum amount of vehicle modification and a minimum effect on vehicle operation and flight characteristics as design goals. The preliminary design features an expandable tunnel that when folded and prepackaged as a unit in the packaging canister, can be delivered to the launch pad as a module and is attached to the launch vehicle only at the Gemini and MSS hatch locations with quick-disconnect fasteners. In the event of mission abort, the entire tunnel system can be jettisoned as a unit, leaving the Gemini hatch clear for astronaut ejection. The packaging canister is designed to present a minimum drag area when the packaged tunnel is attached to the vehicle in the launch configuration. Detail design of the canister for specific mission applications with the attendant aerodynamic loads and aerodynamic heating involved was beyond the scope of this program effort.

The supporting analysis portion of the program, which was conducted in conjunction with the design effort, gave emphasis to the following:

(1) Thermal analysis indicates that the tunnel internal temperature can be maintained at a comfortable level by the use of passive thermal control coatings for most possible orbits and tunnel orientations. The same coatings will also maintain the temperatures of the tunnel structural elements within the thermal limits of material capabilities.

(2) Structural analysis indicates that maintaining safety factors of five on the expandable material and three on the hard structure presents no problems with the use of existing materials and fabrication techniques.

(3) Environmental hazards analysis indicates that the tunnel material has a resistance to high energy space radiation considerably in excess of the expected mission dosage with no significant degradation, while providing micrometeoroid protection with a probability of zero penetrations for a 60-day mission of at least 0.995.

(4) Materials selection, which included the investigation and selection of the most desirable fabrication techniques and the sample qualification testing of candidate materials and processes, was instrumental in establishing the materials designated for use in the tunnel design. The selection resulted in the use of materials that have been proved satisfactory from standpoints of structural integrity, abrasion resistance, fabrication applicability, and resistance to environmental conditions. The latter group includes resistance to radiation damage and micrometeoroid penetration, good permeability and nontoxic off-gassing characteristics in vacuum conditions, and thermal capabilities within the limitations established by the passive thermal control coating.

The prototype tunnel preliminary qualification testing program was successful in the following areas:

(1) The practicality of the launch configuration of the tunnel was established by packaging tests, which determined the most efficient folding procedure to achieve a minimum packaging height. The packaging tests also established the inherent stiffness of the composite wall material by demonstrating that the tunnel maintains its design configuration in a non-pressurized condition even after repeated folding and packaging operations.

(2) The structural integrity and durability of the tunnel were established by the pressure proof test and the cyclic pressure test. The prototype tunnel was pressurized for seven days at 10 psi, 1.33 times the 7.5-psi design pressure, and then subjected to 60 cycles of pressure loading. Each cycle consisted of evacuating the tunnel to an internal vacuum condition and then pressurizing the tunnel to the design pressure of 7.5 psi in approximately 20 seconds. At the completion of these tests, no signs of excessive deformation or damage could be detected.

(3) The leak tightness of the tunnel was established by a one-day leak test prior to packaging, a seven-day ambient atmosphere leak test subsequent to the packaging tests, and a one-day leak test in a vacuum chamber at an average pressure of 4×10^{-5} torr following the vacuum chamber deployment test. Both the one-day and seven-day leak tests under ambient conditions established leak rates converted to orbital conditions of 0.5 lb/day, which is only one-half the allowed value, indicating that folding and packaging have no adverse effects on the leak rate. The one-day vacuum chamber leak test established a converted leak rate of 0.4 lb/day, substantiating the results of the leak tests under ambient conditions.

(4) The vacuum chamber deployment test successfully demonstrated the operational aspects of canister separation and tunnel deployment. The deployment test at a vacuum chamber pressure of 3×10^{-5} torr resulted in a clean and very rapid canister separation and ejection and a partial deployment of the packaged tunnel with no internal pressure. A pressure of about 0.25 psia was necessary to completely expand the tunnel to its design configuration.

Finally, the prototype tunnel will be evaluated and checked out from a human factors standpoint under conditions of no gravity by tests simulating actual transfers in the KC-135 zero-G aircraft at Wright-Patterson AFB. Since zero-G flight tests have already been successfully performed in a simulated tunnel wooden mock-up, no problems are anticipated in this area.

The results of this program effort show that every development objective has been met. The expandable Gemini to MSS modular crew transfer tunnel is entirely feasible and within the present state of the art. In addition, the materials and fabrication techniques used in this program have demonstrated characteristics that should make them attractive for other expandable space structures applications. The characteristics of primary interest include leak tightness, structural integrity, resistance to the effects of space environment, packagability, ability to be integrated with "hard" structure, and adaptability to desired geometric configurations.

B. RECOMMENDATIONS

In view of the results of the preliminary design, prototype fabrication, and preliminary qualification testing program, further detailed definition of the design and extensive qualification testing, culminating in operational space-qualified and man-rated flight hardware via an unmanned space flight, are recommended. Specifically, the following efforts are recommended as a logical extension of the program:

(1) Direct further detailed design efforts toward reducing the packaging height and launch weight of the preliminary design.

(2) Initiate studies of specific mission applications with respect to the design of definite passive thermal control systems associated with specific orbits and orientations.

(3) Construct scale-model canisters and conduct wind tunnel tests to determine aerodynamic loading and heating characteristics on the canister and to determine canister effects on the vehicle system flight characteristics.

(4) Construct several full-scale tunnels for extensive qualification testing and installation compatibility checks. The testing program should terminate in an unmanned test flight to establish the tunnel as space-qualified and man-rated flight hardware.

In line with these recommendations, a program development plan is included in Section VIII.

SECTION VIII

PROGRAM DEVELOPMENT PLAN

A. PHASE II - EXPANDABLE TUNNEL PRELIMINARY QUALIFICATION

The tunnel program development plan is shown in Figure 108. The Phase II program is scheduled for completion in six months. During the program, wind tunnel tests will be run on the Gemini-MSS vehicle with a canister to determine the aerodynamic loads and heating on the canister and the effects of the canister on launch vehicle aerodynamics. A full-scale transfer tunnel will be fabricated using the Phase I design with a modified canister. During Phase III the tunnel will be used as a mock-up and also to run design proof tests of breadboarded subsystems.

Operational analysis tests will be run using the existing tunnel model to determine the most feasible methods for deploying the tunnel from both a mechanical and a human factors viewpoint. Emphasis will also be placed on defining the MSS-tunnel integration requirements. Work will also be started on defining subsystem areas and writing preliminary specifications for each area. Where necessary, procurement specifications will be prepared to shorten the procurement cycle in Phase III. The object of the Phase II effort will be to obtain the necessary design and test data to complete a firm base-line design.

B. PHASE III - EXPANDABLE TUNNEL QUALIFICATION PROGRAM

Phase III includes final detailed design of the tunnel, fabrication of five units, final [illegible] testing, and delivery.

1. Final Design

Phase III detailed design is scheduled to start the seventh month, and by the end of the twelfth month, the final design will be completed and all drawings will have been released to the shop. During the design program, deployment tests will be run using the tunnel fabricated in Phase II. The effort will include astronaut locomotion tests, vision and lighting tests, hatch operation tests, etc.

2. Fabrication

Plans now call for five units to be fabricated. Units No. 1 and 2 will be used for system qualification tests. Unit No. 1 will then be shipped to the launch site to be used for compatability checks. Unit No. 3 will be used for the flight test, and unit No. 4 will be used as the spare. The fifth unit will remain at GAC as backup hardware.

Fabrication of the tooling and handling fixtures will start in the tenth month. Five sets of soft tooling will be required, one for each unit fabricated. There is a possibility that an expandable mandrel could be fabricated and reused, thereby eliminating two sets of soft tooling. The last set of tooling must be completed by the sixteenth month in order to start fabrication of the last flight unit by the middle of the nineteenth month. The fabrication area must be exceptionally clean and free from all types of debris (dirt, metal shavings, dust, etc), and the humidity and temperature must be controlled. Therefore, a specific area will be set aside and improved for the fabrication of the tunnel units.

3. Quality Control and Reliability

A full-fledged reliability and quality control program will be conducted during the Phase III design, fabrication, and testing to provide the maximum degree of assurance that the tunnel

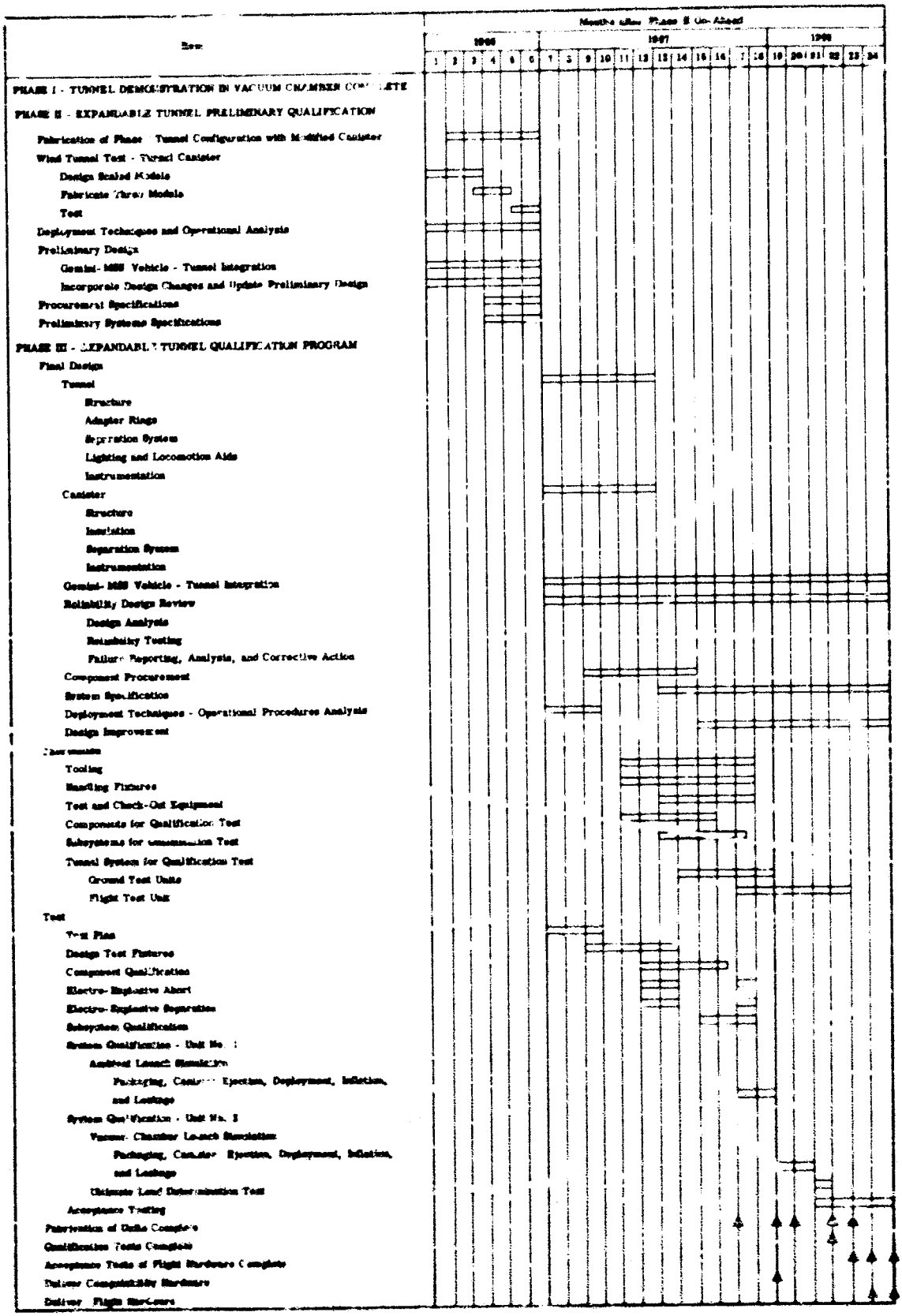

Figure 108. Modular Crew Transfer Tunnel Development Plan and Schedule

units will satisfactorily meet all test objectives. A more detailed set of procurement and system specifications will also be prepared during the Phase III program.

4. Testing

The test program will be designed to space-qualify the hardware prior to the flight test. The tests will include standard component and subsystem qualification, launch simulation and environmental tests, electro-explosive separation and abort deployment tests, and pressurization tests of the expandable crew transfer tunnel.

5. Delivery

The compatibility unit (No. 1) will be shipped to the launch site at the end of the eighteenth month. The flight hardware unit (No. 3) will be delivered the end of the twenty-third month, and the flight unit spare (No. 4) will be shipped on the twenty-fourth month after program go-ahead.

REFERENCES

1. Apisa, J.N., Satellite Radiation Heat Balance Program. GER-10946. Goodyear Aerospace Corporation, Akron, Ohio, 10 January 1962.

2. Oppenheim, A.K., "Radiation Analysis by the Network Method." ASME Transactions. 1956. p. 725.

3. Roark, R.J., Formulas for Stress and Strain. Third Edition. McGraw-Hill Book Company, Inc, New York, 1954.

4. Sutcliffe, A.B., and Reynolds, B.W., Load-Time Tests of Dacron Airship Envelope Fabric at Elevated Temperatures. GER-9657. Goodyear Aerospace Corporation, Akron, Ohio, April 1960.

5. Metallic Materials and Elements for Flight Vehicle Structures. MIL-HDBK-5. Department of Defense, Washington 25, D.C., August 1962.

6. Timoshenko, S., Strength of Materials, Part II. Second Edition. D. Van Nostrand Co, Inc, New York, 1941.

7. Meteoroid Environment in Near-Earth, Cis-Lunar, and Near-Lunar Space. NASA-MSC Bulletin EC-1. 8 November 1963.

8. Attachment B, Request for Proposal Nr. 22583-NB, Expandable Gemini to MOL Crew Transfer Tunnel. Systems Engineering Group, Research and Technology Division, Air Force Systems Command, United States Air Force, Wright-Patterson Air Force Base, Ohio, 13 August 1964.

9. Reynolds, B.W., Effects of Hypervelocity Particle Impact on Composite Materials for Expandable Structures Applications. GER-10663. Goodyear Aerospace Corporation, Akron, Ohio, August 1962.

10. Hess, Wilmont N., "Earth's Radiation Environment." Space/Aeronautics. November 1964. pp. 68 - 76.

11. Goetzel, C.G., and Singletary, J.B., Space Materials Handbook. AD284547. Contract AF04(647)-673. Lockheed Missiles and Space Company, Sunnyvale, California, January 1962.

12. Schulte, H.J., and Shipley, E.N., Models for Space Environmental Hazards: Radiation, Issue II. Bellcomm Inc, Washington, D.C., January 1962.

13. Modisette, J.L., Vinson, T.M., and Hardy, A.C., Model Solar Proton Environments for Manned Spacecraft Design. Technical Note S-48. Manned Spacecraft Center, Houston, Texas, 27 June 1964.

14. Jurich, L., and Emmons, R.H., Study of Radiation in Cis-Lunar Space. GER-10679. Goodyear Aerospace Corporation, Akron, Ohio, June 1962.

15. Rich, M., and Madey, R., Range-Energy Tables. Radiation Laboratory, University of California, Berkeley, California, March 1954.

16. VanAllen, J.A., Recent Observational Work on Trapped Radiation. Presentation at the Third International Space Symposium, COSPAR Meeting, 1962.

17. Swanson, P. G., Solar Reflector Foaming Technology Development. GER-11755. Goodyear Aerospace Corporation, Akron, Ohio, December 1964.

18. Emmons, R. H., Indicated Specular Degradation Rate for Aluminized Mylar Surfaces in Near-Earth Orbit. GER-11521. Goodyear Aerospace Corporation, Akron, Ohio, June, 1964.

19. Plunkett, J. D., NASA Contributions to the Technology of Inorganic Coatings. NASA-SP-5014. 1964.

20. Daugherty, J. W., Radiation Properties of Dielectrics. FD-532. Goodyear Aerospace Corporation, Akron, Ohio, February, 1965.

21. Withey, D. J., Repair of Leaks in an Aerospace Environment. ASD-TDR-62-1-15. Contract AF33(657)-7852. General Electric Co, Philadelphia, Pennsylvania, December 1962.

22. Whipple, C. L., and Cartindale, E. G., Silicone Performance in Thermal-Vacuum Environment. Presentation at the 6th Annual SAMPE National Symposium. November 1963.

23. Thorne, J. A., Radiation Resistance of Silicone and Other Polymeric Materials. Dow-Corning Aerospace Laboratory Report No. 102. Dow Corning Corporation, Midland, Michigan, September 1964.

24. Hoffman, T. L., and Lilley, R. D., Expandable Crew Transfer Tunnel Vacuum Chamber Deployment Test Program. GER-12333. Goodyear Aerospace Corporation, Akron, Ohio, 17 September 1965.

Unclassified
Security Classification

DOCUMENT CONTROL DATA - R&D

(Security classification of title, body of abstract and indexing annotation must be entered when the overall report is classified)

1. ORIGINATING ACTIVITY (Corporate author)	2a. REPORT SECURITY CLASSIFICATION
Goodyear Aerospace Corporation Akron, Ohio	Unclassified
	2b. GROUP

3. REPORT TITLE: UTILIZATION OF ELASTIC RECOVERY MATERIALS FOR THE DEVELOPMENT OF CREW TRANSFER TUNNELS, AIRLOCKS, AND SPACE MAINTENANCE HANGARS
Part II. Expandable Modular Crew Transfer Tunnel Design, Fabrication, and Testing

4. DESCRIPTIVE NOTES (Type of report and inclusive dates)
Final

5. AUTHOR(S) (Last name, first name, initial)
Hoffman, Thomas L.

6. REPORT DATE	7a. TOTAL NO. OF PAGES	7b. NO. OF REFS
June 1966	165	24

8a. CONTRACT OR GRANT NO.	9a. ORIGINATOR'S REPORT NUMBER(S)
AF33(615)-2114 b. PROJECT NO.	AFAPL-TR-66-2, Part II
c.	9b. OTHER REPORT NO(S) (Any other numbers that may be assigned this report) GER 12335
d.	

10. AVAILABILITY/LIMITATION NOTICES
Qualified users may obtain copies of this report from the Defense Documentation Center (DDC), Cameron Station, Bldg. 5, 5010 Duke Street, Alexandria, Virginia, 22314.

11. SUPPLEMENTARY NOTES	12. SPONSORING MILITARY ACTIVITY
	Air Force Aero Propulsion Laboratory, Research and Technology Division, Wright Patterson AFB, Ohio

13. ABSTRACT This report summarizes the design, analysis, fabrication, and testing of the expandable Gemini to Manned Space Station (MSS) modular crew transfer tunnel. The program established the design of a 3.5-ft dia modular tunnel to be used as a pressurized meteoroid protective enclosure for astronauts transferring from the Gemini capsule to the MSS. The transfer tunnel attaches to the elliptical Gemini hatch at one end and to the circular MSS hatch at the other end. A prototype tunnel was fabricated and tested to establish design feasibility. Tunnel construction is a composite wall consisting of an inner triple-barrier pressure bladder for gas retention, a 4-ply Dacron cloth structural layer, a 2-in. thick polyether foam meteoroid barrier, and a film-cloth laminate outer cover with a thermal coating. The expandable composite wall is structurally bonded to a rigid aluminum honeycomb sandwich floor to which the packaging canister is attached when the tunnel is folded to constitute a modular unit. Pressure proof testing for 7 days at 10 psi and cyclic pressure testing from vacuum to the nominal operating pressure of 7.5 psi for 60 cycles established the structural integrity. Pressure leak testing under ambient conditions for 7 days at 7.5 psi established the gas tightness of the structure with a leak rate of 0.50 lb/day of inflation gas under orbital conditions. Pressure leak testing in a vacuum chamber at an average vacuum of 4×10^{-5} mm Hg for one day established a leak rate of 0.40 lb/day of inflation gas under orbital conditions. Tunnel deployment testing in a vacuum chamber confirmed the operational aspects of the design. Fabrication of an operational expandable crew transfer tunnel, which is estimated to weigh 375 pounds including the packaging canister, is entirely feasible and within the present state of the art.

DD FORM 1 JAN 64 1473

Unclassified
Security Classification

14. KEY WORDS	LINK A		LINK B		LINK C	
	ROLE	WT	ROLE	WT	ROLE	WT
Expandable Structures Elastic Recovery Materials Crew Transfer Tunnels						

INSTRUCTIONS

1. ORIGINATING ACTIVITY: Enter the name and address of the contractor, subcontractor, grantee, Department of Defense activity or other organization *(corporate author)* issuing the report.

2a. REPORT SECURITY CLASSIFICATION: Enter the overall security classification of the report. Indicate whether "Restricted Data" is included. Marking is to be in accordance with appropriate security regulations.

2b. GROUP: Automatic downgrading is specified in DoD Directive 5200.10 and Armed Forces Industrial Manual. Enter the group number. Also, when applicable, show that optional markings have been used for Group 3 and Group 4 as authorized.

3. REPORT TITLE: Enter the complete report title in all capital letters. Titles in all cases should be unclassified. If a meaningful title cannot be selected without classification, show title classification in all capitals in parenthesis immediately following the title.

4. DESCRIPTIVE NOTES: If appropriate, enter the type of report, e.g., interim, progress, summary, annual, or final. Give the inclusive dates when a specific reporting period is covered.

5. AUTHOR(S): Enter the name(s) of author(s) as shown on or in the report. Enter last name, first name, middle initial. If military, show rank and branch of service. The name of the principal author is an absolute minimum requirement.

6. REPORT DATE: Enter the date of the report as day, month, year; or month, year. If more than one date appears on the report, use date of publication.

7a. TOTAL NUMBER OF PAGES: The total page count should follow normal pagination procedures, i.e., enter the number of pages containing information.

7b. NUMBER OF REFERENCES: Enter the total number of references cited in the report.

8a. CONTRACT OR GRANT NUMBER: If appropriate, enter the applicable number of the contract or grant under which the report was written.

8b, 8c, & 8d. PROJECT NUMBER: Enter the appropriate military department identification, such as project number, subproject number, system numbers, task number, etc.

9a. ORIGINATOR'S REPORT NUMBER(S): Enter the official report number by which the document will be identified and controlled by the originating activity. This number must be unique to this report.

9b. OTHER REPORT NUMBER(S): If the report has been assigned any other report numbers *(either by the originator or by the sponsor)*, also enter this number(s).

10. AVAILABILITY/LIMITATION NOTICES: Enter any limitations on further dissemination of the report, other than those imposed by security classification, using standard statements such as:

(1) "Qualified requesters may obtain copies of this report from DDC."

(2) "Foreign announcement and dissemination of this report by DDC is not authorized."

(3) "U. S. Government agencies may obtain copies of this report directly from DDC. Other qualified DDC users shall request through

_____."

(4) "U. S. military agencies may obtain copies of this report directly from DDC. Other qualified users shall request through

_____."

(5) "All distribution of this report is controlled. Qualified DDC users shall request through

_____."

If the report has been furnished to the Office of Technical Services, Department of Commerce, for sale to the public, indicate this fact and enter the price, if known.

11. SUPPLEMENTARY NOTES: Use for additional explanatory notes.

12. SPONSORING MILITARY ACTIVITY: Enter the name of the departmental project office or laboratory sponsoring *(paying for)* the research and development. Include address.

13. ABSTRACT: Enter an abstract giving a brief and factual summary of the document indicative of the report, even though it may also appear elsewhere in the body of the technical report. If additional space is required, a continuation sheet shall be attached.

It is highly desirable that the abstract of classified reports be unclassified. Each paragraph of the abstract shall end with an indication of the military security classification of the information in the paragraph, represented as *(TS), (S), (C), or (U)*.

There is no limitation on the length of the abstract. However, the suggested length is from 150 to 225 words.

14. KEY WORDS: Key words are technically meaningful terms or short phrases that characterize a report and may be used as index entries for cataloging the report. Key words must be selected so that no security classification is required. Identifiers, such as equipment model designation, trade name, military project code name, geographic location, may be used as key words but will be followed by an indication of technical context. The assignment of links, rules, and weights is optional.